

Detection and analysis of spin trapped radical adducts using  
thermal desorption gas chromatography mass spectrometry  
(TD/GC/MS)

Kamran Manzoor



Submitted in partial fulfillment of the requirements of the degree of Doctor of Philosophy

School of Environment and Life Sciences

College of Science and Technology

University of Salford, Salford, UK

July 2018

# Table of Contents

|  |       |
|--|-------|
| List of Figures .....                                | x     |
| List of Appendix Figures .....                       | xvi   |
| List of Tables .....                                 | xvii  |
| List of Schemes.....                                 | xix   |
| Acknowledgements.....                                | xxi   |
| Declaration.....                                     | xxii  |
| Abbreviations .....                                  | xxiii |
| Abstract .....                                       | xxv   |
| Introduction.....                                    | 1     |
| 1 Free Radicals .....                                | 2     |
| 1.1 Formation of Free radicals .....                 | 2     |
| 1.2 Sources of Free Radicals .....                   | 3     |
| 1.2.1 The Fenton Reaction .....                      | 4     |
| 1.2.1.1 The Haber-Weiss reaction .....               | 5     |
| 1.2.2 Reactive Oxygen Species (ROS) .....            | 5     |
| 1.2.2.1 Hydroxyl radicals .....                      | 6     |
| 1.2.3 Reactive Nitrogen Species (RNS).....           | 8     |
| 1.3 Oxidative Stress.....                            | 8     |
| 1.3.1 Causes of Oxidative stress .....               | 8     |
| 1.3.2 Consequences of oxidative stress.....          | 9     |
| 1.4 Antioxidants: .....                              | 10    |
| 1.5 Benefits of Free Radicals .....                  | 12    |
| 1.6 Chain reaction and damage by Free radicals ..... | 13    |
| 1.6.1 Lipid hydroperoxide (LOOH).....                | 14    |
| 1.6.2 Protein Oxidation .....                        | 15    |
| 1.6.3 Carbohydrates .....                            | 15    |
| 1.6.4 DNA Oxidation .....                            | 15    |
| 1.7 Free radicals and Human diseases.....            | 15    |
| 1.7.1 Neurodegenerative diseases .....               | 17    |
| 1.7.2 Cardiovascular diseases .....                  | 18    |

|            |  |    |
|------------|--|----|
| 1.7.3      | Rheumatoid arthritis.....                                | 19 |
| 1.7.4      | Cancer .....   | 20 |
| 1.7.5      | Lung diseases .....                                      | 21 |
| 1.7.6      | Hypoglycaemia .....                                      | 21 |
| 1.7.7      | Reproductive system.....                                 | 22 |
| 1.7.8      | Cataract and glaucoma .....                              | 22 |
| 1.7.9      | Immune system .....                                      | 23 |
| 1.7.10     | Ageing.....  | 23 |
| 1.8        | Aldehydes and Free radicals .....                        | 24 |
| 1.8.1      | Aldehyde radicals as potential biomarkers .....          | 25 |
| 1.8.2      | Solvent free approaches to detect aldehyde radicals..... | 25 |
| 1.8.3      | Challenges to detect aldehyde-related radicals .....     | 26 |
| 1.9        | Detection of Free radicals .....                         | 26 |
| 1.9.1      | Spin Trapping.....                                       | 26 |
| 1.9.2      | Nitrones and nitroso spin traps.....                     | 27 |
| 1.9.3      | Nitroxides as spin traps .....                           | 29 |
| 1.9.3.1    | Inhibiting the generation of Fenton-type radicals .....  | 32 |
| 1.9.3.2    | Inhibition of Lipid peroxidation .....                   | 32 |
| 1.9.3.3    | Protection against radiation-induced radicals.....       | 32 |
| 1.9.3.4    | Mutagenicity.....  | 32 |
| 1.9.4      | Secondary Spin trapping .....                            | 33 |
| 1.10       | Extraction approaches .....                              | 34 |
| 1.10.1     | Thermal desorption .....                                 | 34 |
| 1.10.1.1   | Introduction and history.....                            | 34 |
| 1.10.1.2   | General principle .....                                  | 35 |
| 1.10.1.3   | Advantages .....   | 38 |
| 1.10.1.3.1 | Desorption efficiency.....                               | 38 |
| 1.10.1.3.2 | Extraction efficiency.....                               | 38 |
| 1.10.1.3.3 | Reduced solvent interferences.....                       | 38 |
| 1.10.1.3.4 | Exposure risk .....                                      | 38 |
| 1.10.1.3.5 | Low Cost .....   | 38 |
| 1.10.1.4   | Applications of TD.....                                  | 39 |
| 1.10.2     | Solid phase microextraction (SPME).....                  | 39 |

|          |   |    |
|----------|---|----|
| 1.10.2.1 | Working principle.....  | 40 |
| 1.10.2.2 | Sampling techniques .....   | 40 |
| 1.10.2.3 | Polydimethylsiloxane (PDMS) coating .....                                   | 40 |
| 1.10.2.4 | Analytical techniques and SPME .....  | 41 |
| 1.10.2.5 | Advantages and Disadvantages of SPME .....                                  | 41 |
| 1.11     | Analytical techniques and spin tapping .....                                | 43 |
| 1.11.1   | Electron Paramagnetic Resonance and Spin trapping.....                      | 43 |
| 1.11.2   | Spin trapping- Nuclear magnetic resonance (ST-NMR) spectroscopy.....        | 44 |
| 1.11.3   | Liquid Chromatography (LC) and spin trapped free radicals .....             | 45 |
| 1.11.4   | Matrix Assisted Laser Desorption Ionisation time of flight (MALDI-TOF)..... | 46 |
| 1.11.5   | GC-MS and Spin trapping.....  | 47 |
| 1.12     | Other biochemical assays to measure oxidative stress .....                  | 49 |
| 1.12.1   | Total antioxidant capacity (TAC) .....                                      | 49 |
| 1.12.2   | Flow cytometry .....  | 50 |
| 1.12.3   | Assays measuring ROS induced modifications .....                            | 51 |
| 1.12.3.1 | Measuring Lipid peroxidation products .....                                 | 51 |
| 1.12.3.2 | DNA oxidation.....  | 52 |
| 1.12.3.3 | Protein oxidation.....  | 53 |
| 1.13     | Aims and objectives of the research .....                                   | 55 |
| 2        | Materials and methods .....   | 57 |
| 2.1      | Chemicals .....   | 58 |
| 2.2      | Reagents preparation for the Fenton reaction.....                           | 58 |
| 2.2.1    | Standard conditions for the Fenton reaction .....                           | 58 |
| 2.3      | Gas chromatography-Mass spectrometry (GC-MS).....                           | 60 |
| 2.4      | Extraction techniques.....  | 62 |
| 2.4.1    | Headspace solid phase microextraction (HS-SPME) .....                       | 62 |
| 2.4.2    | Thermal desorption gas chromatography mass spectrometry (TD-GC-MS) .....    | 62 |
| 2.5      | Instrumentation for current study .....                                     | 63 |
| 2.5.1    | SPME-GC-MS .....  | 63 |
| 2.5.2    | Thermal desorption.....   | 64 |
| 2.6      | GC-MS method development .....  | 64 |
| 2.6.1    | The Fenton reaction in the presence of a secondary source of radicals ..... | 65 |
| 2.6.2    | Control reaction (Buffer & PBN).....  | 66 |

|       |   |    |
|-------|---|----|
| 2.6.3 | Buffer, PBN & acetaldehyde .....  | 67 |
| 2.6.4 | Comparison of the Fenton reaction with controls .....   | 68 |
| 2.6.5 | Analysis of the Fenton reaction carried out in the absence of a secondary source of free radicals .....   | 69 |
| 2.6.6 | GC-MS analysis of the Fenton reaction in the absence of PBN .....   | 70 |
| 2.6.7 | Analysis of the Fenton reaction containing the spin trap PBN but carried out in the absence of iron and ascorbic acid .....   | 71 |
| 2.6.8 | Analysis of the Fenton reaction containing the spin trap PBN but in the absence of H <sub>2</sub> O <sub>2</sub> .....  | 72 |
| 3     | Detection and analysis of spin-adducts from ethanal and N- <i>tert</i> -butyl- $\alpha$ -phenylnitron (PBN) using thermal desorption-gas chromatography-mass spectrometry ..... | 73 |
| 3.1   | Introduction.....   | 74 |
| 3.2   | Chromatograms.....  | 76 |
| 3.2.1 | Fenton reaction with acetaldehyde and PBN .....   | 77 |
| 3.2.2 | Fenton reaction with d <sub>3</sub> -acetaldehyde {CD <sub>3</sub> C(H)O} and PBN .....   | 78 |
| 3.2.3 | Fenton reaction with acetaldehyde and d <sub>6</sub> -PBN.....  | 79 |
| 3.2.4 | Fenton reaction with acetaldehyde and F-PBN .....   | 80 |
| 3.2.5 | Fenton reaction with acetaldehyde and Cl-PBN .....  | 81 |
| 3.3   | Electron ionisation (EI-MS) mass spectra of the di-methyl adduct of PBN.....  | 82 |
| 3.3.1 | Dimethyl adduct of PBN {PBN(CH <sub>3</sub> ) <sub>2</sub> } .....  | 82 |
| 3.3.2 | PBN (CD <sub>3</sub> ) <sub>2</sub> adduct.....   | 83 |
| 3.3.3 | d <sub>6</sub> -PBN(CH <sub>3</sub> ) <sub>2</sub> adduct.....  | 84 |
| 3.3.4 | d <sub>6</sub> -PBN(CD <sub>3</sub> ) <sub>2</sub> adduct.....  | 85 |
| 3.3.5 | F-PBN(CH <sub>3</sub> ) <sub>2</sub> adduct.....  | 86 |
| 3.3.6 | Cl-PBN(CH <sub>3</sub> ) <sub>2</sub> adduct .....  | 87 |
| 3.4   | Electron ionisation mass spectra (EI-MS) of the H-PBN-CH <sub>3</sub> adduct.....   | 89 |
| 3.4.1 | CH <sub>3</sub> & H adduct of PBN (H-PBN-CH <sub>3</sub> ).....   | 89 |
| 3.4.2 | CD <sub>3</sub> & H adduct of PBN (H-PBN-CD <sub>3</sub> ).....   | 90 |
| 3.4.3 | CH <sub>3</sub> & H adduct of d <sub>6</sub> -PBN (H-d <sub>6</sub> PBN-CH <sub>3</sub> ).....  | 91 |
| 3.4.4 | CD <sub>3</sub> & H adduct of d <sub>6</sub> -PBN (H-d <sub>6</sub> PBN-CD <sub>3</sub> ).....  | 92 |
| 3.4.5 | CH <sub>3</sub> & H adduct of F-PBN {F-PBN(H)CH <sub>3</sub> }.....   | 93 |
| 3.5   | Methyl adduct of <i>tert</i> -butylhydroaminoxyl ( <sup>t</sup> Bu-NOME).....   | 95 |
| 3.5.1 | EI mass spectrum of <sup>t</sup> Bu-NOHMe .....   | 95 |

|        |  |     |
|--------|--|-----|
| 3.5.2  | EI mass spectrum of <sup>1</sup> Bu-NOH(CD <sub>3</sub> ).....   | 96  |
| 3.6    | Di- <i>tert</i> -butyl hydroxylamine.....  | 98  |
| 3.6.1  | EI mass spectrum of Di- <i>tert</i> butyl hydroxylamine.....   | 98  |
| 3.6.2  | EI mass spectrum of Di- <i>tert</i> butyl (d <sub>9</sub> ) hydroxylamine.....   | 99  |
| 3.7    | EI mass spectrum of phenyl methanimine.....  | 101 |
| 3.8    | EI mass spectrum of benzaldehyde.....  | 103 |
| 3.9    | N-methoxy-1-phenylethanamine.....  | 105 |
| 3.9.1  | EI mass spectrum of N-methoxy-1-phenylethanamine.....  | 105 |
| 3.9.2  | EI mass spectrum of N-methoxy-1-phenylethanamine (d <sub>6</sub> ).....  | 106 |
| 3.10   | EI mass spectrum of methoxy-(1-phenylethylidene)amine.....   | 109 |
| 3.11   | EI mass spectrum of DL-2,3-Diphenylbutane.....   | 112 |
| 3.12   | Paraldehyde.....   | 114 |
| 3.12.1 | EI mass spectrum of paraldehyde.....   | 114 |
| 3.12.2 | EI mass spectrum of paraldehyde (d <sub>9</sub> ).....   | 115 |
| 3.13   | Discussion.....  | 116 |
| 4      | Detection and analysis of spin-adducts from propanal and N- <i>tert</i> -butyl- $\alpha$ -phenylnitron (PBN) using Thermal Desorption-Gas Chromatography-Mass Spectrometry (TD-GC/MS)..... | 127 |
| 4.1    | Introduction.....  | 128 |
| 4.2    | Chromatograms.....   | 129 |
| 4.2.1  | Fenton reaction with PBN and propanal (CH <sub>3</sub> CH <sub>2</sub> CHO).....   | 130 |
| 4.2.2  | Fenton reaction with PBN and d <sub>2</sub> -propanal (CH <sub>3</sub> CD <sub>2</sub> CHO).....   | 131 |
| 4.2.3  | Fenton reaction with d <sub>6</sub> -PBN and propanal.....   | 132 |
| 4.2.4  | Fenton reaction with d <sub>6</sub> -PBN and d <sub>2</sub> -propanal.....   | 133 |
| 4.2.5  | Fenton reaction with F-PBN and propanal.....   | 134 |
| 4.2.6  | Fenton reaction with Cl-PBN and propanal.....  | 135 |
| 4.2.7  | Comparison chromatograms (control reactions versus the Fenton reaction; R <sub>t</sub> 1-4 min).....   | 136 |
| 4.2.8  | Comparison chromatograms (control reactions versus the Fenton reaction; R <sub>t</sub> 4.19-14.19 min).....  | 137 |
| 4.3    | EI mass spectra of the di-ethyl adduct of PBN.....   | 138 |
| 4.3.1  | PBN(C <sub>2</sub> H <sub>5</sub> ) <sub>2</sub> adduct.....   | 138 |
| 4.3.2  | PBN(CD <sub>2</sub> CH <sub>3</sub> ) <sub>2</sub> adduct.....   | 140 |
| 4.3.3  | d <sub>6</sub> -PBN(CH <sub>3</sub> CH <sub>2</sub> ) <sub>2</sub> adduct.....   | 141 |

|         |   |     |
|---------|---|-----|
| 4.3.4   | d <sub>6</sub> -PBN(CD <sub>2</sub> CH <sub>3</sub> ) <sub>2</sub> adduct .....   | 142 |
| 4.3.5   | F-PBN(C <sub>2</sub> H <sub>5</sub> ) <sub>2</sub> adduct .....   | 143 |
| 4.3.6   | Cl-PBN(C <sub>2</sub> H <sub>5</sub> ) <sub>2</sub> adduct.....   | 144 |
| 4.4     | Electron ionisation mass spectra (EI-MS) of N-ethoxy-1-phenyl-1-propanamine....   | 146 |
| 4.4.1   | EI mass spectrum of N-ethoxy-1-phenyl-1-propanamine .....   | 146 |
| 4.4.2   | EI mass spectrum of N-ethoxy-1-phenyl-1-propanamine-d <sub>4</sub> .....  | 147 |
| 4.4.3   | EI mass spectrum of N-ethoxy-1-phenyl-1-propanamine-d <sub>6</sub> .....  | 148 |
| 4.4.4   | EI mass spectrum of N-ethoxy-1-phenyl-1-propanamine-d <sub>10</sub> .....   | 149 |
| 4.4.5   | EI mass spectrum of N-ethoxy-1-fluorophenyl-1-propanamine .....   | 150 |
| 4.5     | A hydrogen and ethyl adduct of MNP (H-MNP-C <sub>2</sub> H <sub>5</sub> ).....  | 152 |
| 4.5.1   | EI mass spectrum of the H-MNP-C <sub>2</sub> H <sub>5</sub> adduct.....   | 152 |
| 4.5.2   | EI mass spectrum of the H-MNP-CD <sub>2</sub> CH <sub>3</sub> adduct .....  | 153 |
| 4.6     | EI mass spectra of phenylpropene .....  | 155 |
| 4.6.1   | Phenylpropene.....  | 155 |
| 4.6.2   | d <sub>1</sub> -phenylpropene.....  | 156 |
| 4.7     | Identification of extra peaks found with other derivatives of PBN .....   | 158 |
| 4.7.1   | EI mass spectrum of C <sub>2</sub> H <sub>5</sub> -MNP- <i>tert</i> butyl.....  | 158 |
| 4.7.2   | Hydrogen and <i>tert</i> -ethyl adduct of MNP .....   | 159 |
| 4.7.2.1 | EI mass spectrum of H-MNP- <i>tert</i> ethyl adduct.....  | 159 |
| 4.7.2.2 | EI mass spectrum of H-MNP- <i>tert</i> -ethyl-d <sub>6</sub> adduct.....  | 160 |
| 4.8     | Identification of other peaks (not derived from the Fenton reaction).....   | 161 |
| 4.8.1   | Propanal .....  | 161 |
| 4.8.2.1 | EI mass spectrum of 2-methyl-2-pentenal.....  | 161 |
| 4.8.2.2 | EI mass spectrum of 2-methyl-2-pentenal (d <sub>2</sub> ).....  | 162 |
| 4.8.3   | EI mass spectrum of 2-methylcyclopentenone .....  | 163 |
| 4.9     | Discussion.....   | 164 |
| 4.9.1   | The Fenton reaction derived peaks.....  | 165 |
| 4.9.2   | Peaks not derived from the Fenton reaction.....   | 169 |
| 5       | Detection and analysis of spin-adducts from ethanal and 2,2,6,6-Tetramethylpiperidin-1-yl-oxyl (TEMPO) using Thermal desorption - Gas Chromatography-Mass Spectrometry (TD-GC/MS) (Part 1)..... | 171 |
| 5.1     | Introduction.....   | 172 |
| 5.2     | Chromatograms.....  | 172 |
| 5.2.1   | Fenton reaction with acetaldehyde and TEMPO.....  | 173 |

|   |  |     |
|---|--|-----|
| 5.2.2   | Fenton reaction with d <sub>3</sub> -acetaldehyde and TEMPO.....   | 174 |
| 5.2.3   | Fenton reaction with acetaldehyde and 4-methoxy-TEMPO .....  | 175 |
| 5.2.4   | Fenton reaction with acetaldehyde and 4-oxo-TEMPO .....  | 176 |
| 5.2.5   | Comparison chromatograms (control reactions versus with Fenton reaction).....                                  | 177 |
| 5.3   | Electron ionisation (EI) mass spectra of the methyl adduct of TEMPO and its derivatives.....                   | 178 |
| 5.3.1   | TEMPO-CH <sub>3</sub> adduct .....   | 178 |
| 5.3.2   | TEMPO-CD <sub>3</sub> adduct .....   | 180 |
| 5.3.3   | 4-methoxy-TEMPO-CH <sub>3</sub> adduct .....   | 181 |
| 5.3.4   | 4-oxo-TEMPO-CH <sub>3</sub> adduct.....  | 182 |
| 5.4   | Paraldehyde.....   | 184 |
| 5.5   | Electron ionisation mass spectra (EI-MS) of methyl adduct of 2,2,6,6-tetramethyl-3,6-dihydropyridine.....      | 185 |
| 5.5.1   | EI mass spectrum of 1-methoxy-2,2,6,6-tetramethyl-1,2,3,6-tetrahydropyridine .....                             | 185 |
| 5.5.2   | EI mass spectrum of 1-(methoxy-d <sub>3</sub> )-2,2,6,6-tetramethyl-1,2,3,6-tetrahydropyridine .....           | 187 |
| 5.6   | Electron ionisation mass spectra of the <i>tert</i> -butyl adduct of TEMPO and its derivatives.....            | 188 |
| 5.6.1   | TEMPO- <i>tert</i> butyl adduct.....   | 188 |
| 5.6.2   | TEMPO- <i>tert</i> butyl (d <sub>9</sub> ) adduct .....  | 189 |
| 5.7   | Electron ionisation mass spectra of methyl adduct of 2,2,4,6,6-pentamethylpiperidine .....                     | 190 |
| 5.7.1   | EI mass spectrum of 1-methoxy-2,2,4,6,6-pentamethylpiperidine .....  | 190 |
| 5.7.2   | EI mass spectrum of 1-(methoxy-d <sub>3</sub> )-2,2,4,6-tetramethyl-4-(methyl-d <sub>3</sub> )piperidine ..... | 191 |
| 5.8   | Identification of other peaks when for 4-methoxy-TEMPO is used as the trapping agent.....                      | 192 |
| 5.8.1   | EI mass spectrum of 1,4-dimethoxy-2,6-dimethyl-1,4-dihydropyridine .....                                       | 192 |
| 5.8.2   | EI mass spectrum of 1,4-dimethoxy-2,6-dimethyl-1,2-dihydropyridine .....                                       | 193 |
| 5.8.3   | EI mass spectrum of 1,4-dimethoxy-2,2-dimethyl-1,2-dihydropyridine (isomers) .....                             | 194 |
| 5.8.4   | EI mass spectrum of 1,4-dimethoxy-2,2,6-trimethyl-1,2-dihydropyridine.....                                     | 195 |
| Detection and analysis of spin-adducts from ethanal and 2,2,6,6-Tetramethylpiperidin-1-yl-oxyl (TEMPO) using Solid phase microextraction-Gas Chromatography-Mass Spectrometry (SPME-GC/MS) (Part 2) ..... |  | 196 |



|        |  |     |
|--------|--|-----|
| 5.9    | Chromatograms.....   | 197 |
| 5.9.1  | Fenton reaction with acetaldehyde and TEMPO.....   | 197 |
| 5.9.2  | Fenton reaction with d <sub>3</sub> -acetaldehyde and TEMPO.....   | 198 |
| 5.9.3  | Fenton reaction with acetaldehyde and 4-methoxy-TEMPO .....  | 199 |
| 5.9.4  | Fenton reaction with acetaldehyde and 4-oxo-TEMPO .....  | 200 |
| 5.10   | Detection and analysis of methyl radical adducts.....  | 201 |
| 5.11   | Methyl adduct of 2,2,4,6,6-pentamethylpiperidine .....   | 201 |
| 5.12   | Detection and analysis of <i>tert</i> -butyl adduct of TEMPO and its derivatives .....                                   | 201 |
| 5.13   | Electron ionisation (EI) mass spectra of the acetyl adduct of TEMPO and its derivatives.....                             | 203 |
| 5.13.1 | TEMPO-COCH <sub>3</sub> adduct .....   | 203 |
| 5.13.2 | TEMPO-COCD <sub>3</sub> adduct .....   | 204 |
| 5.14   | Electron ionisation (EI) mass spectra of a methyl adduct of 2,2,6-trimethyl-2,3,4,5-tetrahydropyridin-1-ium .....        | 206 |
| 5.14.1 | EI mass spectrum of 1-methoxy-2,2,6-trimethyl-2,3,4,5-tetrahydropyridin-1-ium  | 206 |
| 5.14.2 | EI mass spectrum of 1-(methoxy-d <sub>3</sub> )-2,2,6-trimethyl-2,3,4,5-tetrahydropyridin-1-ium .....                    | 207 |
| 5.15   | EI mass spectrum of 2,6-dimethyl-1,5-heptadiene .....  | 208 |
| 5.16   | Electron ionisation (EI) mass spectrum of methyl and acetyl adduct of 2,2,6-trimethylpiperidine.....                     | 209 |
| 5.16.1 | EI mass spectrum of 1-(1-methoxy-2,2,6-trimethylpiperidin-4-yl) ethan-1-one .....  | 209 |
| 5.16.2 | EI mass spectrum of 1-(1-(methoxy-d <sub>3</sub> )-2,2,6-trimethylpiperidin-4-yl) ethan-1-one-2,2,2-d <sub>3</sub> ..... | 210 |
| 5.17   | EI mass spectrum of unreacted TEMPO .....  | 211 |
| 5.18   | Discussion.....  | 212 |
| 6      | Conclusions and Further work .....   | 216 |
| 6.1    | Summary and conclusions.....   | 217 |
| 6.2    | Areas of future study.....   | 221 |
|        | References .....   | 223 |
|        | Appendix.....  | 269 |

## List of Figures

|      |  |    |
|------|--|----|
| 1.1  | Different sources of reactive oxygen species .....   | 4  |
| 1.2  | Reduction of molecular oxygen via four and one electron scheme.....  | 6  |
| 1.3  | Mutual association between oxidants and antioxidants.....  | 9  |
| 1.4  | Production of different ROS in the body.....   | 11 |
| 1.5  | Physiological roles of free radicals.....  | 13 |
| 1.6  | Antioxidant/pro-oxidant balance in the cell .....  | 16 |
| 1.7  | Oxidative stress-induced diseases in humans .....  | 17 |
| 1.8  | Commonly used nitroso spin traps .....   | 28 |
| 1.9  | Commonly used nitron Spin traps.....   | 28 |
| 1.10 | General structure of nitroxide.....  | 30 |
| 1.11 | Structure of common nitroxides .....   | 30 |
| 1.12 | Steps of adsorption and desorption of molecules on sorbent material .....  | 36 |
| 1.13 | A diagrammatic view of primary and secondary desorption.....   | 37 |
| 1.14 | Diagram of analysis with solid phase microextraction gas chromatography-mass spectrometry (SPME-GC-MS) .....                       | 42 |
| 1.15 | Schematic of a typical GC system.....  | 49 |
| 1.16 | Formation pathways of different biomarkers of oxidative stress .....   | 54 |
| 2.1  | A schematic of mass spectrometer .....   | 61 |
| 2.2  | Sampling of headspace by using Easy-VOC .....  | 63 |
| 2.3  | The Total ion chromatogram (TIC) for the standard Fenton reaction in the presence of acetaldehyde .....                            | 65 |
| 2.4  | The GC-MS TIC when PBN (Spin trap) was stirred in a buffer and extracted using VOC pump for thermal desorption analysis .....      | 66 |
| 2.5  | The GC-MS TIC when PBN with acetaldehyde was stirred in a buffer and extracted using VOC pump for thermal desorption analysis..... | 67 |
| 2.6  | Comparison of gas chromatography of control samples with the Fenton reaction .....   | 68 |
| 2.7  | The GC-MS TIC of the Fenton reaction carried out in the absence of a secondary source of radicals .....                            | 69 |
| 2.8  | The Gas chromatogram when the Fenton reaction was carried out without PBN.....   | 70 |
| 2.9  | The GC-MS TIC for the Fenton reaction containing the spin trap PBN but carried out in the absence of iron and ascorbate.....       | 71 |

|  |    |
|--|----|
| 2.10 The GC-MS TIC for the Fenton reaction containing the spin trap PBN but carried out in the absence of H <sub>2</sub> O <sub>2</sub> .....                                    | 72 |
| 3.1 The total ion chromatogram (TIC) obtained from the head space thermal desorption GC-MS analysis of the Fenton reaction containing acetaldehyde and PBN.....                  | 77 |
| 3.2 The total ion chromatogram (TIC) obtained from the head space thermal desorption GC-MS analysis of the Fenton reaction containing d <sub>3</sub> -acetaldehyde and PBN.....  | 78 |
| 3.3 The total ion chromatogram (TIC) obtained from the head space thermal desorption GC-MS analysis of the Fenton reaction containing acetaldehyde and d <sub>6</sub> -PBN.....  | 79 |
| 3.4 The total ion chromatogram (TIC) obtained from the head space thermal desorption GC-MS analysis of the Fenton reaction containing acetaldehyde and F-PBN.....                | 80 |
| 3.5 The total ion chromatogram (TIC) obtained from the head space thermal desorption GC-MS analysis of the Fenton reaction containing acetaldehyde and Cl-PBN.....               | 81 |
| 3.6 Electron ionisation (EI) mass spectrum of the peak at 10.26 minutes (figure 3.1) corresponding to PBN(CH <sub>3</sub> ) <sub>2</sub> .....                                   | 82 |
| 3.7 Electron ionisation (EI) mass spectrum of the peak at 10.16 minutes (figure 3.2) corresponding to PBN(CD <sub>3</sub> ) <sub>2</sub> .....                                   | 83 |
| 3.8 Electron ionisation (EI) mass spectrum of the peak at 10.19 minutes (figure 3.3) corresponding to d <sub>6</sub> -PBN(CH <sub>3</sub> ) <sub>2</sub> .....                   | 84 |
| 3.9 Electron ionisation (EI) mass spectrum of the peak at 10.09 minutes (figure A1; appendix) corresponding to d <sub>6</sub> -PBN(CD <sub>3</sub> ) <sub>2</sub> .....          | 85 |
| 3.10 Electron ionisation (EI) mass spectrum of the peak at 10.49 minutes (figure 3.4) corresponding to F-PBN(CH <sub>3</sub> ) <sub>2</sub> .....                                | 86 |
| 3.11 Electron ionisation (EI) mass spectrum of the peak at 15.32 minutes (figure 3.5) corresponding to Cl-PBN(CH <sub>3</sub> ) <sub>2</sub> .....                               | 87 |
| 3.12 Electron ionisation (EI) mass spectrum of the peak at 8.52 minutes (figure 3.1) corresponding to a hydrogen and methyl adduct of PBN.....                                   | 89 |
| 3.13 Electron ionisation (EI) mass spectrum of the peak at 8.48 minutes (figure 3.2) corresponding to a hydrogen and CD <sub>3</sub> adduct of PBN.....                          | 90 |
| 3.14 Electron ionisation (EI) mass spectrum of the peak at 8.46 minutes (figure 3.3) corresponding to a hydrogen and methyl adduct of d <sub>6</sub> -PBN.....                   | 91 |
| 3.15 Electron ionisation (EI) mass spectrum of the peak at 8.40 minutes (figure A1; appendix) corresponding to a hydrogen and CD <sub>3</sub> adduct of d <sub>6</sub> -PBN..... | 92 |
| 3.16 Electron ionisation (EI) mass spectrum of the peak at 8.70 minutes (figure 3.4) corresponding to a hydrogen and methyl adduct of F-PBN.....                                 | 93 |

|      |   |     |
|------|---|-----|
| 3.17 | Electron ionisation (EI) mass spectrum of the peak at 1.63 minutes (figure 3.1) corresponding to <i>tert</i> -butylhydroaminoxyl-CH <sub>3</sub> adduct.....                            | 95  |
| 3.18 | Electron ionisation (EI) mass spectrum of the peak at 1.62 minutes (figure 3.2) corresponding to <i>tert</i> -butylhydroaminoxyl-CD <sub>3</sub> adduct.....                            | 96  |
| 3.19 | Electron ionisation (EI) mass spectrum of the peak at 2.04 minutes (figure 3.1) corresponding to di- <i>tert</i> butyl hydroxylamine .....  | 98  |
| 3.20 | Electron ionisation (EI) mass spectrum of the peak at 2.02 minutes (figure 3.2) corresponding to di- <i>tert</i> butyl (d <sub>9</sub> ) hydroxylamine.....                             | 99  |
| 3.21 | Electron ionisation (EI) mass spectrum of the peak at 2.22 minutes (figure 3.1) corresponding to phenyl methanimine.....  | 101 |
| 3.22 | Electron ionisation (EI) mass spectrum of the peak at 2.61 minutes (figure 3.1) corresponding to benzaldehyde .....   | 103 |
| 3.23 | Electron ionisation (EI) mass spectrum of the peak at 5.22 minutes (figure 3.1) corresponding to N-methoxy-1-phenylethanamine .....   | 105 |
| 3.24 | Electron ionisation (EI) mass spectrum of the peak at 5.13 minutes (figure 3.2) corresponding to N-methoxy-1-phenylethanamine (d <sub>6</sub> ).....                                    | 106 |
| 3.25 | Electron ionisation (EI) mass spectrum of the peak at 6.32 minutes (figure 3.1) corresponding to methoxy-(1-phenylethylidene)amine.....   | 109 |
| 3.26 | Electron ionisation (EI) mass spectrum of the peaks at 15.96 minutes (figure 3.1) corresponding to isomers of 2,3-diphenylbutane.....   | 112 |
| 3.27 | Electron ionisation (EI) mass spectrum of the peak at 1.80 minutes (figure 3.1) corresponding to paraldehyde.....   | 114 |
| 3.28 | Electron ionisation (EI) mass spectrum of the peak at 1.79 minutes (figure 3.2) corresponding to d <sub>9</sub> -paraldehyde .....  | 115 |
| 4.1  | The total ion chromatogram (TIC) obtained from the head space thermal desorption GC-MS analysis of the Fenton reaction containing propanal and PBN..                                    | 130 |
| 4.2  | The total ion chromatogram (TIC) obtained from the head space thermal desorption GC-MS analysis of the Fenton reaction containing d <sub>2</sub> -propanal and PBN.....                 | 131 |
| 4.3  | The total ion chromatogram (TIC) obtained from the head space thermal desorption GC-MS analysis of the Fenton reaction containing propanal and d <sub>6</sub> -PBN.....                 | 132 |
| 4.4  | The total ion chromatogram (TIC) obtained from the head space thermal desorption GC-MS analysis of the Fenton reaction containing d <sub>2</sub> -propanal and d <sub>6</sub> -PBN..... | 133 |
| 4.5  | The total ion chromatogram (TIC) obtained from the head space thermal desorption GC-MS analysis of the Fenton reaction containing propanal and F-PBN.....                               | 134 |

|      |  |     |
|------|--|-----|
| 4.6  | The total ion chromatogram (TIC) obtained from the head space thermal desorption GC-MS analysis of the Fenton reaction containing propanal and Cl-PBN.....     | 135 |
| 4.7  | Comparison chromatograms (control reactions versus the Fenton reaction, $R_t$ 1-4 minutes) .....   | 136 |
| 4.8  | Comparison chromatograms (control reactions versus the Fenton reaction, $R_t$ 4.19-14.19 minutes) .....  | 137 |
| 4.9  | Electron ionisation (EI) mass spectrum of the peak at 12.97 minutes (figure 4.1) corresponding to $\text{PBN}(\text{C}_2\text{H}_5)_2$ .....                   | 138 |
| 4.10 | Electron ionisation (EI) mass spectrum of the peak at 12.90 minutes (figure 4.2) corresponding to $\text{PBN}(\text{CD}_2\text{CH}_3)_2$ .....                 | 140 |
| 4.11 | Electron ionisation (EI) mass spectrum of the peak at 12.89 minutes (figure 4.3) corresponding to $\text{d}_6\text{-PBN}(\text{C}_2\text{H}_5)_2$ .....        | 141 |
| 4.12 | Electron ionisation (EI) mass spectrum of the peak at 12.82 minutes (figure 4.4) corresponding to $\text{d}_6\text{-PBN}(\text{CD}_2\text{CH}_3)_2$ .....      | 142 |
| 4.13 | Electron ionisation (EI) mass spectrum of the peak at 13.20 minutes (figure 4.5) corresponding to $\text{F-PBN}(\text{C}_2\text{H}_5)_2$ .....                 | 143 |
| 4.14 | Electron ionisation (EI) mass spectrum of the peak at 16.52 minutes (figure 4.6) corresponding to $\text{Cl-PBN}(\text{C}_2\text{H}_5)_2$ .....                | 144 |
| 4.15 | Electron ionisation (EI) mass spectrum of the peak at 8.74 minutes (figure 4.1) corresponding to N-ethoxy-1-phenyl-1-propanamine .....                         | 146 |
| 4.16 | Electron ionisation (EI) mass spectrum of the peak at 8.66 minutes (figure 4.2) corresponding to N-ethoxy-1-phenyl-1-propanamine- $\text{d}_4$ .....           | 147 |
| 4.17 | Electron ionisation (EI) mass spectrum of the peak at 8.66 minutes (figure 4.3) corresponding to N-ethoxy-1-phenyl-1-propanamine- $\text{d}_6$ .....           | 148 |
| 4.18 | Electron ionisation (EI) mass spectrum of the peak at 8.60 minutes (figure 4.4) corresponding to N-ethoxy-1-phenyl-1-propanamine- $\text{d}_{10}$ .....        | 149 |
| 4.19 | Electron ionisation (EI) mass spectrum of the peak at 8.90 minutes (figure 4.5) corresponding to N-ethoxy-1-fluorophenyl-1-propanamine .....                   | 150 |
| 4.20 | Electron ionisation (EI) mass spectrum of the peak at 1.69 minutes (figure 4.1) corresponding to a hydrogen & ethyl adduct of the MNP .....                    | 152 |
| 4.21 | Electron ionisation (EI) mass spectrum of the peak at 1.66 minutes (figure 4.2) corresponding to a hydrogen & $\text{CH}_3\text{CD}_2$ adduct of the MNP ..... | 153 |
| 4.22 | Electron ionisation (EI) mass spectrum of the peak at 3.16 minutes (figure 4.1) corresponding to phenylpropene.....  | 155 |
| 4.23 | Electron ionisation (EI) mass spectrum of the peak at 3.15 minutes (figure 4.2) corresponding to $\text{d}_1$ -phenylpropene .....                             | 156 |

|  |     |
|--|-----|
| 4.24 Electron ionisation (EI) mass spectrum of the peak at 2.77 minutes (figure 4.5 & 4.6) corresponding to C <sub>2</sub> H <sub>5</sub> -MNP- <sup>t</sup> Bu .....                | 158 |
| 4.25 Electron ionisation (EI) mass spectrum of the peak at 3.59 minutes (figure 4.5) corresponding to a H-MNP-CET <sub>3</sub> adduct .....  | 159 |
| 4.26 Electron ionisation (EI) mass spectrum of the peak at 3.51 minutes (Figure 4.2) corresponding to a hydrogen and d <sub>6</sub> -CET <sub>3</sub> adduct of MNP.....             | 160 |
| 4.27 Electron ionisation (EI) mass spectrum of the peak at 1.69 minutes (figure 4.1) corresponding to 2-methyl-2-pentenal.....   | 161 |
| 4.28 Electron ionisation (EI) mass spectrum of the peak at 1.95 minutes (figure 4.2) corresponding to 2-methyl-2-pentenal (d <sub>2</sub> ).....                                     | 162 |
| 4.29 Electron ionisation (EI) mass spectrum of the peak at 2.23 minutes (figure 4.1) corresponding to 2-methylcyclopentenone.....  | 163 |
| 5.1 The total ion chromatogram (TIC) obtained from the head space thermal desorption GC-MS analysis of the Fenton reaction containing acetaldehyde and TEMPO.....                    | 173 |
| 5.2 The total ion chromatogram (TIC) obtained from the head space thermal desorption GC-MS analysis of the Fenton reaction containing d <sub>3</sub> -acetaldehyde and TEMPO .....   | 174 |
| 5.3 The total ion chromatogram (TIC) obtained from the head space thermal desorption GC-MS analysis of the Fenton reaction containing acetaldehyde and Methoxy-TEMPO .....           | 175 |
| 5.4 The total ion chromatogram (TIC) obtained from the head space thermal desorption GC-MS analysis of the Fenton reaction containing acetaldehyde and Oxo-TEMPO.....                | 176 |
| 5.5 Comparison chromatograms (control reactions versus the Fenton reaction) .....  | 177 |
| 5.6 Electron ionisation (EI) mass spectrum of the peak at 7.27 minutes (figure 5.1) corresponding to the methyl adduct of TEMPO.....   | 178 |
| 5.7 Electron ionisation (EI) mass spectrum of the peak at 7.23 minutes (figure 5.2) corresponding to the CD <sub>3</sub> adduct of TEMPO .....                                       | 180 |
| 5.8 Electron ionisation (EI) mass spectrum of the peak at 11.71 minutes (figure 5.3) corresponding to the methyl adduct of 4-methoxy-TEMPO .....                                     | 181 |
| 5.9 Electron ionisation (EI) mass spectrum of the peak at 11.59 minutes (figure 5.4) corresponding to the methyl adduct of 4-oxo-TEMPO .....   | 182 |
| 5.10 Electron ionisation (EI) mass spectrum of the peak at 6.55 minutes (figure 5.1) corresponding to 1-methoxy-2,2,6,6-tetramethyl-1,2,3,6-tetrahydropyridine.....                  | 185 |
| 5.11 Electron ionisation (EI) mass spectrum of the peak at 6.52 minutes (figure 5.2) corresponding to 1-(methoxy-d <sub>3</sub> )-2,2,6,6-tetramethyl-1,2,3,6-tetrahydropyridine ... | 187 |

|  |     |
|--|-----|
| 5.12 Electron ionisation (EI) mass spectrum of the peak at 13.85 minutes (figure 5.1) corresponding to <i>tert</i> -butyl adduct of TEMPO.....   | 188 |
| 5.13 Electron ionisation (EI) mass spectrum of the peak at 13.70 minutes (figure 5.2) corresponding to <i>tert</i> -butyl(d <sub>9</sub> ) adduct of TEMPO.....                                    | 189 |
| 5.14 Electron ionisation (EI) mass spectrum of the peak at 10.07 minutes (figure 5.1) corresponding to 1-methoxy-2,2,4,6,6-pentamethylpiperidine .....   | 190 |
| 5.15 Electron ionisation (EI) mass spectrum of the peak at 9.97 minutes (Figure 5.2) corresponding to 1-(methoxy-d <sub>3</sub> )-2,2,6,6-tetramethyl-4-(methyl-d <sub>3</sub> )piperidine.....    | 191 |
| 5.16 Electron ionisation (EI) mass spectrum of the peak at 5.02 minutes (figure 5.3) corresponding to 1,4-dimethoxy-2,6-dimethyl-1,4-dihydropyridine.....  | 192 |
| 5.17 Electron ionisation (EI) mass spectrum of the peak at 5.74 minutes (figure 5.3) corresponding to 1,4-dimethoxy-2,6-dimethyl-1,2-dihydropyridine.....  | 193 |
| 5.18 Electron ionisation (EI) mass spectrum of the peak at 13.11 minutes (figure 5.3) corresponding to 1,4-dimethoxy-2,2-dimethyl-1,2-dihydropyridine.....   | 194 |
| 5.19 Electron ionisation (EI) mass spectrum of the peak at 15.93 minutes (figure 5.3) corresponding to 1,4-dimethoxy-2,2,6-trimethyl-1,2-dihydropyridine .....                                     | 195 |
| 5.20 The total ion chromatogram (TIC) obtained from the headspace Solid phase microextraction (SPME)-GC-MS analysis of the Fenton reaction containing acetaldehyde and TEMPO .....                 | 197 |
| 5.21 The total ion chromatogram (TIC) obtained from the headspace Solid phase microextraction (SPME)-GC-MS analysis of the Fenton reaction containing d <sub>3</sub> -acetaldehyde and TEMPO ..... | 198 |
| 5.22 The total ion chromatogram (TIC) obtained from the headspace Solid phase microextraction (SPME)-GC-MS analysis of the Fenton reaction containing acetaldehyde and methoxy-TEMPO.....          | 199 |
| 5.23 The total ion chromatogram (TIC) obtained from the headspace Solid phase microextraction (SPME)-GC-MS analysis of the Fenton reaction containing acetaldehyde and oxo-TEMPO.....              | 200 |
| 5.24 Electron ionisation (EI) mass spectrum of the peak at 9.7 minutes (figure 5.20) corresponding to TEMPO-COCH <sub>3</sub> .....  | 203 |
| 5.25 Electron ionisation (EI) mass spectrum of the peak at 9.7 minutes (figure 5.21) corresponding to TEMPO-COCD <sub>3</sub> .....  | 204 |
| 5.26 Electron ionisation (EI) mass spectrum of the peak at 8.6 minutes (figure 5.20) corresponding to 2,2,6-trimethyl-2,3,4,5-tetrahydropyridin-1-ium.....   | 206 |
| 5.27 Electron ionisation (EI) mass spectrum of the peak at 8.5 minutes (Figure 5.21) corresponding to 1-(methoxy-d <sub>3</sub> )-2,2,6-trimethyl-2,3,4,5-tetrahydropyridin-1-ium.                 | 207 |
| 5.28 Electron ionisation (EI) mass spectrum of the peak at 8.9 minutes (figure 5.20 & 5.21) corresponding to 2,6-Dimethyl-1,5-heptadiene.....  | 208 |

|   |     |
|---|-----|
| 5.29 Electron ionisation (EI) mass spectrum of the peak at 9.5 minutes (figure 5.20) corresponding to methyl and acetyl adduct of 2,2,6-trimethylpiperidin .....                      | 209 |
| 5.30 Electron ionisation (EI) mass spectrum of the peak at 9.4 minutes (Figure 5.21) corresponding to CD <sub>3</sub> and COCD <sub>3</sub> adduct of 2,2,6-trimethylpiperidine ..... | 210 |
| 5.31 Electron ionisation (EI) mass spectrum of the peak at 8.7 minutes (Figure 5.20) corresponding to untreated TEMPO .....   | 211 |

## List of Appendix Figures

|   |     |
|---|-----|
| A1 The total ion chromatogram (TIC) obtained from the headspace Thermal desorption TD-GC-MS analysis of the Fenton reaction containing d <sub>3</sub> -acetaldehyde {CD <sub>3</sub> C(H)O} and d <sub>6</sub> -PBN ..... | 270 |
| A2 Aldol condensation of acetaldehyde into paraldehyde .....  | 271 |
| A3 A standard mass spectrum of 2-methylcyclopentenone .....   | 272 |
| A4 Comparison of chromatograms: Chromatograms generated for control experiments containing 4-methoxy-TEMPO (spin trap) and acetaldehyde (secondary source of radicals) using TD-GC-MS .....                               | 273 |



## List of tables

|     |  |     |
|-----|--|-----|
| 1.1 | Sources of free radicals .....   | 3   |
| 2.1 | Volumes of different aldehydes used as a source of secondary free radicals generated in the Fenton reaction.....   | 59  |
| 3.1 | Summary of GC-MS data for the dimethyl adduct of PBN and its derivatives .....   | 88  |
| 3.2 | Summary of GC-MS data for the hydrogen and methyl adduct of PBN and its derivatives.....   | 94  |
| 3.3 | Summary of GC-MS data for <sup>t</sup> Bu-NOMe when PBN and its derivatives were used as trapping agents .....   | 97  |
| 3.4 | Summary of GC-MS data for di-tert butylhydroxylamine when the reaction was carried by using PBN and its derivatives as trapping agents and acetaldehyde/deuterated acetaldehyde as a secondary source of radicals .....                        | 100 |
| 3.5 | Summary of GC-MS data for X-phenyl methanimine when the reaction was carried using PBN and its derivatives as trapping agents and acetaldehyde/deuterated acetaldehyde as a secondary source of radicals .....                                 | 102 |
| 3.6 | Summary of GC-MS data for X-benzaldehyde when the reaction was carried using PBN and its derivatives as trapping agents and acetaldehyde/deuterated acetaldehyde as a secondary source of radicals .....                                       | 104 |
| 3.7 | Summary of GC-MS data for X-(N-methoxy-1-phenylethanamine) when the reaction was carried using PBN and its derivatives as trapping agents and acetaldehyde/deuterated acetaldehyde as a secondary source of radicals .....                     | 108 |
| 3.8 | Summary of GC-MS data for methoxy-(1-phenylethylidene)amine when the reaction was carried using PBN and its derivatives as trapping agents and acetaldehyde/deuterated acetaldehyde as a secondary source of radicals .....                    | 111 |
| 3.9 | Summary of GC-MS data for X-(2,3-diphenylbutane) when the reaction was carried using PBN and its derivatives as trapping agents and acetaldehyde/deuterated acetaldehyde as a secondary source of radicals .....                               | 113 |
| 4.1 | Summary of GC-MS data for the diethyl adduct of PBN and its derivatives.....   | 145 |
| 4.2 | Summary of GC-MS data for X-(N-ethoxy-1-phenylethanamine), when the reaction was carried out by using PBN and its derivatives as trapping agents and propionaldehyde/deuterated propionaldehyde as a secondary source of free radicals.....    | 151 |
| 4.3 | Summary of GC-MS data for hydrogen & ethyl adduct of the MNP, when the reaction was carried out by using PBN and its derivatives as trapping agents and propionaldehyde/deuterated propionaldehyde as a secondary source of free radicals..... | 154 |

|     |   |     |
|-----|---|-----|
| 4.4 | Summary of GC-MS data for X-phenylpropene, when the reaction was carried out by using PBN and its derivatives as trapping agents and propionaldehyde/deuterated propionaldehyde as a secondary source of free radicals..... | 157 |
| 5.1 | Summary of GC-MS data for methyl adduct of TEMPO and its derivatives.....   | 183 |
| 5.2 | Summary of GC-MS data for <i>tert</i> -butyl adduct of TEMPO and its derivatives.....   | 202 |
| 5.3 | Summary of GC-MS data for acetyl adduct of TEMPO and its derivatives .....  | 205 |

## List of schemes

|       |   |     |
|-------|---|-----|
| 1.1   | Formation of radical cation by the loss of an electron.....                         | 2   |
| 1.2   | Formation of radical anion by the gain of an electron.....                          | 2   |
| 1.3   | Formation of free radicals by the homolytic fission of an organic molecule .....    | 2   |
| 1.4   | The Fenton reaction .....   | 4   |
| 1.5   | Haber-Weiss reaction.....   | 5   |
| 1.6   | Production of an alkyl radical.....   | 13  |
| 1.7   | Production of peroxy radical .....  | 14  |
| 1.8.1 | Formation of Lipid hydroperoxide.....   | 14  |
| 1.8.2 | Formation of Fatty acid peroxy free radical.....                                    | 14  |
| 1.8.3 | Formation of alkyl radical during lipid peroxidation.....                           | 14  |
| 1.9   | Trapping of free radical with nitron.....   | 29  |
| 1.10  | Trapping of free radical with nitroso compound .....                                | 29  |
| 1.11  | Reduction of a nitroxides radical .....   | 31  |
| 1.12  | Oxidation of a nitroxides radical .....   | 31  |
| 1.13  | Trapping of radical by nitroxide and formation of stable radical adduct .....       | 31  |
| 1.14  | The reaction of a hydroxyl radical with DMSO to produce a methyl radical .....      | 33  |
| 3.1   | Metabolism of ethanol into acetaldehyde .....                                       | 75  |
| 3.2   | The Fenton reaction .....   | 116 |
| 3.3   | Generation of methyl radicals from acetaldehyde during the Fenton reaction.....     | 116 |
| 3.4   | Trapping of methyl radicals by PBN .....  | 117 |
| 3.5   | Fragmentation pattern of the PBN-di-methyl adduct .....                             | 119 |
| 3.6   | Fragmentation pattern of hydrogen and methyl adduct of PBN.....                     | 120 |
| 3.7   | Pathway of methyl adduct of <i>tert</i> -butylhydroainoxyl formation from MNP ..... | 122 |
| 3.8   | Pathway of di- <i>tert</i> -butyl hydroxylamine formation from MNP .....            | 123 |
| 3.9   | Fragmentation pattern of di- <i>tert</i> -butyl hydroxylamine.....                  | 123 |
| 3.10  | Fragmentation pathway of phenyl methanimine .....                                   | 124 |
| 4.1   | The fragmentation scheme for PBN-diethyl adduct .....                               | 139 |
| 4.2   | Formation of ethyl radicals from propanal .....                                     | 164 |
| 4.3   | Formation of PBN-diethyl adduct .....   | 166 |
| 4.4   | Suggested mechanism of phenyl propene formation from the mono-ethyl adduct ...      | 168 |
| 5.1   | Possible fragmentation pathways for TEMPO-methyl adduct .....                       | 179 |

|   |     |
|---|-----|
| 5.2 Possible mechanism of 1-methoxy-2,2,6,6-tetramethyl-1,2,3,6-tetrahydropyridine formation..... | 186 |
|---|-----|

## Acknowledgements

First of all, I would like to thank my supervisor Dr Ian Podmore for all his guidance, attention, patience and encouragement throughout my stay at Salford. You have been a tremendous mentor for me.

I would like to mention two of my brilliant Lab colleagues Dr Sanat Mishra & Dr Kamila Schmidt who guided me about use, maintenance and troubleshooting of the instruments. I also pay my gratitude to academic staff and fellow PhD students for their support.

A special thanks to my family who believe in me, I would achieve my goal. Word can't express how grateful I am for the sacrifices they made so that I can fulfil my dream. I might not be at this point without the prayers of my parents.

Above all, Thanks to Almighty for the blessings and guidance.

## Declaration

This thesis is the result of research carried out under the supervision of Dr Ian Podmore at School of Environment and Life Sciences at the University of Salford.

Except where acknowledged in the customary manner, the material presented in this thesis is, to the best of my knowledge, original and has not been submitted in whole or part for a degree in any university.

---

Kamran Manzoor

## Abbreviations

|        |  |
|--------|--|
| CKD    | chronic kidney disease                       |
| COX    | cyclooxygenase                               |
| CVD    | cardiovascular disease                       |
| Da     | dalton                                       |
| DLLME  | dispersive liquid-liquid microextraction     |
| DMPO   | 5,5-dimethyl-1-pyrroline N-oxide             |
| DMSO   | dimethyl sulfoxide                           |
| DNA    | deoxyribonucleic acid                        |
| ED     | electrochemical detection                    |
| EDTA   | ethylene di-amine-tetra-acetic acid          |
| EPA    | environment protection agency                |
| EPR    | electron paramagnetic resonance              |
| ESI-MS | electron spray ionisation- mass spectrometry |
| ESR    | electron spin resonance                      |
| Et     | Ethyl  |
| GC-MS  | gas chromatography- mass spectrometry        |
| HPLC   | high performance liquid chromatography       |
| HS     | headspace                                    |
| LC-MS  | liquid chromatography- mass spectrometry     |
| LDL    | low density lipoproteins                     |
| LDME   | liquid dispersive microextraction            |
| LMW    | low molecular weight                         |
| LOX    | Lipoxygenase                                 |
| LPO    | Lipid peroxidation                           |
| MALDI  | matrix assisted laser desorption ionisation  |

|       |  |
|-------|--|
| MDA   | malondialdehyde                                    |
| MNP   | 2-methyl-2-nitrosopropane                          |
| NADPH | nicotinamide adenine dinucleotide phosphate        |
| NIST  | national institute of standards and technology     |
| NMR   | nuclear magnetic resonance                         |
| NOS   | nitric oxide synthase                              |
| PBN   | N-tert-Butyl- $\alpha$ -phenylnitron               |
| PDMS  | polydimethylsiloxane                               |
| PEG   | polyethylene glycol                                |
| POBN  | N-tert-Butyl- $\alpha$ -(4-pyridyl)nitron N'-oxide |
| PUFA  | poly unsaturated fatty acids                       |
| RA    | rheumatoid arthritis                               |
| RNA   | ribonucleic acid                                   |
| RNS   | reactive nitrogen species                          |
| ROS   | reactive oxygen species                            |
| RT    | room temperature                                   |
| SDME  | single drop microextraction                        |
| SIM   | selected ion monitoring                            |
| SOD   | superoxide dismutase                               |
| SPME  | solid phase microextraction                        |
| ST    | spin trapping                                      |
| TD    | thermal desorption                                 |
| TEMPO | 2,2,6,6-tetramethyl-1-piperinyloxy                 |
| TIC   | total ion chromatogram                             |
| TMS   | trimethylsilylation                                |
| UV    | ultraviolet  |
| VOCs  | volatile organic compounds                         |



## Abstract

Certain oxygen free radicals are produced constantly in cells by metabolism and exogenous agents. Some, such as the hydroxyl radical, may react with various biomolecules like DNA, lipids or proteins, and thus be involved in the pathogenesis of various diseases. It is often difficult to detect oxygen free radicals due to their relatively short half-life. This problem may be overcome, however, using the spin trapping technique. In this technique, the spin-trap compound is used to trap free radicals, making them stable enough to be analysed using techniques like Electron Paramagnetic Resonance (EPR) spectroscopy or Mass Spectrometry (MS).

In the current study, Fenton chemistry has been used to generate hydroxyl radicals. Since the hydroxyl radical adduct of the spin-trap *N-tert-butyl- $\alpha$ -phenylnitrone* (PBN) is short-lived at room temperature a secondary trapping technique is employed. The resulting spin-trapped species have been sampled using solvent-free extraction approaches i.e. Headspace Solid Phase Microextraction (HS-SPME) or Thermal desorption (TD), and the extracted products then detected and identified by using gas chromatography-mass spectrometry (GC-MS). GC-MS provides an alternative to other traditional techniques like EPR spectroscopy, as it provides more detailed information about structure of the radical adduct.

Aldehydes are some of the most important products of oxidative stress, mostly produced through lipid peroxidation, and potentially may be used as biomarkers for different diseases. Their reactivity, production in low quantities and need of derivatisation are some of the challenges faced by analytical chemists to detect them. In the current research, aldehydes are used as secondary source of radicals in the Fenton reaction to produce aldehyde related free radicals. The developed method is not only a solvent free approach but also there is no need of derivatisation. It has the potential to be used as a biomarker assay of oxidative stress.



# Chapter 1

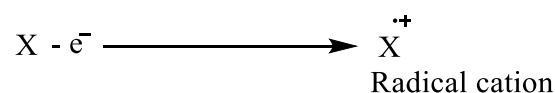
## Introduction

## 1. Free radicals

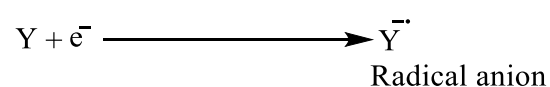
In most of the stable atoms and molecules, electrons are in pairs. In contrast, free radicals are atoms or molecules with one or more unpaired electrons; the unpaired electron is usually represented by a dot on atom/molecule (Webb, 2013; Halliwell, 2001b). Some examples of free radicals include: hydroxyl (OH<sup>•</sup>), the hydrogen atom (H<sup>•</sup>) and superoxide (O<sub>2</sub><sup>•-</sup>) free radicals. Due to paramagnetic behaviour, free radicals are attracted towards a magnetic field (McMillan, 1961). They also tend to be highly reactive species. Free radicals generally try to capture an electron from another molecule/atom/ion to gain stability and this feature makes them potentially destructive to cells (Sarma, Mallick & Ghosh, 2010).

### 1.1 Formation of Free radicals:

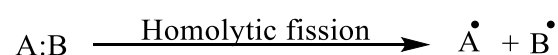
Radicals may be formed by losing or gaining a single electron from a non-radical species. A cationic radical is formed when the electron is lost (Scheme 1.1) whilst anionic radicals are the result of gaining an electron (Scheme 1.2). Homolytic fission of covalent bonds also results in the formation of free radicals (Scheme 1.3). Ultraviolet light, heat or ionizing radiation provides sufficient energy to break covalent bonds (Halliwell and Gutteridge, 2015).



Scheme 1.1: Formation of a radical cation by the loss of an electron



Scheme 1.2: Formation of the radical anion by the gain of an electron



Scheme 1.3: Formation of free radicals by the homolytic fission of an organic molecule

## 1.2 Sources of Free Radicals:

The mitochondrial electron transport chain, oxidation in the endoplasmic reticulum, inflammatory cell activities, and other enzymatic activities are some of the biochemical processes where free radicals are being produced within the human body. The mitochondrion is the powerhouse of the cell which has a central role in the respiratory chain and thus the generation of reactive oxygen species (ROS) (Poyton, Ball & Castello, 2009; Chance, Sies & Boveries, 1979; Inoue *et al.*, 2003). Free radicals help fight against infections and foreign invaders like micro-organisms that is why they are produced regularly by the immune system. Energy production increases during the condition of stress which in turn results in the production of more free radicals. Reduction of oxygen to water is a continuous process and a major source of ROS in the body (Sarma, Mallick & Ghosh, 2010). Different sources of ROS are shown in Table 1.1 (Bagchi and Puri, 1998) and Figure 1.1 (Al-Dalaen & Al-Qtaitat, 2014).

Cigarette smoke, inflammation, radiation constituents of ozone, alcohol, compounds of chlorine and metal ions are some of the external factors which can trigger the production of free radicals (Sivanandham, 2011; Klaunig *et al.*, 1997; Miller, Buettner & Aust, 1990; Poyton, Ball and Castello, 2009; Chance, Sies and Boveries, 1979). Other sources include cleaning products, paints, perfumes and even some medications. Exposures to X-rays also increase the level of ROS in the body. Coffee, alcohol, food of animal origin, food cooked at high temperature, hydrogenated vegetable oils and sugar are also responsible for the increased production of ROS (Sarma, Mallick & Ghosh, 2010).

Table 1.1: Sources of Free radicals (Bagchi & Puri, 1998)

| <b>Internally generated sources</b> | <b>Externally generated sources</b> |
|-------------------------------------|-------------------------------------|
| Mitochondria                        | Cigarette smoke                     |
| Phagocytes                          | Environmental pollutant             |
| Exercise                            | Radiation                           |
| Inflammation                        | UV light                            |
| Peroxisomes                         | Certain drugs/ Pesticides           |
| Ischaemia/reperfusion               | Ozone                               |

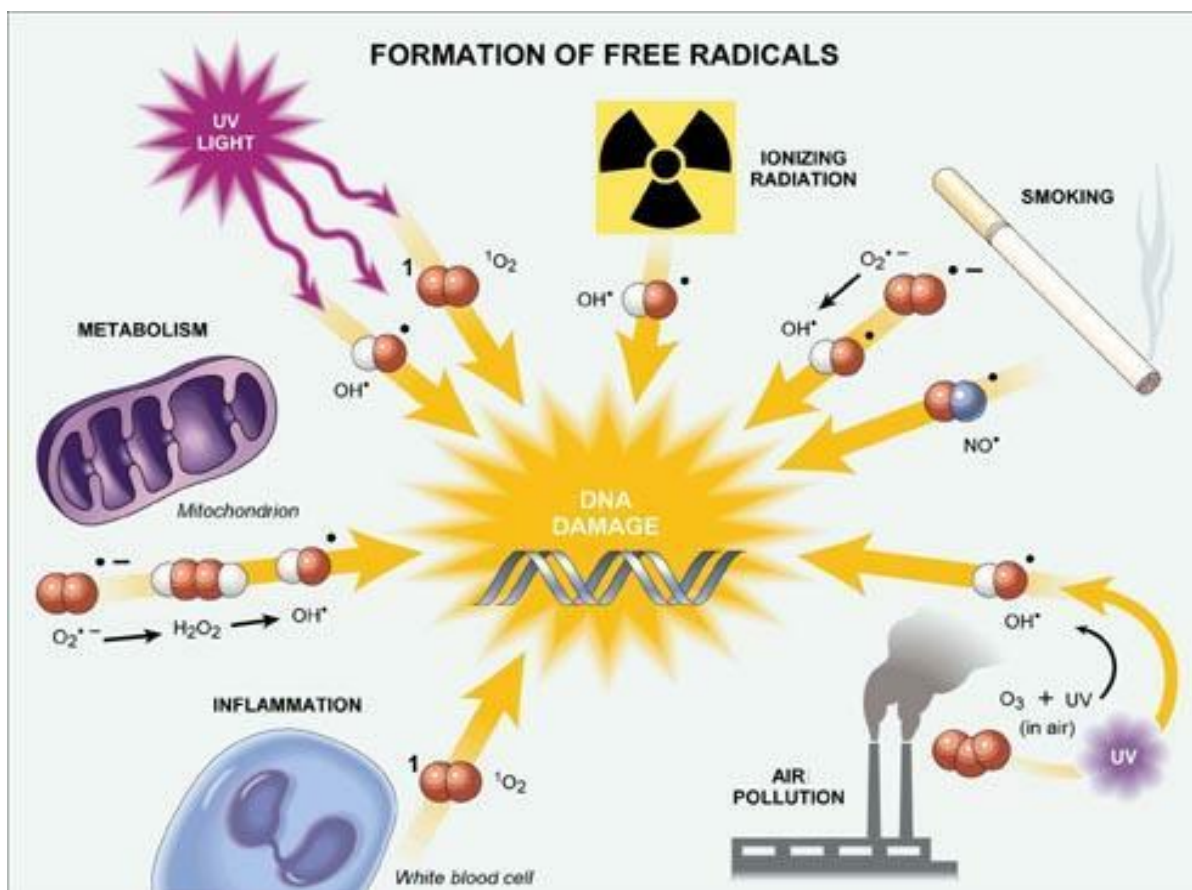
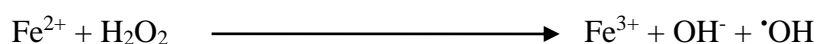


Figure 1.1: Different sources of Reactive Oxygen Species (Al-Dalaen & Al-Qtaitat, 2014)

### 1.2.1 The Fenton reaction:

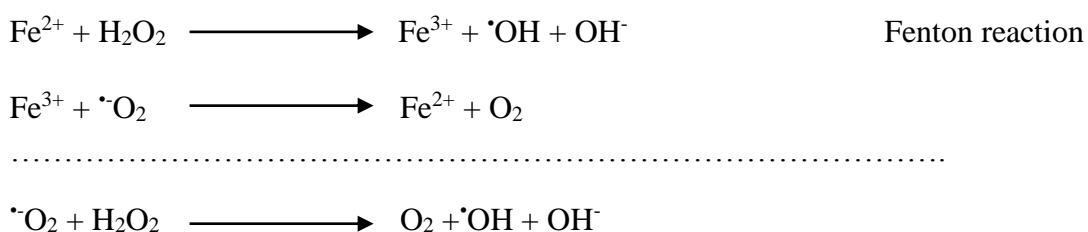
Most of the hydroxyl radicals generated in a living system are produced by this mechanism (Melin *et al.*, 2015). Under controlled conditions, this reaction may be used to generate  $\cdot\text{OH}$  in laboratories for studies. The reaction is named after H. Fenton who described it in 1894. The reaction involves the reduction of  $\text{H}_2\text{O}_2$  by  $\text{Fe}^{2+}$  to produce a hydroxyl radical and hydroxyl ion (Scheme 1.4).



Scheme 1.4: The Fenton reaction

### 1.2.1.1 The Haber-Weiss reaction:

A chain reaction of free radical generation is triggered by the superoxide radical.  $\text{Fe}^{3+}$ , a product of the Fenton reaction, is reduced by  $\text{O}_2^{\cdot-}$  to  $\text{Fe}^{2+}$ . The net reaction is termed as Haber-Weiss reaction and is shown in scheme 1.5 (Lemire, Harrison & Turner, 2013; Powell & Hall, 1990; Kissner *et al.*, 1997).



Scheme 1.5: Haber-Weiss reaction

Besides the Fenton reaction, highly reactive hydroxyl radicals are also produced when water is exposed to ionizing radiation (Attri *et al.*, 2015). Reduction of many oxidases also produces  $\text{H}_2\text{O}_2$  in the human body (Sivanandham, 2011).

### 1.2.2 Reactive Oxygen Species (ROS)

Radical species derived from molecular oxygen which are more reactive than oxygen itself are termed as Reactive Oxygen Species (ROS) (Halliwell and Gutteridge, 2015). It is the most important class of free radicals. Both exogenous and endogenous sources contribute to the production of ROS; smoke, drugs, radiation, and pollution are exogenous (Miller *et al.*, 1990) while inflammation, peroxisomes, and mitochondria are some of the endogenous sources contributing to an increased level of ROS (Klaunig *et al.*, 1997; Al-Dalaen & Al-Qtaitat, 2014).

Oxygen may accept an unpaired electron which results in the formation of the superoxide anion ( $\text{O}_2^{\cdot-}$ ). This in turn leads to the formation of hydrogen peroxide ( $\text{H}_2\text{O}_2$ ) and then the hydroxyl ( $\cdot\text{OH}$ ) radical (Figure 1.2) which may start chain reactions, the potentially damaging process for the cells (Riley, 1994; Lushchak, 2014).

The superoxide anion radical ( $\text{O}_2^{\cdot-}$ ) has a very short half-life and acts as an intermediate in the production of  $\text{H}_2\text{O}_2$  (Figure 1.2). Hydrogen peroxide is a stable molecule but may be converted into hydroxyl radicals, highly reactive species with a half-life of  $10^{-9}$

seconds and thus potentially damaging to biomolecules (Dalle-Done *et al.*, 2006; Erzsebet *et al.*, 2016). However, further one-electron reduction of the hydroxyl radical, as occurs in mitochondria, leads to the generation of water. The overall process whereby molecular oxygen is reduced to water is called oxidative phosphorylation (Alessio and Blasi, 1997).

The peroxy radical (ROO<sup>•</sup>; also known as hydroperoxyl radical) is another ROS and may be formed by the protonation of superoxide anion (O<sub>2</sub><sup>•-</sup>) (De Grey, 2002). It can initiate lipid peroxidation and thus a chain reaction which is potentially destructive to the cellular membrane (Aikens and Dix, 1991).

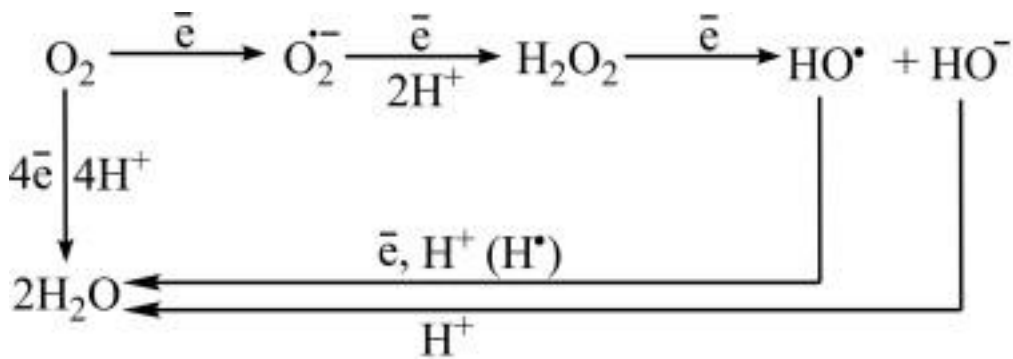


Figure 1.2; Reduction of molecular oxygen to water via four one-electron steps (Lushchak, 2014)

### 1.2.2.1 The hydroxyl radical

The hydroxyl radical is the most reactive known oxygen radical (Halliwell and Gutteridge, 2015). It is mainly produced inside the cell from hydrogen peroxide through the Fenton reaction (Scheme 1.4). Besides this reaction, there are other ways it can be produced inside the living cells e.g. homolytic fission of hydrogen peroxide by UV light may produce hydroxyl radicals (Dizdaroglu and Jaruga, 2012). High energy ionizing radiation may also produce hydroxyl radicals from water in cells. Exposure to ultrasound waves is also known to produce hydroxyl radicals. For example, hydroxyl radicals have been generated during cataract removal when using an ultrasonic probe (Murano *et al.*, 2008) and also from fragmentation of a kidney stone using shock wave lithotripsy



(Ghulam *et al.*, 2011). In addition, hydroxyl radicals are produced during oxidative stress and during the period of ischaemia when the body is in the condition of hypoxia (Lipinski, 2011).

Reactions of the hydroxyl radical include hydrogen atom abstraction, addition and electron transfer reactions (Schacker *et al.*, 1991). The hydroxyl radical may abstract a hydrogen atom from an organic compound e.g. ethanal to form water and carbon centered radical by leaving behind an unpaired electron on the carbon. In “addition” reactions, the hydroxyl radical may react with aromatic compounds like benzene or with compounds having double bond. In electron transfer reactions,  $\cdot\text{OH}$  may react with ions (e.g halides) to exchange ions and convert them into free radical (Halliwell and Gutteridge, 2015).

The hydroxyl radical may react with all types of biomolecules including lipids, proteins and DNA thus causing them damage which may lead to various consequences (Imlay, 2003). Directly or indirectly hydroxyl radicals are the cause of many life-threatening diseases like stroke, Alzheimer’s disease, rheumatoid arthritis, respiratory, kidney failure, cardiovascular diseases and cancer (Baradaran *et al.*, 2014; Nasri and Rafieian-Kopaei, 2014; Bocci and Valacchi, 2013; Halliwell, 1996; Shigenaga, Hagen & Ames, 1994; Halliwell, 1994).

Due to high reactivity and short lifetime, it is difficult to measure hydroxyl radicals. The three general approaches usually used to measure them are (a) Electron paramagnetic resonance (EPR) spectroscopy, for the measurement of radicals following spin-trapping, (b) the measurement of hydroxyl radical-induced damage, e.g. oxidised DNA, protein etc, after the reaction of free radicals with these molecules, and (c) the measurement of hydroxylation products of aromatic compounds like aromatic amino acids (Themann *et al.*, 2001). Examples of techniques that may be used to measure hydroxyl radical-induced damage include deoxyribose assay, EPR (Halliwell and Gutteridge, 2015), GC-MS (Dizdaroglu, 1991), HPLC coupled with a variety of detectors including electrochemical detection (ED) (Bergh *et al.*, 2000).

### **1.2.3 Reactive Nitrogen Species (RNS)**

Reactive Nitrogen Species (RNS) include a wide range of compounds derived from nitric oxide (NO<sup>•</sup>). In biological tissues, nitric oxide synthases (NOSs) generate nitric oxide (Ghafourifar and Cadenas, 2005). Nitric oxide is relatively stable and plays an important role in regulating different vital physiological processes such as cellular defence and blood pressure regulation if present in a small amount (Bergendi *et al.*, 1999). It reacts with other free radicals to produce RNS, for example, the reaction of nitric oxide with superoxide will produce peroxynitrite anion (ONOO<sup>-</sup>). This anion may react with thiols to produce thiyl radicals leading to thiol oxidation (Patel *et al.*, 1999). It can also potentially break the DNA strand as well when to attack the sugar-phosphate backbone through the process of oxidation and nitration (Carr *et al.*, 2000). Increased production of RNS is called “nitrosative stress” which is potentially damaging to the cell constituents (Volka *et al.*, 2007).

## **1.3 Oxidative Stress:**

Sies (1991) introduced the term “oxidative stress” in the title of a book in 1985. The term was defined in the second edition of the book published in 1991 as “a disturbance in the prooxidant antioxidant balance in favour of the former, leading to potential damage”. Velavan *et al.* (2007) defined it as an imbalance between ROS and antioxidants (defence system).

### **1.3.1 Causes of Oxidative stress**

Two major reasons behind oxidative stress are reduced levels of antioxidants or increased levels of ROS/RNS production. Decreased level of dietary antioxidants can be the cause of dropped level of antioxidants in the body while elevated toxin levels or inflammation can increase the production of ROS. Mutual association between oxidants and antioxidants in the body is shown in Figure 1.3 (Durackova, 2010).

### 1.3.2 Consequences of oxidative stress

Oxidative stress may lead to a situation where cells can die (necrosis) thus initiating/accelerating some fatal diseases. Three possible scenarios are:

- i- Cells may adapt to survive oxidative stress, for example, rats exposed to elevated oxygen can tolerate oxidative stress much longer than control rats.
- ii- All the molecular targets like protein and DNA will be damaged during the oxidative stress.
- iii- Apoptosis and necrosis are phenomena triggered by oxidative stress. The intrinsic “suicide mechanism” of the cell is activated during the former, thus leading to the death of the cell. This happens in many neurodegenerative diseases. In the latter process, the cell swells and ruptures, affecting adjacent cells by the contents released (Halliwell, 2001).

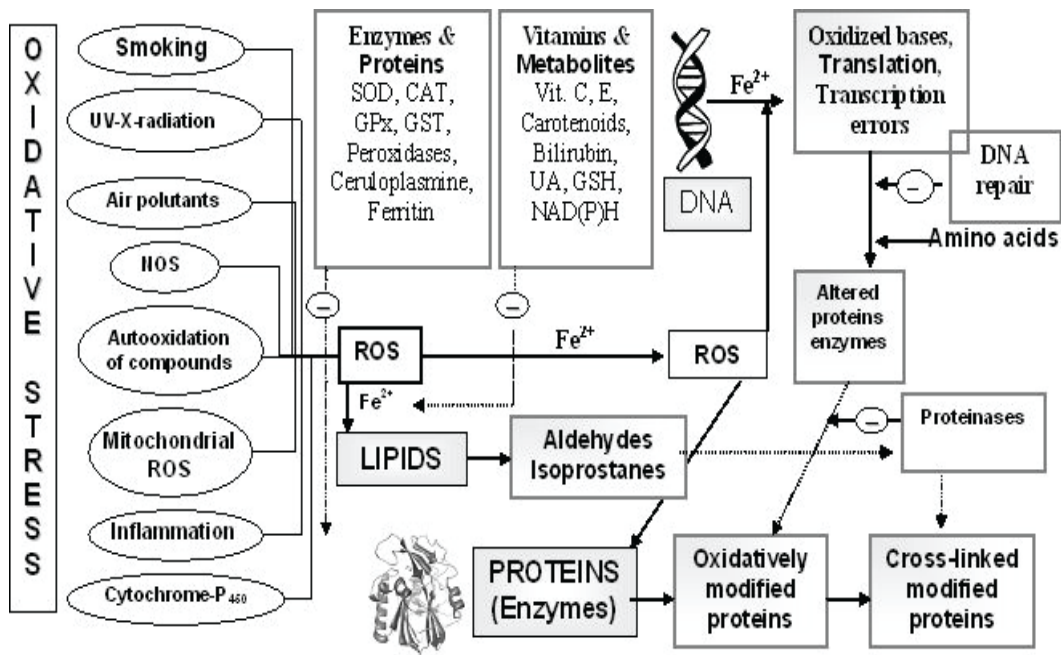


Figure 1.3: Mutual associations between oxidants and antioxidants (Durackova, 2010).

NOS- NO-synthase                      ROS- reactive oxygen species      CAT- catalase      SOD- superoxide  
dismutase

GPx- glutathione peroxidase      GST- glutathione S-transferase      UA- uric acid      GSH- glutathione reduce

## 1.4 Antioxidants:

Antioxidants are compounds (natural or synthesized) which prevent oxidative damage by reacting with free radicals before they target important bio-molecules of the cell. Antioxidants react with free radicals to terminate the chain reaction thus helping to reduce the damage.  $\cdot\text{OH}$  radicals have a strong affinity for double bonds converting them to single bonds after the reaction. This is the basic phenomenon behind the scavenging activity of compounds like polyphenolic natural substances and omega-3-fatty acids. All compounds with double bonds show scavenging activity thus lowering the effect of ROS (Liu *et al.*, 2011; Czapski, 1984). Salicylates having a phenolic ring in their structure, and with an “available” ortho-position, also act as scavengers and protect against free radicals (Podhaisky *et al.*, 1997; Kim *et al.*, 2001). Flavonoids present naturally in fruits and vegetables are also antioxidants (Areias *et al.*, 2001). Soybean contains genistein which can scavenge  $\cdot\text{OH}$  radicals (Zielonka, Gebicki & Grynkiewicz, 2003). Many reducing agents like ascorbate, tocopherols, and purines act as antioxidants which can reduce the ROS to less reactive forms (Proctor & Reynolds, 1984; Carr, Zhu & Frei, 2000; Al-Dalaen & Al-Qtaitat, 2014).

To take more antioxidants is a way to neutralize the effects of free radicals thus reducing oxidative stress. Various natural foods like beans and berries are high in antioxidants. By lowering the concentration of free radicals, it may be possible to reduce the damage caused by oxidative stress and help to avoid many diseases (Mastaloudis, Lenoard and Traber, 2001).

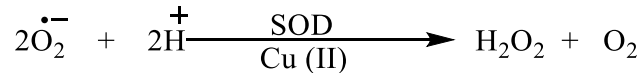
Physical activity plays a vital role as a natural antioxidant “booster” but strenuous exercise can lower the antioxidant level (Vinna *et al.*, 2008). Living species have antioxidants specific to radical species but this natural defence system is not strong enough to stop all free radicals from reacting with biomolecules thus potentially leading to cancer-like consequences (Alessio & Blasi, 1997; Sarma, Mallick & Ghosh, 2010).

There are different working mechanisms of antioxidants:

- i- Scavenging active free radicals.
- ii- Repairing/clearing damage.
- iii- Reduction of hydroperoxides ( $\text{ROO}\cdot$ ) and  $\text{H}_2\text{O}_2$  by suppression of active species production.

Oxidative stress can be minimized by natural antioxidants which strengthen the endogenous antioxidant defence system to restore balance (Velavan *et al.*, 2007). Both endogenous and diet-derived molecules make a network complex of antioxidant defence, for example:

- i-  $O_2^{\cdot-}$  is removed by converting it into  $H_2O_2$ . The enzyme system responsible is superoxide dismutase (SOD).



- ii- The  $H_2O_2$  produced is also dangerous for living cells and is then converted into water and  $O_2$  by the catalase enzyme.

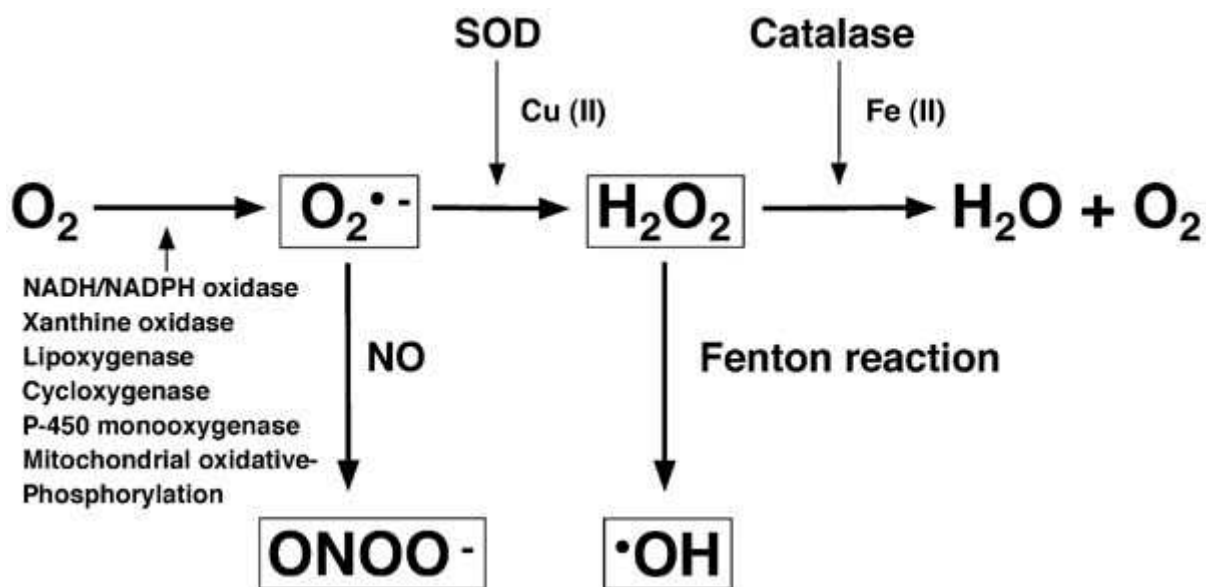


Figure 1.4: Production of different ROS in the body (Al-Dalaen & Al-Qtaitat, 2014).

Glutathione peroxidase and catalase are also part of antioxidant defence (Heilek & Noller, 1996; Barciszewski *et al.*, 1997). Non-enzymatic antioxidants like ascorbic acid/ascorbate, alpha-tocopherol and beta-carotene also operate inside the body to break the chain reaction of free radicals (Petersen *et al.*, 2000; Caro & Puntarulo, 1996). Nicotinamide adenine dinucleotide phosphate (NADPH) production helps to maintain

the reducing environment of the cell which in turn lowers the production of free radicals (Beckman & Ames, 1998). Many scavengers of low molecular weight (LMW) also help to neutralize the effect of free radicals. A balanced diet containing fruits, vegetables, and whole grain lowers the free radical stress, thus, helps defend the body from many diseases (Dauchet, Amouyel & Dallongeville, 2009). The mechanism of production of key ROS and related species in the body is outlined in Figure 1.4 (Al-Dalaen & Al-Qtaitat, 2014).

### **1.5 Benefits of Free Radicals:**

Although in general, free radicals are harmful to living organisms, this is not always the case. They help in the normal functioning of many systems both physiologically and biochemically. For example, phagocytes activation produces a burst of ROS which attack and inactivate microorganisms thus helping to defend the body against foreign invaders. Free radicals also play an important role in growth and regulation when serving as a physiological messenger for cell signaling (Saugstad, 2000; Droge, 2002). Some free radicals have a role in controlling the blood flow through arteries which, in turn, is helpful to keep the brain alert and active, especially during exercise (Trinity, Broxterman and Richardson, 2016). Also, cancer cells may be destroyed by free radicals (Sarma, Mallick & Ghosh, 2010). Polyunsaturated fatty acids (PUFAs) produce lipid peroxides that contribute to oxidative stress but, in a recent study, their beneficial effect was noted in diseases known to be associated with ROS (Schmidt, 1997). In fact, PUFAs protect the body when oxygen supply is low. Fibrosis and wound healing promoted by the growth of epithelial cells and fibroblasts may also be initiated by ROS (Turner, 1996) but crucially important is their concentration, which can cause different disorders when increased. Some of the pathological aspects of free radicals are outlined in Figure 1.5 (Sivanandham, 2011).

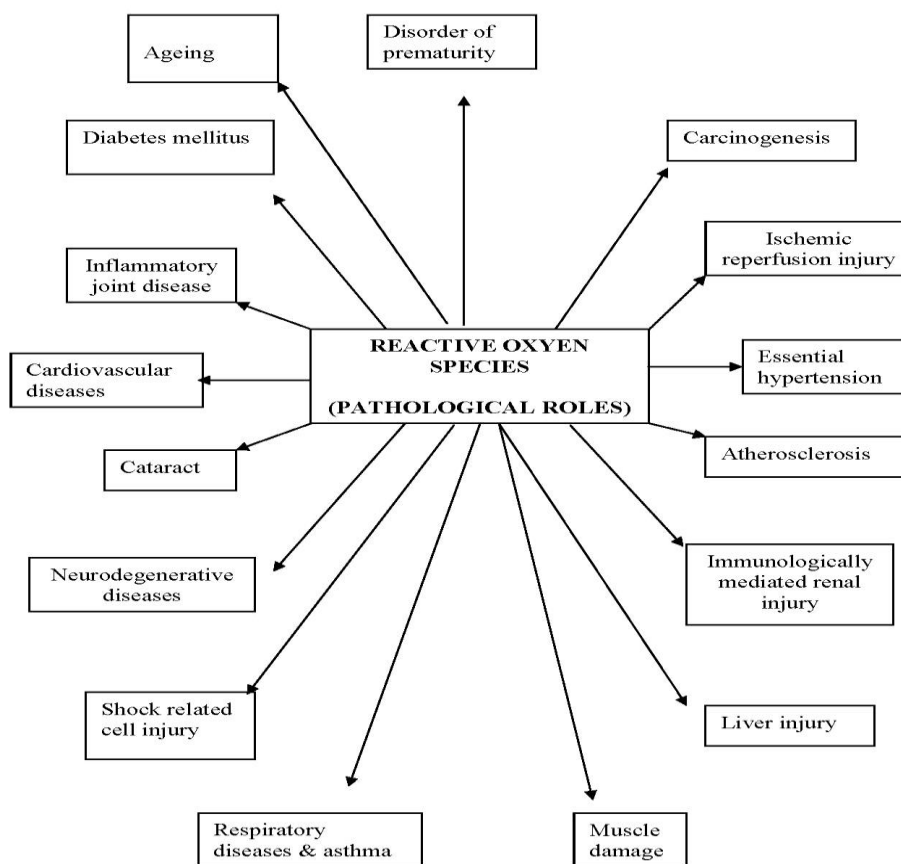
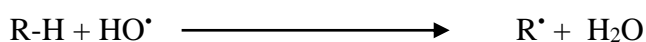


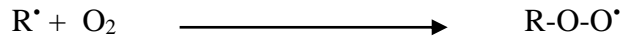
Figure 1.5 Pathological roles of ROS (adapted from Sivanandham, 2011).

### 1.6 Chain reaction and damage by free radicals

Free radicals initiate chain reactions when reacting with other non-radical molecules of the body, a very damaging process. Most biological molecules are non-radicals. New radicals are generated when these non-radicals are attacked by free radicals. For example, a carbon-centered radical is generated when hydrocarbons are attacked by an  $\cdot\text{OH}$  radical. Newly generated carbon-centered radicals react readily with oxygen to form peroxy radicals (scheme 1.6 & 1.7). Bio-molecules attacked by free radicals result in impaired cell function leading to ageing and eventually cell death. (Sarma, Mallick & Ghosh, 2010).

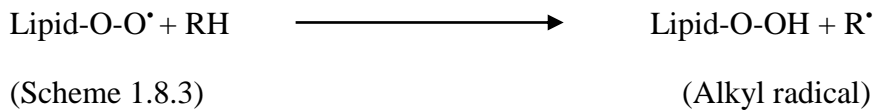
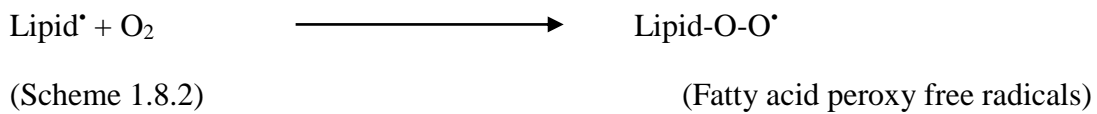
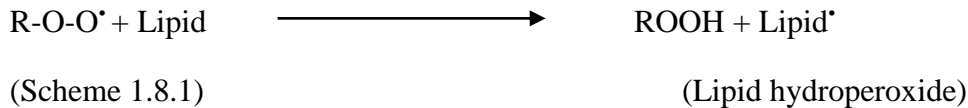


Scheme 1.6: Production of an alkyl radical when a hydrocarbon is attacked by hydroxyl radical



Scheme 1.7: Production of peroxy radical from an alkyl radical

Carbon-centered peroxy radicals will then attack membranes to produce lipid hydroperoxides and a new carbon-centered radical (Scheme 1.8.1). This newly generated carbon-centered radical will continue the chain propagation (Halliwell, 2001).



Peroxy radical attacks lipid to generate lipid hydroperoxide radical (scheme 1.8.1), which is further oxidised to produce fatty acid peroxy free radical (scheme 1.8.2) which in turn may attack hydrocarbon to produce an alkyl radical (scheme 1.8.3)

## Types of Damage

All constituents of the cell are a target of free radicals. Some of the major cell constituents with consequences of a free radical attack are summarized below.

### 1.6.1 Lipid hydroperoxide (LOOH)

Lipid peroxidation is defined as an oxidative destruction of poly unsaturated fatty acids (PUFAs). A fatty acid radical (L<sup>•</sup>) is produced by the oxidation of a PUFA. Fatty acid radicals rapidly change into fatty acid peroxy radicals (LOO<sup>•</sup>) when exposed to oxygen (Scheme 1.8.1 & 1.8.2). By-products of the reaction can cause direct destruction of the membrane or indirectly to other structures, right from protein to DNA & RNA. Peroxidation of lipids affects the function of enzymes and receptors (Halliwell, 2001).



### **1.6.2 Protein oxidation**

ROS and RNS can cause oxidative modification of proteins resulting in the pathogenesis of various diseases. The biochemical functions may be lost if the protein is oxidatively damaged, especially at an active site. Modification of protein may lead to cancer, ischaemia-reperfusion injury, and atherosclerosis (Sarma, Mallick & Ghosh, 2010).

### **1.6.3 Carbohydrates**

Carbon-centered free radicals are produced when  $\cdot\text{OH}$  reacts with carbohydrates. This can cause chain breaks in important molecules like hyaluronic acid. There is evidence that rheumatoid arthritis is induced by an excess production of oxy-radicals but the mechanism is not fully understood and need further investigation (Sivanandham, 2011).

### **1.6.4 DNA oxidation**

The poly (ADP-ribose) synthetase enzyme is activated when free radicals cause damage to DNA. Protective properties of the cell are lost when damage is extensive (Sarma, Mallick & Ghosh, 2010). Damage to DNA can be considered as most destructive as it affects the cell cycle. DNA mutation can trigger many diseases like diabetes mellitus (Dandona *et al.*, 1996), cancer (Shu *et al.*, 2017), inflammatory and liver diseases (Sipowicz *et al.*, 1997) and is suggested to be part responsible in the ageing process (Nakao *et al.*, 1999; Fraga *et al.*, 1990).

## **1.7 Free radicals and Human diseases**

As defined earlier, oxidative stress is the “imbalance between free radicals and reactive metabolites called oxidants” (Reuter *et al.*, 2010). A diagrammatic description of the phenomenon is given in figure 1.6. The first documented evidence of oxidative stress was a chromosomal mutation in pollens caused by higher oxygen level pressure (Conger and Fairchild, 1952). The antioxidant defence system of the body copes with oxidative stress under normal circumstances. However, increase in oxidative stress may induce cancer (Sosa *et al.*, 2013), rheumatoid arthritis, inflammation, diabetes, asthma, ageing

(Lee, Koo & Min, 2004) and neurodegenerative diseases (Pham-Huy, He & Pham-Huy, 2008; Uttara *et al.*, 2009).

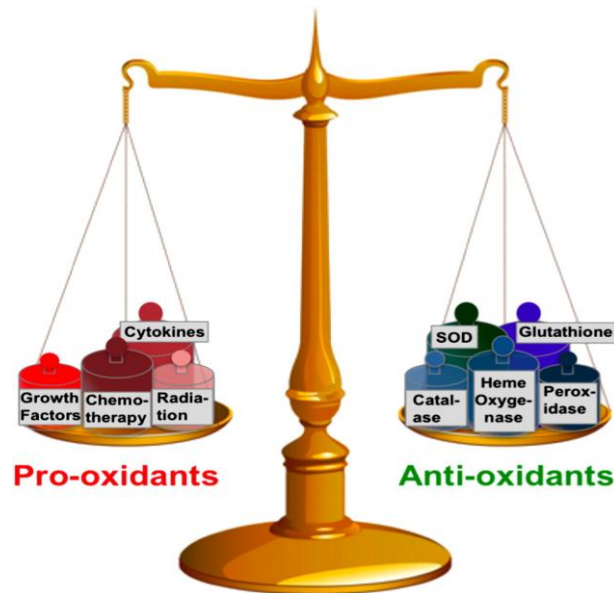


Figure 1.6: Antioxidant/pro-oxidant balance in the cell (adapted from Reuter *et al.*, 2010)

In biological systems, ROS plays a dual role since they can be beneficial or harmful (Volka *et al.*, 2007). However, damage is done when the balance is disrupted between free radicals and antioxidants in favour of former. Some of the diseases which can be induced by oxidative stress are listed in Figure 1.7 (Pham-huy, He & Pham-huy, 2008).

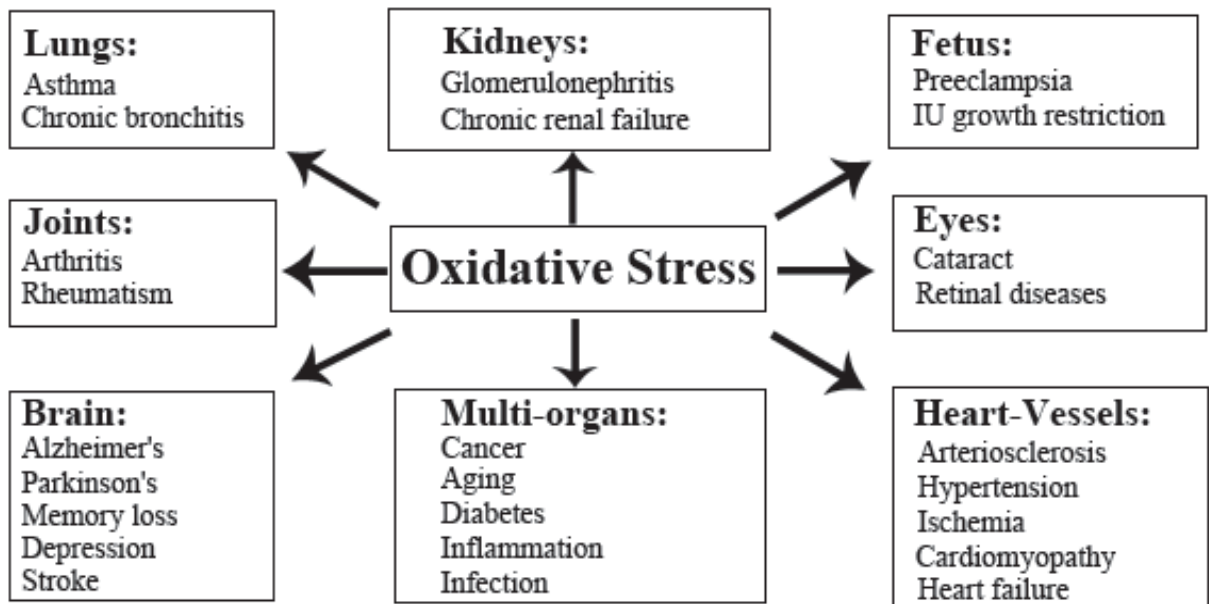


Figure 1.7: Oxidative stress-induced diseases in humans (Pham-Huy, He & Pham-Huy, 2008).

### 1.7.1 Neurodegenerative diseases

Large amount of oxygen is needed for the functioning of the brain thus leading to a large turnover of free radicals. Low levels of antioxidants around the brain and limited activity from protective enzymes (Ferber *et al.*, 1999) and high levels of ascorbate and iron ( $Fe^{2+}$ ) are the main causes of oxidative stress in the brain (Floyd & Carney, 1992) which can lead to ataxia or dementia. Ataxia is a condition when there is functional loss whereas, in dementia, there is sensory dysfunction of brain cells (Mattson, 2004).

Neurodegenerative diseases like Parkinson's disease or Alzheimer's may be initiated or triggered if the oxidative stress balance sways in the favour of pro-oxidants (Kumar *et al.*, 2012; Nikolova, 2012; Uttara *et al.*, 2009; Simonian, 1996; Aslan & Ozben, 2004; Perry *et al.*, 2002).

Aggregation of proteins is associated with loss of specific neuronal cells which can lead to neurodegenerative conditions like Alzheimer's disease (AD), Parkinson's disease (PD) and sclerosis. Death or dysfunction of neuronal cells resulting in the loss of specific population of the neuronal cell might be caused by oxidative stress thus contributing to the pathogenesis of neurodegenerative diseases (Rahman *et al.*, 2012).

Products of LPO i.e. 2-hydroxy nonanal (2-HNE), malondialdehyde and F<sub>2</sub>-isoprostanes were all elevated in the brains of patients with AD when compared to healthy controls (Arlt, Beisiegel and Kontush, 2002). In another study, levels of F<sub>2</sub>-isoprostanes were elevated in cerebrospinal fluid of patients with Huntington's disease as compared to a healthy group (Montine *et al.*, 1999). These studies provide some evidence of free radical damage in the pathogenesis of neurodegenerative diseases.

DNA modification is another possibility when cells are under oxidative stress. One study found that levels of 8-hydroxyguanine and 8-hydroxy-2-deoxyguanosine (formed by the attack of hydroxyl radical on guanine base of the DNA) were elevated in patients with PD disease (Alam *et al.*, 1997). In Parkinson's disease  $\alpha$ -synuclein, a protein that plays role in the functioning of mitochondria was modified by the products of LPO and accumulated in the cytoplasm, thus providing evidence of oxidative damage during the progression of neurodegenerative disease (Dasgupta and Klein, 2014).

Neuronal cells are more vulnerable with increasing age. This is because high concentrations of redox metals like copper, zinc, and iron accelerate the production of free radicals at the junction of neuronal environment, thus triggering various neurodegenerative diseases (Takahashi *et al.*, 2001; Uttara *et al.*, 2009). Moreover, high levels of PUFA in neuronal cells and a poor antioxidant defence system make the nervous system vulnerable to oxidative stress (Dasgupta and Klein, 2014).

### **1.7.2 Cardiovascular diseases**

Raised level of cholesterol, smoking, hyperglycemia, stress and physical inactivity are some of the risk factors in developing cardiovascular disease (CVD). In recent years, various studies have established a strong link between oxidative stress and development/progression of CVD (Bhattacharya, Ahmed and Chakraborty, 2011). Cardiovascular function is affected by oxidative stress in two ways, either by the development of atherosclerosis on a long-term basis or involving sudden damage during stroke or heart attack (Dhalla, Temsah & Netticadan, 2000).

Atherosclerosis is a condition, in which, lipoproteins are deposited in arteries, which can lead to plaque formation and thus obstructing the arterial blood flow. Free radical mediated oxidative damage can play an important role in the inflammatory state of

atherosclerosis and its pathogenesis (Steinberg, 1997; Al-Dalaen & Al-Qtaitat, 2014). Low density lipoproteins (LDL) may react with ROS to form oxidised form of low density lipoproteins (oxLDL) which, in turn, can initiate the process of atherosclerosis.

Uncontrolled lipid peroxidation causes cellular damage with the result of plaque formation causing coronary artery disease (McIntyre & Hazen, 2010). Leukocyte binding is facilitated by the expression of cellular adhesion molecules up-regulated by oxLDL, which in turn can increase the rate of plaque formation leading to different medical conditions including stroke and heart attack (Devasagayam *et al.*, 2004). There is evidence that ischemic injury can be reduced by the reversal of oxidative stress with antioxidants (Wang *et al.*, 2016).

### **1.7.3 Rheumatoid arthritis**

Rheumatoid arthritis (RA) is an autoimmune disease in which joints are mistakenly attacked by body's immune system resulting in inflammation, which can lead to cartilage and bone destruction in a chronic condition. Although there is no established link between oxidative stress and RA, increased levels of LPO products, protein oxidation and an impaired antioxidant system have been reported in patients with rheumatoid arthritis. The level of MDA and protein carbonyls formed by the oxidation of lipids and proteins, respectively, were higher while the levels of antioxidants were significantly lower in RA patients as compared to healthy controls (Mateen *et al.*, 2016). In another study, similar results suggested that oxidative stress may be involved in the pathophysiology of RA. The levels of reactive aldehydes, which are the products of LPO i.e. malondialdehyde (MDA) & 4-hydroxy nonanal (4-HNE) were at a higher level both in plasma and urine while the level of antioxidants was lower when compared with control group (Łuczaj *et al.*, 2016). Structural and functional alterations of biomolecules caused by ROS may have a significant role in the pathogenesis of RA. Phull *et al.* (2018) demonstrated a strong association between oxidative stress and RA severity score. Oxidative stress may not be the direct cause of RA but it may be triggered if levels of ROS are elevated (Lemarechal *et al.*, 2006).

### 1.7.4 Cancer

Cancer is a multistage process having three distinct phases i.e. initiation, promotion and progression. All three stages are affected by oxidative stress (Klaunig and Kamendulis, 2004). Damage to DNA may occur during initiation stage resulting in gene mutation and structural changes. During the promotion phase, expression of the gene is affected by reactive oxygen species resulting in an increased cell proliferation. Further DNA alterations are added by oxidative stress in the progression phase (Klaunig *et al*, 1998). Damage to bases and backbone of DNA causes gene mutations leading to cancer (Al-Dalaen & Al-Qtaitat, 2014). Initially, it was thought that ROS increases the mutation rate by acting simply as a tumour initiator (Jackson and Loeb, 2001) but later studies revealed that in addition to tumour initiation, they are involved in certain signaling pathways which can contribute to tumour formation (Storz, 2005). A direct link has been suggested between the product of oxidised DNA, 8-hydroxyguanine (8-OH-G) adduct and the size of a benign tumour; for example, an increase of up to 17-fold in primary breast tumours as compared to non-malignant tissues of the breast has been observed (Musarrat, Arezina-Wilson and Wani, 1996). Further understanding of this link might be helpful to explain benign to malignant tumour transformation (Loft and Poulsen, 1996).

Inflammation is a part of the immune system in which body tries to remove harmful stimuli. Radiation, allergens, chemicals, chronic diseases, tobacco, viruses and microbes are some of the sources of inflammation (Reuter *et al.*, 2010). Acute and chronic are the two stages of inflammation. Acute inflammation is for short term only and is usually counter attacked by the immune system for neutralization, while inflammation lasting for a longer period-of-time is called as chronic inflammation. Various chronic illnesses including cancer may be caused by chronic inflammation (Lin and Karin, 2007). Chronic inflammation produces oxidative stress which may change the immune responses to various external and internal stimuli thus creating an immune system chaos leading to various chronic conditions including cancer (Rahal *et al.*, 2014).

Metals like iron, copper, and chromium are essential for the normal functioning of various enzymes and proteins. These metals act as a catalyst in Fenton-type chemistry. Accumulation of iron is closely associated with colorectal (Huang, 2003) and renal cancer (Toyokuni, 1996). Iron loading can also lead to the promotion of a liver tumour

(Mizukami *et al.*, 2010). Hydroxyl radicals produced by the Fenton reaction may activate redox-sensitive transcription factors leading to tumour promotion (Vogt & Bos, 1990).

Lipid peroxidation (mentioned earlier in section 1.6) may cause malignant neoplasia of the breast, ovaries and rectum (Barrera, 2012). In a recent review, clinical evidence of oxidative stress in different types of cancers was discussed in detail. The levels of MDA were elevated in patients with ovarian, oral, breast, lung and cervical cancer patients (Sharma, Shrivastav and Shirvastav, 2014).

### **1.7.5 Lung diseases**

Chronic inflammation and oxidative stress may be involved in the respiratory system diseases like asthma and chronic obstructive pulmonary disease. Inflammation is enhanced through activation of different kinases and redox transcription factors by the oxidants (Hoshino & Mishima, 2008).

In many studies, it has been suggested that pathogenesis of asthma could be linked to oxidative stress. Airway inflammation might be exacerbated by oxidative stress which in turn stimulates mucin secretion and induction of chemical mediators, believed to be linked with asthma (Rahman, 2003). More cases of asthma have been reported in areas of air pollution, a major exogenous source of oxidants (Battaglia *et al.*, 2005).

Pulmonary fibrosis is another condition in which lung tissues become thickened and scarred over a period-of-time. There are many factors like radiation, drugs, an autoimmune reaction that can initiate fibrosis, but several studies suggested that a critical role is played by the oxidant/antioxidant imbalance in the pathogenesis of fibrosis (Cantin *et al.*, 1987; Montuschi *et al.*, 1998).

### **1.7.6 Hypoglycaemia**

Free radicals' production can be triggered by hypoglycemia which can further aggravate the complications of diabetes (Johansen *et al.*, 2005). Elevated levels of MDA has been detected in patients with longer duration of disease as compared to newly diagnosed type

1 diabetes mellitus which indicates that production of free radicals has increased as the disease has progressed (El-samahy *et al.*, 2009).

### **1.7.7 Reproductive system**

Fertility status may also be affected by oxidative stress (Makker, Agarwal and Sharma, 2009). Approximately 4000 compounds are present in tobacco smoke; which may cause oxidative stress. There is also strong evidence of sperm DNA fragmentation with smoking (Sun, Jurisicova and Casper, 1997). In another study, it was found that the sperm of smokers are more sensitive to DNA mutation than non-smokers (Potts, *et al.*, 1999). In addition, reduced levels of antioxidants like vitamin C & vitamin E can increase the risk of abortion (Barrington *et al.*, 1996).

### **1.7.8 Cataract and glaucoma**

Loss of retinal ganglion cells and increased intraocular pressure are characteristic features of glaucoma. Mitochondria may lose their function in glaucoma patients thus leading to oxidative stress which in turn can cause secondary degeneration (Chrysostomou *et al.*, 2013).

Opacification of the eye lens is termed as cataract. In human beings, UV light filter becomes weaker with increasing age resulting in elevated oxidative stress if exposed to sunlight (Vinson, 2006). Kaur *et al.* (2012) found the levels of LPO products were significantly elevated in a group of cataract patients as compared to control group. In addition, levels of antioxidants were severely depleted suggesting a role for oxidative stress in the progression of cataracts. In another study, similar observations i.e. increased LPO products and lower level of antioxidants were found when age-related macular degeneration was studied in 25 patients and results were compared with a group of healthy controls (Yildirim, Ucgun and Tildirim, 2011). Age-related disorders of the retina and cataracts are also caused by oxidative stress (Tavafi, 2013; Bagchi & Puri, 1998; Dalle-Donne *et al.*, 2006). The leading cause of irreversible blindness is primary open angle glaucoma, which may be triggered by ROS damage (Izzotti, Bagnis & Sacca, 2006).



### **1.7.9 Immune system**

The immune system of the body aids the defence against oxidative stress (Poli *et.al.*, 2004). The immune system of the body becomes weaker with the age and thus lowers the fighting capabilities against diseases resulting in oxidative stress. This increases the susceptibility to free radical damage with age (Yu, 1994; Halliwell and Gutteridge, 1989).

A correlation between disease and oxidative stress may also depend on the type of ROS responsible for that oxidation. For example an amino acid, methionine oxidation produce sulfonate derivative when attacked by singlet oxygen while a reaction with hydroxyl radical gives hydroxyl methionine (Suto *et al.*, 2006).

### **1.7.10 Ageing**

Ageing is defined as a progressive decline in physiological functions with increased chances of mortality. Although ageing is a universal phenomenon the underlying mechanism behind it is largely elusive. There are two different types of ageing theories: the programmed theory and the free radical/mitochondrial theory. Programmed theory of ageing implies that ageing follows a timetable programmed in the genes. Regulation depends on the change in gene expression which in turn affects immune, repair and maintenance systems (Jin, 2010; Halliwell and Gutteridge, 2015).

Free radical theory of ageing proposes ROS as the main cause of ageing. The function of mitochondrial DNA (mtDNA) is adversely affected, when under oxidative stress which in turn enhances the production of ROS thus causing more damage to mtDNA (Cui, Kong and Zang, 2012).

The free radical theory of ageing was first proposed by Herman in 1957 which hypothesizes that the age-related damage is because of oxidative stress (Herman, 1957; Ziegler, Wiley and Valerade, 2015; Turner, 1996). There are many studies which suggest this theory by showing the increased levels of 8-oxo-dG (formed by the breakdown of DNA because of oxidative stress) in aged tissues suggesting oxidative stress as a contributory factor in the ageing process (Maynard *et al.*, 2009).

After genetic factors, metabolic rate also affects the process of ageing. The high metabolic rate will produce more ROS thus making life span shorter. In general, reduced production of free radicals in mitochondria, resistance to oxidative stress and improved antioxidant resistance was seen in long-lived species (Simm & Bromme, 2005).

There are many pieces of evidence that show molecular damage by ROS can lead to disorders, diseases and death. This evidence also suggests that oxidative stress is strongly linked to cellular damage leading to ageing (Rattan, 2006; Simm and Bromme, 2005).

### **1.8 Aldehydes and free radicals**

Aldehydes are low molecular weight compounds produced in the human body during lipid peroxidation (Pillai *et al.*, 2009). Aldehydes are some of the most important products of oxidative stress, mostly produced through lipid peroxidation, and potentially may be used as biomarkers of many pathological conditions (Deng and Zhang, 2004; Lili *et al.*, 2010).

Polyunsaturated lipids of the membrane can undergo peroxidation to initiate a chain reaction leading to tissue damage (Rosen, Elmer and Rauckman, 1981). Cyclooxygenase (COX) and lipoxygenase (LOX) (involved in fatty acid metabolism) are two main pathways to do lipid peroxidation in the human body resulting in the production of free radicals. These radicals then can target many other molecules like DNA/RNA or proteins, thus causing different structural changes leading to a variety of consequences (Xu, Gu and Qian, 2012).

Aliphatic aldehydes are produced during the peroxidation of polyunsaturated fatty acids (PUFA). Enhanced activity of malignant tissues could be the reason for the increased level of aldehydes. The body may recognise a tumour as an inflammation which can also be another reason for causing oxidative stress thus elevating aldehyde levels (Fuchs *et al.*, 2010).

### **1.8.1 Aldehyde radicals as potential biomarkers**

Free radical induced lipid peroxidation produces aldehydes which can be used as biomarkers for diseases such as atherosclerosis, carcinogenesis and dysplasia of the pancreas (Basu and Marnett, 1983). Raised levels of many other aldehydes like acetaldehyde, acrolein, hexanal and heptanal has been used as biomarkers for different diseases (Gordon *et al.*, 1985; Kato *et al.*, 2001).

The type of aldehyde produced greatly depends on the type of PUFA in the membrane of tumour cells. Pentanal is considered as a strong candidate as a biomarker of lipid peroxidation in mammals (Eggink *et al.*, 2008). Formaldehyde has been suggested as a lung malignancy biomarker (Kushch *et al.*, 2008). Higher concentrations of pentanal, hexanal, octanal and nonanal were detected in cancer patients as compared to a control group so these could also be used as a biomarker for lung cancer (Fuchs *et al.*, 2010). In another study levels of hexanal, heptanal and nonanal were elevated in patients with blood cancer, showing potential to be used as biomarkers (Li *et al.*, 2005a). Although it is well established that lipid peroxidation increases the level of aldehydes, the exact mechanism about their presence in body fluids and breath is still not fully understood (Eggink *et al.*, 2010; Hakim *et al.*, 2012).

### **1.8.2 Solvent free approaches to detect aldehyde radicals**

Aldehyde-based biomarkers were extracted successfully by solid phase microextraction (SPME) after aqueous or on-fiber derivatisation and then analysed by GC-MS (Shin, 2009; Deng and Zhang, 2004). Liquid dispersive microextraction (LDME) or single drop microextraction (SDME) is another method used for the extraction of volatiles like aldehydes (Li *et al.*, 2005b; Fiamegos and Stalikas, 2007).

Dispersive liquid-liquid microextraction (DLLME), introduced by Rezaee and his colleagues is a fast and sensitive technique in which a dispersive solvent is used with an appropriate extractant (Rezaee *et al.*, 2006). The drawback of the method is limiting the number of extracting solvents available because the density of solvent should be higher than water for an extracting solvent. All the commonly used solvents like chloroform, tetrachloromethane and chlorobenzene are toxic and not environment-friendly (Rezaee, Yamini & Faraji, 2010; Chen *et al.*, 2009; Moinfar and Hosseini, 2009).

### 1.8.3 Challenges to detect aldehyde-related radicals

Aldehydes are reactive and decompose in a short period of time. They are produced in low quantities, thus there is a need for derivatisation before analysis (Kato *et al.*, 2001; Schmarr *et al.*, 2008; Fiamegos and Stalikas, 2008; Stashenko *et al.*, 2000). For aliphatic aldehydes the most commonly applied method is to react them with PFBHA O-(2,3,4,5,6-pentafluorophenyl) methyl hydroxylamine hydrochloride to produce stable oximes (Cancilla and Que Hee, 1992). Furthermore, separation of derivatised product from unreacted derivatising reagent before chromatographic separation makes it harder and less accurate. There is clearly a need to develop a method for the detection of aldehyde-related radicals without derivatisation.

In the present project, solvent-free approaches are used without any derivatisation to detect aldehyde related radicals produced from acetaldehyde and propionaldehyde by using the Fenton chemistry, thus allowing indirect detection of the aldehyde.

## 1.9 Detection of free radicals

Damage made/induced by free radicals at the molecular level is quite severe and may be detected by the use of biological markers produced by the reaction of free radicals like  $\cdot\text{OH}$  with other biological entities. Aromatic compounds such as 2-hydroxybenzoate have been used to detect and measure the level of hydroxyl radicals (Ste-Marie *et al.*, 1996). Free radicals can be measured by trapping or by a process called “fingerprinting”, where damage caused by free radicals is measured to quantify them (Halliwell and Gutteridge, 2015).

### 1.9.1 Spin trapping

As free radicals are short-lived, it is difficult to detect and analyze them directly (Holley & Cheeseman, 1993). Spin trapping was introduced by Janzen’s group in 1968 in which detection and identification of short-lived free radicals was achieved with more ease (Janzen 1971). In this technique diamagnetic compounds called spin trapping agents, such as nitron or nitroso, react with a free radical to form spin adduct which is stable enough to be used for further analysis by using techniques like EPR spectroscopy or MS (Suezawa *et al.*, 1981; Galkin *et al.*, 1997; Halliwell & Gutteridge, 2007).

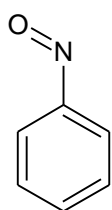
### 1.9.2 Nitrones and nitroso spin traps

Nitroso (R-NO) and nitrone (R-CH=NO-Y) are two important categories of spin traps used. An EPR detectable nitroxide radical adduct is produced by the reaction of free radicals with a spin trap (Janzen & Blackburn, 1968; Lagercrantz, 1971) e.g. nitrones can react with free radicals to form nitroxide radical adducts (Scheme 1.9) (Janzen *et al.*, 1988). The radical adds directly to the nitrogen atom in the case of the nitroso trap, whereas it adds to an adjacent carbon atom for the nitrone. With both spin-traps an aminoxyl radical adduct (nitroxide) is produced which can be detected by EPR spectroscopy (Rosselin *et al.*, 2016). The nitroso trapped radical may influence the EPR spectrum more and generate extra hyperfine splitting, whereas with spectra of nitrones spin traps tend to be broadly similar irrespective of the trapped radical. However, less stable adducts are produced with nitroso compound (Scheme 1.10) when compared to nitrone-trapped radicals, because nitrones are thermally and photochemically stable as compared to nitroso compounds (Abe, Suezawa and Hirota, 1984). In addition, they tend to be toxic to living organisms; hence nitrones are more common in use both *in vivo* and *in vitro*. Ideal spin traps should react rapidly with specific radicals that needed to be trapped, produce chemically stable adducts, should not be metabolised by cellular systems and have unique EPR spectra (Britigan, Cohen and Rosen, 1987).

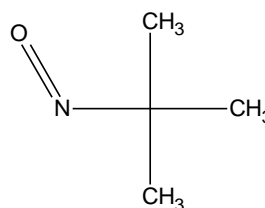
Nitrones are used extensively for spin trapping studies because of their low toxicity. N-*tert*-butyl- $\alpha$ -Phenylnitron (PBN),  $\alpha$ -(4-pyridyl-1-oxide)-N-*tert*-butylnitron (POBN) and 5,5-dimethyl-1-pyrroline-N-oxide (DMPO) are the most utilized nitrones. The first cyclic nitrone used was DMPO which was mostly used to trap oxygen centered radicals like superoxide (Buettner, 1993). The superoxide adduct of DMPO can decompose into the hydroxyl adduct in less than a minute which has limited its use to detect this entity (Samuni, Samuni and Swartz, 1989). POBN is another most commonly used spin trap for the detection of hydroxyl and carbon centered radicals. POBN have been used successfully not only in many EPR spin trapping studies (Kennedy *et al.*, 1992; Panchenko *et al.*, 2004) but also using GC-MS (Ireland and Valinieks, 1992, Mistry *et al.*, 2008) and MALDI-TOF-MS (Podmore *et al.*, 2013; Tian *et al.*, 2007) studies. PBN is another very common spin trapping agent which can stabilize free radicals thus reducing their reactivity. It is mostly used for the detection of carbon centered radicals as its radical adducts of oxygen centered radicals are less stable (Kotake and Janzen, 1991)

Hydrolysis of PBN yields *tert*-butyl hydroxylamine. It can also be formed by the decomposition of PBN-OH adduct (Jerzykiewics *et al.*, 2011; Turnbull *et al.*, 2001). Nitric oxide is involved in signal transduction and the physiology of cardiovascular and immune systems, thus affecting many important physiological functions other than acting as a spin trap (Chamulitrat *et al.*, 1993) but an abnormal production of nitric oxide may cause neuronal injury by inducing apoptotic death of neuronal cells (Wei *et al.*, 2000). Nitrones like PBN are an effective carrier of it in an inert form (Saito and Cutler, 1995).

In several experiments, nitrones have shown promising anticancer effects and thus potentially have a future use as therapeutics for cancer (Floyd *et al.*, 2008). PBN has shown good pharmacokinetic properties when administrated to rats (Chen *et al.*, 1990). Nitronone analogues of PBN have shown promising neuroprotective effects after cerebral ischemia in rats (Kuroda *et al.*, 1999). In the Mongolian Gabriel, age-related parameters were reversed using PBN (Carney *et al.*, 1991).

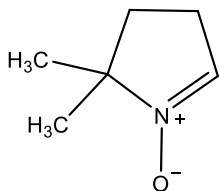


Nitrosobenzene

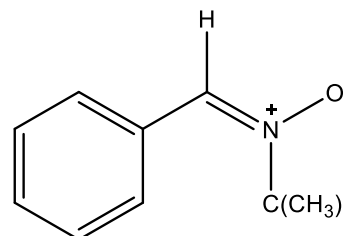


2-methyl-2-nitrosopropane

Figure 1.8: Commonly used nitroso spin traps

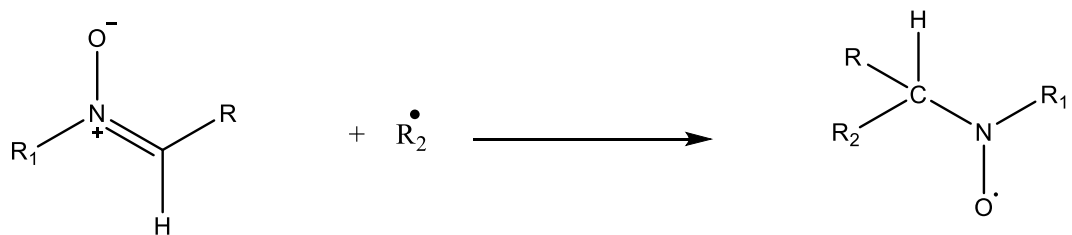


DMPO (5,5-Dimethyl-1-Pyrroline-N-Oxide)



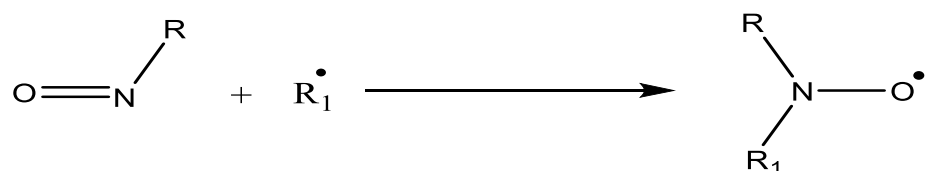
PBN

Figure 1.9: Commonly used nitronone Spin traps



Nitronium spin trap + reactive radical  $\longrightarrow$  Nitroxide radical

Scheme 1.9: Trapping of a free radical with a nitronium compound resulting in the formation of a stable nitroxide radical adduct.



Nitroso spin trap + reactive radical  $\longrightarrow$  Nitroxide radical

Scheme 1.10: Trapping of a free radical with a nitroso compound resulting in the formation of a stable nitroxide radical adduct.

### 1.9.3 Nitroxides as spin traps

Nitroxides (also known as aminoxyls or nitroxyls) are fairly stable free radicals that can interact with other free radicals to help scavenge them. They often consist of a five or six membered ring stabilized by methyl groups (Soule *et al.*, 2007). The unpaired electron is highly delocalized over the nitrogen and oxygen atom, making them stable even at room temperature (RT) for many days (Likhtenshtein *et al.*, 2008). The general structure of nitroxides is shown in figure 1.10.

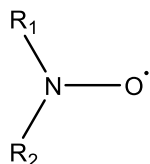
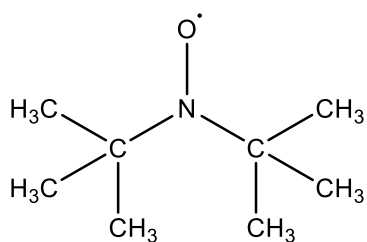
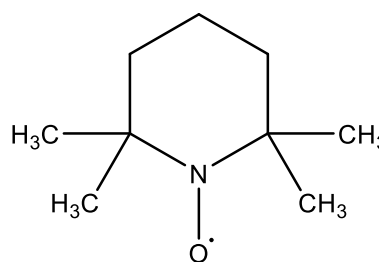


Figure 1.10 General structure of nitroxide.

Typically, inert groups like methylated carbon atoms are attached giving them stability as shown in Figure 1.11. 2,2,6,6-Tetramethyl-1-piperidinyloxy (TEMPO) and its derivatives are the most studied nitroxides. Structure of TEMPO is given in Figure 1.11 (b).



(a) (Di-*tert*-butylamino)oxidanyl



(b) TEMPO

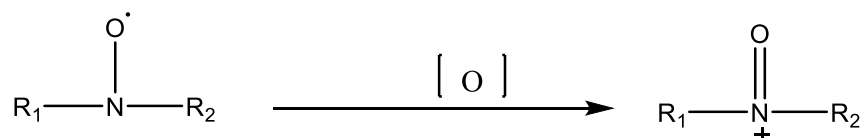
Figure 1.11 Structure of nitroxides (a) (Di-*tert*-butylamino)oxidanyl (b) (2,2,6,6-tetramethylpiperidin-1-yl)oxyl (TEMPO)

Nitroxides can undergo both oxidation and reduction, but in the presence of ascorbic acid, nitroxides reduced rapidly (Scheme 1.11). A nitroxonium ion is produced when nitroxide undergoes oxidation in the presence of the strong oxidising agent (scheme 1.12) (Janzen *et al.*, 1985).





Scheme 1.11: Reduction of a nitroxide radical



Scheme 1.12: Oxidation of a nitroxide radical

Nitroxides are the most studied spin labels and make a stable non-radical compound when reacting with a free radical (scheme 1.13) (Hideg, Kalai and Sar, 2005). They can act as reporter group when inserted at a specific site in large biomolecules. Labeled site emit exclusive EPR signals giving dynamical information about biological molecules (Guzzi and Bartucci, 2015). Because of their stability and paramagnetic properties, they have been used as spin trapping agents for a long time to detect free radicals (Wang, Lei and Wu, 2005).



Scheme 1.13: Trapping of radical by nitroxide and formation of the stable radical adduct

Nitroxides have shown promising benefits as a class of spin traps. However, some of the benefits other than spin trapping abilities are as follows:

### 1.9.3.1 Inhibiting the generation of Fenton-type radicals:

Nitroxides can accept an electron from reduced metal complex to prevent the generation of hydroxyl radicals in the Fenton-type system (Mitchell *et al.*, 1990).



### 1.9.3.2 Inhibition of lipid peroxidation

As discussed earlier, lipid peroxidation can cause cellular injury. Lipid peroxidation has three phases i.e. initiation, propagation, and termination. Generally, antioxidants inhibit the initiation step thus retarding the propagation of a chain reaction. Nitroxides may be considered as antioxidants because by participating in redox reaction they can break the chain at all three stages thus providing more protection (Miura, Utsumi and Hamada, 1993).

### 1.9.3.3 Protection against radiation-induced radicals

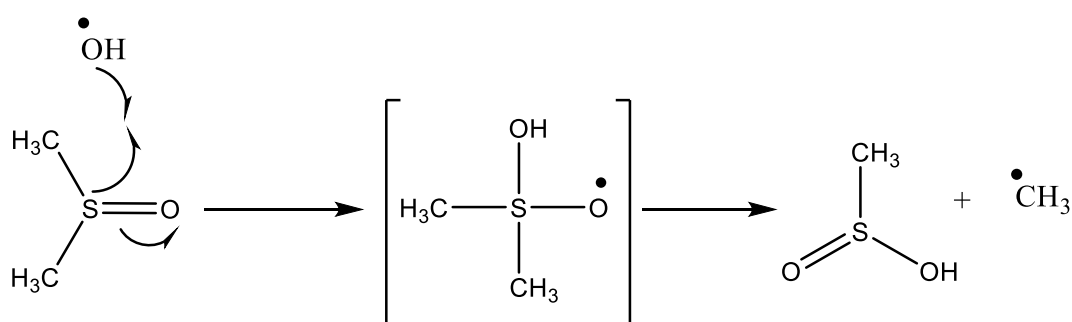
Ionizing radiation produces hydroxyl radicals from water. These primary radicals can react with other chemical species and biologically important molecules to produce secondary radicals. These secondary radicals with a lifetime of microseconds may be very damaging to the cells. Nitroxides not only help in scavenging the free radicals but also in chemical repair by restoring damaged target molecules (donation of hydrogen atom is an interaction to do this). Radical-radical recombination reactions are another detoxification pathway to eliminate free radicals (Soule *et al.*, 2007).

### 1.9.3.4 Mutagenicity

Nitroxides are free radicals by nature which gives rise to the concern about them as potential mutagens. 4-hydroxy-TEMPO (TEMPOL) as a model was investigated for mutagenicity. Studies showed that TEMPOL is neither mutagenic nor cytotoxic. Interestingly, chromosomal aberrations were reversed by this nitroxide in radiation exposed lymphocytes (DeGraff *et al.*, 1992a; DeGraff *et al.*, 1992b).

### 1.9.4 Secondary spin trapping

It is not easy to detect short-lived hydroxyl radicals directly since they have a half-life of less than a second. A secondary radical trapping technique is generally employed to identify and quantify this most reactive species. In this technique, the  $\cdot\text{OH}$  radical reacts with a compound like dimethyl sulfoxide (DMSO) to form methyl ( $\cdot\text{CH}_3$ ) and methoxy radicals ( $\cdot\text{OCH}_3$ ) which will make more stable compounds/radicals when spin traps like 2,2,6,6-Tetramethyl-1-piperidinyloxy (TEMPO) or PBN are used. In the Fenton reaction, excess DMSO is added before reaction starts so that  $\cdot\text{OH}$  produced reacts readily with it to form  $\cdot\text{CH}_3$  radicals (Scheme 1.14). Methyl radicals then react with a spin trap to form methyl adduct which is stable enough to be detected using analytical techniques such as HPLC-MS (Janzen *et al.*, 1990), GC-MS (Mistry *et al.*, 2008) and MALDI-TOF-MS (Podmore *et al.*, 2013).



Scheme 1.14: The reaction of a hydroxyl radical with DMSO to produce a methyl radical (Jerzykiewicz *et al.*, 2011).

Isotopically labelled DMSO has been used to confirm the identity of the radical adduct where normal DMSO is replaced with a deuterated analogue. Mass spectra of normal and deuterated versions are compared to interpret data for the identification of adducts formed (Burkitt & Mason, 1991). Based on this established technique, instead of DMSO other organic compounds like acetaldehyde may be used in the Fenton reaction to generate secondary radicals.

Various analytical techniques are used to detect and analyse free radicals. Every method has its own pros and cons. Before discussing analytical techniques in detail, it is worth

looking at sample extraction techniques i.e thermal desorption (TD) and solid phase microextraction (SPME) used in the current project.

## **1.10 Extraction approaches**

It is not possible to inject the products of the Fenton reaction directly onto a GC column as the reaction is carried out in an aqueous medium which can damage the column. In addition, direct injection onto an HPLC column will lead to rapid degradation of the column. Thus, analytes need to be extracted prior to separation on a column. Extraction of the analytes into a suitable solvent such as chloroform is laborious, time consuming, will often lead to loss/decomposition of target analytes and is a multi-stage process with more chances of contamination leading to errors (Kuanglin *et al.*, 2013; Koning, Janssen and Brinkman, 2009). In addition, it is not easy to couple directly traditional methods of sample preparation with techniques such as GC. A lot of work has been done in past two decades on sample preparation techniques for GC analysis. The main aims of developing new sample preparation techniques are for better isolation of analytes from solid phase during separation and improved detection for molecules of interest (Koning, Janssen and Brinkman, 2009).

It is beyond the scope of this thesis to discuss the pros and cons of every sampling technique, however, for reviews showing their benefits and limitations see Kuanglin *et al.*, 2013; Koning, Janssen and Brinkman, 2009.

### **1.10.1 Thermal desorption (TD)**

#### **1.10.1.1 Introduction and history**

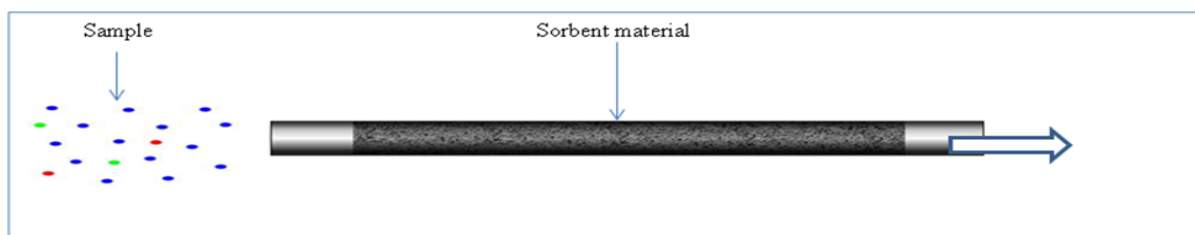
The history of TD goes back to the mid-1970s. Initially, injector liners packed with sorbent material were used for sampling air or gas and then inserted back into the GC inlet for the analysis. Loss of highly volatile compounds and contamination from the liner were among some of the disadvantages. Purge and trap GC methods were developed by the US Environment Protection Agency (EPA) to measure volatile organic compounds (VOCs) in drinking water (Li, 2010).

During the late-1970s a group from UK scientists (known as WG5) worked on the development of thermal desorption as a sampling approach, which had better sensitivity than conventional approaches used at that time. In 1981, PerkinElmer developed ATD 50 addressing all the issues faced by WG5. They were able to quantitatively analyze a wide range of compounds (Kristensson & Widen, 1987).

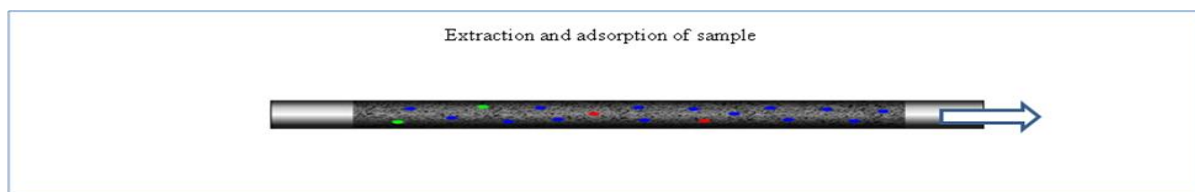
#### **1.10.1.2 General principles**

Thermal desorption units include a trap (sorbent tubes) which can be used to collect the samples. These are heated for the release of adsorbed compounds to be analyzed by GC/MS. Sampling with this solvent free approach can be done in minutes or even in seconds (Woolfenden, 2010). The headspace of the sample is extracted in sorbent tube after the required concentration is achieved. The sample can be extracted multiple times if the concentration of the analyte is low. This helps to achieve the required sensitivity/detection limit. Sorbent tubes are heated at high temperatures in a thermal desorber connected with GC. Retained volatiles and semi-volatiles from the tube desorb and are carried to GC using carrier gas (Woolfenden, 2012). Steps involved in adsorption and desorption are shown in Figure 1.12.

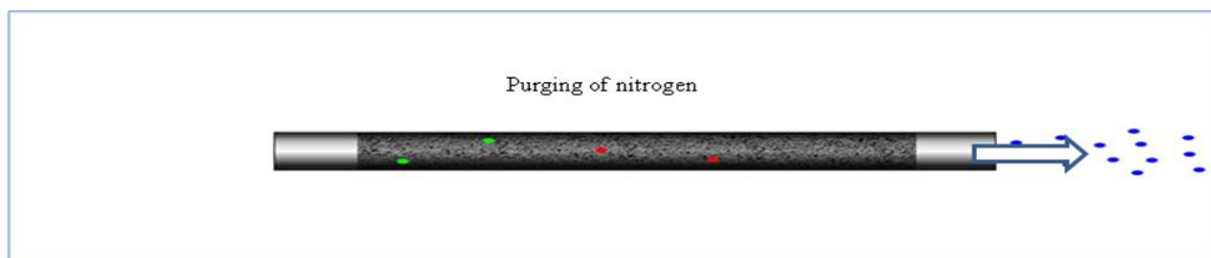
A



B



C



D

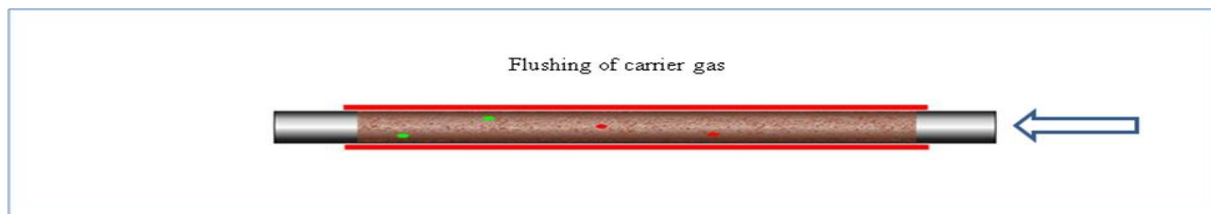


Figure 1.12: Steps of adsorption and desorption of molecules on sorbent material: (A) sample and internal view of sorbent tube; (B) adsorption of a compound of interest on sorbent material; (C) purging of nitrogen through sorbent tube; (D) the carrier gas is flushed in a reversed flow to desorb molecules of interest (Hebestreit, 2011).

Desorption is a two-step procedure i.e. primary and secondary desorption. The tube is heated for a certain amount of time to desorb the volatiles from the tube, which is then transferred to a cold trap. During secondary desorption, the cold trap is heated rapidly which transfers the compounds to the GC column. By using two stages, problems like peak broadening can be avoided as volatiles will enter the column at once (because of rapid temperature rise) during the secondary desorption. A diagrammatic view of primary and secondary desorption is shown in Figure 1.13.

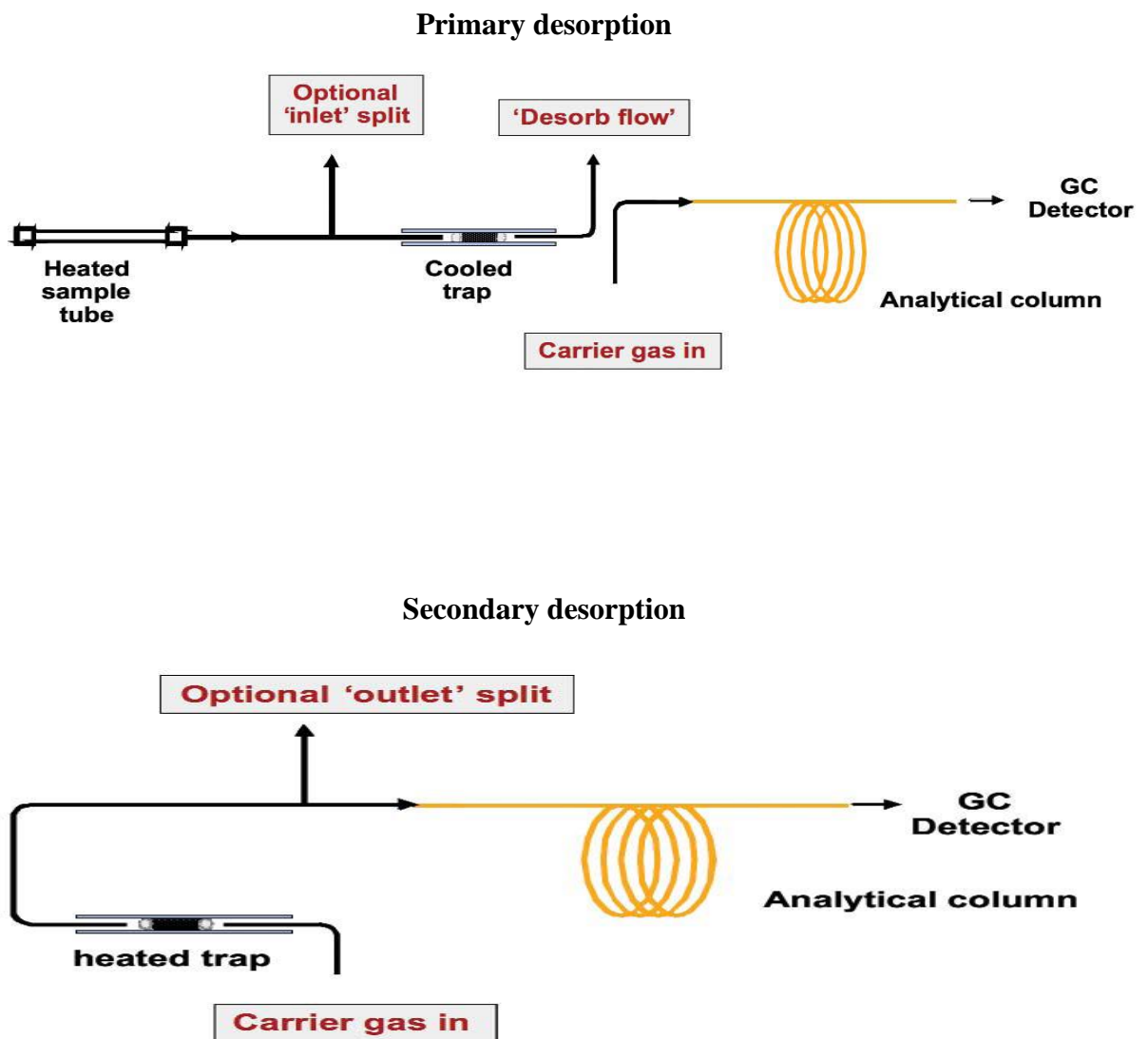


Figure 1.13: A diagrammatic view of primary and secondary desorption (Plant and Keen, 2007)

### **1.10.1.3 Advantages**

#### **1.10.1.3.1 Desorption efficiency**

It is possible to transfer more than 95% of the extracted sample to GC for analysis which is of great advantage as compared to conventional liquid-liquid extraction where generally only a microliter of the milliliter extract is being injected (Woolfenden, 2012). High recovery of analytes is achieved by the fact of continuous purging from sorbent tube as soon as retained sample enters the vapour phase by increasing the temperature. Contrary to this, in liquid extraction approaches the analyte molecules are partitioned between the vapour (HS), the solvent and the sorbent (extracting material) which limits the desorption efficiency to a maximum of 75% (ISO 16200-1).

#### **1.10.1.3.2 Extraction efficiency**

The compound of interest and type of interference can affect the efficiency of extraction in traditional approaches eventually effecting sensitivity. For example, extraction of polar compounds in the presence of moisture can lower the extraction efficiency to 20-30% (Callan, Walsh & Dowding, 1993). This can lead to false results when samples are collected from the field and the analyst has no information about the water level.

#### **1.10.1.3.3 Reduced solvent interferences**

The solvent can interfere when extraction is done by traditional approaches. Some of the common issues include masking of the peak of interest (i.e. having the same retention time as the peak of interest) and solvent and base line interferences. As TD is a solvent free approach so all the above-mentioned disadvantages can be avoided.

#### **1.10.1.3.4 Exposure risk**

Many commonly used extraction solvents are potentially a health and safety hazard. By using TD, all risks related to solvent can be avoided thus leading to the safer working environment.

#### **1.10.1.3.5 Low Cost**

Although sorbent tubes are expensive as compared to traditionally used charcoal tubes, they can be used around 100 times. In addition, they have advantage of being cleaned



automatically by TD thus having longer lifetime which in turn reduces the cost per analysis (Woolfenden, 2012).

#### **1.10.1.4 Applications of TD**

Thermal desorption can be used for air monitoring in an occupational place (Grote and Kennedy, 2002), breath sampling for potential diagnostic biomarkers (Phillips, 1992, Gordon *et al.*, 1985), off line sampling of the outdoor environment (Ras *et al.*, 2009), measuring semi-volatiles in wine & fruit juices (Lee *et al.*, 2011), forensic labs (Jones, 2000; Carter *et al.*, 2003), measuring low molecular weight esters produced in fruit (Agelopoulos and Pickett, 1998), pollutants in the air (Vu *et al.*, 2018, Juillet *et al.*, 2014), VOCs in dairy (Rabaud *et al.*, 2002) and other food products (Dong *et al.*, 2013), It may be also be used to identify different compounds in tobacco smoke (Savareear *et al.*, 2017), VOCs from industrial exhaust gas (Huilian *et al.*, 2017), narcotics and explosives traces (Forbes *et al.*, 2017), contamination in soil (Zhao *et al.*, 2016), aerosols from electronic cigarettes (Rawlinson *et al.*, 2017), volatiles in edible oil (Cacho *et al.*, 2016), flavour compounds in grilled beef (Ruan *et al.*, 2015), ink dating (Koenig *et al.*, 2014), detecting biomarkers for chronic kidney disease (CKD) (Grabowska-Polanowska *et al.*, 2013) and VOCs from automobiles (Cheng-ping, 2011).

#### **1.10.2 Solid phase microextraction (SPME)**

Solid Phase Microextraction (SPME), as the name indicates, is an extraction technique. It was invented by Janusz Pawliszyn and, in last decade, it has gained much importance for the sampling a wide variety of analytes from liquids, solids, and gases (Spietelum *et al.*, 2010).

The fiber assembly and holder are the two main parts of the SPME device (figure 1.14). Fiber assembly has a retractable (1-2 cm) fiber (Vas & Vekey, 2004) contained in a modified syringe (Zhang and Pawliszyn 1993; Lord & Pawliszyn 2000). The septum is pierced through by SPME needle to extend the fiber into the vial (figure 1.15). The fiber is exposed for a pre-determined time according to the experimental protocol for achieving an equilibrium (Merkle, Kleeberg and Fritsche, 2015).

### **1.10.2.1 Working principle**

A polymeric sorbent or an immobilized liquid is coated on a silica fiber as a thin layer (5-100 $\mu$ m) is used as a stationary phase helping to absorb/desorb the analyte (Spietelum *et al.*, 2010). There are two types of SPME fibers, absorption, and adsorbent type. In absorbent type fibers, the analyte is extracted by its partitioning into a liquid-like phase while in adsorbent type; physical interaction will be used to extract the analyte (Luks-Betlej *et al.*, 2001).

### **1.10.2.2 Sampling techniques**

Based on the type of fiber, there are two categories of sampling, immersion and headspace (HS) sampling. As the name indicates there is exposure of the fiber in the headspace above the sample for HS sampling whilst the fiber is immersed in the aqueous phase to extract the analyte in the case of immersion type sampling (Lord and Pawliszy, 2000). HS sampling works well for low molecular weight analytes and temperature enhances extraction (Kirkbride *et al.* 1998). Direct immersion (DI) has not been used to the same extent, however recently it has been used successfully for food analysis (Naccarato and Pawliszyn, 2016). The SPME technique is based on analyte partitioning between the sample and stationary phase (coated fiber). Time and temperature of the sample to equilibrate, fiber exposure time, and temperature of the sample before and during extraction and time of head space saturation are some of the factors by which HS-SPME is affected (Lona-Ramirez *et al.*, 2016).

### **1.10.2.3 Polydimethylsiloxane (PDMS) coating**

PDMS is an immobilized liquid at the extracting temperature and is the most extensively used sorbent in SPME analysis. Although it is a non-polar phase it can be used to extract polar compounds as well. It can easily be identified in MS because of its known decomposition products as it is commonly used stationary phase in GC. Other advantages of PDMS are its thermostability and inertness. Analytes interact with the sorbent and can easily be desorbed thus ruling out their decomposition (Baltussen, Cramers and Sandra, 2002)

Extraction of polar analytes may be enhanced by combining polar and non-polar materials (Alpendurada, 2000), for example, Carboxen/Polydimethylsiloxane (CAR/PDMS) and Divinylbenzene/ Polydimethylsiloxane (DVB/PDMS) are more polar than coating containing only polar material and this is the reason why these fibers are used to extract polar molecules like alcohols and ethers. Mechanical stability also increases by using the homogenous mixture of adsorbents (Penalver *et al.*, 1999). These fibers have been used to detect various volatile analytes in a variety of samples (Laguerre *et al.*, 2007; Zeng *et al.*, 2008; Bryant and McClung, 2011).

#### **1.10.2.4 Analytical techniques and SPME**

SPME is used extensively for the analysis of organic compounds because of its convenience to combine the pre-concentration and sampling steps (Lindholm *et al.*, 2014). It has been used successfully for the analysis of food (Jelen, Majeher and Dziadas, 2012), wine (Lona-Ramirez *et al.*, 2016), environment samples (Vidal *et al.*, 2009), drugs (Kataoka, 2010), in clinical investigations (Bojko *et al.*, 2012, Monteleone *et al.*, 2012, Naccarato *et al.*, 2014) and to determine compound toxicity (Pragst, 2007).

In the past two decades, this very sensitive sampling technique has been combined with other techniques like GC-MS (Hu and Chen, 2009; Luo *et al.*, 2009; Griglione *et al.*, 2015), gas chromatography (Krogh, Grefslie and Ramsussen, 1997; Vita, Abdel-Rehim and Nilsson, 2005), LC-MS (Caris, Chaves and Queiroz, 2012; Bojko, Vuckovic and Cudjoe, 2011), and HPLC-UV (Rajabi *et al.*, 2013; Buszewski *et al.*, 2011) for the separation and analysis of the different analytes.

SPME interfaced with LC has had little attention from researchers. This is largely due to longer equilibration times, no automation system and a lack of commercially available interfaces (Merkle, Kleeberg and Fritsche, 2015)

#### **1.10.2.5 Advantages and Disadvantages of SPME**

Like any other technique, SPME has many pros and cons. There is a partial loss of fiber coating in conditioning step which can result in extra peaks during analysis (Psillakis and kalogerakis, 2001; Lindholm *et al.*, 2014). Bending of the needle, the limited lifetime of the fiber, which is mechanically weak as well, not being cost-effective, low selectivity

and limited availability of fibers (Dietz, Sanz and Camara, 2006) are some other challenges faced by this technique.

Although SPME has some disadvantages it is still one of the most reliable sampling technique. It is a solvent-free approach which is not only rapid and sensitive but also provides linear results for many analytes and over a wide range of concentration. It also avoids the losses that occur during traditional extraction procedures (Nerin *et al*, 2009). SPME is considered as an eco-friendly technique and has been presented as a greener alternative to other extraction methods (Pena-Pereira *et al.*, 2015). Operational simplicity, time efficiency, the possibility of automation and can be directly linked to an analytical instrument like GC are some of its other advantages (Spietelun *et al.*, 2010).

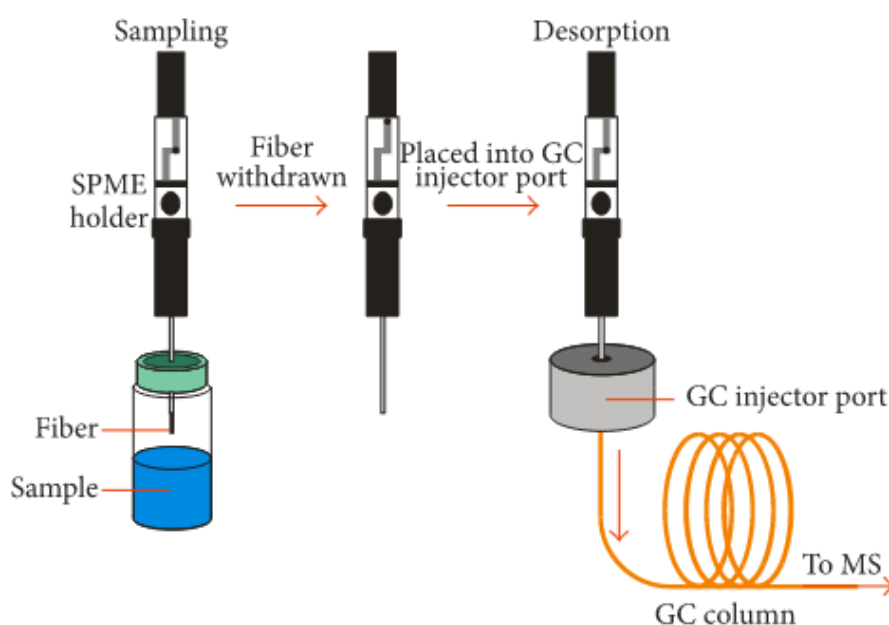


Figure 1.14: Diagram of analysis with solid phase microextraction gas chromatography-mass spectrometry (SPME-GC-MS) (Schmidt and Podmore, 2015)

## **1.11 Analytical techniques and spin trapping**

Various analytical techniques have been used to study spin trapped free radicals. An overview of their working principle, pros and cons and important work is outlined in this section.

### **1.11.1 Electron Paramagnetic Resonance spectroscopy and spin trapping**

Electron Paramagnetic Resonance (EPR) spectroscopy also known as Electron spin resonance (ESR) spectroscopy or Electron Magnetic Resonance (EMS) spectroscopy is the most commonly used technique to detect stable free radicals in biological & chemical systems (Davies, 2016; Janzen and Nutter, 1998). The principle of EPR lies in electromagnetic radiation absorption by paramagnetic species, placed in a magnetic field. Depending on the type of species, radiation absorption occurs at a specific frequency (microwave region) and magnetic field combination, producing lines at different regions of the magnetic field (Davies, 2016). An unpaired electron behaves like a small magnet because of its spin which could be either  $+1/2$  or  $-1/2$ . Two energy levels will be created when the unpaired electron is exposed to the external magnetic field. When exposed to electromagnetic radiation, the electron resonates between the energy levels and thus an absorption spectrum is produced.

Spin trapping is a traditional method to identify the radical adducts by using EPR (Janzen and Nutter, 1998). Radical adducts of nitrones/nitroso are EPR active and thus can easily be detected. The EPR signal intensity can be affected by a number of factors like oxidation and reduction of radical/radical adducts in the system (Swartz, Khan & Khramtsov, 2007).

In a study in 1997, high power UV radiation was used to produce acetaldehyde derived radicals, which were further trapped by PBN and detected by EPR. Irradiation of deoxygenated acetaldehyde with direct sunlight produces PBN-acetyl adducts whereas acetoxyl ( $\text{CH}_3\text{CO}_2^\cdot$ ) radicals were trapped when oxygenated acetaldehyde was irradiated (Jenkins *et al.*, 1997). In another study, DMPO was used as a spin trap to detect PUFA derived alkoxyl radicals. Computer simulation was performed to identify the radical adducts, as it was difficult to interpret the data because of overlapping EPR spectra (Dikalov and Mason, 2001). Stolze and his colleagues used the Fenton system to produce

linoleic acid derived radicals in the presence of DMPO. Computer simulation was used to interpret the data and three radical adducts were identified including hydroxyl and acyl adducts of DMPO. All three adducts were detected successfully when 5-(Diethoxyphosphoryl)-5-methyl-1-pyrroline-N-oxide (DEPMPO) was used as spin trap instead of DMPO (Stolze, Udilova and Nohl, 2000).

Hydroxyl radicals were used to oxidize DMSO, thus producing methyl and methoxy radicals which were further detected by EPR as PBN adducts. Initially, the methyl adduct of PBN was in abundance but with time signals for PBN-methoxy adduct became more prominent. Breakdown of PBN by the attack of hydroxyl radicals also produced MNP which was detected as MNP-CH<sub>3</sub> and MNP-*tert*-butyl adducts (Jerzykiewicz *et al.*, 2011). In another study, hydroxyl adducts of DMPO and PBN were identified while di-*tert*-butyl nitroxide was detected by using MNP as a spin trap by using EPR (Spulber & Schlick, 2010).

The EPR spectrum of the spin adduct is helpful in detecting the original radical but it is difficult to identify overlapping EPR spectra when a mixture of spin adducts are under analysis or spin adducts are unknown (Janzen, Krygsmann & Haire, 1988). Free radicals in biological systems are not only short lived but low in concentration as well, which makes it really difficult to detect them by using EPR (Jerzykiewicz *et al.*, 2011; Swartz, Khan & Khramtsov, 2007). Furthermore, species with unpaired electrons can only be detected by this method (Davies, 2016).

When coupled with HPLC-MS (or tandem mass spectrometry) EPR provides more detailed information (Steven, Yi & Yan, 2012). From the hyperfine splitting it is possible to classify the type of radical but often no structural information is obtained (Tian *et al.*, 2007). Many radicals have a similar pattern of hyperfine splitting making interpretation difficult. In addition, signals are unstable and become weak with time. This has led to the need for alternative approaches to identify free radicals (Ste-Marie *et al.*, 1996).

### **1.11.2 Spin trapping- Nuclear Magnetic Resonance (ST-NMR) spectroscopy**

During 1995, Tordo and his co-workers synthesised 5-diethoxyphosphoryl-5-methyl-1-pyrroline-N-oxide (DEPMPO), a phosphorous containing analog of DMPO. By taking the advantage of phosphorus (<sup>31</sup>P) in the structure, a new technique called nuclear

magnetic resonance (NMR) spin trapping (ST) was introduced to study the radical reaction and degradation pathway of radical adducts (Khramtsov *et al.*, 1999).

It is difficult for paramagnetic adducts to accumulate in a reducing environment of biological systems. To overcome this limitation spin trapping with NMR (ST-NMR) was used in the late nineties. It was demonstrated that diamagnetic products formed by the decay of spin trapped radical adducts (paramagnetic species) can be identified by NMR. These diamagnetic adducts are stable enough to be accumulated up to NMR detectable levels (Khramtsov *et al.*, 1999). Detection of stable diamagnetic products makes ST-NMR a valuable tool for spin trapping studies in biological systems (Zoia and Argyropoulos, 2010).

Multiple resonances of more commonly used nuclei i.e.  $^1\text{H}$  and  $^{13}\text{C}$  can be avoided by using spin traps containing  $^{31}\text{P}$  or  $^{19}\text{F}$ . Any molecule which is a stable diamagnetic adduct can be used potentially for ST-NMR, unlike EPR where nitroxides are the only choice (Khramtsov and Clanton, 2011).

Many oxygen and carbon-centered radicals were detected using  $^{31}\text{P}$  ST-NMR. Stable radical adducts were produced by using the nitron, 5-diisopropoxy-phosphoryl-5-methyl-1-pyrroline-N-oxide (DIPPMPO) and detected and identified by using  $^{31}\text{P}$  NMR. EPR detectable paramagnetic radical adducts were produced when free radicals reacted with this spin trap. These paramagnetic adducts have shorter half life and dissociate into stable diamagnetic species which can be further quantified by using ST-NMR giving more details about the structure of the radical adducts (Zoia and Argyropoulos, 2010; Zoia *et al.*, 2011).

Selinsky and co-workers suggested the use of  $^{19}\text{F}$  to get insight about spin trapped radical adducts. They successfully detected *in vitro* organic free radicals but were not able to extrapolate the method because of the low level of free radicals in biological systems. Low concentration of radical adducts results in paramagnetic broadening of NMR spectrum which in turn made its use difficult for the detection of spin trapping studies (Berliner *et al.*, 2002).

### **1.11.3 Liquid Chromatography (LC) and spin trapped free radicals**

LC-MS has the advantage over GC-MS in that the radicals may be analysed in an aqueous solution. It means LC-MS can be used to identify spin adducts which are not

volatile. LC-EPR has been used successfully to identify linoleic acid-derived radicals trapped by nitrosobenzene (Iwahashi *et al.*, 1991). MS combined with LC and using either EPR or Thermospray (TSP) was used to identify and characterize methanol and ethanol-derived free radicals in the Fenton system. Deuterated methanol and ethanol were used to confirm the structure of carbon-centered free radicals (Iwahashi *et al.*, 1990).

Parker and his co-workers (1991) used HPLC-ESI-MS to identify ethyl and pentyl radicals trapped by 4-POBN. Spin trapped radical adducts were not only identified but also proved as a powerful tool to determine their structure. A POBN-ethyl adduct was identified at  $m/z$  224 and a POBN-pentyl radical adduct at  $m/z$  266, which were confirmed by using HPLC-EPR technique (Parker *et al.*, 1991).

Cationic intermediates of radicals (multi-phenyl substituted) were detected and characterized successfully by using ESI-MS and ESI-MS/MS (Zhang *et al.*, 2005). Spin traps TEMPO and DMPO were used successfully to detect intermediates of radicals by ESI-MS. Cationic intermediates were detected at  $m/z$  260 for styrene and  $m/z$  274 for alpha-methyl styrene when TEMPO was used as radical trap while fluorine radicals and radical adducts were detected at  $m/z$  131, 132 and 152 with DMPO (Zhang *et al.*, 2006).

#### **1.11.4 Matrix Assisted Laser Desorption Ionisation time of flight (MALDI-TOF) mass spectrometry**

Matrix Assisted Laser Desorption Ionisation time-of-flight (MALDI-TOF) mass spectrometry is a soft ionisation technique developed for thermolabile and non-volatile compounds of higher molecular weight. It has been used successfully for the analysis of macromolecules like proteins and peptides. Single charged ions are produced which make the spectra much easier to interpret (Cohen & Gusev, 2002). As the name indicates matrices, which are low molecular weight compounds are used to aid the ionisation process. It is usually difficult to use “MALDI” for the analysis of low molecular weight compounds because of interference caused by matrix ions in the low mass range (Hashir *et al.*, 2007; Jing, Hao-Yang & Yin-Long, 2005). During the ionisation process, fragments and cluster ions of low molecular weight compounds are generated which can significantly mask the analyte signals thus limiting the analytical ability.



Previous studies include the trapping of  $\cdot\text{OH}$  radicals by DMPO which was then detected at  $m/z$  128 while using 2,5-dihydroxybenzoic acid (DHB) as a matrix using the MALDI-FTMS approach. Several radicals were identified with their structure and mechanism of formation by using this high throughput instrument (Tian *et al.*, 2007).

A secondary spin trapping technique was used to produce methyl radicals from hydroxyl radicals by using DMSO in a Fenton-type reaction as described earlier. POBN was used successfully as a spin trap for methyl radicals. POBN/dimethyl adducts were identified. Identification was confirmed by substituting DMSO with a deuterated analogue ( $\text{d}_6$ -DMSO) (Podmore, Cunliffe & Heshmati, 2013).

### 1.11.5 GC-MS and Spin trapping

GC-MS is another popular technique used to study free radicals. Each compound elutes from the column at a certain time which allows a more specific identification of spin-trapped adducts by mass spectrometry. Because of different molecular masses, different adducts can be recognised easily. Moreover, each adduct has a specific fragmentation pattern which provides more reliable identification. Several spin adducts can be identified in the same run by using mass spectrometric information of the molecular ion, isotope peaks, fragment ions and pattern of fragmentation (Abe, Suezawa & Hirota, 1984). A typical GC-MS is shown in figure 1.15 (Chromedia.org, 2015).

GC-MS in selected ion monitoring (SIM) mode has been used successfully to detect hydroxyl and 1-hydroxyethyl (1-HEt) radicals produced by the Fenton system. Hydroxyl and 1-Hydroxyethyl radicals were detected as DMPO-OH and DMPO-1HEt adducts when DMPO was used as a trapping agent in the presence of ethanol. The concentration of 1-HEt was low despite the varied amount of ethanol used. Ethanol adducts were detected more efficiently as PBN-1-HEt adduct by using PBN as trapping agent instead of DMPO (Castro and Castro, 2002).

Abe and co-workers used GC-MS to identify aryl and hydroxyl radicals. Adducts of hydroxyl radicals were generated by reacting sodium peroxodisulphate and water in the presence of nitron spin trap. Substituted phenyl azo triphenylmethane (PAT) was thermally decomposed to generate aryl radicals. Radical adducts were trimethylsilylated

to make them volatile and thermally stable, suitable for GC-MS analysis. Silylated spin adducts of hydroxyl and various aryl radicals were identified successfully in this study (Abe, Suezawa & Hirota, 1984). Methyl radicals produced by the reaction of DMSO and hydroxyl radicals generated chemically in Fenton system were detected by using POBN. A novel POBN-dimethyl adduct was identified by using GC-MS. This was confirmed by replacing normal DMSO with  $d_6$ -DMSO (Mistry *et al.*, 2008).

4-hydroxybenzoate and salicylates were used to trap free radicals. GC-MS and HPLC-EC (electrochemical detection) were used to identify the products. Hydroxyl radicals were successfully measured by using both methods with enhanced sensitivity compared to previous methods. While comparing different trapping agents, 4-hydroxybenzoate was much more sensitive than salicylates (Ste-Marie *et al.*, 1996).

The pesticide fenvalerate was irradiated using ultraviolet (UV) light source to produce free radicals which were trapped by PBN. These aminoxyl spin adducts were detected and analysed successfully by using GC-MS (Mikami *et al.*, 1985). Alkyl spin adducts produced by Grignard addition to PBN followed by oxidation of the resulting hydroxylamine were detected by using GC-MS. They successfully produced and explained the dimethyl adduct of the PBN (Janzen *et al.*, 1985). In addition, mass spectrometry was used to investigate the structure of hydrazyl-PBN adduct formed in microsome of rat livers (Ortiz de Montellano *et al.*, 1983).

GC-MS was used to analyse trimethylsilylated (TMS) PBN-methyl radical adduct (PBN-methyl OTMS) with a molecular ion at  $m/z$  265. Repeating the same experiment but using deuterated ( $d_3$ ) methyl confirmed the molecular ion at  $m/z$  268 (PBN-methyl- $d_3$  OTMS) thus proving it as a reliable procedure for the detection of spin trapped free radicals by using GC-MS. Silylated radical adducts gave strong signals as they are more stable. Also, isotopes of silicon may help to deduce the structure of a compound (Janzen *et al.*, 1988).

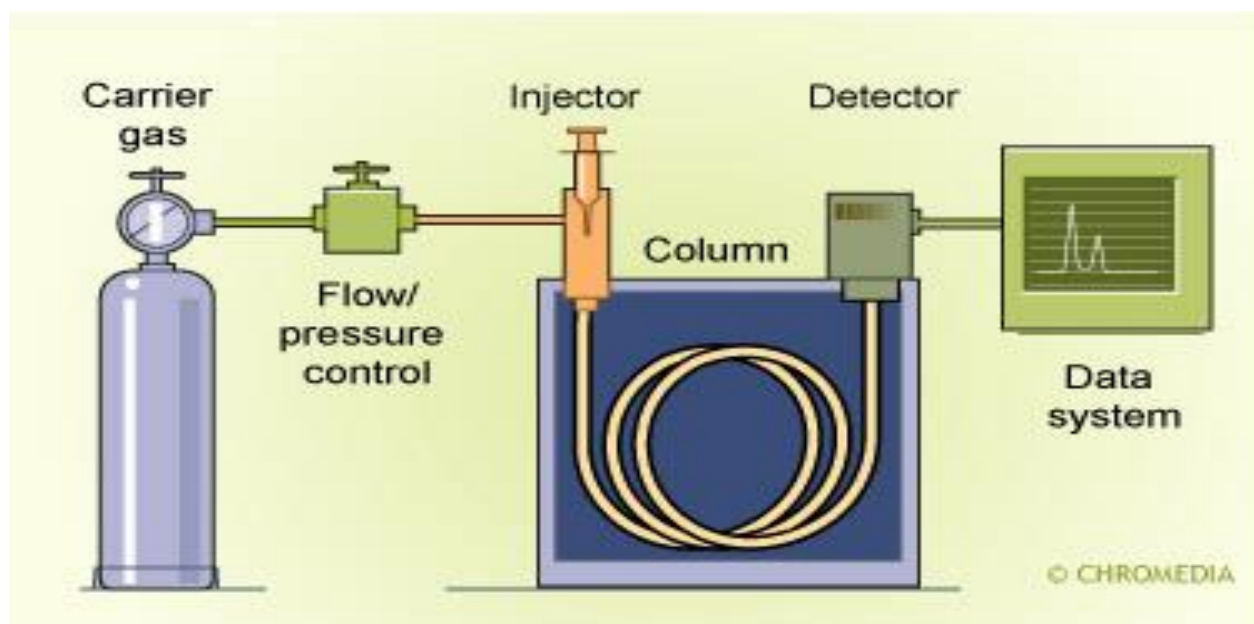


Figure 1.15: Schematic of a typical GC system (Chromedia.org, 2015).

## 1.12 Other biochemical assays to measure oxidative stress

### 1.12.1 Total antioxidant capacity (TAC)

Free radical damage is mediated by antioxidants thus the level of the antioxidant in biofluids has been used to measure the extent of oxidative stress. Measuring concentration of different antioxidants can give an idea about the level of oxidative stress but it is neither easy nor economical. Hence, an overall level of antioxidants known as TAC is measured. Secondly, the activity of enzymes like superoxide dismutase (SOD) which can convert free radicals into less toxic products can be useful to get an idea about risk reduction of disease by oxidative stress. The level of these two major groups i.e. low molecular weight antioxidants and enzymes like SOD, catalase and glutathione peroxidase decreases when oxidative stress increases (Young, 2001). Measurement of TAC in biofluids and tissues can be done easily which is a big advantage of this process (Somogyi *et al.*, 2007).

Another major *in vivo* radical scavenger, ascorbic acid has also been used as a biomarker of oxidative stress. Ascorbic acid is converted into dehydroascorbic acid when the cell is under oxidative stress. An elevated level of dehydroascorbic acid is indicative of oxidative stress and can be measured easily in biofluids (Lykkesfeldt, 2007).

Catalases, glutathione peroxidases and SOD are major enzymes of the antioxidant defence system. Measurement of these three enzymes together may be helpful to evaluate the antioxidant status of the cell. Various disorders have been associated with the change of activity of these enzymes (Halliwell, 2001). Another family of enzymes which is involved in the metabolism of carcinogens in the liver are glutathione S-transferases (GSTs). To protect the cell from electrophilic entities, they bind with them and neutralise their effects. GST has a potential to be used as a biomarker for oxidative stress in some cancers (Khan *et al.*, 2010).

Some important effects might be missed if only the level of individual antioxidants is measured. Similarly, variation in enzyme activity can make it difficult to measure antioxidant status. Simultaneous measurement of low molecular weight antioxidants and enzyme activity may potentially be used as an indication of oxidative stress (Lowe, 2014).

### **1.12.2 Flow cytometry**

Fluorescent probes like 2'-7'-Dichlorodihydrofluorescein diacetate (DCFH-DA) can be used for the detection of ROS at the cellular level. DCFH-DA is a non-fluorescent precursor of Dichlorodihydrofluorescein which can pass through the cell easily. Cleavage of DCFH-DA produces H<sub>2</sub>DCF, a non-fluorescent probe which is polar and thus not cell-impermeable. Highly fluorescent molecules of DCF are produced from H<sub>2</sub>DCF when the cell is under oxidation (Marrocco, Altieri & Peluso, 2017), which will accumulate thus increasing the fluorescence. The increase in fluorescence at 530 nm can be measured by using a flow cytometer which is assumed to be directly proportional to the level of H<sub>2</sub>O<sub>2</sub>. Hydrogen peroxide does not actually react with most molecules itself; it may form hydroxyl radicals which do (Eruslanov and Kusmartsev, 2009).

It is a sensitive technique which is not only easy to use but relatively inexpensive as well. A very simple technique where data is read by increase or decrease in fluorescence. The biggest advantage is no need for trypsinization of cells. When coupled with confocal

microscopy, cells can be viewed in real time which in turn can be helpful to understand the role of different cell organelles in oxidative stress.

On another hand, its main weakness is that it gives an idea about the general state of oxidative stress rather than measuring individual reactive oxygen species. Secondly, superoxide can be converted to hydrogen peroxide by SOD, which can result in accumulation of DCF in the cell. Lastly, hydrolysis of DCFH-DA requires esterases and some cells have limited esterase activity which in turn can affect the results (Eruslanov and Kusmartsev, 2009).

### **1.12.3 Assays measuring ROS induced modifications**

Reactive oxygen species can modify the molecules of DNA, protein and lipids which in turn affect the function of target molecules like enzymatic function inhibition.

#### **1.12.3.1 Measuring lipid peroxidation products**

Unsaturated double bonds in PUFAs make them highly susceptible to oxidative damage (Negre-Salvayre *et al.*, 2010). End products of LPO i.e. lipid hydroperoxides and secondary carbonyl compounds like aldehydes may be used as potential biomarkers of oxidative damage (Niki, 2018). The most investigated products are malondialdehyde (MDA) and 2-hydroxy-2-nonenal (HNE) while the long list of end products includes many aldehydes, alkanes and alkenes (Sousa, Pitt & Spickett, 2017).

LMW aldehydes may react with biological molecules especially DNA to form DNA-aldehyde adducts (Voulgaridou, 2011). 4-hydroxy-2-nonenal (4-HNE), malondialdehyde (MDA) and acrolein are some of the reactive aldehydes which can modify DNA bases thus leading to mutagenic and carcinogenic effects (Voulgaridou *et al.*, 2011). HNE can be detected directly by using HPLC coupled with electrochemical detector (Goldring *et al.*, 1993) or can be derivatised by using 2,4-dinitrophenylhydrazine followed by GC-MS detection (Zelzer *et al.*, 2015). In another study, HPLC-MS was used to correlate COPD and MDA levels. They found elevated levels of MDA in COPD patients when compared with healthy controls (Milevoj Kopčinović *et al.*, 2016). In many other studies levels of

MDA was elevated in patients with ovarian (Bandeubuche and Melinkeri, 2011), cervical (Looi *et al.*, 2008), oral (Beevi *et al.*, 2004) and breast cancer (Gupta *et al.*, 2012).

Thiobarbituric acid reactive substances (TBARS) assay is widely used to detect LPO products. In this assay, the major products of LPO i.e. lipid peroxides, MDA and other LMW aldehydes reacts with 2-thiobarbituric acid (TBA) to form compounds exhibiting a characteristic pink colour. A spectrophotometer is used to measure the concentration of the product formed and this is an indicator of oxidative stress. Although it is a most widely used assay, TBA is able to react with several compounds like albumin, sugars and amino acids, thus causing interference in measurements which can lead to misleading results (Dreissigacker *et al.*, 2010; Natarajan *et al.*, 2015).

The reaction of free radicals with PUFA of membrane phospholipids produces chemically stable F<sub>2</sub>-isoprostanes (F<sub>2</sub>-IsoPs) which can be used as a biomarker of oxidative stress (Diniz *et al.*, 2018). Although it is considered as one of the more reliable methods it needs costly instrumentation, i.e. GC-MS or LC-MS (Natarajan *et al.*, 2015).

Although measurement of F<sub>2</sub>-IsoPs in biofluids is a complex process but these small molecules might be used as potential biomarkers of oxidative stress (Van 't Erve, 2017).

### **1.12.3.2 DNA oxidation**

DNA modifications induced by oxidative stress includes oxidised nucleotides, a basic sites and formation of adducts. A variety of products are formed when DNA is attacked by hydroxyl radicals, of which the most common is 8-hydroxy-2'-deoxyguanosine (8OxodG) (Cadet *et al.*, 2003).

Addition of a methyl group to the cytosine ring resulting in the formation of 5-methylcytosine is one aspect of a process of DNA methylation which is a regular part of cellular differentiation in living organisms. This can inhibit the binding of transcriptional machinery (Jenuwain & Allis, 2001) which in turn results into preventing the gene expression, which might lead to the development of various pathological conditions (Lowe, 2014).

Oxidative stress related aberrant methylation of genes like the formation of 5-methylcytosine at the individual or multiple sites could possibly serve as a biomarker of

oxidative stress (Zukiel *et al.*, 2004; Menezo, 2016), although understanding of the methylation process needs more thorough investigation (Shenker & Flanagan, 2012).

Reactive products formed by ROS-induced damage of other macromolecules like lipids can also cause DNA damage, for example, producing etheno-DNA adducts which may also be used as indicators of oxidative damage (Li *et al.*, 2015).

### **1.12.3.3 Protein oxidation**

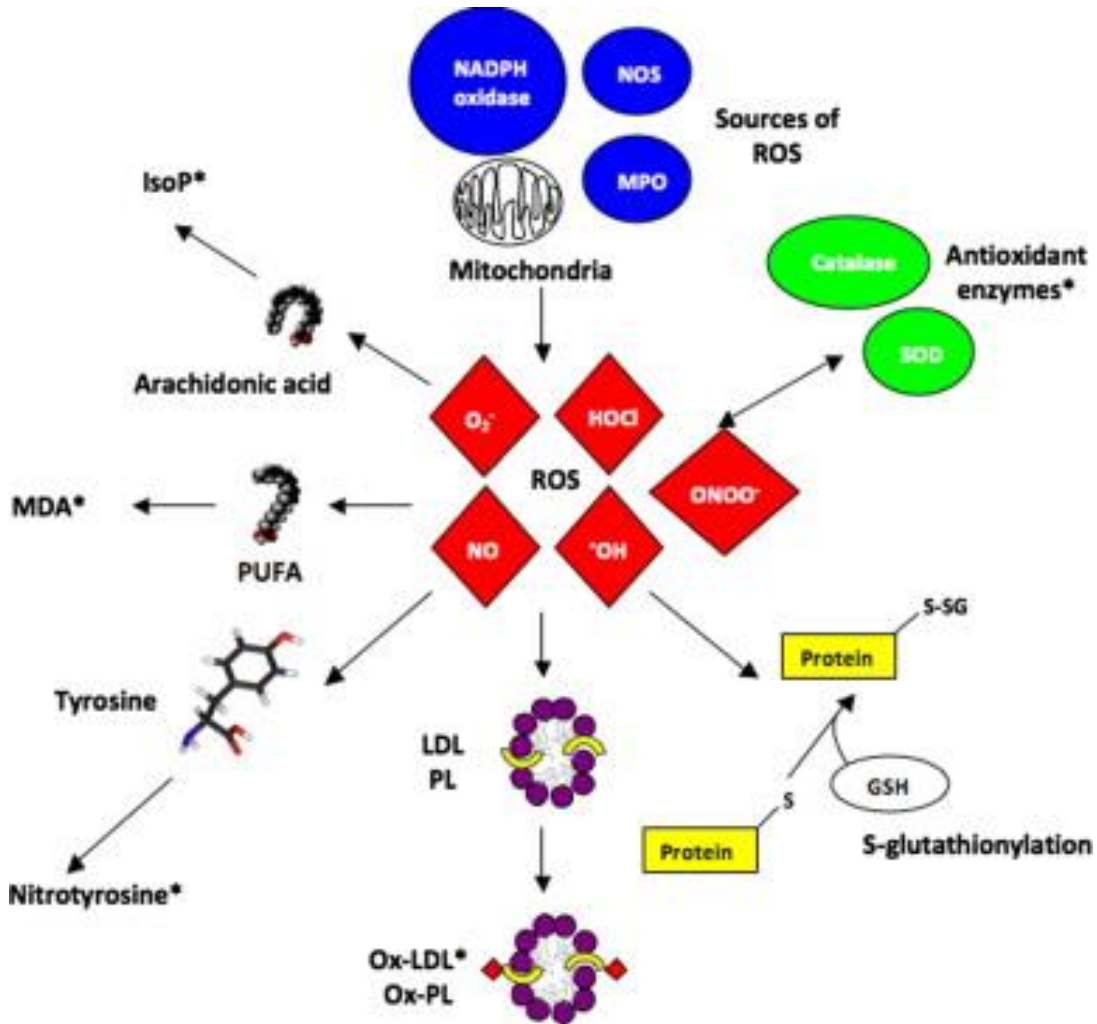
Oxidative modification of amino acids includes aromatic & aliphatic group hydroxylation, oxidation of residues containing sulfur and the modification of cysteine (Davies, 2016). Aggregation of oxidatively cleaved cross-linked proteins can also be the result of ROS damage to proteins (Hohn, Jung & Grune, 2014).

The high levels of carbonyls are also used as an indicator of protein damage which is considered as a most abundant by-product (Zinellu *et al.*, 2016). Carbonyls are produced by different mechanisms which include cleavage of the protein backbone and attack of hydroxyl radicals on some of the amino acids such as proline, lysine, arginine & threonine (Stadtman & Levine, 2003). Carbonyl compounds are relatively more stable thus can be measured easily but their levels not only increase with age but also in several pathological conditions which elevate them (Gil *et al.*, 2006; Sultana, Perluigi & Butterfield, 2006).

Protein carbonyl content (PCC) assay is used to measure the products of protein oxidation. The sample is incubated for one hour after the addition of 2,4-dinitrophenylhydrazine (DNPH) which, in turn, follows the addition of 50% (v/v) trichloroacetic acid (TCA). The supernatant is washed after centrifugation followed by incubation for 30 minutes at 60°C and then overnight incubation at room temperature. For each sample, a control tube is used and the absorbance at 370 nm measured and compared to evaluate the levels of oxidative stress. The drawback of this assay is the need to derivatise which is not only laborious but time consuming as well (Reznick & Packer, 1994).

Oxidative damage can change the three-dimensional structure of the protein, which in turn will change the biochemical properties. Many methods have been developed to

detect the modification of proteins but still their use as a biomarker is limited because there is no concrete method for the identification and quantification of protein modifications (Marrocco, Altieri & Peluso, 2017).



MDA- Malondialdehyde

GSH- Glutathione

IsoP- Isoprostanes

SOD- superoxide dismutase

PUFA-Polyunsaturated fatty acids

MPO-myeloperoxidase

LDL- low density lipoproteins

PL-phospholipids

NOS- nitric oxide synthase

NADPH-Nicotinamide adenine dinucleotide phosphate

SG- S-glutathionylation

Figure 1.16: Formation pathways of different biomarkers of oxidative stress (Ho *et al.*, 2013).



More relevant biomarkers are needed as the role of oxidative stress in many pathological conditions is still not clear. Oxidative injury may also be seen as a pre-disease stage like hepatitis B & C infections, diabetes and alcohol related disease. Biomarkers which can help identify the pre-disease stage could be beneficial for an early diagnosis of the disease. Although the discovery of oxidative stress related biomarkers is a complex their detection would help better understanding of underlying biology which in turn will be helpful in the diagnosis of various diseases (Lowe, 2014).

### **1.13 Aims and objectives of the research**

The primary aim of the current study is the separation and mass spectrometric analysis of spin trapped aldehyde free radicals by using *N-tert-butyl- $\alpha$ -phenylnitron* (PBN) and 2,2,6,6-tetramethyl-1-piperidinyloxy (TEMPO) and their derivatives as trapping agents. Gas chromatography-mass spectrometry (GC-MS) using headspace thermal desorption (TD) and solid phase microextraction (SPME) as extraction techniques will be used, having the advantage of being solvent free and much sensitive over traditional method of extraction.

Fenton chemistry will be used to produce hydroxyl radicals which will then react with aldehydes to produce free radicals. This secondary spin trapping may then be used to confirm the presence of the primary radical (hydroxyl in this case) as well as identify the radical adduct itself. Nitrones like PBN and nitroxides like TEMPO may be used to trap free radicals both in chemical and biological systems.

Electron paramagnetic resonance (EPR) spectroscopy, a traditional method used to detect spin trapped free radicals is not so useful for the detection of trapped free radicals, especially when they are unknown. This is because the stable nitroxide produced when the spin trap reacts with free radical gives limited structural information. In addition, the hydroxyl radical adduct of PBN and its derivatives are unstable and decay in seconds making them difficult to be identified and quantified by the spin trapping method. GC-MS provides an alternative to EPR for the detection and identification of spin trapped free radicals since chromatography will separate out the adducts and mass spectrometry may detect and characterize them (Mistry *et al.*, 2008).

Hydroxyl radicals generated by using the Fenton system react with aldehydes like acetaldehyde and propionaldehyde to generate methyl (Nakao *et al.*, 2000; Jenkins *et al.*, 1997) and ethyl radicals (Wang, Lei and Wu, 2005) respectively. In this study these radicals were trapped by nitroxides such as TEMPO and its derivatives or nitrones like PBN and its derivatives. Headspace sampling techniques were used as they are solvent free and more efficient than traditional solvent extraction – see earlier for discussion. Effectiveness of all these techniques and derivatives of TEMPO and PBN will be used for comparative study.

## Chapter 2

### Materials and Methods

## 2.1 Chemicals

Ethylene di-amine-tetra-acetic acid (EDTA), L-ascorbic acid, di-potassium hydrogen phosphate ( $K_2HPO_4$ ), N-*tert*-Butyl- $\alpha$ -phenylnitron (PBN), and propionaldehyde ( $d_2$ ) were purchased from sigma-Aldrich. Acetaldehyde- $d_3$  was purchased from CDN Isotopes, UK. Ammonium ferrous sulfate Hexahydrate  $Fe(NH_4)_2(SO_4)_2 \cdot 6H_2O$  was purchased from Fluka, Biochemika. Acetaldehyde, 30% (w/v) hydrogen peroxide ( $H_2O_2$ ), 2,2,6,6-Tetramethyl-1-piperidinyloxy (TEMPO), 4-Hydroxy-TEMPO, 4-Oxo-TEMPO and 4-Methoxy-TEMPO were purchased from Alfa Aesar, UK. All derivatives of the PBN were synthesised in the lab using the method of Hinton and Janzen (1992).

## 2.2 Reagent preparation for the Fenton reaction

The reagents were prepared at specific concentrations to give optimum generation of free radicals and adducts, as described previously (Mishra, 2016). The stock solutions were prepared by using distilled water in following concentrations:

100 mmole  $dm^{-3}$  potassium phosphate buffer (pH 7.4)

11 mmole  $dm^{-3}$  EDTA (sodium salt)

3% (w/v) hydrogen peroxide solution

100 mmole  $dm^{-3}$  ascorbic acid

10 mmole  $dm^{-3}$   $Fe(NH_4)_2(SO_4)_2 \cdot 6H_2O$

### 2.2.1 Standard conditions for the Fenton Reaction

A standard method was used throughout the experiment to generate and spin trap free radicals by using different spin traps (one at a time). Two main spin traps used were PBN and TEMPO. Their derivatives were used for the confirmation of the identified spin adducts. The Fenton reaction produces hydroxyl radicals which attack the secondary source of free radicals to produce secondary radicals with comparatively longer half-life.

Various sources (one at a time) of secondary radicals were used in the Fenton system, which is summarised in Table 2.1 with their volume.

Table 2.1: Volumes of different aldehydes used as a source of secondary free radicals generated in the Fenton reaction

| <b>A secondary source of free radicals</b>  | <b>Volume (<math>\mu\text{L}</math>)</b> | <b>Molarity (mM)</b> |
|---|--|----------------------|
| Acetaldehyde                                | 132                                      | 2.4                  |
| Deuterated acetaldehyde ( $\text{d}_3$ )    | 132                                      | 2.4                  |
| Propionaldehyde                             | 174                                      | 2.4                  |
| Deuterated propionaldehyde ( $\text{d}_2$ ) | 174                                      | 2.4                  |

The prepared reagents were added to a 25 mL beaker in a strict order as stated below:

100 mmole  $\text{dm}^{-3}$  phosphate buffer (pH 7.4) (5 mL),

11 mmole  $\text{dm}^{-3}$  EDTA solution (1 mL),

100 mmole  $\text{dm}^{-3}$  spin-trap compound (1 mL),

3% hydrogen peroxide solution (1 mL),

100 mmole  $\text{dm}^{-3}$  ascorbic acid solution (1 mL) and

Aldehyde (see table 2.1).

To initiate the reaction 10 mmole  $\text{dm}^{-3}$   $\text{Fe}(\text{NH}_4)_2(\text{SO}_4)_2 \cdot 6\text{H}_2\text{O}$  (1 mL) was added to the mixture. The reaction was left for 5 minutes with continuous stirring.

The aldehyde was introduced into the Fenton system to generate secondary radicals. Hydroxyl radicals produced during the Fenton reaction attacked the aldehyde to produce secondary radicals (the type of radical depending on a chain length of the aldehyde) i.e. methyl and ethyl radicals were produced in the presence of acetaldehyde and propanal respectively (demonstrated in chapters 3, 4 and 5).

### 2.3 Gas chromatography-mass spectrometry (GC-MS)

Gas chromatography (GC) is a technique used in analytical chemistry to separate, analyse and identify volatile compounds. Like any other chromatography technique, the stationary phase helps to separate the chemical entities. However, unlike other chromatography techniques the mobile phase (known as a carrier gas) does not take part in the separation, but merely transport the sample mixture through the column (Blumberg, 2012). Helium was used as the carrier gas in this study.

In the gas chromatograph (see figure 1.15) the sample is injected through the injection port, which has been set at a high temperature, typically 250°C, to vaporise the sample without dissociation. The carrier gas transfers the vapours of the sample to the column which is placed in an oven. The column is usually about 25-30 meters in length and internally lined with a liquid or solid stationary phase (Christian, 1994). Compounds will be retained by the stationary phase to different extents because of differences in their chemical properties. From the GC, through a transfer line, the separated compounds transfer to the mass spectrometer, which has three main parts: an ion source, a mass analyser and an ion collection system (figure 2.1). The ion source ionises the molecules which will then be separated by the mass analyser according to their mass-to-charge ( $m/z$ ) ratio. Finally ions are detected by the ion collection system and recorded in the form of a graph called a mass spectrum. The size of the peak and the amount of detected compound are generally directly related to each other i.e. higher amount of detected compound the more intense the peak, however this is not always the case. The most commonly used ion source is electron ionisation (EI) in which an electron beam from a heated filament is used to ionise the sample molecules. These high energy electrons remove an electron from a parent molecule thus converting it to a molecular ion ( $M^{+\bullet}$ ) which has a positive charge with an odd number of electrons (radical cation) as shown in following reaction (Christian, 1994).



A reaction showing the formation of molecular ion ( $M^{+\bullet}$ ), by removing an electron from a parent molecule (M) (Christian, 1994).

As the mass of an electron is negligible when compared to the parent molecule, the identification of the compound becomes easier since the molecular ion will have the same mass as the neutral molecule (assuming the charge  $z = 1$ ). The energy absorbed during the ionisation process can cause the molecular ion to break into fragments. Every compound has its own fragmentation fingerprint under certain EI conditions which can be used to identify the compound, a major advantage of mass spectrometry. The molecular ion with its fragmentation pattern is presented in the form of the mass spectrum.

In the present study, two different GC-MS systems were used. A Varian CP-3800 GC coupled with 1200 MS/MS mass spectrometer was used for SPME analysis whilst a PerkinElmer Turbomatrix 300 thermal desorber attached with Clarus 5800 GC and Clarus 800 MS was used for thermal desorption experiments.

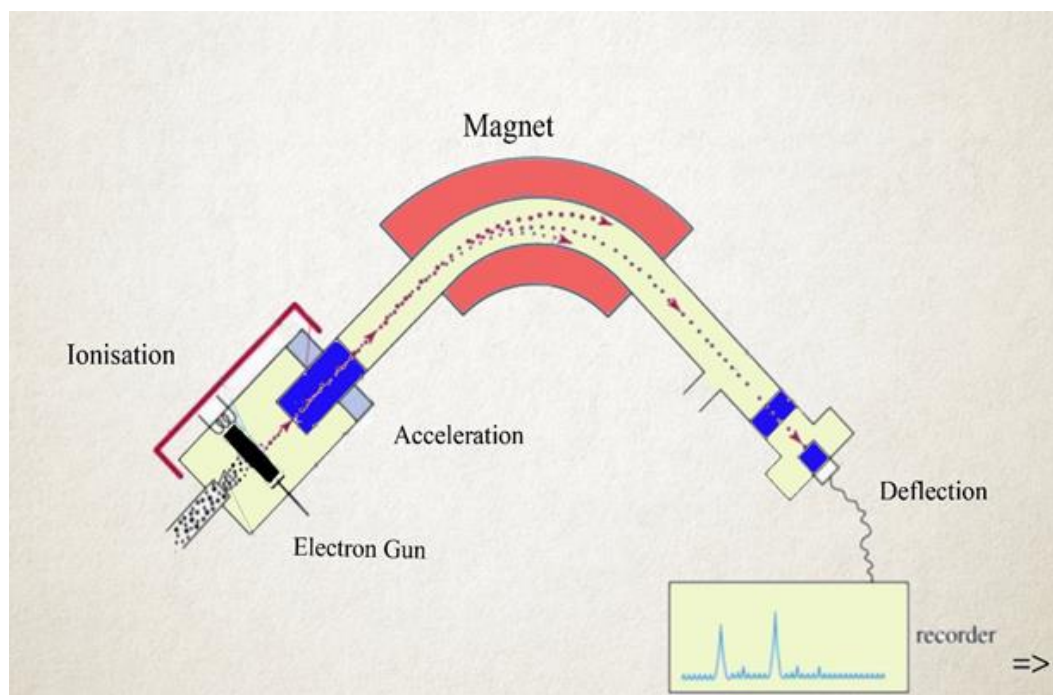


Figure 2.1: A schematic of mass spectrometer (adapted from Tring, 2018)

## **2.4 Extraction Techniques**

### **2.4.1 Headspace solid phase microextraction (HS-SPME)**

As described in Chapter 1, SPME is a solvent-free extraction technique in which sampling, isolation, and enrichment are achieved in a single step. In SPME, a fiber coated with the polymer is exposed to the headspace (HS) above the sample for several minutes to achieve equilibrium between the sample and fiber coating. Once equilibrium has been established, the extracted quantity will remain constant (Lord and Pawliszyn, 2000).

The fiber is then transferred into the GC-MS for the analysis. Different products including spin trapped free radicals are desorbed when the temperature is increased. This is known as thermal desorption. After desorption, analytes are carried onto the GC column for separation and then further detection according to their mass/charge ( $m/z$ ) ratio by MS (figure 2.1). For this study, a carboxen-polydimethylsiloxane (CARB/PDMS) SPME fiber of 75  $\mu\text{m}$  was used with needle size of 23 ga (Supelco, UK) to extract radical adducts.

### **2.4.2 Thermal desorption gas chromatography mass spectrometry (TD-GC-MS)**

The Fenton reaction solution carried out in a beaker (9.1mL) was transferred to 40 mL vial which was set aside for 3 minutes for headspace saturation. Easy-VOC pump (Markes International, UK) was used to extract the headspace as shown in figure 2.2. SVI<sup>TM</sup> sorbent tubes were used for sampling which were conditioned before the analysis. The collected headspace volume was set at 50 mL and the pump released after 30 seconds so that analytes have enough time for adsorption.

At least one “blank” (i.e. headspace in a vial with no sample) was taken after each analysis to remove any carry over from the previous sample.





Figure 2.2: Sampling of headspace by using Easy-VOC

## 2.5 Instrumentation for current study

### 2.5.1 Solid-phase microextraction gas chromatography-mass spectrometry (SPME- GC-MS)

As mentioned earlier, for SPME analysis Varian GC (GC-3800) was coupled with a Mass Spectrometer (1200). Data handling was done by using the application package for a Varian workstation. The GC column used for separation of the analytes was 30 meters in length with a diameter of 0.25 mm and film coating thickness of 0.25  $\mu\text{m}$ .

The SPME fiber was conditioned before first use according to the supplier instructions. Optimized extraction time (exposure of fiber in the HS) was 3 minutes and then analytes on the fiber were desorbed for 5 minutes at 250°C into the injection port, operated in splitless mode. Standard GC conditions used throughout the experiment were gas flow rate 1 mL/minute, oven temperature 100°C for 10 minutes which was increased to 320°C by 15°C/min and held for 1 minute. The scan range for the electron ionisation (EI) mass

spectra was 50-500 m/z. A photomultiplier voltage of 900 V was used to detect the generated ions.

### **2.5.2 Thermal desorption gas chromatography-mass spectrometry (TD-GC-MS)**

A Turbomatrix 300 thermal desorber (Perkin Elmer, UK) was used to extract the adsorbed analytes from the sorbent tubes. A sorbent tube with adsorbed analytes was loaded and purged for 5 minutes by using oxygen-free nitrogen gas (BOC, UK). Primary desorption was conducted at 330°C for 5 minutes. This step removes adsorbed analyte from the sorbent tube and takes them to the GC by using helium as a carrier gas, where separation takes place according boiling point and interaction with the stationary phase. This separation was conducted by using Clarus 5800 gas chromatograph (Perkin Elmer, UK) which was equipped with a Restek capillary column using mainly polydimethylsiloxane as the stationary phase (Rtx-5). The capillary column was 30 meters in length with a diameter of 0.25 mm and film coating thickness of stationary phase was 0.25  $\mu\text{m}$ .

The initial column temperature was set at 100°C for 5 minutes and was set to increase at 5°C/minute to 150°C and finally to increase until 300°C by 40°C/minute and held for 2 minutes. Electron ionisation mass spectra were obtained from scan range of 45-500 m/z.

## **2.6 GC-MS method development**

Free radicals were produced by using Fenton chemistry as detailed earlier in the chapter. A series of experiments was carried out to validate the Fenton system. Acetaldehyde was used as a secondary source of free radicals for the development and validation of the method. Standard conditions described in section 2.4.2 were used to develop a method. Although it is well established and one of the most studied reactions, it was necessary to develop a method to optimise the conditions.

## 2.6.1 The Fenton reaction in the presence of a secondary source of radicals

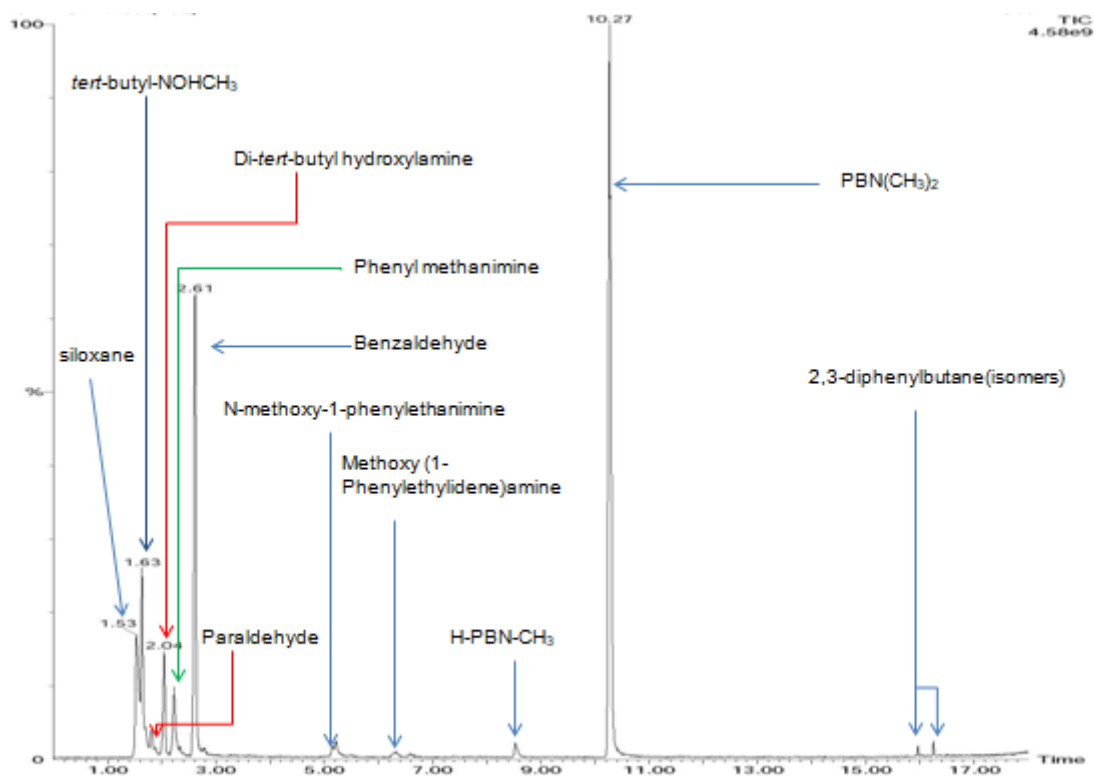


Figure 2.3: The total ion chromatogram (TIC) for the standard Fenton reaction in the presence of acetaldehyde. For identification of peaks see chapter 3.

GC-MS analysis of the Fenton reaction by using acetaldehyde as a secondary source of free radicals was carried out under standard conditions mentioned in section 2.3. Many different peaks are shown which are identified and explained in chapter 3.

Various control experiments were performed to identify the products of the Fenton reaction and the source of free radicals.

## 2.6.2 Control reaction (Buffer & PBN)

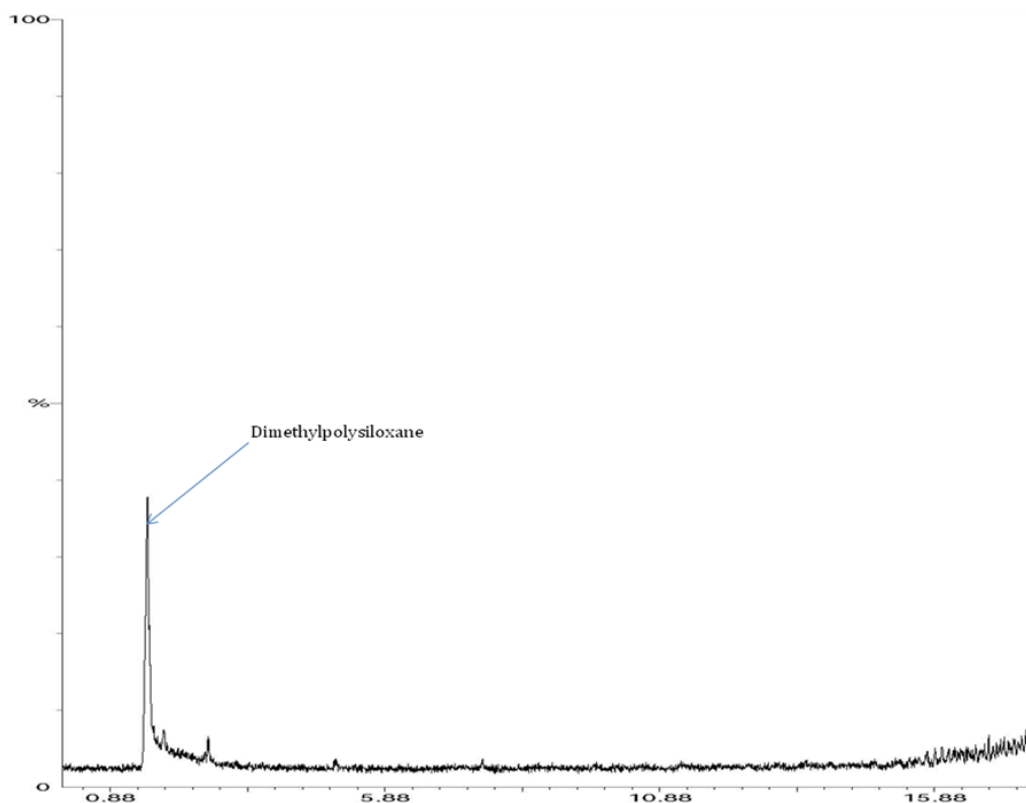


Figure 2.4: The GC-MS TIC when PBN (spin trap) was stirred in a phosphate buffer (pH 7.4) and extracted using VOC pump for thermal desorption analysis

A very important control was carried out by stirring PBN in the buffer for five minutes under standard conditions (at room temperature with continuous stirring). The EI-mass spectrum of peak retained at 1.53 minutes was identified as dimethylpolysiloxane following a search on mass spectral library of National Institute of Standards and Technology (NIST). It is coming out because of a column bleed (i.e. very slight breakdown of the stationary phase). Since the peak has been identified it can be eliminated.

### 2.6.3 Buffer, PBN & acetaldehyde

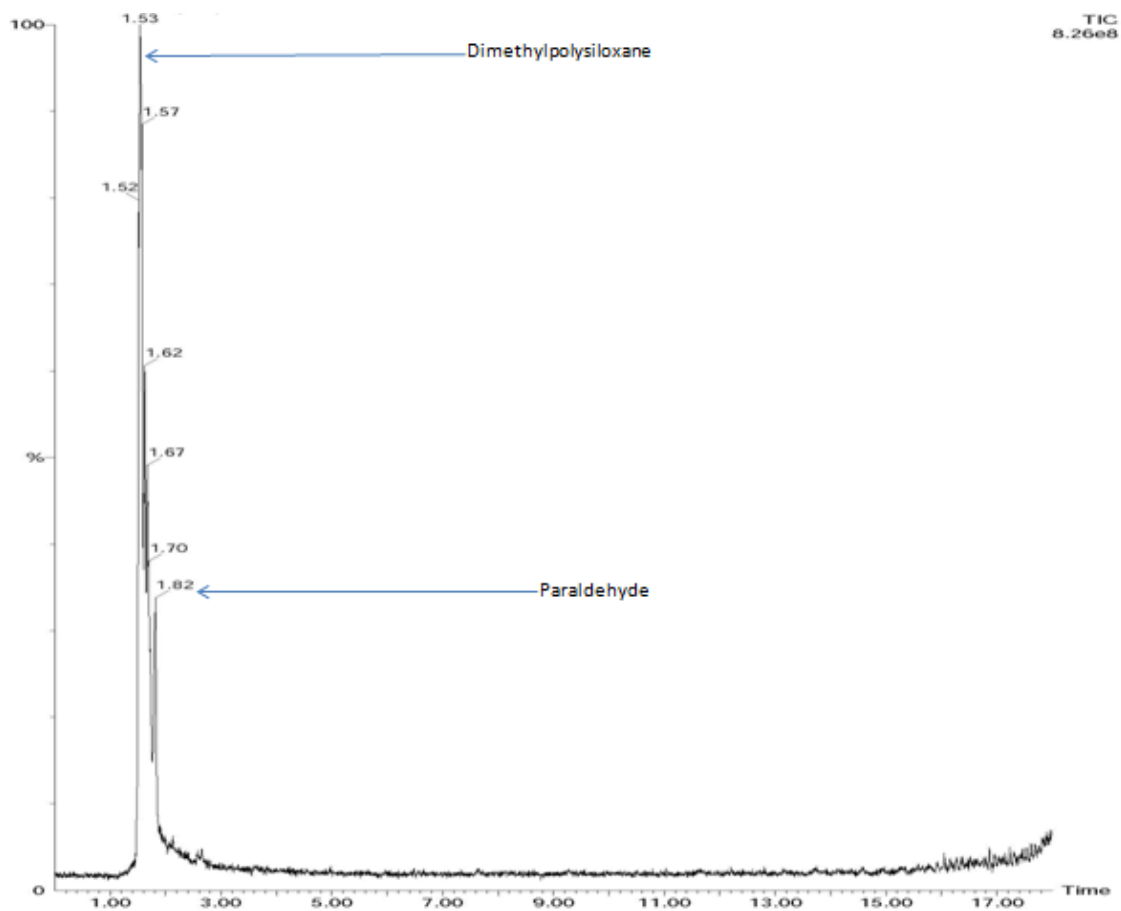


Figure 2.5: The GC-MS TIC when PBN (spin trap) with acetaldehyde was stirred in a phosphate buffer (pH 7.4) and extracted using VOC pump for thermal desorption analysis.

This control was carried out to determine if any peaks in the chromatogram from fig. 2.3 were derived from acetaldehyde other than those from it behaving as a secondary source of free radicals in the Fenton reaction. In addition to dimethylpolysiloxane, a peak, retained at 1.82 minutes, was identified as paraldehyde by comparison to the NIST library (see chapter 3). This control indicates that these are not the products of the Fenton reaction.

## 2.6.4 Comparison of the Fenton reaction with controls

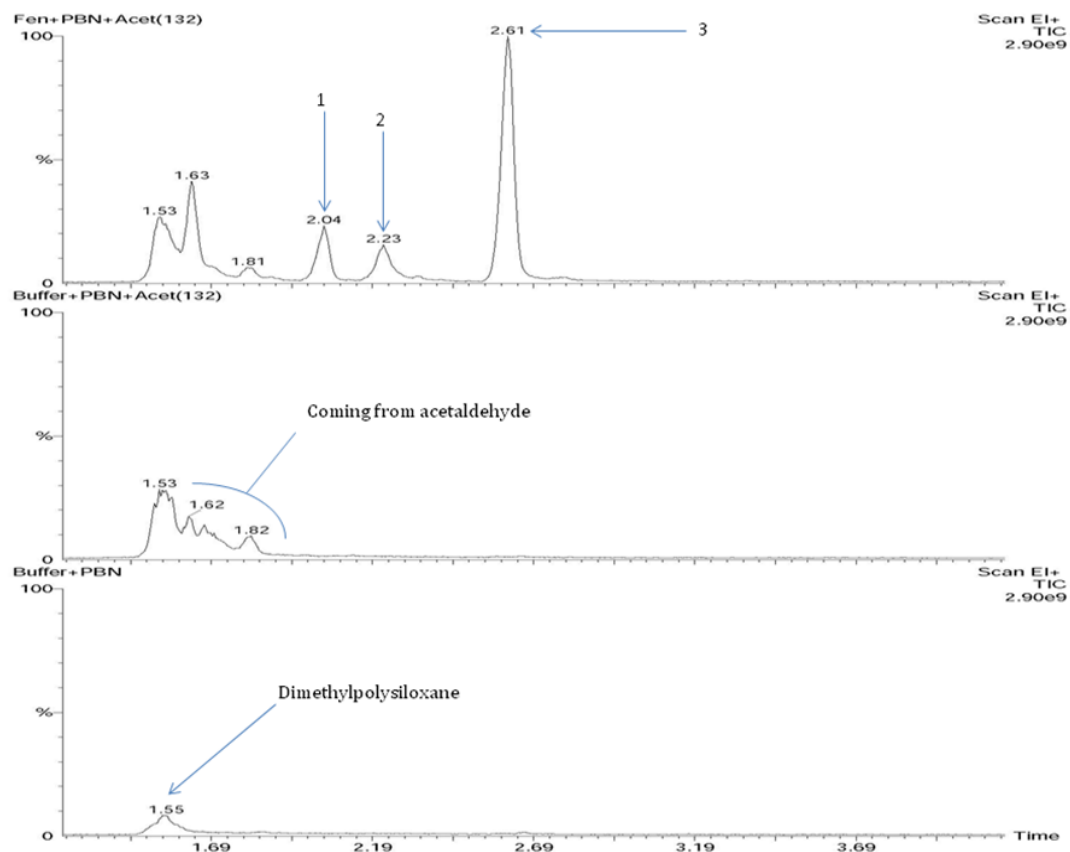


Figure 2.6: Comparison of gas chromatograms of control samples with the Fenton reaction ( $R_t$  1-4 minutes). Chromatograms shown are [(Buffer and PBN), (Buffer, PBN and acetaldehyde), (Fenton reaction when acetaldehyde was used as secondary source of radicals)], from bottom to top respectively.

The gas chromatogram of the Fenton reaction (figure 2.3) compared with controls showed that initial peaks are not products of the Fenton reaction. Peaks eluting at  $R_t$  2.04, 2.23 & 2.61 minutes represented as 1, 2 and 3 are di-*tert* butyl hydroxylamine, phenyl methanimine and benzaldehyde. These are produced as a result of Fenton chemistry. These are peaks of interest which are identified by looking into respective mass spectra (see section 3.6-3.8 in chapter 3 for the detailed analysis).

## 2.6.5 Analysis of the Fenton reaction containing the spin trap PBN carried out in the absence of a secondary source of free radicals

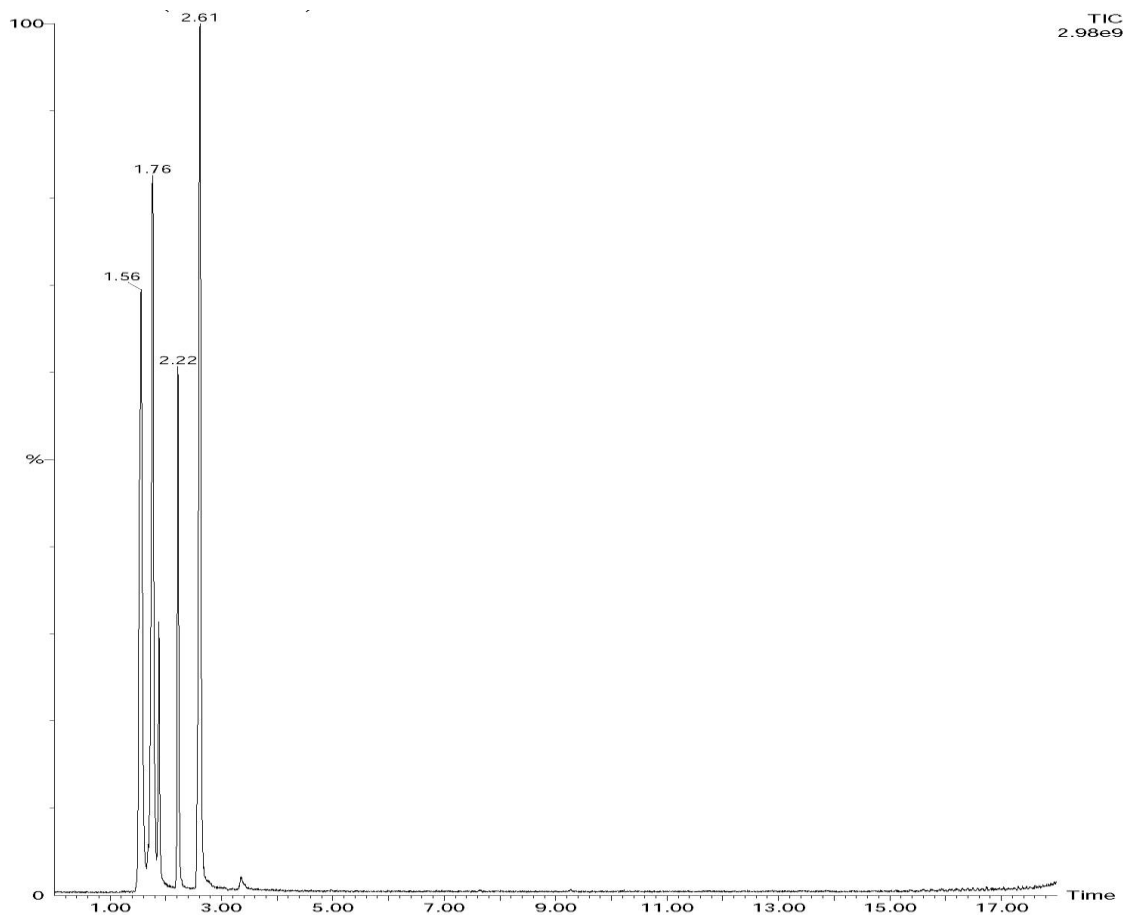


Figure 2.7: The GC-MS TIC of the Fenton reaction containing the spin trap PBN carried out in the absence of a secondary source of radicals showing five peaks.

To confirm the generation of spin-trapped free radicals in figure 2.3 from acetaldehyde, the Fenton reaction was carried out in the absence of a secondary source (i.e. acetaldehyde). Hydroxyl radicals produced during the Fenton reaction reacts with PBN at the  $\alpha$ -carbon atom to break it down and produce different adducts which are identified as tert-butylaminoxyl-CH<sub>3</sub> ( $R_t$  1.56 minutes), di-tert-butyl hydroxylamine ( $R_t$  2.04 minutes), phenyl methanimine ( $R_t$  2.22 minutes), benzaldehyde ( $R_t$  2.61 minutes) – see chapter 3 for EI-mass spectra and peak identification.

### 2.6.6 GC-MS analysis of the Fenton reaction in the absence of PBN

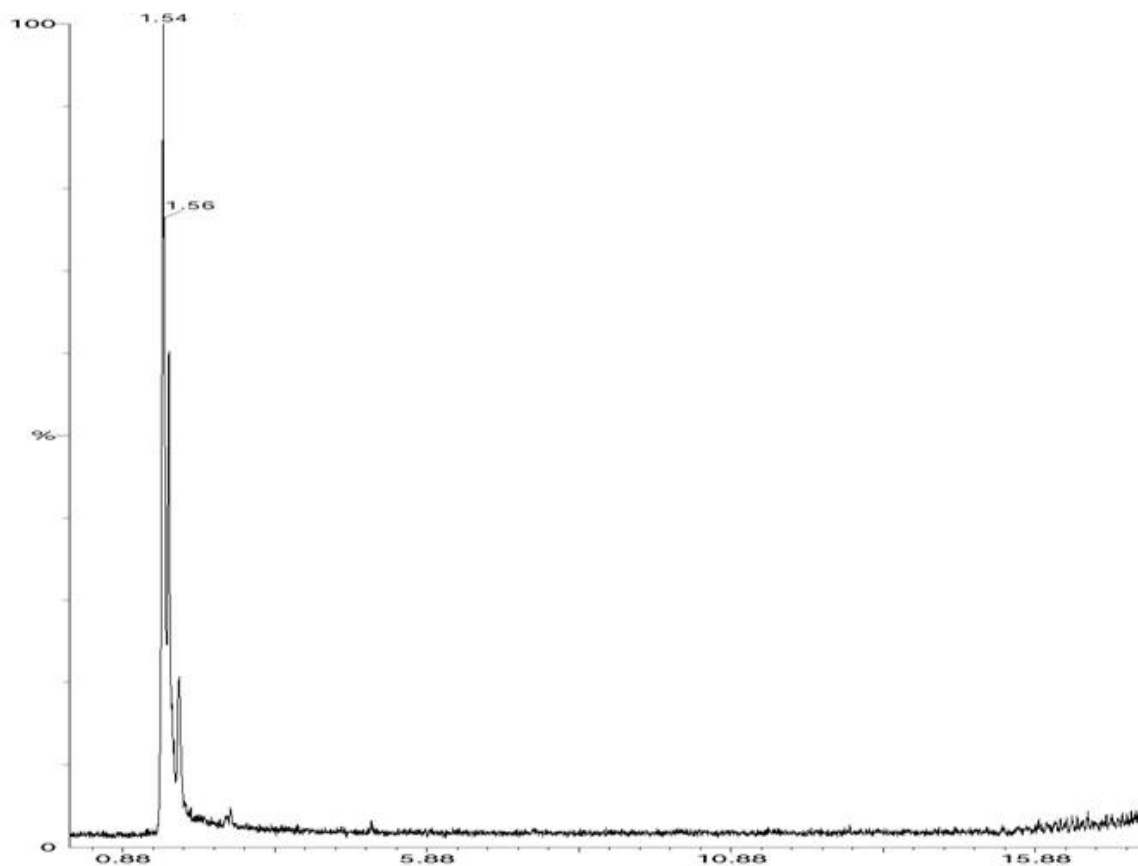


Figure 2.8: Gas chromatogram when the Fenton reaction was carried out without PBN showing only dimethylpolysiloxane peak.

The GC-MS TIC generated following sampling of the Fenton reaction in the absence of spin trap is shown in figure 2.8. While looking at corresponding mass spectrum (data not shown), peak retained at 1.54 minutes is identified as dimethylpolysiloxane (from the column). The result demonstrates that all peaks in the chromatogram of the Fenton reaction (Figure 2.3) are derived from PBN, except those that are present in this chromatogram.



### 2.6.7 Analysis of the Fenton reaction containing the spin trap PBN but carried out in the absence of $\text{Fe}^{2+}$ and ascorbic acid

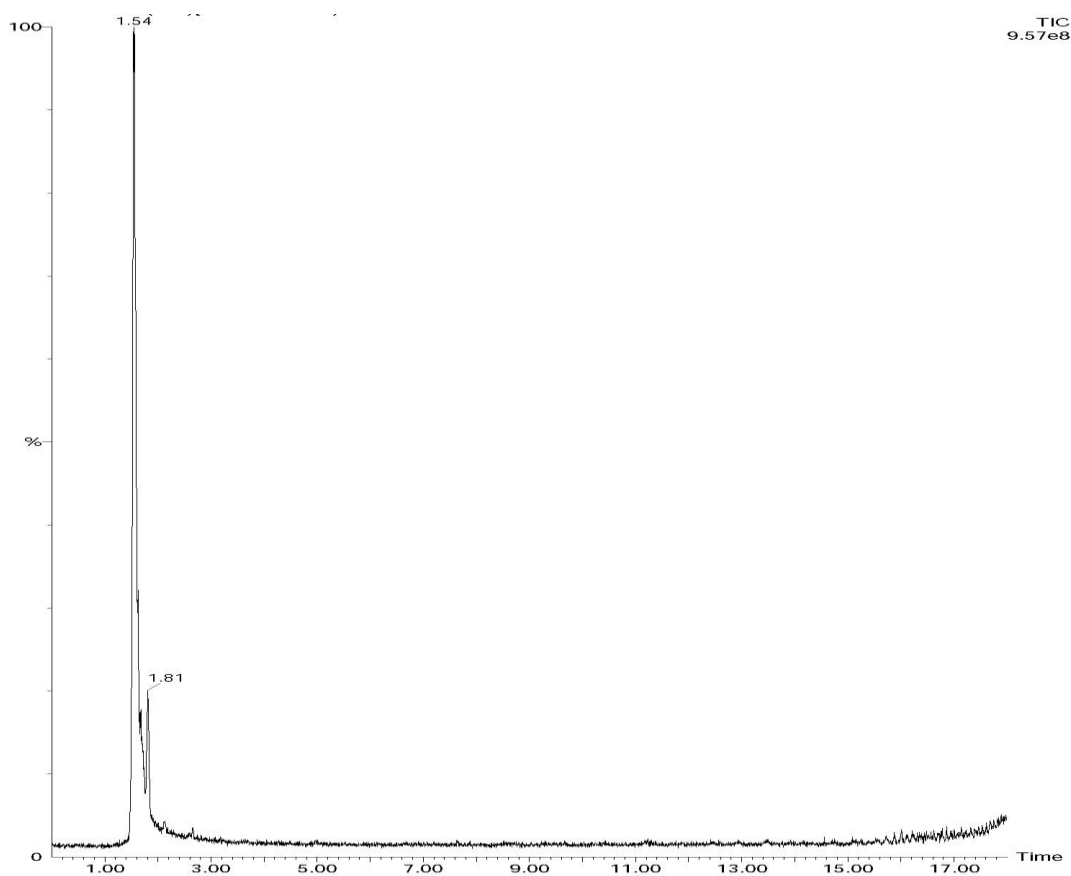


Figure 2.9: The GC-MS total ion chromatogram for the Fenton reaction containing the spin trap PBN but carried out in the absence of  $\text{Fe}^{2+}$  and ascorbic acid showing dimethyl polysiloxane and paraldehyde retained at 1.54 and 1.81 minutes respectively.

In the Fenton reaction  $\text{Fe}^{2+}$  reduces hydrogen peroxide to generate hydroxyl radicals which may then react with compounds like acetaldehyde to form secondary radicals. Ascorbic acid acts as a reducing agent which converts  $\text{Fe}^{3+}$  to  $\text{Fe}^{2+}$ , thus a continuous supply of  $\text{Fe}^{2+}$  is maintained during the reaction which in turn increases the yield of hydroxyl radicals.

To confirm the importance of ascorbic acid and  $\text{Fe}^{2+}$ , the Fenton reaction was carried out in the absence of these chemicals. The GC-MS TIC shows peaks which are also present in other control experiments, demonstrating, as expected, that ascorbic acid and  $\text{Fe}^{2+}$  play a significant role in the Fenton reaction.

## 2.6.8 Analysis of the Fenton reaction containing the spin trap PBN but in the absence of H<sub>2</sub>O<sub>2</sub>

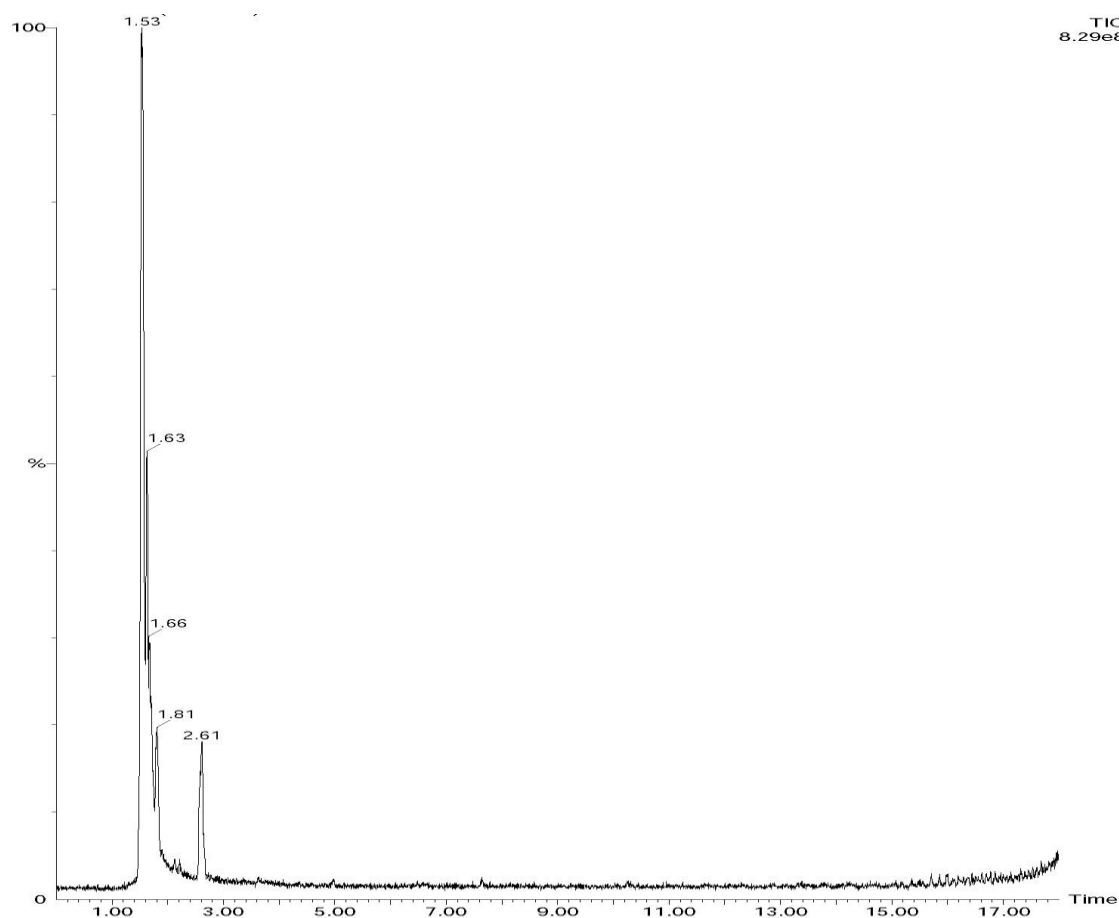


Figure 2.10: GC-MS total ion chromatogram for the Fenton reaction containing the spin trap PBN but carried out in the absence of H<sub>2</sub>O<sub>2</sub> showing dimethylpolysiloxane, paraldehyde and benzaldehyde retained at 1.53, 1.81 and 2.61 minutes respectively.

The source of hydroxyl radicals in the Fenton reaction is H<sub>2</sub>O<sub>2</sub> which may then react with a secondary source (e.g. acetaldehyde) to produce secondary radicals (e.g. methyl). To confirm this, the Fenton reaction was carried out in the absence of H<sub>2</sub>O<sub>2</sub> while keeping all other conditions same. Only one new peak is generated, at R<sub>t</sub> 2.61 minutes, and has been identified as benzaldehyde, formed by the breakdown of PBN – see chapter 3 for EI-mass spectra and identification. Since the TIC does not show any other peaks, when compared to figure 2.3, it is clear that H<sub>2</sub>O<sub>2</sub>, as expected, is the primary source of radicals in the Fenton system.

## Chapter 3

Detection and analysis of spin-adducts from ethanal and *N*-*tert*-Butyl- $\alpha$ -Phenylnitron (PBN) using Thermal Desorption-Gas Chromatography-Mass Spectrometry (TD-GC/MS)

### 3.1 INTRODUCTION

Ethanol is metabolised into ethanal (acetaldehyde) by alcohol dehydrogenase in the liver which is further converted to acetate by aldehyde dehydrogenase (Edenberg, 2007; Scheme 3.1), therefore, biological fluids may contain acetate (Hipolito *et al.*, 2007).

Catalase and cytochrome p4502E1 are other enzymes involved in the production of acetaldehyde from ethanol (scheme 3.1), though their part is minor (Edenberg, 2007; Mezey, 1976; Khanna and Israel, 1980). Acetaldehyde is a class 1 carcinogen and can cause mutagenesis at the concentration of 50-100  $\mu\text{M}$  (2.2-4.4 mg/L) (Seitz and Stickel, 2007) and is 30 times more toxic than ethanol (Zakhari, 2006)

Alcohol is distributed to other body parts including the brain after being absorbed by the stomach and intestine lining. Catalase and CYP2E1 are the enzymes which can convert ethanol to acetaldehyde in the brain (Zimatkin *et al.*, 2006). The pancreas and gastrointestinal (GI) tract are other sites of alcohol metabolism that can face the damaging effects of acetaldehyde (Vonlaufen *et al.*, 2007).

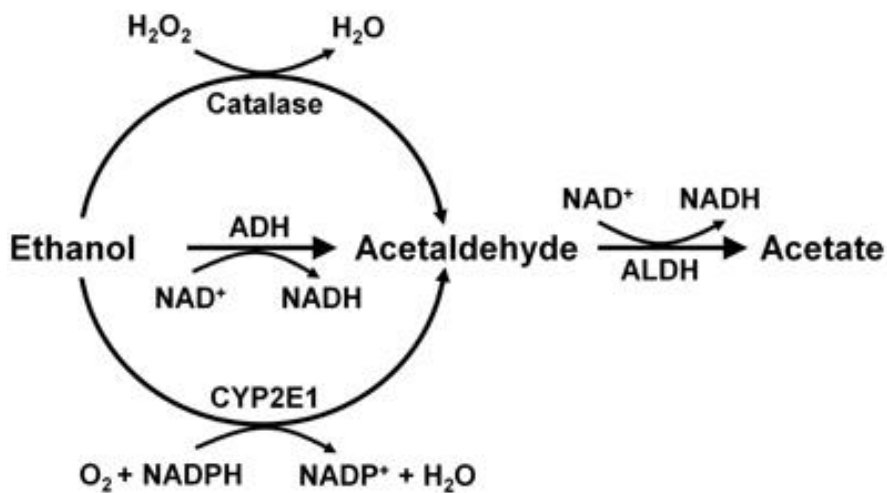
Although acetaldehyde is an intermediate product which is short lived, it can cause significant damage, especially in the liver where alcohol is being metabolised (Zakhari, 2006). Acetaldehyde may be the cause of some of the behavioural and physiological effects previously associated with alcohol (Deitrich *et al.*, 2006), for example, sleepiness, lack of coordination and memory loss symptoms (Quertemont and Didone, 2006). The presence of acetaldehyde in the brain is more damaging as it can combine with neurotransmitters like dopamine to produce salsolinol which is an opiate like addictive biochemical (Juricic *et al.*, 2012; Blum and Payne, 1991). It can also damage the red blood cells (RBC) by making their membrane less flexible making it hard for RBCs to pass through capillaries, making the cells oxygen deficient (Tusboi *et al.*, 1981). It can promote carcinogenesis by interfering with replication and inhibiting the repairing process of the DNA (Seitz and Becker, 2007).

Ethanol is not the only source of acetaldehyde in the body. Some medical conditions and pollution also contribute. For example, *candida* is a medical condition when a yeast

called *Candida albicans* starts producing acetaldehyde by sugar fermentation in GI tract. Acetaldehyde can reach other body parts from GI tract thus increasing the risk of damage (Truss, 1984).

A variety of aldehydes including acetaldehyde are produced by burning wood, natural gas, fuels and tobacco. According to the Environmental Protection Agency (EPA), fireplaces in the home, campfires, stoves and burning plastic all release acetaldehyde as a pollutant (Environmental Protection Agency, 2000)

Measurement of acetaldehyde levels in biological fluids also has significance as a biomarker, in acute alcohol intoxication and diagnosis of alcohol disorder (Schlattler *et al.*, 2014).



Scheme 3.1: Metabolism of ethanol into acetaldehyde (Zimatkin *et al.*, 2006)

## 3.2 Chromatograms

Figure 3.1 shows the chromatogram produced following the introduction of acetaldehyde into the Fenton system. Methyl radicals are primarily produced on reaction of hydroxyl radicals with the acetaldehyde, and these are then trapped by PBN (Scheme 3.4). The Fenton reaction was carried out under standard conditions for five minutes then reactants (9.13 mL) were transferred into 40 mL vial and the headspace sampled (see section 2.4.2 for experimental procedure).

### 3.2.1 Fenton reaction with acetaldehyde and PBN

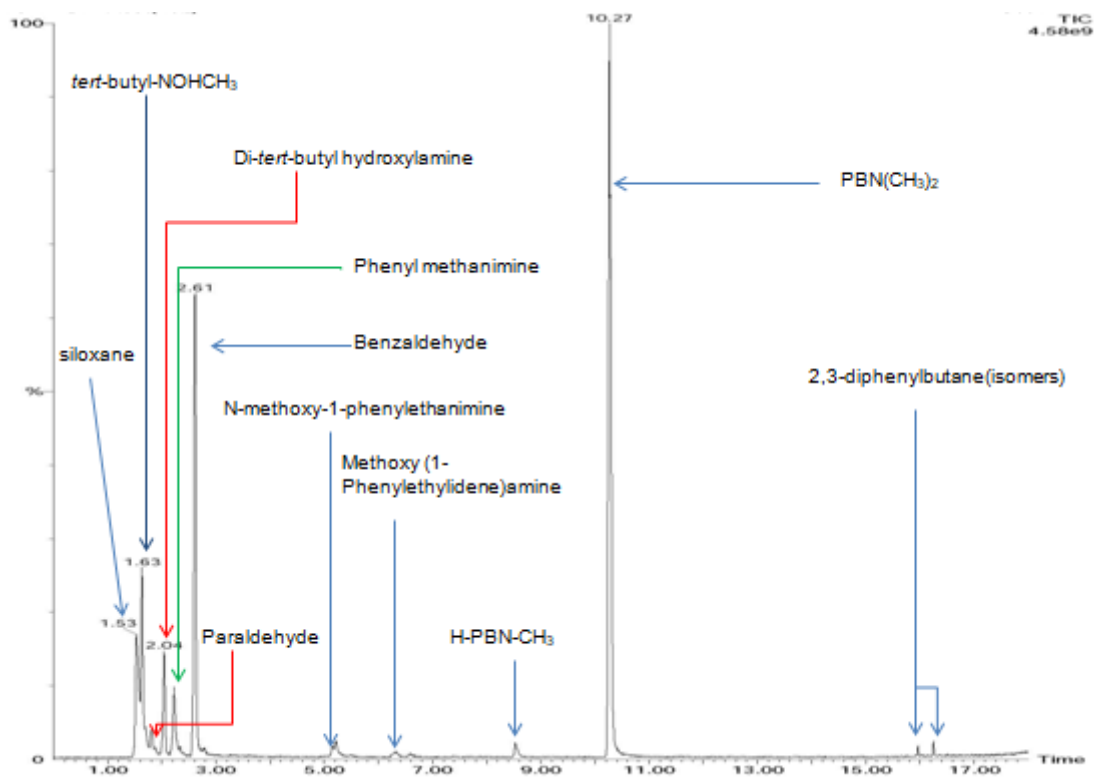


Figure 3.1: The total ion chromatogram (TIC) obtained from the headspace Thermal desorption (TD)-GC-MS analysis of the Fenton reaction containing acetaldehyde and PBN.

Figure 3.1 shows the detection of *tert*-butylhydroaminoxyl-CH<sub>3</sub> ( $R_t$  1.63 minutes), di-*tert*-butyl hydroxylamine ( $R_t$  2.04 minutes), phenyl methanimine ( $R_t$  2.23 minutes), benzaldehyde ( $R_t$  2.61 minutes), N-methoxy-1-phenylethanamine ( $R_t$  5.22 minutes), methoxy(1-phenylethylidene)amine ( $R_t$  6.32 minutes), hydrogen & methyl adduct of PBN (H-PBN-CH<sub>3</sub>;  $R_t$  8.52 minutes), a dimethyl adduct of the PBN (PBN-Me<sub>2</sub>;  $R_t$  10.27 minutes) and 2,3-Diphenylbutane isomers ( $R_t$  15.91 and 16.25 minutes). For a detailed analysis of EI-mass spectra see sections 3.3 – 3.12.

### 3.2.2 Fenton reaction with $d_3$ -acetaldehyde $\{CD_3C(H)O\}$ and PBN

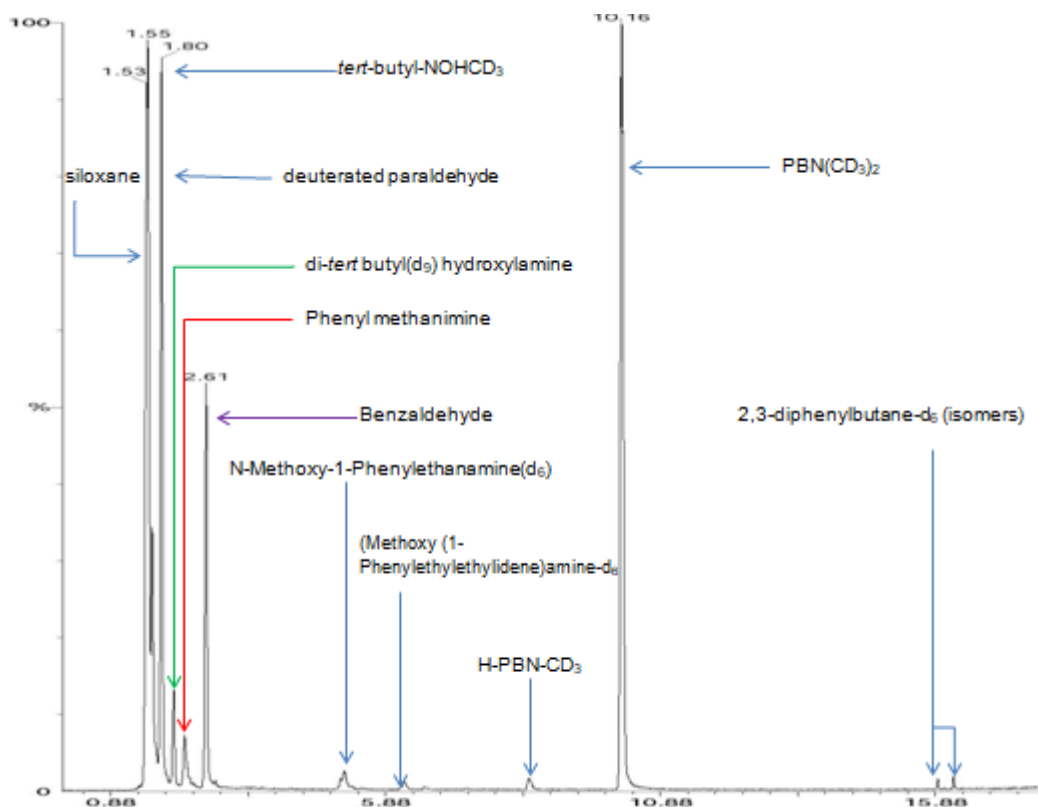


Figure 3.2: The total ion chromatogram (TIC) obtained from the headspace Thermal desorption TD-GC-MS analysis of the Fenton reaction containing  $d_3$ -acetaldehyde  $\{CD_3C(H)O\}$  and PBN.

Figure 3.1 shows the detection of tert-butylhydroaminoxyl- $CD_3$  ( $R_t$  1.65 minutes), deuterated paraldehyde- $d_9$  ( $R_t$  1.80), di-tert-butyl( $d_9$ ) hydroxylamine ( $R_t$  2.04 minutes), phenyl methanimine ( $R_t$  2.23 minutes), benzaldehyde ( $R_t$  2.61 minutes), N-methoxy-1-phenylethanamine( $d_6$ ) ( $R_t$  5.22 minutes), methoxy(1-phenylethylidene)amine- $(d_6)$  ( $R_t$  6.32 minutes), hydrogen & deuterium-methyl adduct of PBN (H-PBN- $CD_3$ ;  $R_t$  8.52 minutes), a di-deuterium-methyl adduct of the PBN (PBN- $(CD_3)_2$ ;  $R_t$  10.27 minutes) and 2,3-diphenylbutane ( $d_{12}$ ) isomers ( $R_t$  15.91 and 16.25 minutes). For a detailed analysis of EI-mass spectra see sections 3.3 – 3.12.



### 3.2.3 Fenton reaction with acetaldehyde and d<sub>6</sub>-PBN

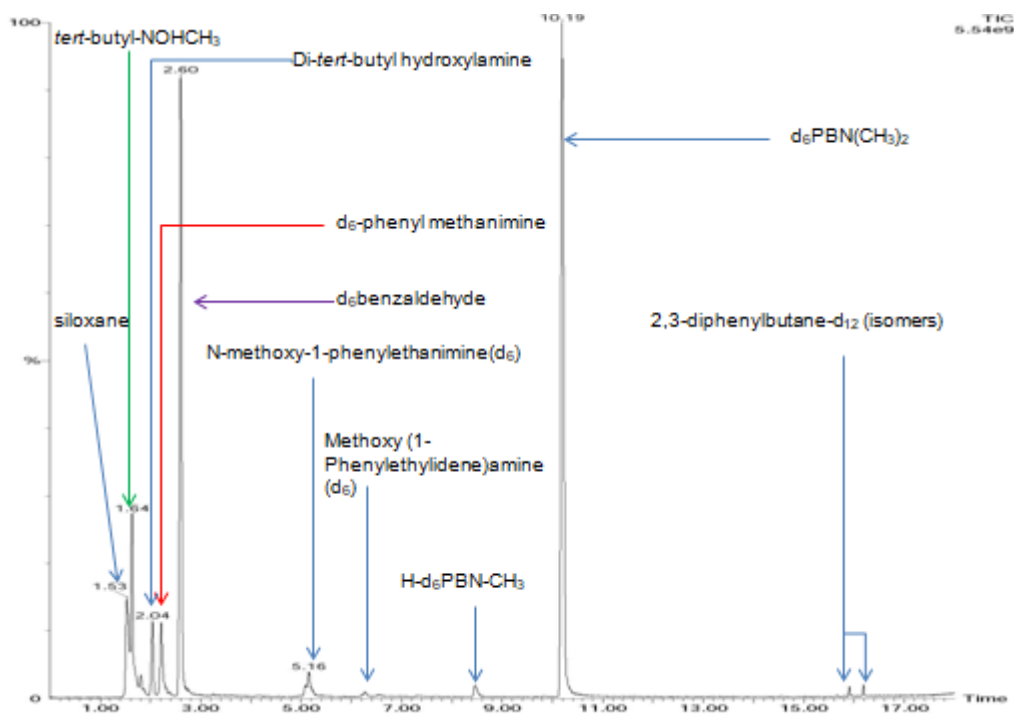


Figure 3.3: The total ion chromatogram (TIC) obtained from the headspace Thermal desorption (TD)-GC-MS analysis of the Fenton reaction containing acetaldehyde and d<sub>6</sub>-PBN.

Figure 3.3 shows the detection of tert-butylhydroaminoxyl-CH<sub>3</sub> (R<sub>t</sub> 1.63 minutes), di-tert-butyl hydroxylamine (R<sub>t</sub> 2.04 minutes), d<sub>6</sub>-phenyl methanimine (R<sub>t</sub> 2.23 minutes), d<sub>6</sub>-benzaldehyde (R<sub>t</sub> 2.60 minutes), d<sub>6</sub>-N-methoxy-1-phenylethanamine (R<sub>t</sub> 5.16 minutes), methoxy(1-phenylethylidene)amine(d<sub>6</sub>) (R<sub>t</sub> 6.29 minutes), hydrogen & methyl adduct of d<sub>6</sub>-PBN (H-d<sub>6</sub>-PBN-Me; R<sub>t</sub> 8.46 minutes), a dimethyl adduct of d<sub>6</sub>-PBN (d<sub>6</sub>-PBN-Me<sub>2</sub>; R<sub>t</sub> 10.19 minutes) and 2,3-diphenylbutane isomers (d<sub>12</sub>) (R<sub>t</sub> 15.91 and 16.25 minutes). For a detailed analysis of EI-mass spectra see sections 3.3 – 3.12.

### 3.2.4 Fenton reaction with acetaldehyde and F-PBN

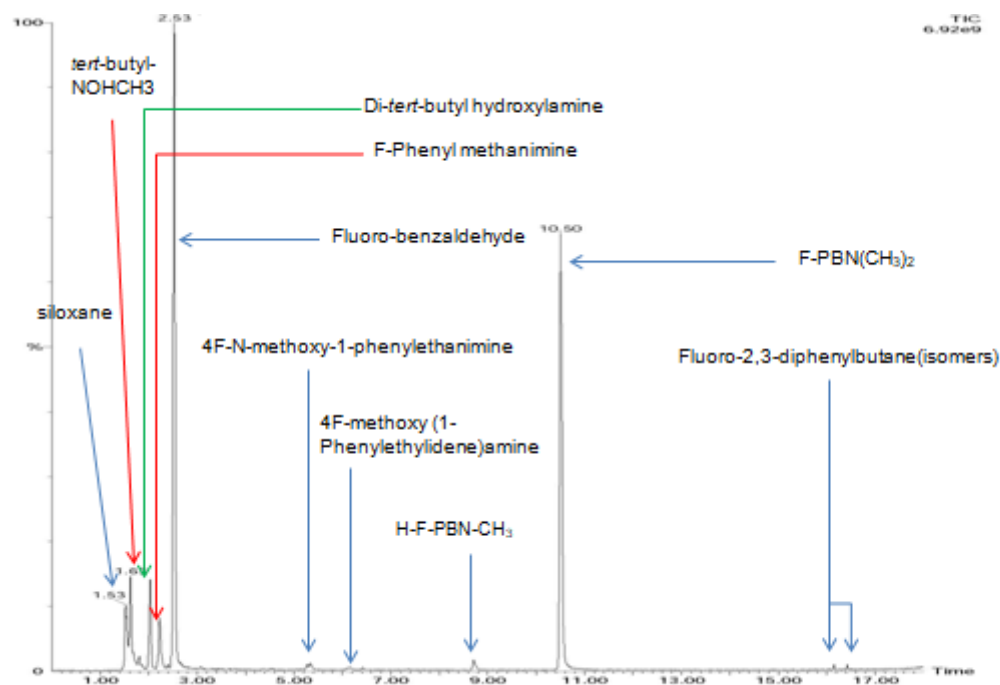


Figure 3.4: The total ion chromatogram (TIC) obtained from the headspace Thermal desorption (TD)-GC-MS analysis of the Fenton reaction with acetaldehyde and F-PBN.

Figure 3.4 shows the detection of tert-butylhydroaminoxyl-CH<sub>3</sub> (R<sub>t</sub> 1.63 minutes), di-tert-butyl hydroxylamine (R<sub>t</sub> 2.04 minutes), F-phenyl methanimine (R<sub>t</sub> 2.23 minutes), F-benzaldehyde (R<sub>t</sub> 2.53 minutes), F-N-methoxy-1-phenylethanamine (R<sub>t</sub> 5.34 minutes), 4F-methoxy(1-phenylethylidene)amine (R<sub>t</sub> 6.15 minutes), hydrogen & methyl adduct of F-PBN (F-PBN(H)Me; R<sub>t</sub> 8.70 minutes), a dimethyl adduct of the F-PBN (F-PBN-Me<sub>2</sub>; R<sub>t</sub> 10.50 minutes) and 2,3-diphenylbutane isomers (R<sub>t</sub> 15.91 and 16.25 minutes). For a detailed analysis of EI-mass spectra see sections 3.3 – 3.12.

### 3.2.5 Fenton reaction with acetaldehyde and Cl-PBN

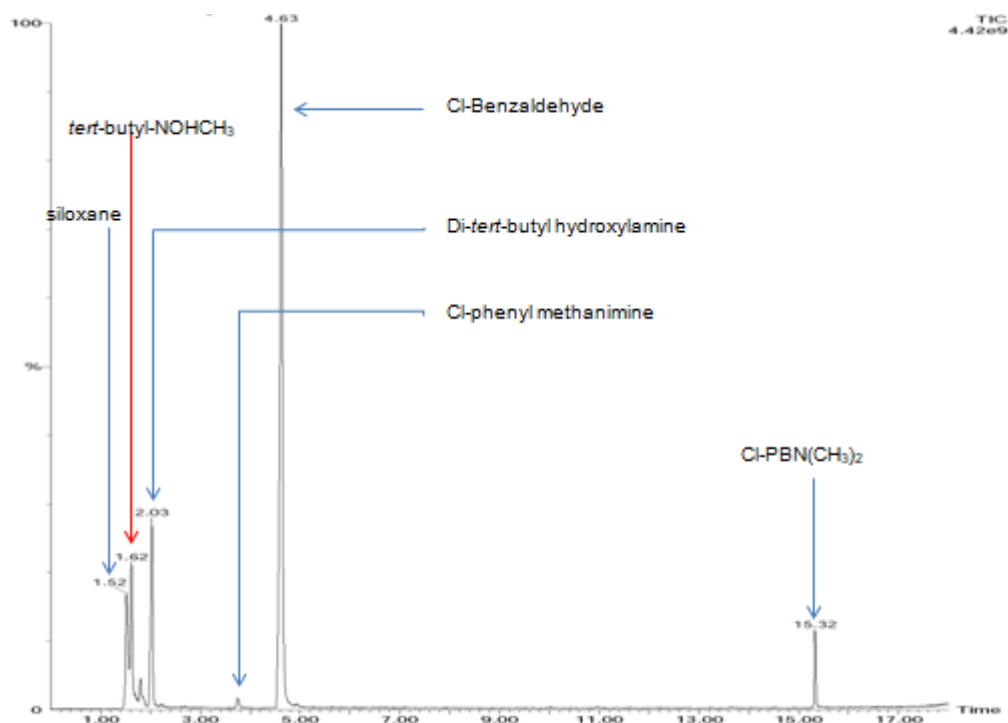


Figure 3.5: The total ion chromatogram (TIC) obtained from the headspace Thermal desorption (TD)-GC-MS analysis of the Fenton reaction containing acetaldehyde and Cl-PBN.

Figure 3.5 shows the detection of tert-butylhydroaminoxyl-CH<sub>3</sub> ( $R_t$  1.63 minutes), di-tert-butyl hydroxylamine ( $R_t$  2.04 minutes), Cl-phenyl methanimine ( $R_t$  3.75 minutes), Cl-benzaldehyde ( $R_t$  4.63 minutes) and a dimethyl adduct of the Cl-PBN (Cl-PBN-Me<sub>2</sub>;  $R_t$  15.32 minutes). For a detailed analysis of EI-mass spectra see sections 3.3 – 3.12.

### 3.3 Electron ionisation mass spectra (EI-MS) of the di-methyl adduct of PBN

#### 3.3.1 Dimethyl adduct of PBN {PBN (CH<sub>3</sub>)<sub>2</sub>}

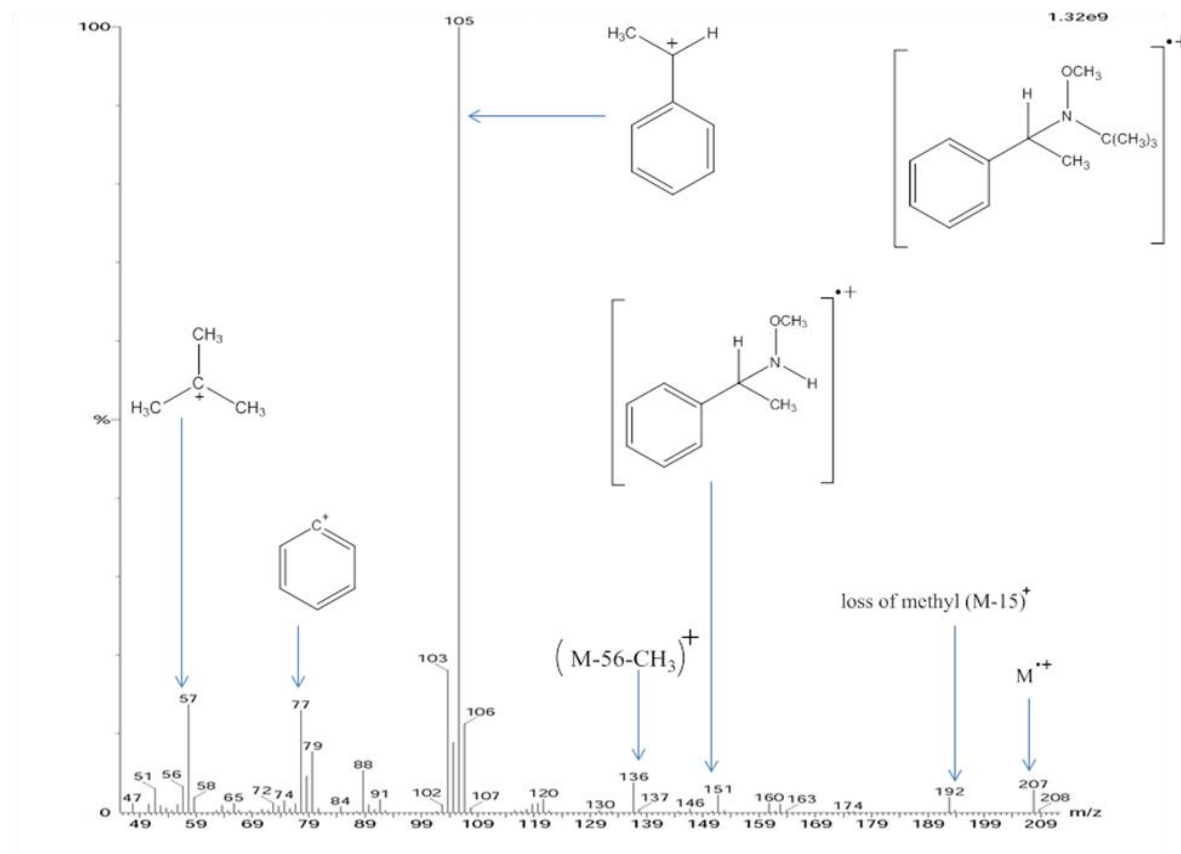


Figure 3.6: Electron ionisation (EI) mass spectrum of the peak at 10.26 minutes (figure 3.1) corresponding to PBN(CH<sub>3</sub>)<sub>2</sub>. The structure given in the top right corner is that of the molecular ion ( $\text{M}^+$ ) of PBN(CH<sub>3</sub>)<sub>2</sub>, corresponding to the peak at  $m/z$  207.

The EI mass spectrum shown in figure 3.6 corresponds to the PBN dimethyl adduct PBN(CH<sub>3</sub>)<sub>2</sub>. The peak at  $m/z$  207 corresponds to the molecular ion of PBN-Me<sub>2</sub> (Scheme 3.4). The fragment at  $m/z$  192 is formed by the loss of a methyl radical from the <sup>t</sup>Bu group of the molecular ion, while the loss of 2-methyl-1-propene (from  $\text{M}^+$ ) gives the peak at  $m/z$  151. Dissociation of the molecular ion between the alpha carbon and nitrogen gives the base peak at  $m/z$  105; further, break down of the molecular ion gives a phenyl peak at  $m/z$  77. The fragment at  $m/z$  57 corresponds to the *tert*-butyl cation.

### 3.3.2 PBN (CD<sub>3</sub>)<sub>2</sub> adduct

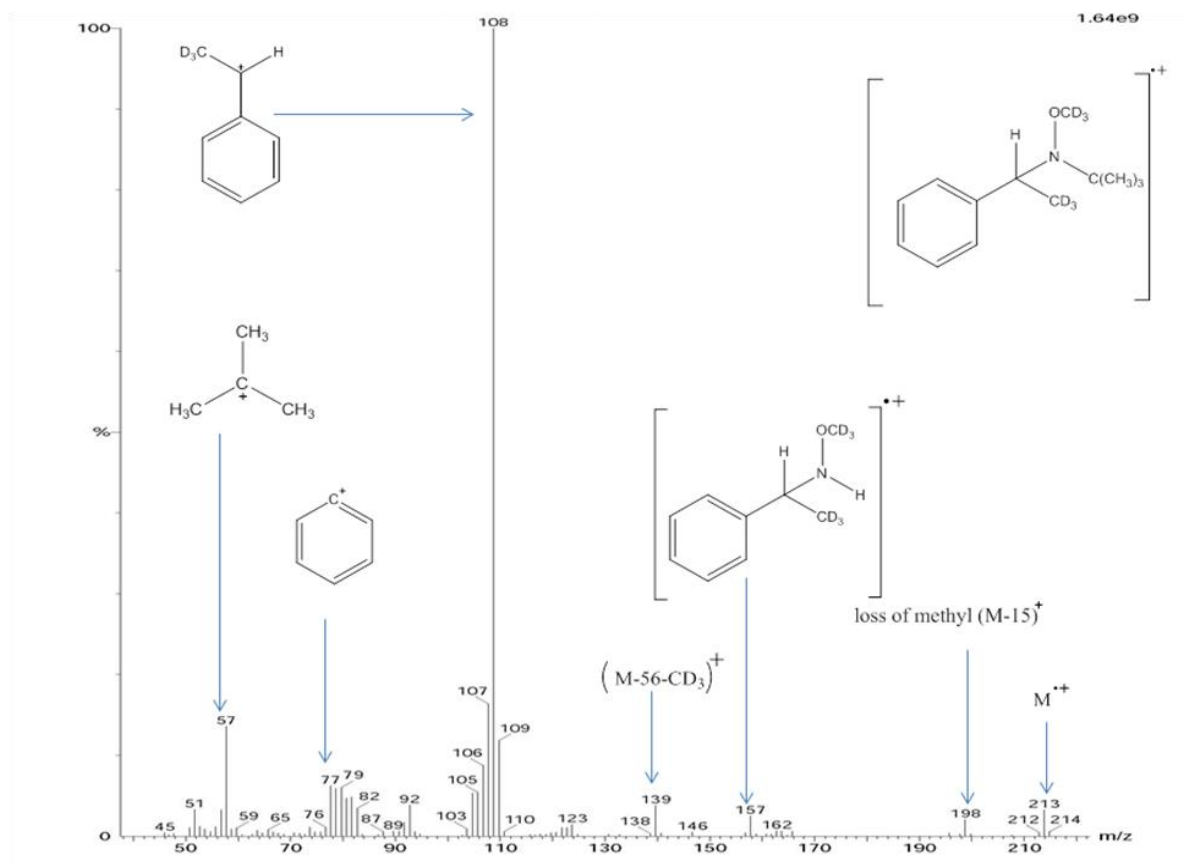


Figure 3.7: Electron ionisation (EI) mass spectrum of the peak at 10.16 minutes (figure 3.2) corresponding to the di-deuteron-methyl adduct of PBN {PBN(CD<sub>3</sub>)<sub>2</sub>}. The structure given in the top right corner is that of the molecular ion (M<sup>++</sup>) of PBN(CD<sub>3</sub>)<sub>2</sub>, corresponding to the peak at *m/z* 213.

The EI mass spectrum shown in figure 3.7 corresponds to PBN(CD<sub>3</sub>)<sub>2</sub> detected at 10.16 minutes when the reaction was carried out by using d<sub>3</sub>-acetaldehyde (the methyl hydrogen atoms replaced by deuterium) as a secondary source of radicals in the Fenton reaction system. The molecular ion can be clearly seen at *m/z* 213 (difference of 6 *m/z* units when compared to the molecular ion of PBN-Me<sub>2</sub>) which confirms the trapping of two deuterium-methyl (CD<sub>3</sub>) radicals by PBN. The fragment at *m/z* 198 is formed by the loss of a methyl radical (from the <sup>t</sup>Bu group of the molecular ion), while the loss of 2-methyl-1-propene (from M<sup>+</sup>) gives a peak at *m/z* 157. Dissociation of a molecular ion between alpha carbon and nitrogen generates the base peak at *m/z* 108, thus retaining one CD<sub>3</sub> group; further break down gives a phenyl peak at *m/z* 77. The fragment at *m/z* 57 corresponds to the *tert*-butyl cation.

### 3.3.3 d<sub>6</sub>-PBN(CH<sub>3</sub>)<sub>2</sub> adduct

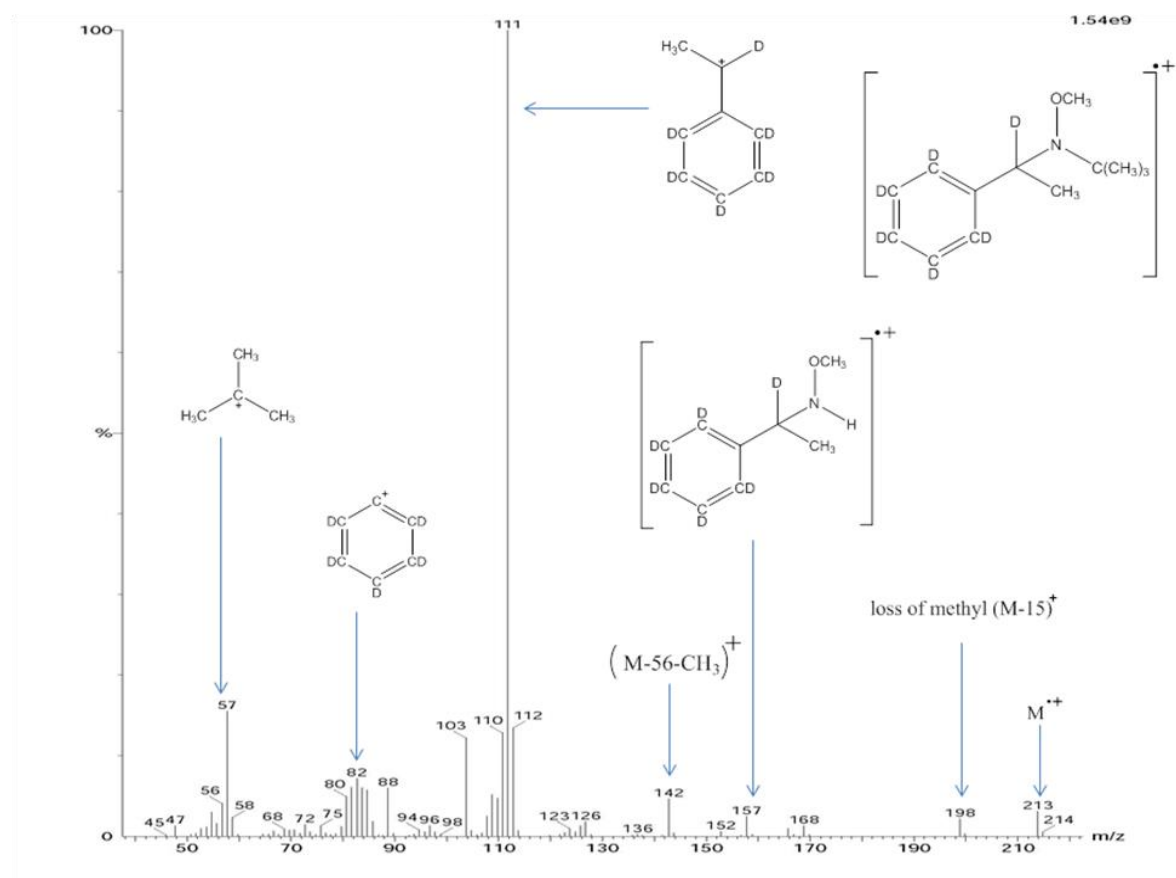


Figure 3.8: Electron ionisation (EI) mass spectrum of the peak at 10.19 minutes (figure 3.3) corresponding to d<sub>6</sub>-PBN(CH<sub>3</sub>)<sub>2</sub>. The structure given in the top right corner is that of the molecular ion ( $M^+$ ) of d<sub>6</sub>-PBN(CH<sub>3</sub>)<sub>2</sub>, corresponding to the peak at  $m/z$  213.

The EI mass spectrum shown in figure 3.8 corresponds to the d<sub>6</sub>-PBN(CH<sub>3</sub>)<sub>2</sub>. The molecular ion can be clearly seen at  $m/z$  213 when d<sub>6</sub>-PBN was used as the spin-trapping agent. The  $m/z$  value for the molecular ion is 6 units higher than when non-deuterated PBN was used, thus confirming the identity of adduct and the trapping of two methyl radicals. The fragment at  $m/z$  198 is formed by the loss of a methyl radical (from the *t*-Bu group of the molecular ion), while the loss of 2-methyl-1-propene (again directly from the *t*-Bu group of the molecular ion) gives a peak at  $m/z$  157. Dissociation of the molecular ion between alpha carbon and the nitrogen atom gives the base peak at  $m/z$  111. The fragment at  $m/z$  57 corresponds to the *tert*-butyl cation.

### 3.3.4 d<sub>6</sub>-PBN(CD<sub>3</sub>)<sub>2</sub> adduct

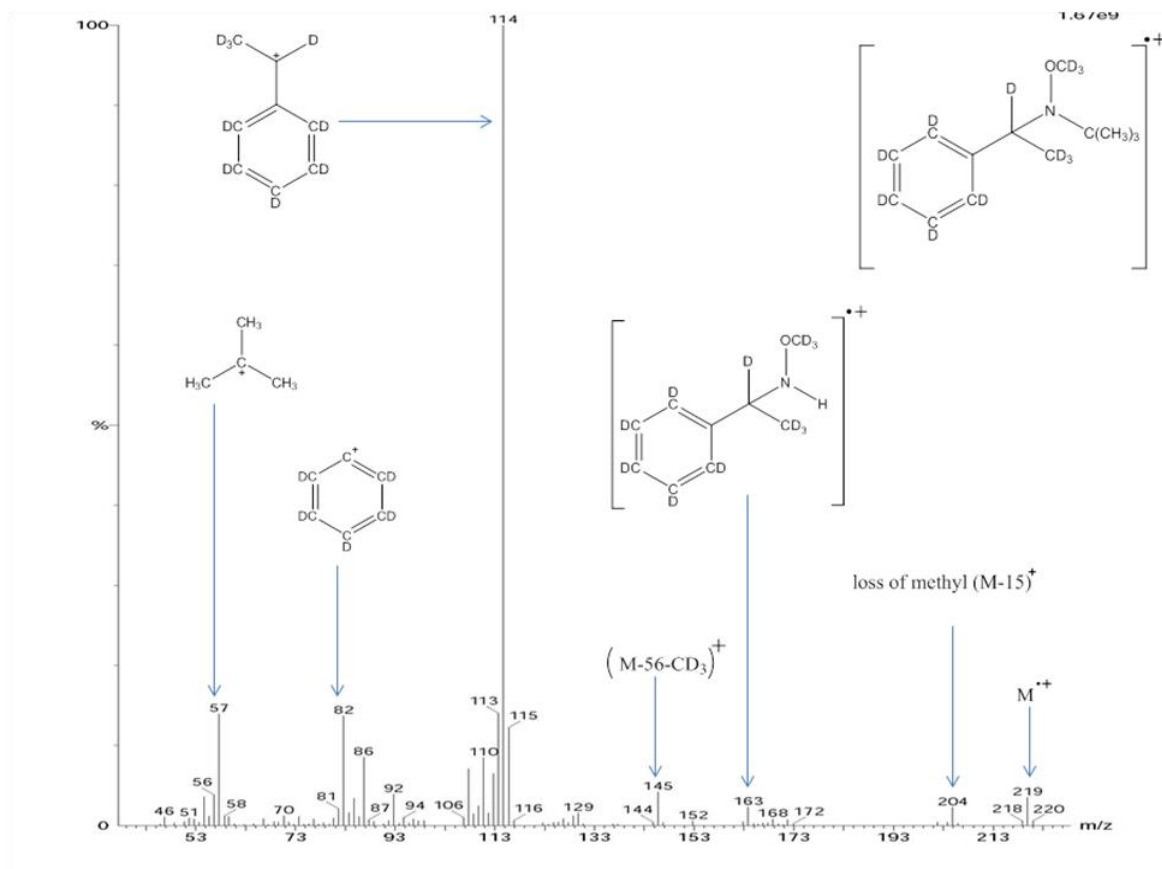


Figure 3.9: Electron ionisation (EI) mass spectrum of the peak at 10.09 minutes (figure A1; appendix) corresponding to d<sub>6</sub>-PBN(CD<sub>3</sub>)<sub>2</sub>. The structure given in the top right corner is that of the molecular ion (M<sup>+</sup>) of d<sub>6</sub>-PBN(CD<sub>3</sub>)<sub>2</sub>, corresponding to the peak at *m/z* 219.

The EI mass spectrum shown in figure 3.9 corresponds to d<sub>6</sub>-PBN(CD<sub>3</sub>)<sub>2</sub>. The molecular ion has shifted to *m/z* 219 (a difference of 12 *m/z* units when compared to the molecular ion of PBN(CH<sub>3</sub>)<sub>2</sub>; figure 3.6). As for spectra shown as figure 3.9, the fragment at *m/z* 204 is formed by the loss of a methyl radical (from the *t*-Bu group of the molecular ion), while the loss of 2-methyl-1-propene (from M<sup>+</sup>) gives a peak at *m/z* 163. Dissociation of the molecular ion between the alpha carbon and nitrogen atom gives the base peak at *m/z* 114. The fragment at *m/z* 57 corresponds to the *tert*-butyl cation.

### 3.3.5 F-PBN(CH<sub>3</sub>)<sub>2</sub> adduct

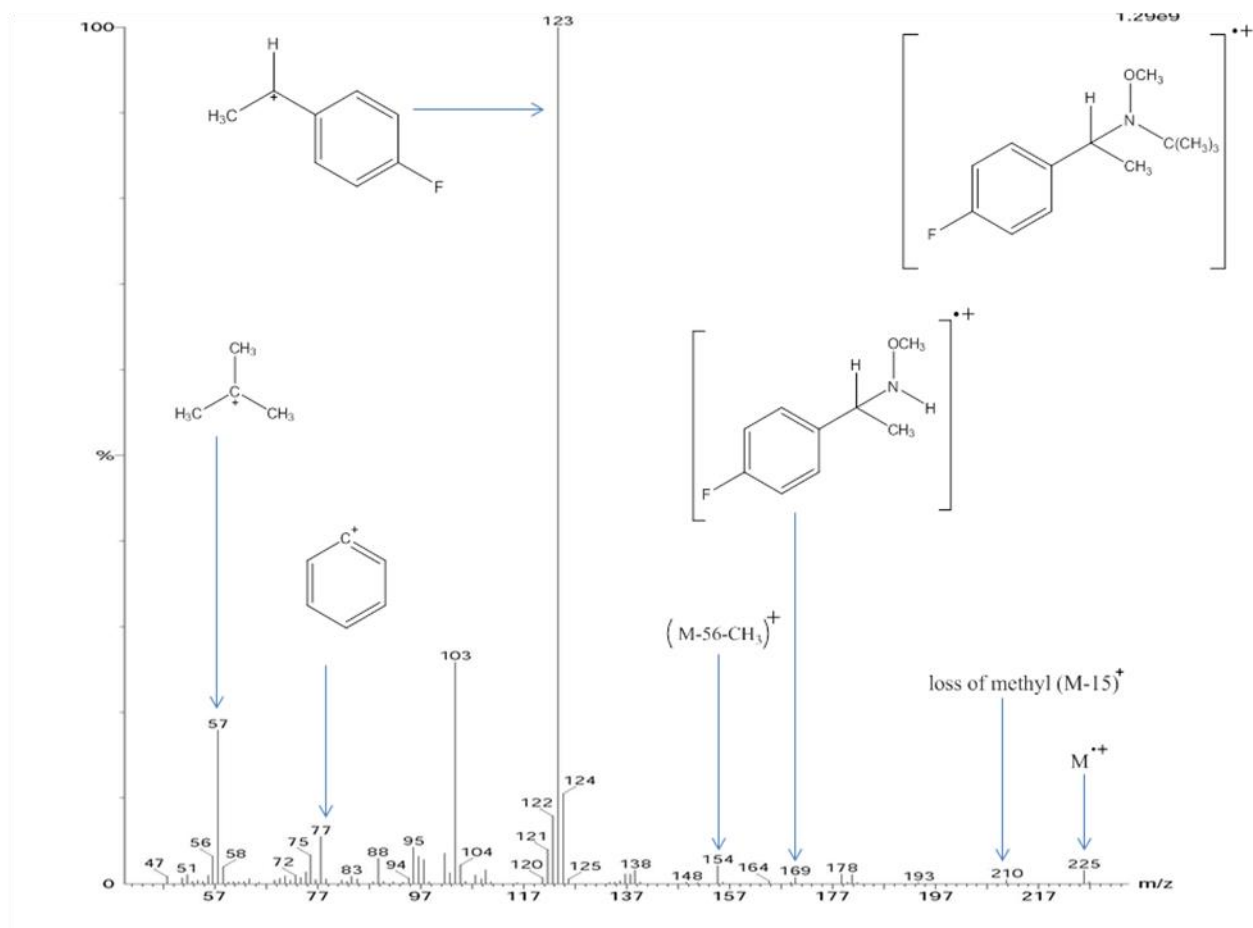


Figure 3.10: Electron ionisation (EI) mass spectrum of the peak at 10.49 minutes (figure 3.4). The structure given in the top right corner is that of the molecular ion ( $M^{++}$ ) of F-PBN(CH<sub>3</sub>)<sub>2</sub>, corresponding to the peak at  $m/z$  225.

The EI mass spectrum shown in figure 3.10 corresponds to the F-PBN(CH<sub>3</sub>)<sub>2</sub>. The molecular ion is at  $m/z$  225 (a difference of 18  $m/z$  units when compared to the molecular ion of PBN(CH<sub>3</sub>)<sub>2</sub>; figure 3.6), thus confirming the identity of the di-methyl adduct. The fragment at  $m/z$  210 is formed by the loss of methyl radical (from the t-Bu group of the molecular ion), while the loss of 2-methyl-1-propene (from  $M^{\bullet+}$ ) gives a peak at  $m/z$  169. Dissociation of the molecular ion between the alpha carbon and nitrogen atom gives the base peak at  $m/z$  123.



### 3.3.6 Cl-PBN(CH<sub>3</sub>)<sub>2</sub> adduct

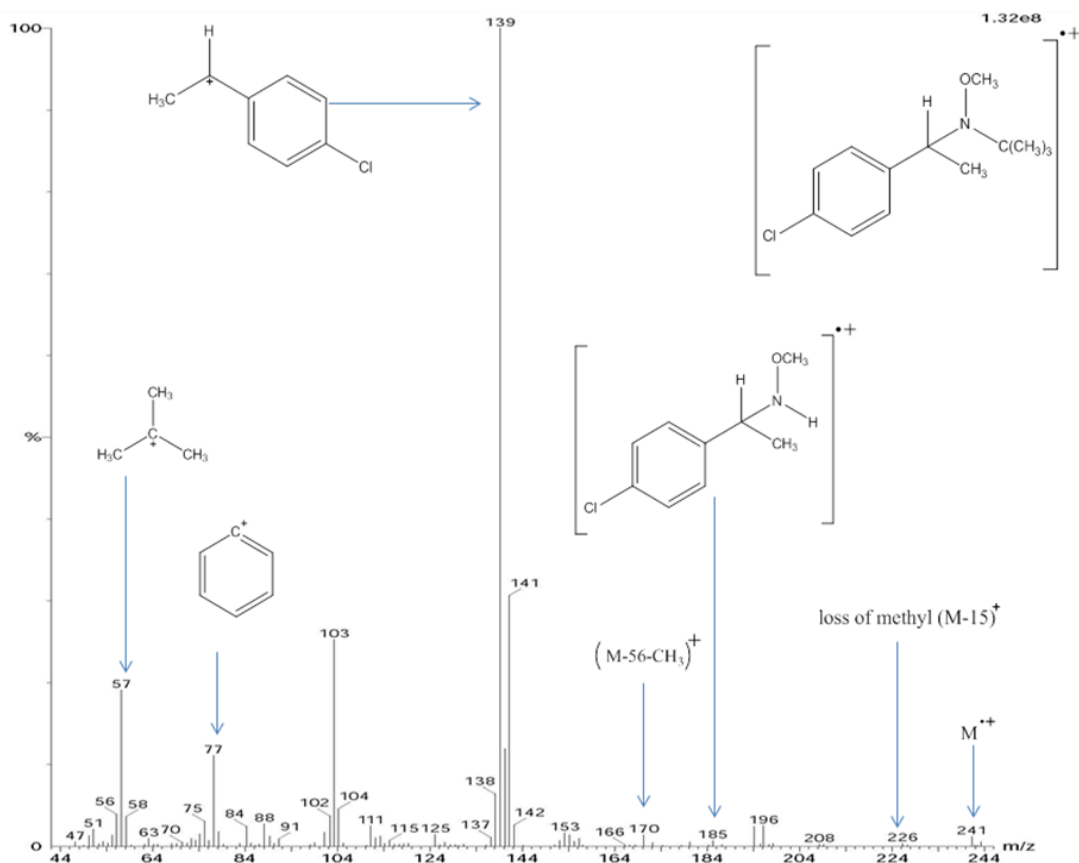


Figure 3.11: Electron ionisation (EI) mass spectrum of the peak at 15.32 minutes (figure 3.5). The structure given in the top right corner is the molecular ions (M<sup>+</sup>) of Cl-PBN(CH<sub>3</sub>)<sub>2</sub>, corresponding to the peaks at *m/z* 241/243 (depending upon the Cl isotope present).

The EI mass spectrum shown in figure 3.11 corresponds to the Cl-PBN(CH<sub>3</sub>)<sub>2</sub>. The molecular ion is at *m/z* 241 or 243, depending upon which isotope of chlorine is present (<sup>35</sup>Cl or <sup>37</sup>Cl). This difference of 34/36 *m/z* units when compared to the molecular ion of PBN (figure 3.6) confirms the detection of the di-methyl adduct. The fragment at *m/z* 226/228 is formed by the loss of a methyl radical (from the t-Bu group of the molecular ions), while the loss of 2-methyl-1-propene (from M<sup>+</sup>) gives rise to peaks at *m/z* 185/187. Dissociation of the molecular ion between the alpha carbon and nitrogen atom gives a base peak at *m/z* 139 (containing the <sup>35</sup>Cl isotope) and the peak at *m/z* 141 (containing the <sup>37</sup>Cl isotope).

Table 3.1: Summary of GC-MS data for the dimethyl-adduct of PBN and its derivatives

| Spin adduct                                       | Retention time (R <sub>t</sub> ; minutes) | Molecular ion ( <i>m/z</i> ) | Base peak ( <i>m/z</i> ) | Characteristic fragment peaks ( <i>m/z</i> ) |
|---|---|------------------------------|--------------------------|--|
| PBN(CH <sub>3</sub> ) <sub>2</sub>                | 10.26                                     | 207                          | 105                      | 192, 151, 136, 77, 57                        |
| PBN(CD <sub>3</sub> ) <sub>2</sub>                | 10.16                                     | 213                          | 108                      | 198, 157, 139, 77, 57                        |
| d <sub>6</sub> PBN(CH <sub>3</sub> ) <sub>2</sub> | 10.19                                     | 213                          | 111                      | 198, 157, 142, 82, 57                        |
| d <sub>6</sub> PBN(CD <sub>3</sub> ) <sub>2</sub> | 10.09                                     | 219                          | 114                      | 219, 163, 145, 82, 57                        |
| F-PBN(CH <sub>3</sub> ) <sub>2</sub>              | 10.49                                     | 225                          | 123                      | 210, 169, 154, 77, 57                        |
| Cl-PBN(CH <sub>3</sub> ) <sub>2</sub>             | 15.32                                     | 241/243                      | 139/141                  | 226/228, 185/187, 170/172, 77, 57            |

### 3.4 Electron ionisation mass spectra (EI-MS) of the H-PBN-CH<sub>3</sub> adduct

#### 3.4.1 CH<sub>3</sub> & H adduct of PBN (H-PBN-CH<sub>3</sub>)

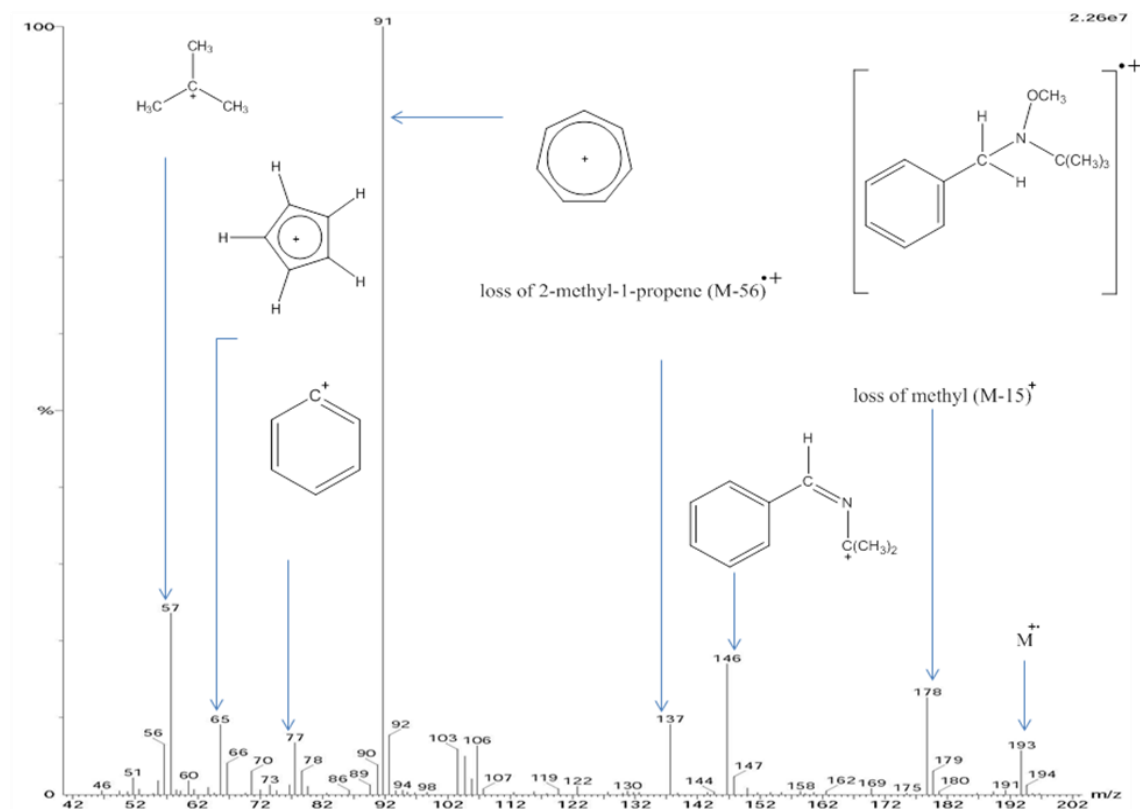


Figure 3.12: Electron ionisation (EI) mass spectrum of the peak at 8.52 minutes (figure 3.1) corresponding to a hydrogen and methyl radical-adduct of PBN (H-PBN-CH<sub>3</sub>). The structure given in the top right corner is that of the molecular ion (M<sup>+</sup>), corresponding to the peak at  $m/z$  193.

The EI mass spectrum shown in Figure 3.12 corresponds to the hydrogen & methyl radical-adduct of PBN (H-PBN-CH<sub>3</sub>). The molecular ion can be seen at  $m/z$  193. The fragment at  $m/z$  178 is formed by the loss of a methyl radical from the <sup>t</sup>Bu group of the molecular ion, while the loss of 2-methyl-1-propene (from M<sup>+</sup>) gave a peak at  $m/z$  137. The fragment at  $m/z$  91 is a tropylium cation formed by the rearrangement of a benzyl cation. The fragment at  $m/z$  77 corresponds to a phenyl cation while one at  $m/z$  57 is a *tert*-butyl cation.

### 3.4.2 CD<sub>3</sub> & H adduct of PBN (H-PBN-CD<sub>3</sub>)

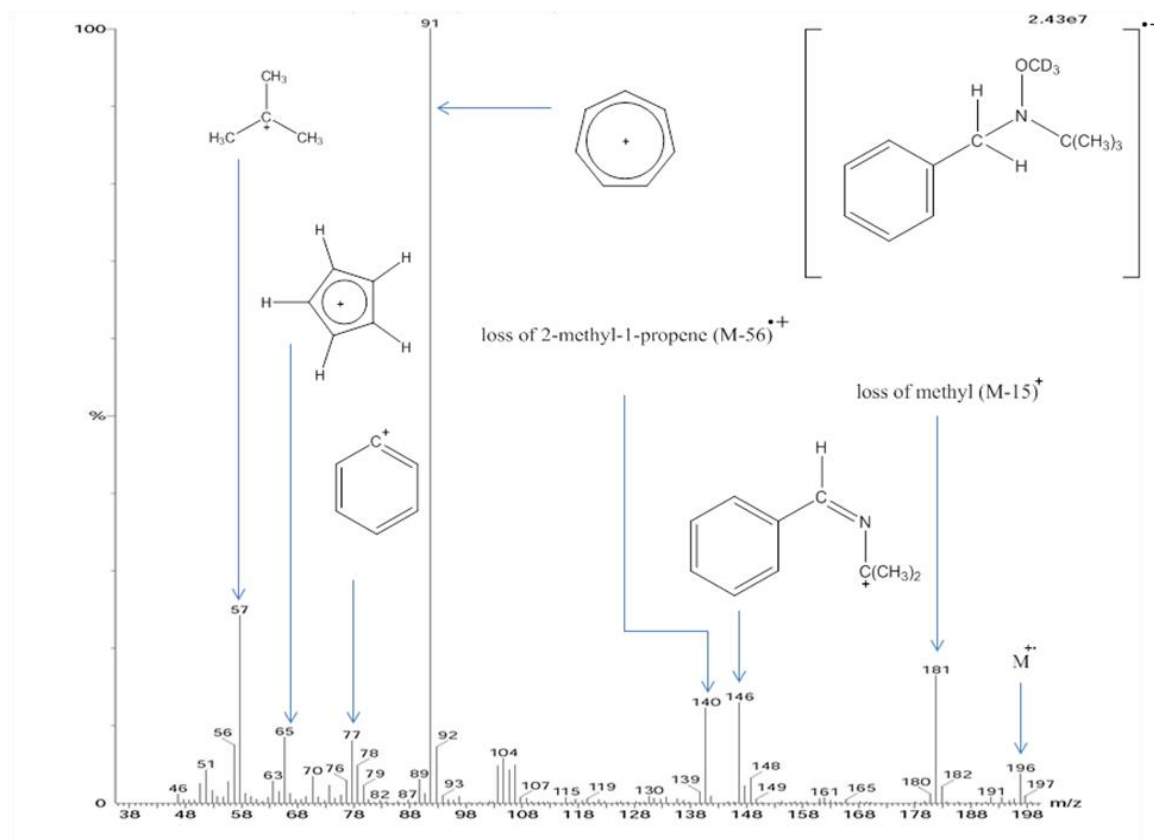


Figure 3.13: Electron ionisation (EI) mass spectrum of the peak at 8.48 minutes (figure 3.2) corresponding to a hydrogen and CD<sub>3</sub> radical adduct of PBN. The structure given in the top right corner is that of the molecular ion ( $\text{M}^+$ ) of H-PBN-CD<sub>3</sub>, corresponding to the peak at  $m/z$  196.

The EI mass spectrum shown in figure 3.13 corresponds to H-PBN-CD<sub>3</sub> detected at 8.48 minutes when the reaction was carried out by using d<sub>3</sub>-acetaldehyde (the methyl hydrogen atoms replaced by deuterium) as a secondary source of radicals in the Fenton reaction system. The molecular ion can be clearly seen at  $m/z$  196 (difference of 3  $m/z$  units when compared to the molecular ion of H-PBN-CH<sub>3</sub>; figure 3.12) which confirms the trapping of one deuterium methyl (CD<sub>3</sub>) radical by PBN. The fragment at  $m/z$  181 is formed by the loss of a methyl radical from the t-Bu group of the molecular ion, while the loss of 2-methyl-1-propene (from  $\text{M}^+$ ) gives a peak at  $m/z$  140. The fragment at  $m/z$  91 corresponds to a tropylium cation which is also the base peak; in addition, break down gives a phenyl peak at  $m/z$  77. The fragment at  $m/z$  57 corresponds to the *tert*-butyl cation

### 3.4.3 CH<sub>3</sub> & H adduct of d<sub>6</sub>-PBN (H-d<sub>6</sub>PBN-CH<sub>3</sub>)

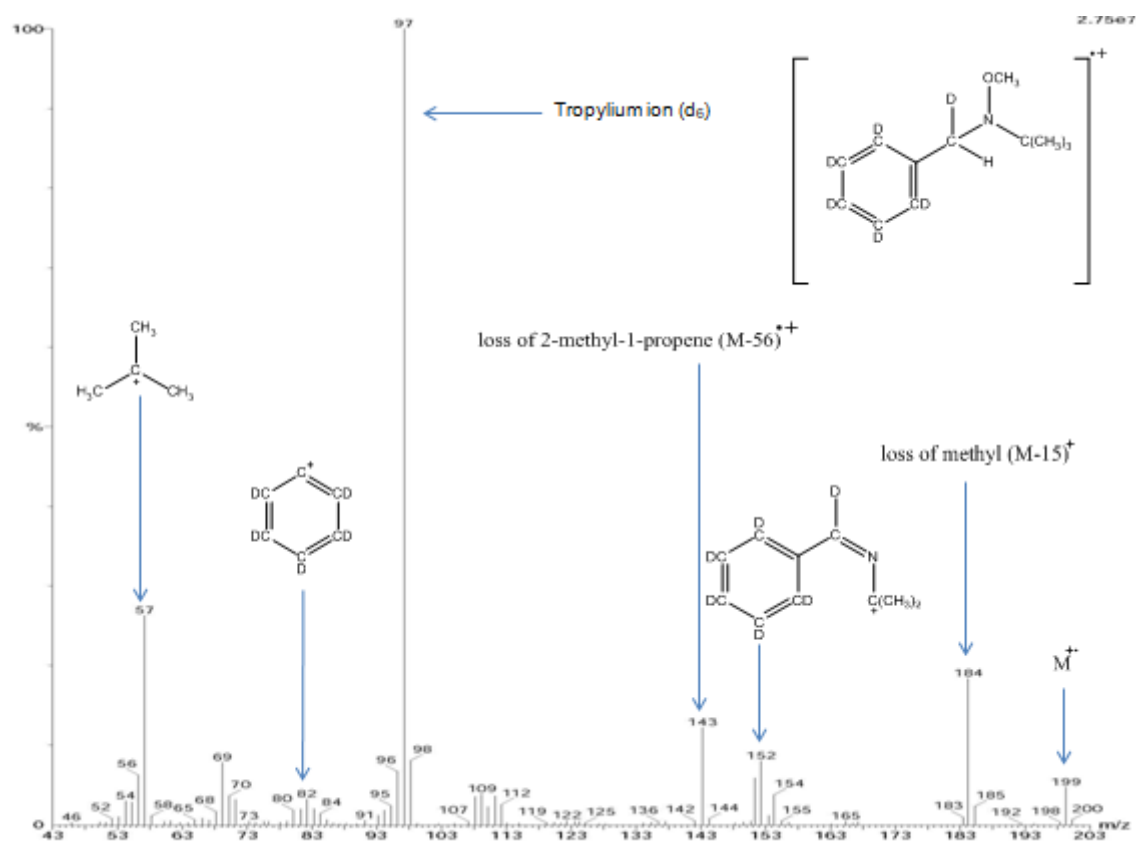


Figure 3.14: Electron ionisation (EI) mass spectrum of the peak at 8.46 minutes (figure 3.3) corresponding to a hydrogen and methyl radical-adduct of d<sub>6</sub>-PBN. The structure given in the top right corner is that of the molecular ion (M<sup>+</sup>) of H-d<sub>6</sub>-PBN-CH<sub>3</sub>, corresponding to the peak at *m/z* 199.

The EI mass spectrum shown in figure 3.14 corresponds to the hydrogen and methyl radical-adduct of PBN (H-d<sub>6</sub>-PBN-CH<sub>3</sub>). The molecular ion can be seen at *m/z* 199 when d<sub>6</sub>-PBN was used as the spin trapping agent. The *m/z* value for the molecular ion is 6 units higher than when non-deuterated PBN is used, thus confirming the identity of the adduct and the trapping of a hydrogen atom and a methyl radical. The fragment at *m/z* 184 is formed by the loss of a methyl radical from the t-Bu group of the molecular ion, while the loss of 2-methyl-1-propene (also directly from the t-Bu group of the molecular ion) gives a peak at *m/z* 143. The fragment at *m/z* 97 corresponds to tropylium (d<sub>6</sub>) cation which is also the base peak; in addition, break down gives a phenyl (d<sub>5</sub>) peak at *m/z* 82. The fragment at *m/z* 57 corresponds to the *tert*-butyl cation.

### 3.4.4 CD<sub>3</sub> & H adduct of d<sub>6</sub>-PBN (H-d<sub>6</sub>PBN-CD<sub>3</sub>)

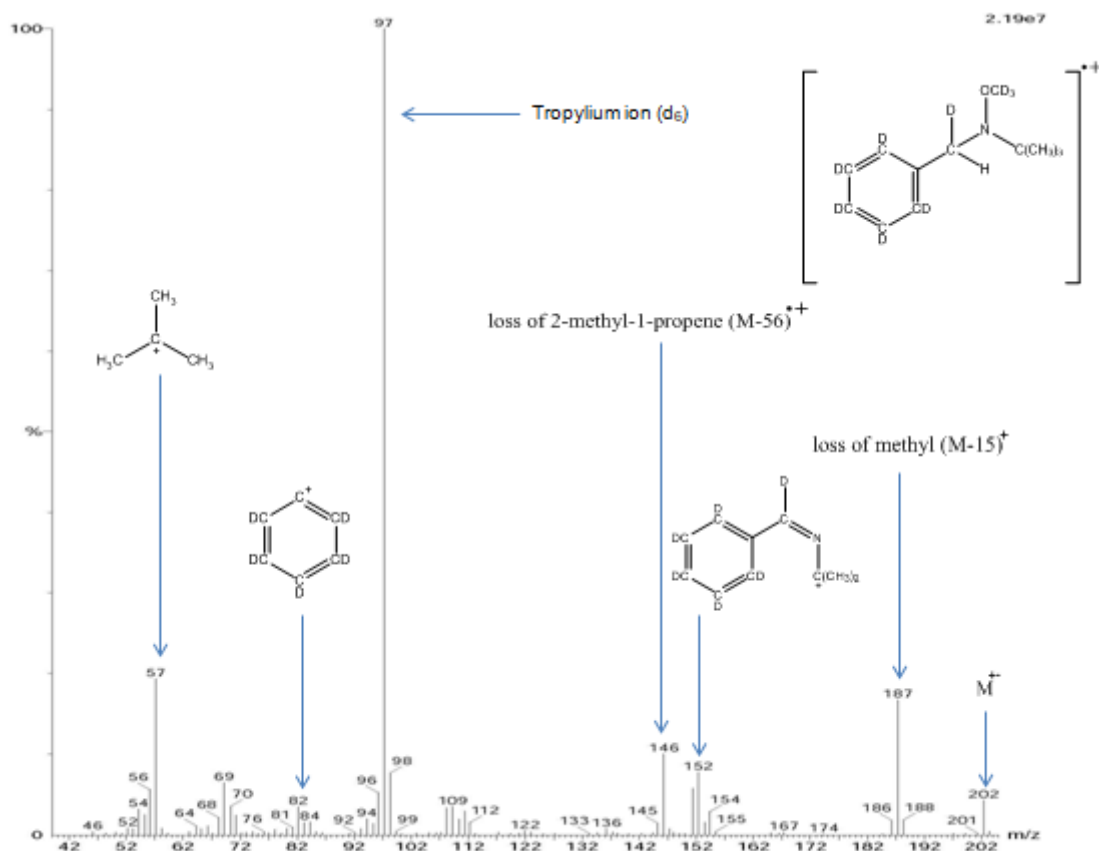


Figure 3.15: Electron ionisation (EI) mass spectrum of the peak at 8.40 minutes (figure A1; appendix) corresponding to a hydrogen atom and a CD<sub>3</sub> radical-adduct of d<sub>6</sub>-PBN. The structure given in the top right corner is that of the molecular ion (M<sup>++</sup>) of H-d<sub>6</sub>-PBN-CD<sub>3</sub> corresponding to the peak at *m/z* 202.

The EI mass spectrum shown in figure 3.15 corresponds to H-d<sub>6</sub>-PBN-CD<sub>3</sub>. The molecular ion has shifted to *m/z* 202 (a difference of 9 *m/z* units when compared to the molecular ion of H-PBN-CH<sub>3</sub>; figure 3.12) thus confirming the identity of adduct. The fragment at *m/z* 187 is formed by the loss of a methyl radical from the *t*-Bu group of the molecular ion, while the loss of 2-methyl-1-propene (also directly from the <sup>1</sup>Bu group of the molecular ion) gives a peak at *m/z* 146. The fragment at *m/z* 97 corresponds to tropylium (d<sub>6</sub>) cation which is also the base peak; in addition, break down gives a phenyl (d<sub>5</sub>) peak at *m/z* 82. The fragment at *m/z* 57 corresponds to the *tert*-butyl cation.

### 3.4.5 CH<sub>3</sub> & H adduct of F-PBN {F-PBN(H)CH<sub>3</sub>}

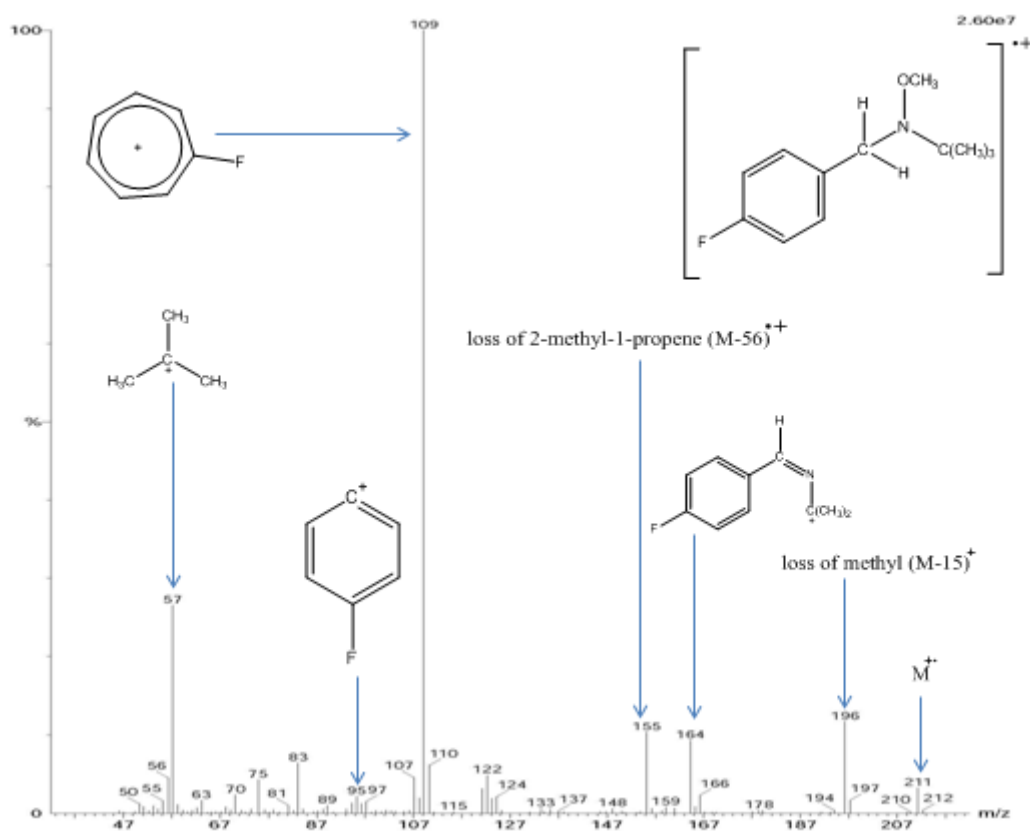


Figure 3.16: Electron ionisation (EI) mass spectrum of the peak at 8.70 minutes (figure 3.4) corresponding to a hydrogen atom and methyl radical-adduct of F-PBN. The structure given in the top right corner is that of the molecular ion ( $M^{+\bullet}$ ) of F-PBN(H)CH<sub>3</sub> corresponding to the peak at  $m/z$  211.

The EI mass spectrum shown in Figure 3.16 corresponds to a hydrogen & methyl radical-adduct of PBN {F-PBN(H)CH<sub>3</sub>}. The molecular ion can be seen at  $m/z$  211 (a difference of 18  $m/z$  units when compared to the molecular ion of H-PBN-CH<sub>3</sub>) thus confirming the identity of the adduct. The fragment at  $m/z$  196 is formed by the loss of a methyl radical from the <sup>t</sup>Bu group of the molecular ion, while the loss of 2-methyl-1-propene (from  $M^{+\bullet}$ ) gave a peak at  $m/z$  155. The fragment at  $m/z$  109 is a fluorotropylium cation formed by the rearrangement of F-benzyl cation; in addition, breakdown gives a F-phenyl peak at  $m/z$  95 while the fragment at  $m/z$  57 corresponds to *tert*-butyl cation.

Table 3.2: Summary of GC-MS data for the hydrogen & methyl adducts of PBN and its derivatives.

| Spin adduct                           | Retention time ( $R_t$ ; minutes) | Molecular ion ( $m/z$ ) | Base peak ( $m/z$ ) | Characteristic fragment peaks ( $m/z$ ) |
|---------------------------------------|-----------------------------------|-------------------------|---------------------|---|
| H-PBN-CH <sub>3</sub>                 | 8.52                              | 193                     | 91                  | 178, 146, 137, 103, 91, 77, 57          |
| H-PBN-CD <sub>3</sub>                 | 8.48                              | 196                     | 91                  | 181, 146, 140, 103, 91, 77, 57          |
| H-d <sub>6</sub> -PBNCH <sub>3</sub>  | 8.46                              | 199                     | 97                  | 184, 152, 143, 109, 97, 82, 57          |
| H-d <sub>6</sub> -PBN-CD <sub>3</sub> | 8.40                              | 202                     | 97                  | 187, 152, 146, 109, 97, 82, 57          |
| F-PBN(H)CH <sub>3</sub>               | 8.70                              | 211                     | 109                 | 196, 164, 155, 109, 95, 57              |



### 3.5 Methyl adduct of *tert*-butylhydroaminoxyl (<sup>t</sup>Bu-NOMe)

#### 3.5.1 EI mass spectrum of <sup>t</sup>Bu-NOHMe

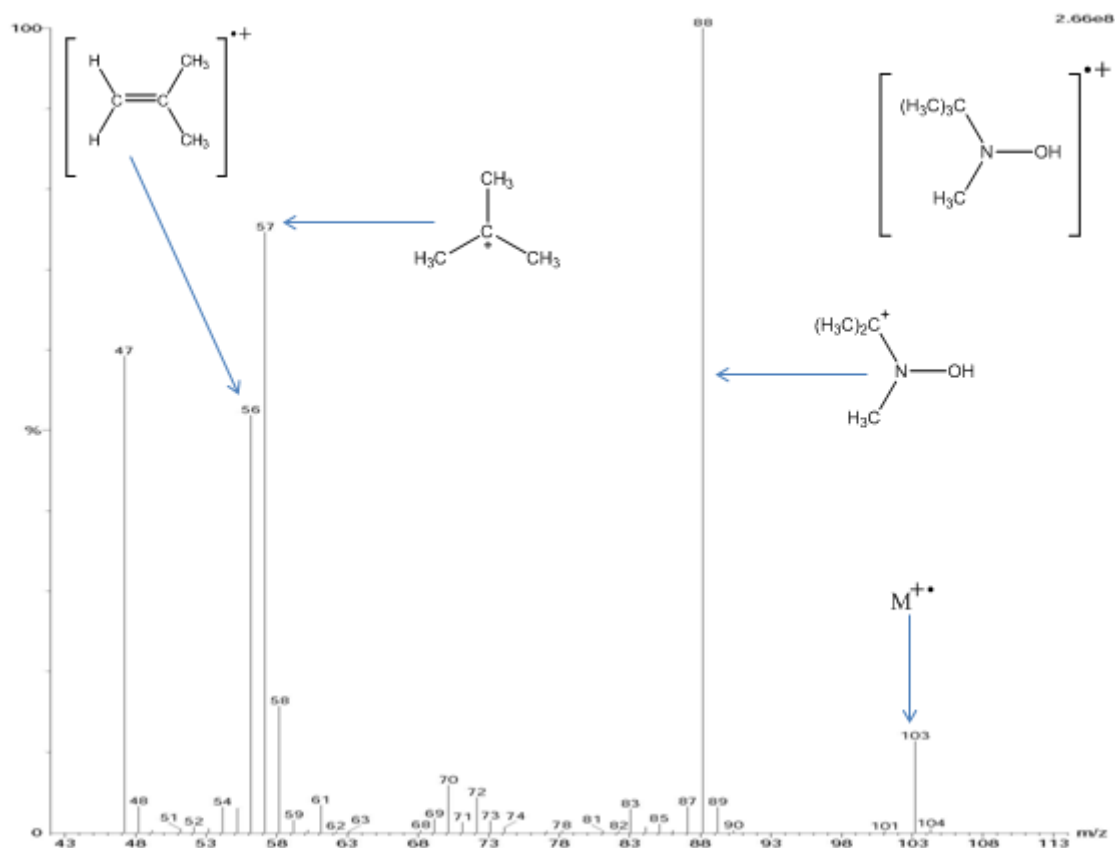


Figure 3.17: Electron ionisation (EI) mass spectrum of the peak at 1.63 minutes (figure 3.1) corresponding to <sup>t</sup>Bu-NOHMe. The structure given in the top right corner is that of the molecular ion ( $M^{\bullet+}$ ) corresponding to the peak at  $m/z$  103.

The EI mass spectrum shown in figure 3.17 corresponds to *tert*-butylhydroaminoxyl (<sup>t</sup>Bu-NOHMe). The molecular ion may be seen at  $m/z$  103. Loss of methyl radical from the molecular ion gives a peak at  $m/z$  88 which is also the base peak. The fragment at  $m/z$  57 corresponds to the *tert*-butyl cation.

### 3.5.2 EI mass spectrum of <sup>t</sup>BuNOH(CD<sub>3</sub>)

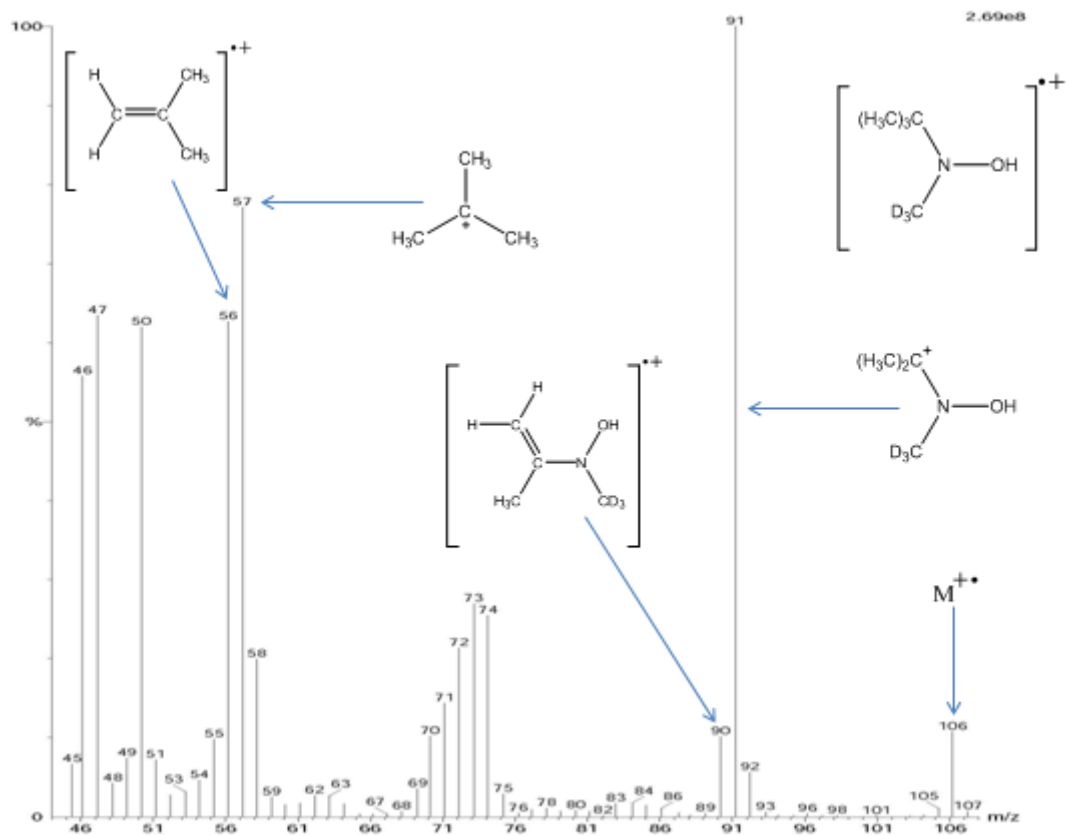


Figure 3.18: Electron ionisation (EI) mass spectrum of the peak at 1.62 minutes (figure 3.2) corresponding to <sup>t</sup>Bu-NOH(CD<sub>3</sub>). The structure given in the top right corner is that of the molecular ion (M<sup>+</sup>) corresponding to the peak at *m/z* 106.

The EI mass spectrum shown in figure 3.18 corresponds to <sup>t</sup>Bu-NOH(CD<sub>3</sub>) detected at 1.62 minutes when the reaction was carried out by using d<sub>3</sub>-acetaldehyde- (the methyl hydrogen atoms replaced by deuterium) as a secondary source of radicals in the Fenton reaction system. The molecular ion can be seen clearly at *m/z* 106 which helps to confirm the identity. Loss of a methyl group from the <sup>t</sup>Bu group of the molecular ion gives a peak at *m/z* 91 which is also the base peak. The fragment at *m/z* 57 corresponds to the *tert*-butyl cation.

Table 3.3: Summary of GC-MS data for <sup>t</sup>Bu-NOHMe when PBN and its derivatives were used as trapping agents

| Reagents in the Fenton system                      | Identified adduct                  | Retention time (R <sub>t</sub> ; minutes) | Molecular ion ( <i>m/z</i> ) |
|--|------------------------------------|---|------------------------------|
| PBN and acetaldehyde                               | <sup>t</sup> Bu-NOHMe              | 1.63                                      | 103                          |
| PBN & d <sub>3</sub> -acetaldehyde                 | <sup>t</sup> Bu-NOHCD <sub>3</sub> | 1.63                                      | 106                          |
| d <sub>6</sub> -PBN & acetaldehyde                 | <sup>t</sup> Bu-NOHMe              | 1.63                                      | 103                          |
| d <sub>6</sub> -PBN & d <sub>3</sub> -acetaldehyde | <sup>t</sup> Bu-NOHCD <sub>3</sub> | 1.63                                      | 106                          |
| F-PBN & acetaldehyde                               | <sup>t</sup> Bu-NOHMe              | 1.63                                      | 103                          |
| Cl-PBN & acetaldehyde                              | <sup>t</sup> Bu-NOHMe              | 1.62                                      | 103                          |

### 3.6 Di-*tert* butyl hydroxylamine

#### 3.6.1 EI mass spectrum of di-*tert* butyl hydroxylamine

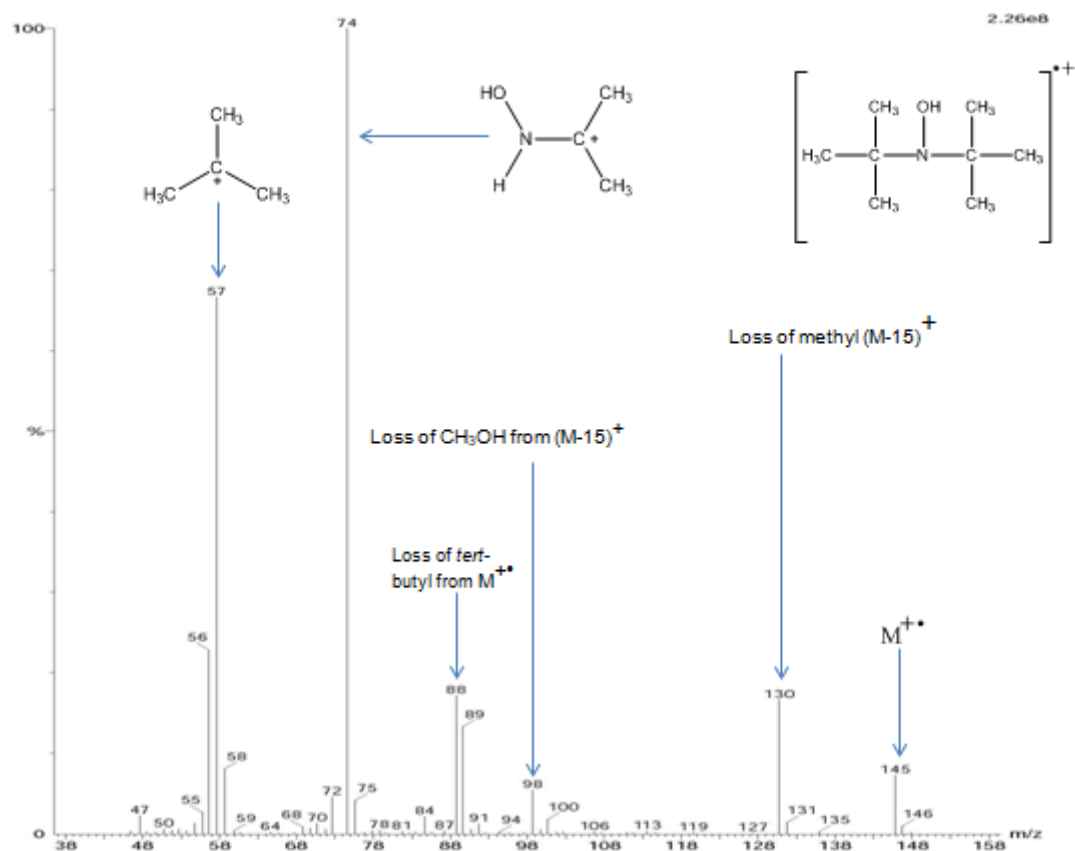


Figure 3.19: Electron ionisation (EI) mass spectrum of the peak at 2.04 minutes (figure 3.1) corresponding to di-*tert* butyl hydroxylamine. The structure given in the top right corner is that of the molecular ion ( $M^{+\bullet}$ ) corresponding to the peak at  $m/z$  145.

The EI mass spectrum shown in figure 3.19 corresponds to the di-*tert* butyl hydroxylamine. This is formed from the *tert*-butyl part of the PBN. 2-methyl-2-nitrosopropane (MNP) is one of the products formed by the breakdown of PBN during the reaction. Di-*tert* butyl hydroxylamine is formed when MNP gains another *tert*-butyl group (formed by the breakdown and rearrangement of acetaldehyde) and a hydrogen on the oxygen of the nitroxide to attain stability (Turnbull *et al.*, 2001). Loss of a methyl group from a molecular ion gives a peak at  $m/z$  130 which further loses *tert*-butyl to give a base peak at  $m/z$  74. The fragment at  $m/z$  113 corresponds to the loss of methanol from the molecular ion while loss of methanol from the (M-15)<sup>+</sup> fragment gives a peak at  $m/z$  98. The fragment at  $m/z$  88 is formed by the loss of a *tert*-butyl group from molecular ion while the fragment at  $m/z$  57 corresponds to the *tert*-butyl cation.

### 3.6.2 EI mass spectrum of di-*tert* butyl (d<sub>9</sub>) hydroxylamine

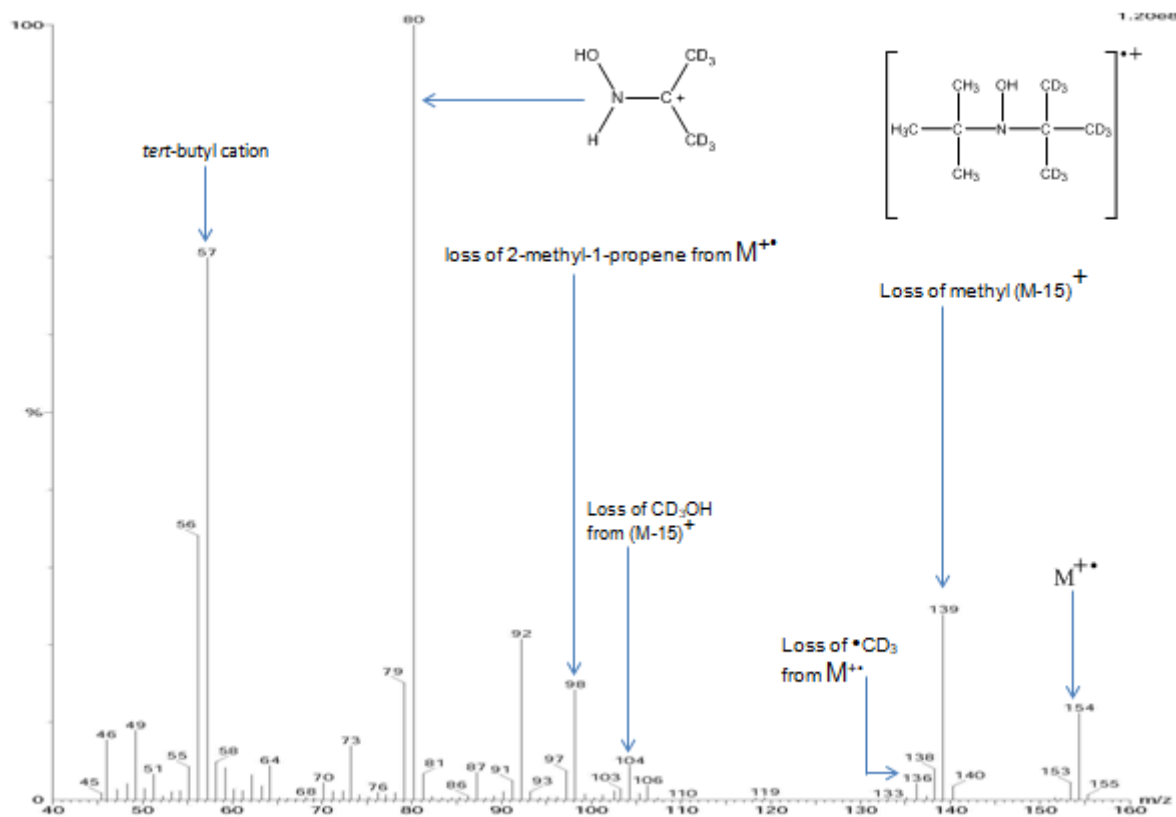


Figure 3.20: Electron ionisation (EI) mass spectrum of the peak at 2.02 minutes (figure 3.2) corresponding to di-*tert* butyl (d<sub>9</sub>) hydroxylamine. The structure given in the top right corner is that of the molecular ion ( $M^{++}$ ) corresponding to the peak at *m/z* 154.

The EI mass spectrum shown in figure 3.20 corresponds to di-*tert* butyl (d<sub>9</sub>) hydroxylamine detected at 2.02 minutes when the reaction was carried out by using d<sub>3</sub>-acetaldehyde (the methyl hydrogen atoms replaced by deuterium) as a secondary source of radicals in the Fenton reaction system. The molecular ion can be clearly seen at *m/z* 154 (a difference of 9 *m/z* units when compared to the molecular ion of Di-*tert* butyl hydroxylamine) which confirms the gain of three deuterium-methyl ( $CD_3$ ) groups. As for previous spectra, the fragment at *m/z* 139 is formed by the loss of a methyl radical (from MNP part of the molecular ion), while the loss of  $CD_3OH$  gives a fragment at *m/z* 119. The fragment at *m/z* 104 is formed by the loss of  $CD_3OH$  from  $(M-15)^+$  fragment. The fragment at *m/z* 57 corresponds to the *tert*-butyl cation.

The identity of di-*tert* butyl hydroxylamine was confirmed when the Fenton reaction was carried out by using other derivatives of PBN and by using either acetaldehyde or deuterated acetaldehyde (d<sub>3</sub>) as a secondary source of free radicals. Summary of identified compound with its retention times and molecular ion (*m/z*) is presented in Table 3.4.

Table 3.4: Summary of GC-MS data for di-*tert* butyl hydroxylamine when the reaction was carried by using PBN and its derivatives as trapping agents and acetaldehyde/deuterated acetaldehyde as a secondary source of free radicals

| Reagents in the Fenton system                      | Identified compound                                   | Retention time (R <sub>i</sub> ; minutes) | Molecular ion ( <i>m/z</i> ) |
|--|---|---|------------------------------|
| PBN and acetaldehyde                               | Di- <i>tert</i> butyl hydroxylamine                   | 2.04                                      | 145                          |
| PBN & d <sub>3</sub> -acetaldehyde                 | Di- <i>tert</i> butyl (d <sub>9</sub> ) hydroxylamine | 2.02                                      | 154                          |
| d <sub>6</sub> -PBN & acetaldehyde                 | Di- <i>tert</i> butyl hydroxylamine                   | 2.04                                      | 145                          |
| d <sub>6</sub> -PBN & d <sub>3</sub> -acetaldehyde | Di- <i>tert</i> butyl (d <sub>9</sub> ) hydroxylamine | 2.02                                      | 154                          |
| F-PBN & acetaldehyde                               | Di- <i>tert</i> butyl hydroxylamine                   | 2.03                                      | 145                          |
| Cl-PBN & acetaldehyde                              | Di- <i>tert</i> butyl hydroxylamine                   | 2.03                                      | 145                          |

### 3.7 EI mass spectrum of phenyl methanimine

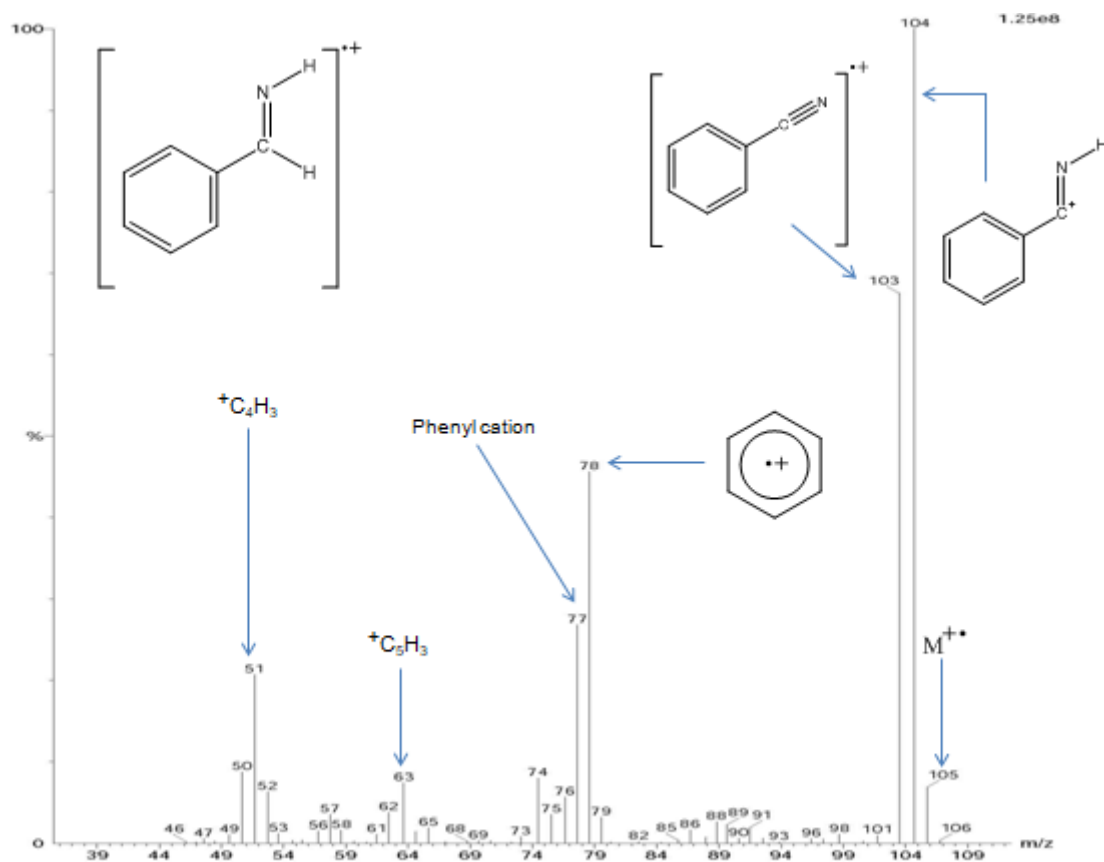


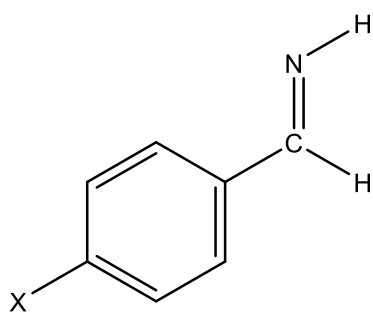
Figure 3.21: Electron ionisation (EI) mass spectrum of the peak at 2.22 minutes (figure 3.1) corresponding to phenyl methanimine. The structure given in the top left corner is that of the molecular ion ( $M^{+\bullet}$ ) corresponding to the peak at  $m/z$  105.

The EI mass spectrum shown in figure 3.21 corresponds to phenyl methanimine. The molecular ion can be seen at  $m/z$  105. The base peak is formed by the loss of a hydrogen atom from molecular ion. The fragment at  $m/z$  78 corresponds to the benzene radical cation ( ${}^{\bullet+}C_6H_6$ ) while  $m/z$  77 is a common fragment of PBN breakdown identified as a  $C_6H_5^+$  cation.

The identity of the compound was confirmed when the Fenton reaction was carried out using other derivatives of PBN and/or using either acetaldehyde or deuterated acetaldehyde as a secondary source of free radicals. Summary of identified compounds with their retention times and molecular ions ( $m/z$ ) is presented in Table 3.5

Table 3.5: Summary of GC-MS data for X-phenyl methanimine (where X is H, F or Cl) when the reaction was carried using PBN and its derivatives as trapping agents and acetaldehyde/deuterated acetaldehyde as a secondary source of free radicals

| Reagents in the Fenton system        | Identified compound                | Retention time (R <sub>t</sub> ; minutes) | Molecular ion ( <i>m/z</i> ) |
|--------------------------------------|------------------------------------|---|------------------------------|
| PBN and acetaldehyde                 | phenyl methanimine                 | 2.23                                      | 105                          |
| PBN and d <sub>3</sub> -acetaldehyde | phenyl methanimine                 | 2.23                                      | 105                          |
| d <sub>6</sub> -PBN & acetaldehyde   | d <sub>6</sub> -phenyl methanimine | 2.23                                      | 111                          |
| F-PBN & acetaldehyde                 | F-phenyl methanimine               | 2.22                                      | 123                          |
| Cl-PBN & acetaldehyde                | Cl-phenyl methanimine              | 3.75                                      | 140/142                      |



X= H (PBN)  
 F (4-FPBN)  
 Cl (4-CIPBN)

X-Phenyl methanimine

For d<sub>6</sub>-phenyl methanimine, all five hydrogen atoms on the ring and the hydrogen attached to alpha carbon are replaced by deuterium.



### 3.8 EI mass spectrum of benzaldehyde

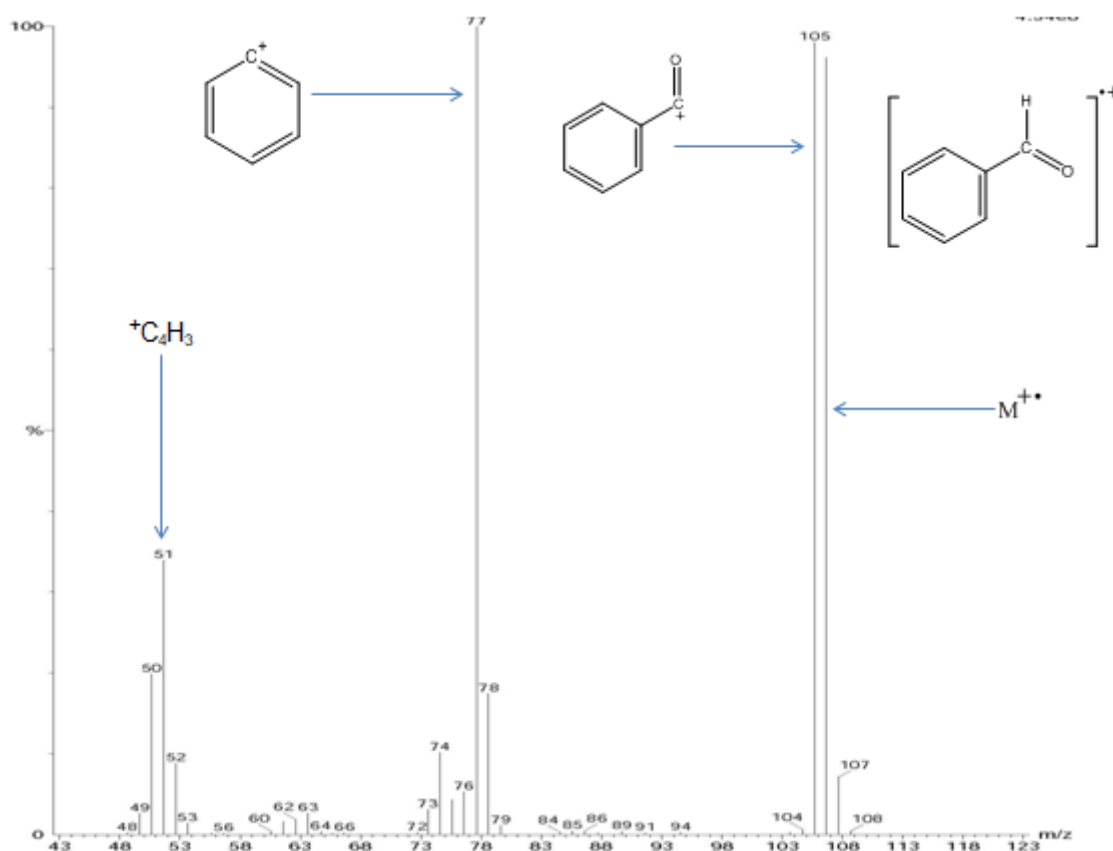


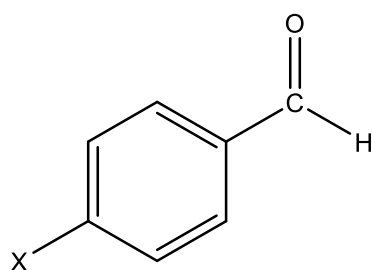
Figure 3.22: Electron ionisation (EI) mass spectrum of the peak at 2.61 minutes (figure 3.1) corresponding to benzaldehyde. The structure given in the top right corner is that of the molecular ion ( $M^{++}$ ) corresponding to the peak at  $m/z$  106.

The EI mass spectrum shown in figure 3.22 corresponds to benzaldehyde. The fragment at  $m/z$  105 is formed by the loss of hydrogen atom from the molecular ion. The fragment at  $m/z$  77 corresponds to the  $C_6H_5$  cation.

The identity of the compound was confirmed when the Fenton reaction was carried out using other derivatives of PBN and/or using either acetaldehyde or deuterated acetaldehyde as a secondary source of free radicals. A summary of benzaldehyde derivatives with their retention times and molecular ion ( $m/z$ ) is presented in Table 3.6

Table 3.6: Summary of GC-MS data for X-Benzaldehyde (where X is H, F or Cl) when the reaction was carried by using PBN and its derivatives as trapping agents and acetaldehyde or d<sub>3</sub>-acetaldehyde as a secondary source of free radicals

| Reagents in the Fenton system        | Identified benzaldehyde derivative | Retention time (R <sub>t</sub> ; minutes) | Molecular ion ( <i>m/z</i> ) |
|--------------------------------------|------------------------------------|---|------------------------------|
| PBN and acetaldehyde                 | Benzaldehyde                       | 2.61                                      | 106                          |
| PBN and d <sub>3</sub> -acetaldehyde | Benzaldehyde                       | 2.61                                      | 106                          |
| d <sub>6</sub> -PBN & acetaldehyde   | d <sub>6</sub> -benzaldehyde       | 2.60                                      | 112                          |
| F-PBN & acetaldehyde                 | F-benzaldehyde                     | 2.52                                      | 124                          |
| Cl-PBN & acetaldehyde                | Cl-benzaldehyde                    | 4.63                                      | 140                          |



X= H (PBN)  
 F (4-FPBN)  
 Cl (4-CIPBN)

X-benzaldehyde

For d<sub>6</sub>-benzaldehyde all five hydrogen atoms on the ring and the hydrogen attached to alpha carbon are replaced by deuterium

### 3.9 N-methoxy-1-phenylethanamine

#### 3.9.1 EI mass spectrum of N-methoxy-1-phenylethanamine

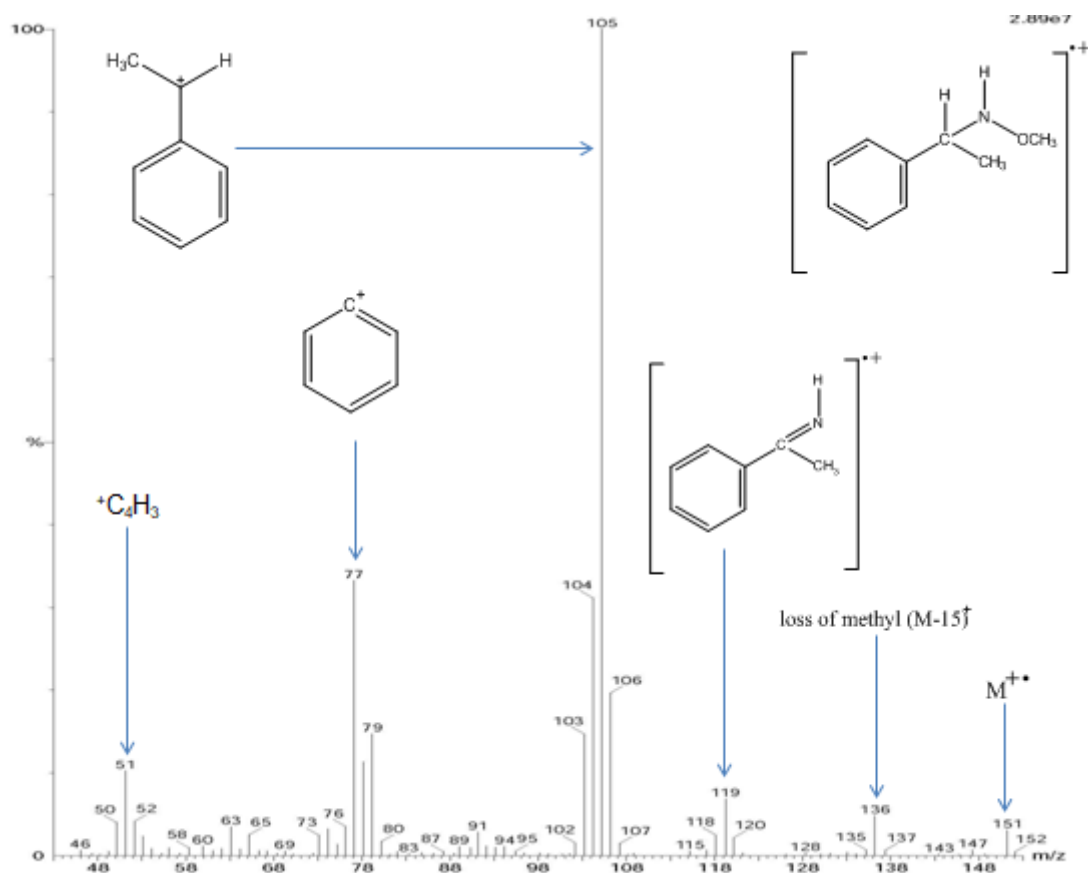


Figure 3.23: Electron ionisation (EI) mass spectrum of the peak at 5.22 minutes (figure 3.1) corresponding to N-methoxy-1-phenylethanamine. The structure given in the top right corner is that of the molecular ion ( $M^+$ ) corresponding to the peak at  $m/z$  151.

The EI mass spectrum shown in figure 3.23 corresponds to N-methoxy-1-phenylethanamine detected at 5.22 minutes. The fragment at  $m/z$  136 is formed by the loss of a methyl radical from the molecular ion. Dissociation of the molecular ion between the alpha carbon and nitrogen gives the base peak at  $m/z$  105. The fragment at  $m/z$  57 corresponds to the *tert*-butyl cation.

### 3.9.2 EI mass spectrum of N-methoxy-1-phenylethanamine (d<sub>6</sub>)

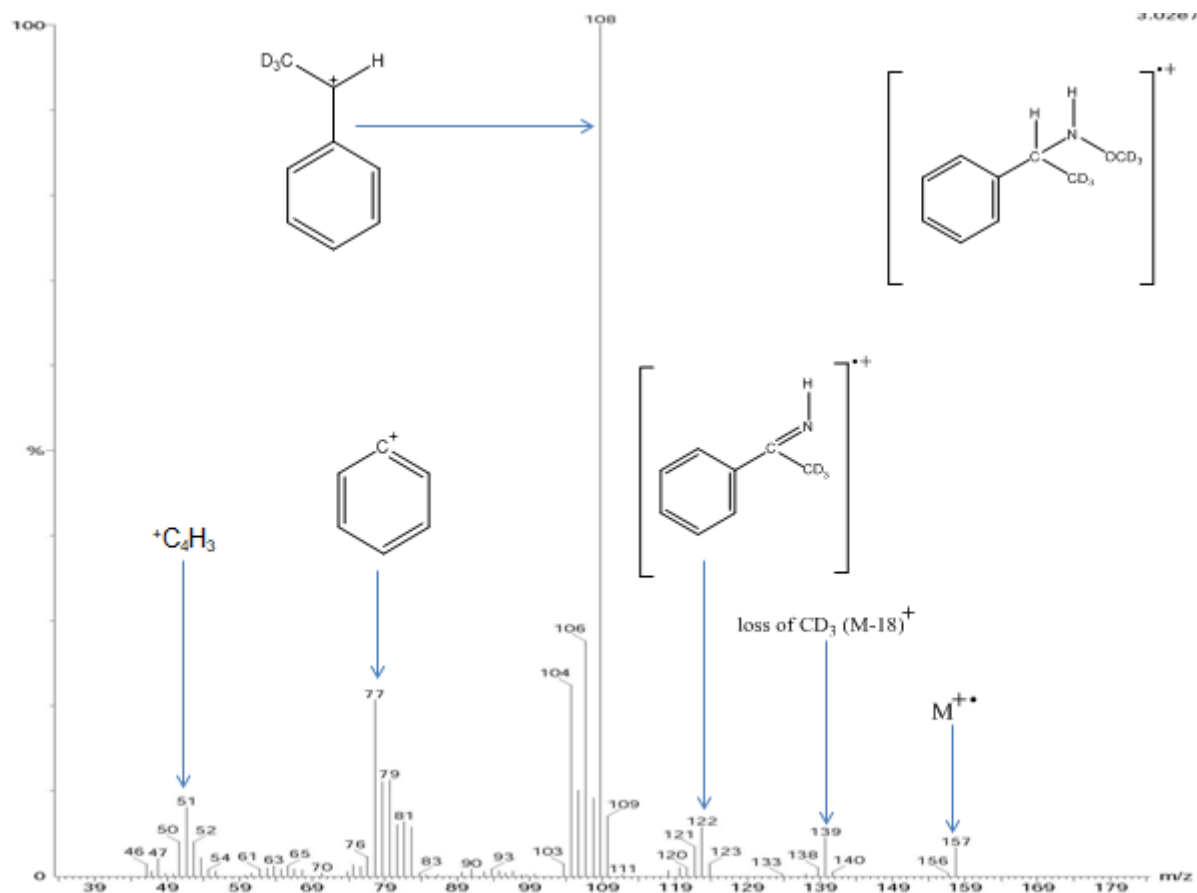
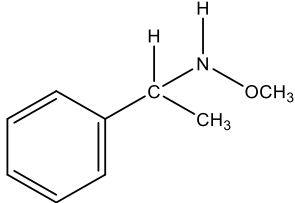
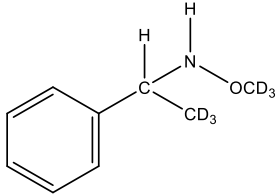
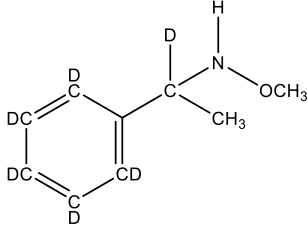
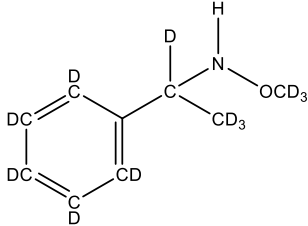
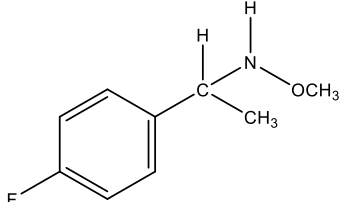


Figure 3.24: Electron ionisation (EI) mass spectrum of the peak at 5.13 minutes (figure 3.2) corresponding to N-methoxy-1-phenylethanamine (d<sub>6</sub>). The structure given in the top right corner is that of the molecular ion (M<sup>+</sup>) corresponding to the peak at m/z 157.

The EI mass spectrum shown in figure 3.24 corresponds to N-methoxy-1-phenylethanamine (d<sub>6</sub>) detected at 5.13 minutes when the reaction was carried out using d<sub>3</sub>-acetaldehyde (the methyl hydrogen atoms replaced by deuterium) as a secondary source of radicals in the Fenton reaction system. The molecular ion can be seen at m/z 157 (difference of 6 m/z units when compared to the mass spectrum when using non-deuterated acetaldehyde; figure 3.23) which confirms the trapping of two deuteromethyl (<sup>•</sup>CD<sub>3</sub>) radicals. The fragment at m/z 139 is formed the loss of a <sup>•</sup>CD<sub>3</sub> from the molecular ion. Dissociation of the molecular ion between the alpha carbon and nitrogen gives the base peak at m/z 108. The fragment at m/z 57 corresponds to the *tert*-butyl cation.

Furthermore, the identity of the compound was confirmed when the Fenton reaction was carried out using other derivatives of PBN and/or using either acetaldehyde or deuterated acetaldehyde as a secondary source of free radicals. Summary of identified compounds with their retention times and molecular ions ( $m/z$ ) is presented in Table 3.7

Table 3.7: Summary of GC-MS data for N-methoxy-1-X-phenylethanamine (where X is H, F or Cl) when the reaction was carried out by using PBN and its derivatives as trapping agents and acetaldehyde/deuterated acetaldehyde as a secondary source of free radicals

| Reagents in the Fenton system                      | Identity  | Retention time ( $R_t$ ; minutes) | Molecular ion ( $m/z$ ) | Base Peak ( $m/z$ ) | Characteristic fragment peaks ( $m/z$ ) |
|--|---|-----------------------------------|-------------------------|---------------------|---|
| PBN & acetaldehyde                                 |    | 5.21                              | 151                     | 105                 | 136, 119, 77                            |
| PBN & d <sub>3</sub> -acetaldehyde                 |   | 5.13                              | 157                     | 108                 | 139, 122, 77                            |
| d <sub>6</sub> -PBN & acetaldehyde                 |  | 5.16                              | 157                     | 111                 | 142, 125, 82                            |
| d <sub>6</sub> -PBN & d <sub>3</sub> -acetaldehyde |  | 5.08                              | 163                     | 114                 | 145, 128, 82                            |
| F-PBN & acetaldehyde                               |  | 5.34                              | 169                     | 123                 | 154, 137, 95                            |
| Cl-PBN & acetaldehyde                              | Not detected  |                                   |                         |                     |   |

### 3.10 EI mass spectrum of methoxy-(1-phenylethylidene)amine

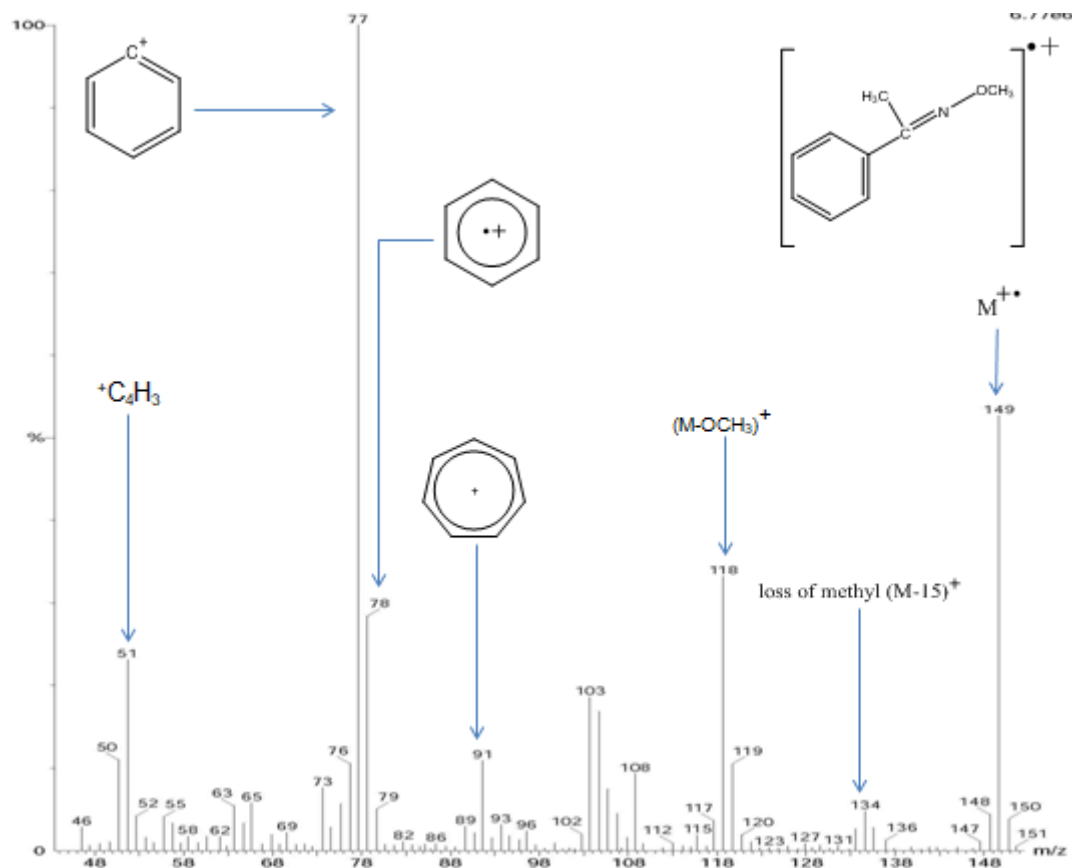


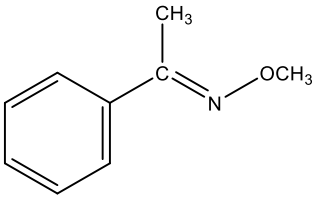
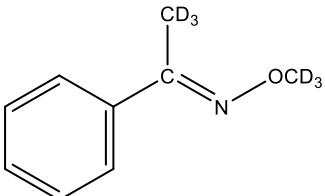
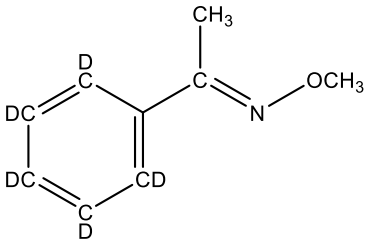
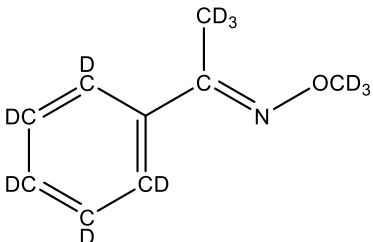
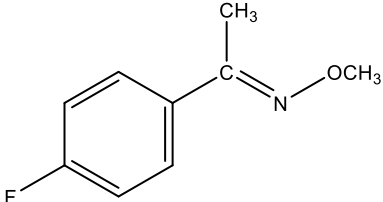
Figure 3.25: Electron ionisation (EI) mass spectrum of the peak at 6.32 minutes (figure 3.1) corresponding to methoxy-(1-phenylethylidene)amine. The structure given in the top right corner is that of the molecular ion ( $M^+$ ) corresponding to the peak at  $m/z$  149.

The EI mass spectrum shown in figure 3.25 corresponds to methoxy-(1-phenylethylidene)amine detected at 6.32 minutes. The suggested adduct is formed by trapping two methyl radicals and loss of *tert*-butyl group from PBN & loss of both hydrogens i.e. from alpha carbon and nitrogen. Loss of the methoxy group from molecular ion gives a peak at  $m/z$  118. Dissociation of the molecular ion between the alpha carbon and nitrogen gives the base peak at  $m/z$  105. The fragment at  $m/z$  57 corresponds to the *tert*-butyl cation. The fragment at  $m/z$  77 is a  $C_6H_5$  cation which is also the base peak.

The identity of adduct was confirmed when the Fenton reaction was carried out using other derivatives of PBN and using either acetaldehyde or deuterated acetaldehyde as a secondary source of free radicals. Summary of identified compounds with their retention times and molecular ion ( $m/z$ ) is presented in Table 3.8



Table 3.8: Summary of GC-MS data for methoxy(1-phenylethylidene)amine derivatives, when reaction was carried out by using PBN and its derivatives as trapping agent and acetaldehyde/deuterated acetaldehyde as a secondary source of free radicals

| Reagents in the Fenton system    | Identity  | Retention time ( $R_t$ ; minutes) | Molecular ion ( $m/z$ ) | Base Peak ( $m/z$ ) | Characteristics fragment peaks ( $m/z$ ) |
|----------------------------------|---|-----------------------------------|-------------------------|---------------------|--|
| PBN & acetaldehyde               |    | 6.32                              | 149                     | 77                  | 134, 118, 105                            |
| PBN & $d_3$ -acetaldehyde        |   | 6.22                              | 155                     | 77                  | 137, 122,                                |
| $d_6$ -PBN & acetaldehyde        |  | 6.29                              | 154                     | 82                  | 139, 123, 108                            |
| $d_6$ -PBN & $d_3$ -acetaldehyde |  | 6.18                              | 160                     | 82                  | 142, 126, 108                            |
| F-PBN & acetaldehyde             |  | 6.15                              | 167                     | 95                  | 152, 136, 122                            |

### 3.11 EI mass spectrum of 2,3-diphenylbutane

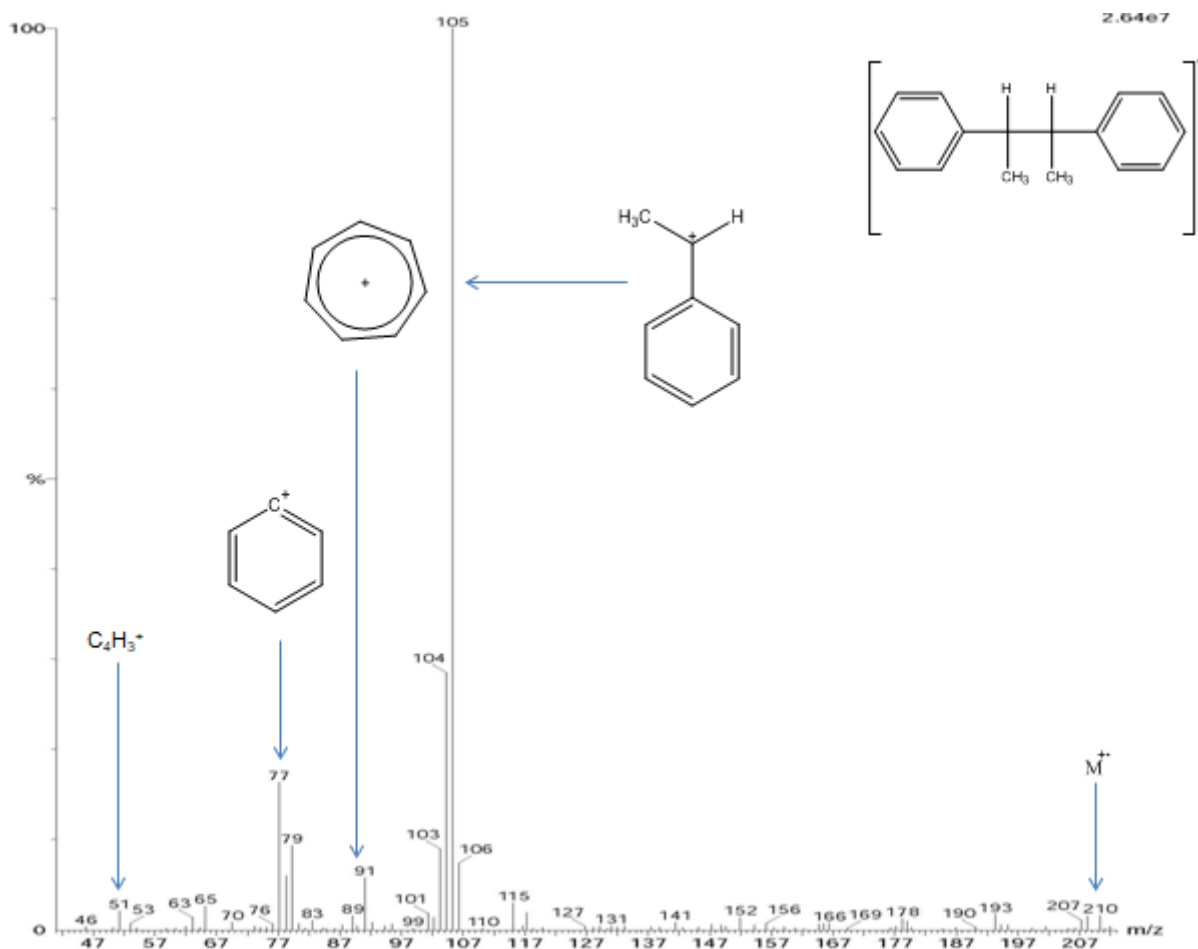


Figure 3.26: Electron ionisation (EI) mass spectrum of the peaks at  $R_t$  15.96 & 16.25 minutes (figure 3.1) corresponding to isomers of 2,3-diphenylbutane. The structure given in the top right corner is that of the molecular ion ( $M^+$ ) corresponding to the peak at  $m/z$  210.

The EI mass spectrum shown in figure 3.26 corresponds to isomers of 2,3-diphenylbutane detected at 15.96 & 16.25 minutes. Dissociation of the molecular ion at the C-C bond gives the base peak at  $m/z$  105. The fragment at  $m/z$  57 corresponds to the *tert*-butyl cation. The fragment at  $m/z$  77 is a  $C_6H_5^+$  cation while the fragment at  $m/z$  91 corresponds to the tropylium cation.

The identity of compound was confirmed when the Fenton reaction was carried out using other derivatives of PBN and using either acetaldehyde or deuterated acetaldehyde as a secondary source of free radicals. Summary of identified diphenylbutane derivatives with their retention times and molecular ions ( $m/z$ ) is presented in Table 3.9

Table 3.9: Summary of GC-MS data for 2,3-X-diphenylbutane (where X is H, F or Cl) when the reaction was carried out using PBN and its derivatives as trapping agents and acetaldehyde/deuterated acetaldehyde as a secondary source of free radicals

| Reagents in the Fenton system    | Identity                     | Retention time ( $R_t$ ; minutes) | Molecular ion ( $m/z$ ) | Base Peak ( $m/z$ ) |
|----------------------------------|------------------------------|-----------------------------------|-------------------------|---------------------|
| PBN & acetaldehyde               | 2,3-diphenylbutane           | 15.96/16.25                       | 210                     | 105                 |
| PBN & $d_3$ -acetaldehyde        | 2,3-diphenylbutane- $d_6$    | 15.92/16.21                       | 216                     | 108                 |
| $d_6$ -PBN & acetaldehyde        | 2,3-diphenylbutane- $d_{12}$ | 15.91/16.19                       | 222                     | 111                 |
| $d_6$ -PBN & $d_3$ -acetaldehyde | 2,3-diphenylbutane- $d_{18}$ | 15.86/16.14                       | Not detected            | 114                 |
| F-PBN & acetaldehyde             | Fluoro-2,3-diphenylbutane    | 16.15/16.42                       | 246 very weak           | 123                 |

### 3.12 Paraldehyde:

#### 3.12.1 EI mass spectrum of paraldehyde

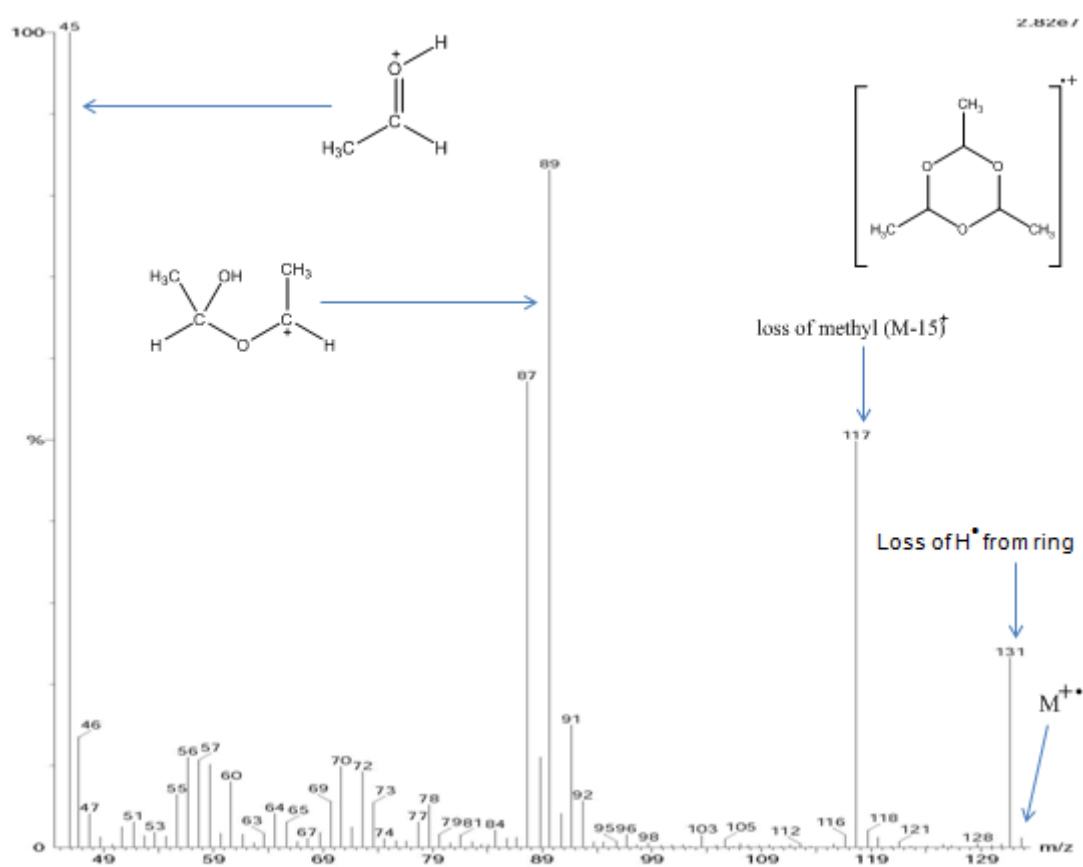


Figure 3.27: Electron ionisation (EI) mass spectrum of the peak at  $R_t$  1.80 minutes (figure 3.1) corresponding to paraldehyde. The structure given in the top right corner is that of the molecular ion ( $M^{+\bullet}$ ) corresponding to the peak at  $m/z$  132.

The EI mass spectrum shown in figure 3.27 corresponds to paraldehyde detected at 1.80 minutes. The peak is present in non-Fenton control experiments (data not shown) when acetaldehyde is used and suggests that the compound is derived from acetaldehyde and not from the Fenton reaction. A search of the NIST library suggests it to be paraldehyde, which is not only a precursor of acetaldehyde but can also be formed by self-aldol condensation of acetaldehyde molecules in the presence of protons (Hill, Miessner & Ohlmann, 1989; Georgieff, 1966). Scheme of paraldehyde formation from acetaldehyde is presented in appendix as figure A2. Fragments at  $m/z$  131, 89 and a base peak at 45 are the characteristic fragments of paraldehyde

### 3.12.2 EI mass spectrum of paraldehyde (d<sub>9</sub>)

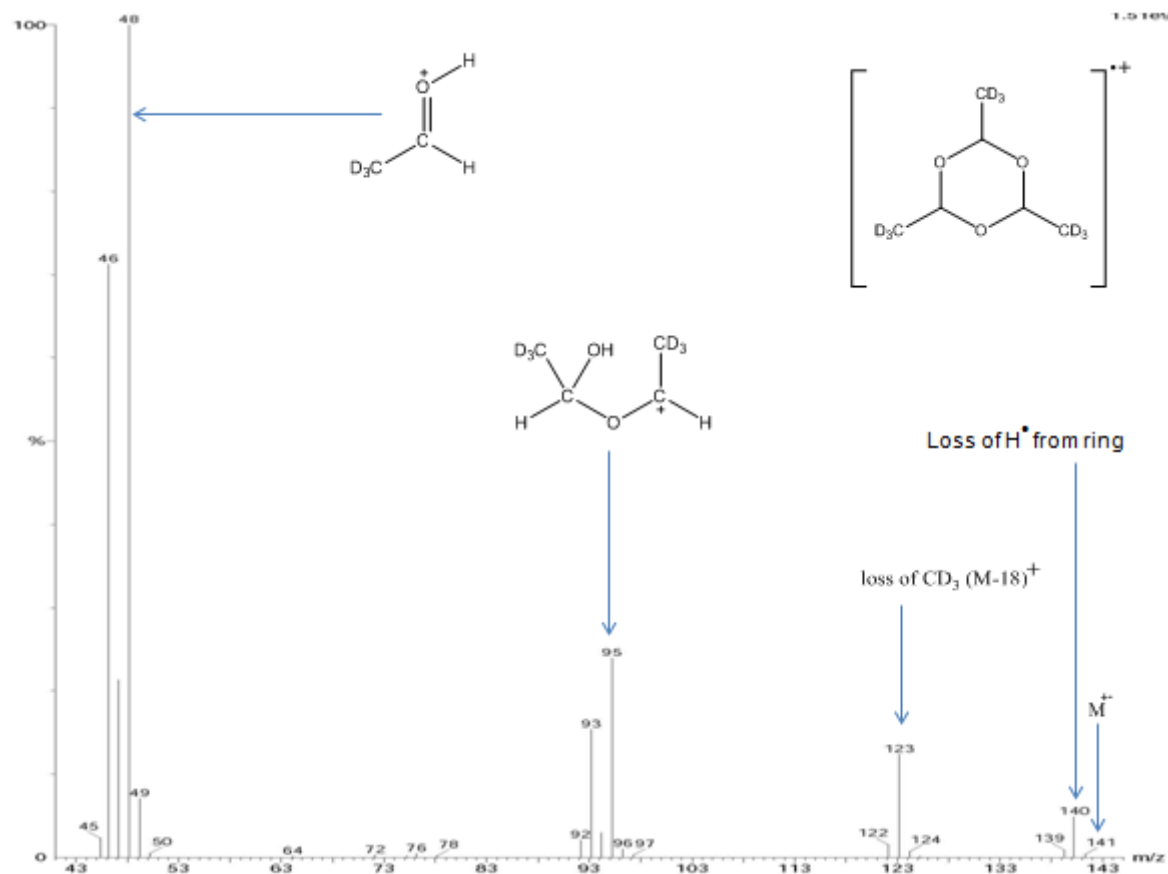


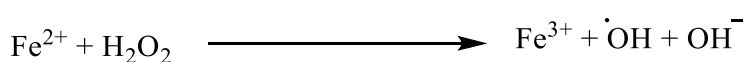
Figure 3.28: Electron ionisation (EI) mass spectrum of the peak at *R<sub>t</sub>* 1.79 minutes (Figure 3.2) corresponding to d<sub>9</sub>-paraldehyde. The structure given in the top right corner is that of the molecular ion (M<sup>+</sup>) corresponding to the peak at *m/z* 141.

The EI mass spectrum shown in Figure 3.28 corresponds to d<sub>9</sub>-paraldehyde detected at 1.79 minutes when the reaction was carried out by using d<sub>3</sub>-acetaldehyde (the methyl hydrogen atoms replaced by deuterium) as a secondary source of radicals in the Fenton reaction system. The molecular ion is just visible at *m/z* 141 (difference of 9 *m/z* units when compared to that in figure 3.27 where non-deuterated acetaldehyde was used) thus confirming the formation of paraldehyde.

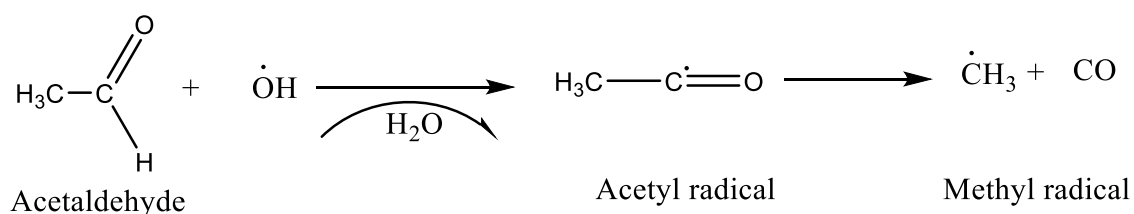
### 3.13 Discussion:

The aim of the study in this chapter was to develop a solvent free method for the detection and analysis of the spin trapped free radicals generated by acetaldehyde as a secondary source of radicals in the Fenton system. The Fenton reaction is one that generates hydroxyl radicals (scheme 3.2) which can be damaging to different constituents of the cell. Hydroxyl radicals are short-lived which makes them very hard to detect. They can react with many organic molecules at near diffusion-controlled rates to produce other radicals and possibly initiate a chain reaction which is even more destructive to the living body (Dalle-Donne *et al.*, 2006).

Spin trapping is a technique used to trap these radicals. Spin traps are chemical compounds which react with free radicals to produce comparatively stable radical adducts which can be measured by using different analytical techniques, principally electron paramagnetic resonance (EPR) spectroscopy (Halliwell & Gutteridge, 2015). In this study, the Fenton reaction was used to generate hydroxyl radicals which then reacted with acetaldehyde to produce acetyl radicals, which further decompose into methyl radicals and hydrogen atoms by decarbonylation (Nakao *et al.*, 2000) as shown in scheme 3.3. In another study hydrogen radicals produced from acetaldehyde were spin trapped by PBN and detected by EPR (Jenkins *et al.*, 1997). These free radicals then react with PBN derivatives to produce stable radical adducts which may be extracted and analysed by using TD-GC-MS.



Scheme 3.2: The Fenton reaction

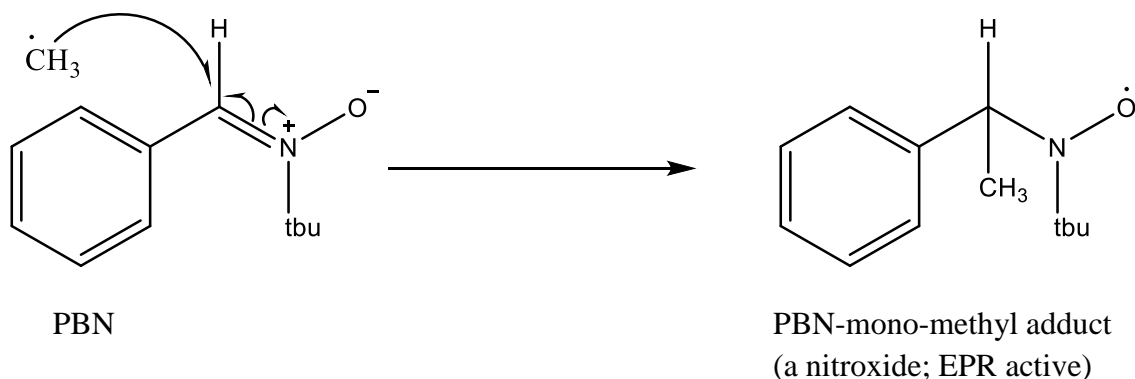


Scheme 3.3: Generation of methyl radicals from acetaldehyde during the Fenton reaction

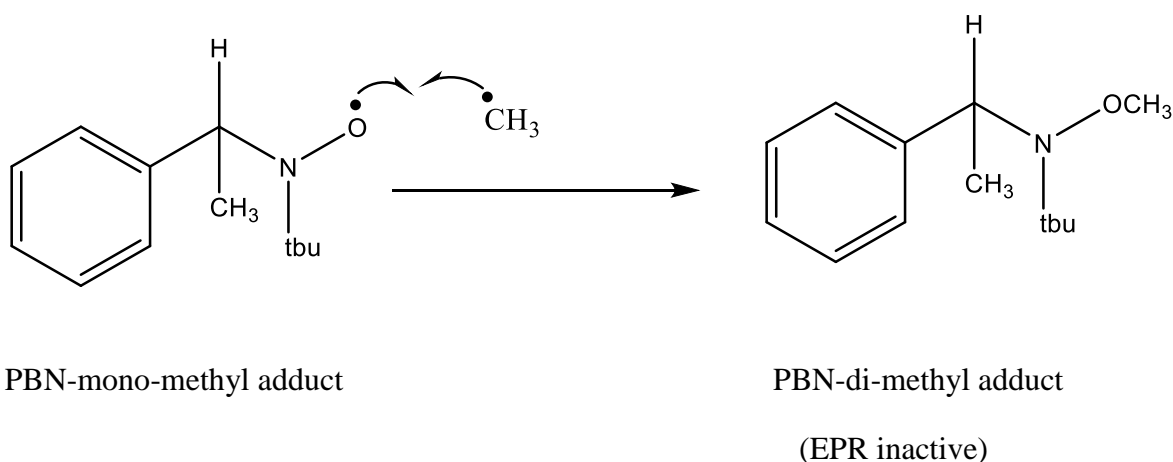
The chromatogram in figure 3.1 shows several peaks which are not present in “non-Fenton” control reactions thus confirming them as products of the Fenton reaction. These peaks have been identified by carrying out the Fenton reaction with PBN or its derivatives in the presence of acetaldehyde or deuterated acetaldehyde ( $d_3$ ).

The most intense peak at 10.27 minutes in figure 3.1 has been identified as a di-methyl adduct of PBN (PBN-Me<sub>2</sub>). Formation of the di-methyl adduct of PBN is a two-step process. In the first step, methyl radicals are trapped at the alpha carbon, converting the molecule into a nitroxide which, in turn, traps another methyl group at the oxygen and generates a stable non-radical adduct (scheme 3.4).

### Step 1: Formation of mono-methyl adduct



### Step 2: Formation of the di-methyl adduct



Scheme 3.4: Trapping of methyl radicals by PBN (Janzen *et al.*, 1985).

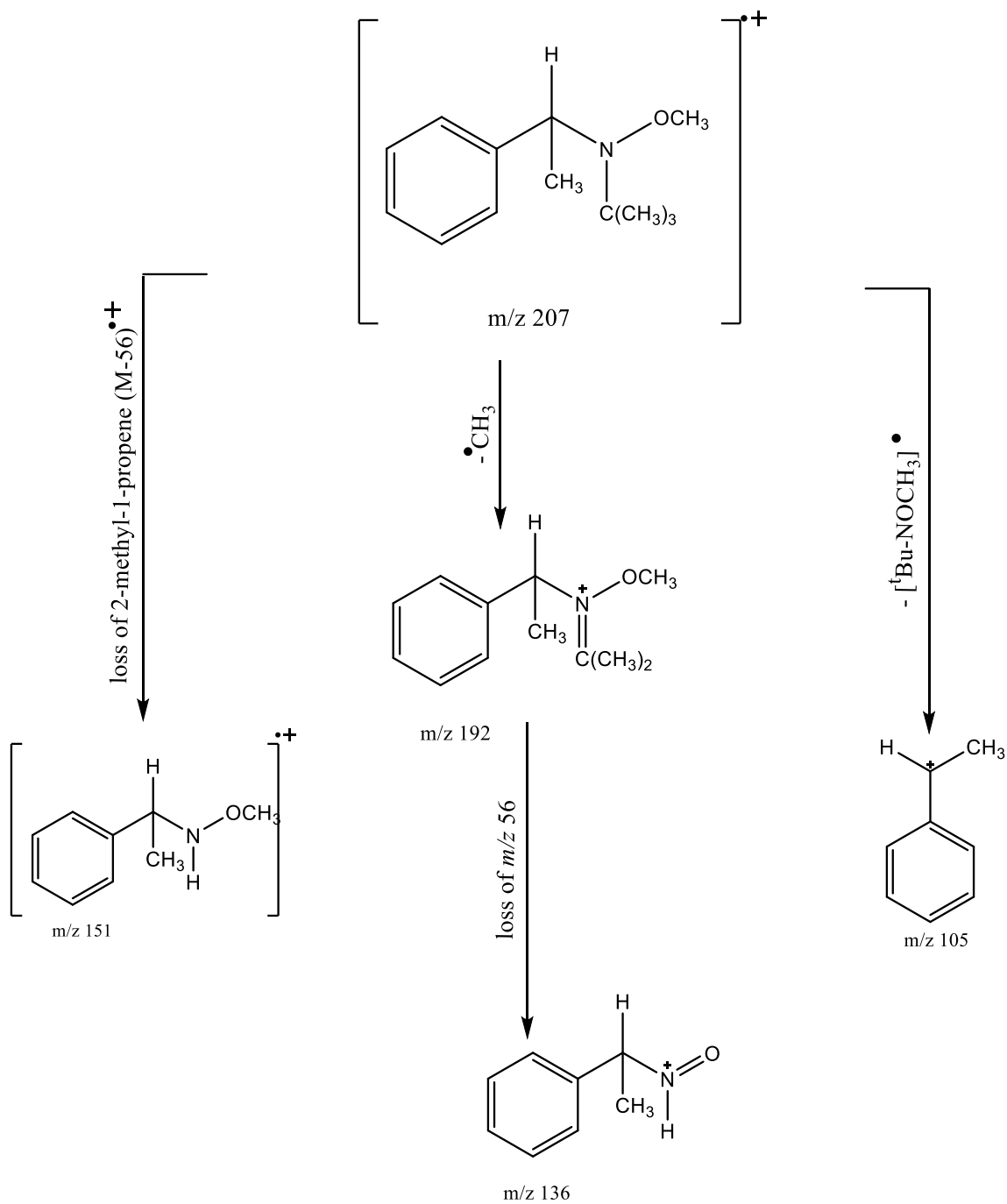
The mass spectrum in figure 3.6 clearly shows a molecular ion at  $m/z$  207 which loses a methyl radical to give a fragment at  $m/z$  192. The methyl radical is lost from the <sup>1</sup>Bu group as indicated by experiments using d<sub>3</sub>-acetaldehyde as the source of secondary radicals. One of the trapped methyl groups may also be lost which further loses *tert*-butyl to give a peak at  $m/z$  136. Loss of 2-methyl-1-propene from the molecular ion gives a fragment at  $m/z$  151. Dissociation of the molecular ion between the alpha carbon and nitrogen gives the base peak at  $m/z$  105 (shown in scheme 3.5).

To confirm the source of the methyl radicals, deuterated acetaldehyde was used in the Fenton system. Deuteron-methyl radicals (<sup>2</sup>CD<sub>3</sub>) were generated and then trapped by PBN to form a PBN(CD<sub>3</sub>)<sub>2</sub> adduct (Figure 3.7). This clearly demonstrates that acetaldehyde is the source of the trapped methyl radicals in the system. Furthermore, the identity of the adduct was confirmed by using different combinations of spin trap and acetaldehyde/deuterated-acetaldehyde, summarised in Table 3.1.

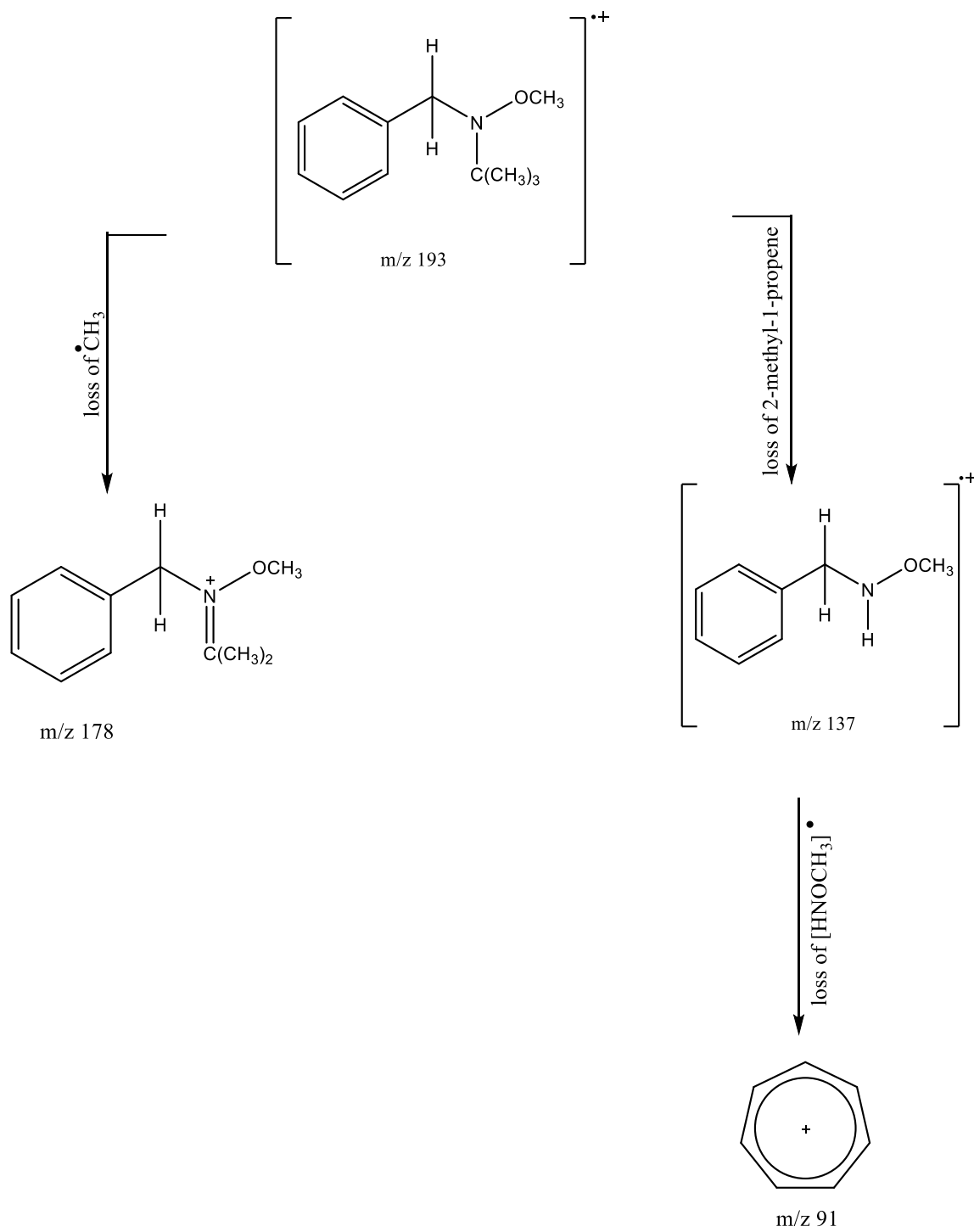
The chromatogram shown in figure 3.1 has a small peak retained at 8.52 minutes. This is hydrogen & methyl adduct of PBN (H-PBN-Me). A hydrogen atom is trapped by the alpha carbon to give an unstable nitroxide, which then traps a methyl radical to stabilise itself (Janzen *et al.*, 1985). The molecular ion can be seen at  $m/z$  193 (figure 3.12) which then loses a methyl group to give a peak at  $m/z$  178. The methyl radical is lost from the <sup>1</sup>Bu group as demonstrated by experiments using d<sub>3</sub>-acetaldehyde. Loss of 2-methyl-1-propene from parent molecular ion gives a peak at  $m/z$  137. Further loss of [HNOCH<sub>3</sub>]<sup>•</sup> from this fragment generates a peak at  $m/z$  91 (scheme 3.6). Janzen and his colleagues also observed same fragmentation pattern for the adduct in 1985.

The identity of adduct was confirmed using deuterated acetaldehyde in the Fenton reaction. A small peak retained at 8.48 minutes (figure 3.2) is the hydrogen and CD<sub>3</sub> adduct of PBN (H-PBN-CD<sub>3</sub>). The molecular ion has shifted to  $m/z$  196 confirming the addition of one deuteron-methyl radical. Furthermore, experiments using different combinations of PBN or its derivatives and acetaldehyde/d<sub>3</sub>-acetaldehyde help to confirm the identity of the adduct; retention times, the  $m/z$  value of the molecular ions and characteristic fragments are all summarised in table 3.2.





Scheme 3.5: Fragmentation pattern of the PBN-di-methyl adduct



Scheme 3.6: Fragmentation pattern of hydrogen & methyl adduct of PBN (H-PBN-Me)

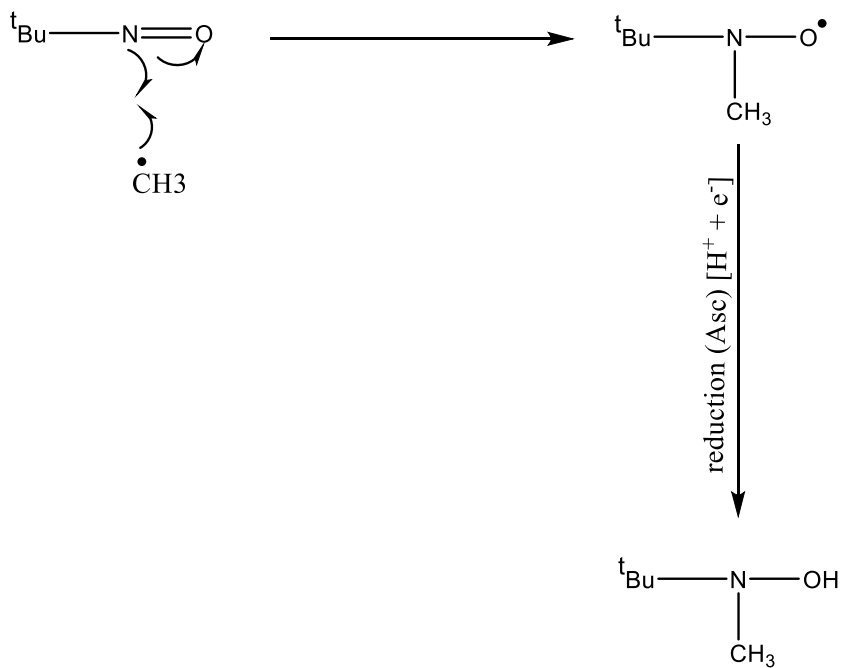
The chromatogram shown in figure 3.1 gives two peaks retained at 15.91 and 16.25 minutes with the same mass spectrum suggesting that these are isomers. The suggested compound is 2,3-diphenylbutane. The adduct is most probably formed in the Fenton system although mechanism of its formation needs further investigation (figure 3.26). The base peak at  $m/z$  105 is formed by the dissociation of the molecule from the centre point.

An experiment carried out by using deuterated acetaldehyde with PBN showed a molecular ion at  $m/z$  216, demonstrating the presence of two deuterium-methyl radicals. Further experiments involving  $d_6$ -PBN and acetaldehyde or  $d_3$ -acetaldehyde suggest that the compound is 2,3-diphenylbutane. A summary of retention times and  $m/z$  values for the base peaks and characteristic fragments is presented in table 3.9.

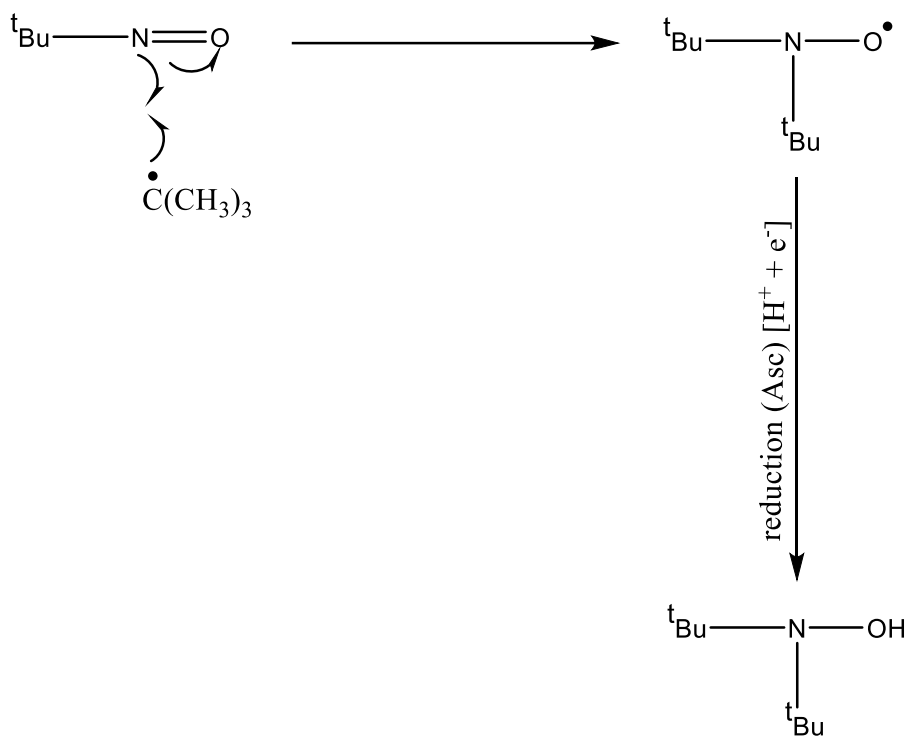
A peak retained at 1.63 minutes (figure 3.1) has been identified as a methyl adduct of *tert*-butylhydroaminoxyl. Hydroxyl radical attack on PBN may lead to the formation of 2-methyl-2-nitrosopropane (MNP) (Turnbull *et al.*, 2001). MNP is a known free radical spin trap which, in this study, may trap a methyl radical & then be reduced to the *tert*-butylhydroaminoxyl in the presence of ascorbate (scheme 3.7). Production of *tert*-butylhydroaminoxyl by the degradation of PBN is well documented (Kotake and Janzen, 1991; Jerzykiewics *et al.*, 2011). The molecular ion of the adduct is seen at  $m/z$  103 (figure 3.17). In the corresponding experiment, using  $d_3$ -acetaldehyde the  $m/z$  value of the molecular ion increases by 3 units to 106 (figure 3.18) thus confirming the addition of methyl in the structure (summarised in table 3.3).

The peak retained at 2.04 minutes (figure 3.1) is di-*tert* butyl hydroxylamine with a molecular ion at  $m/z$  145 (figure 3.19). It is believed that MNP, formed from the breakdown of PBN, traps a *tert*-butyl radical to produce di-*tert*-butylnitroxide radical (Makino, Moriya and Hatano, 1985; Turnbull *et al.*, 2001; Jerzykiewics *et al.*, 2011), which subsequently reduces in the presence of ascorbate to generate di-*tert* butyl hydroxylamine (scheme 3.8). Loss of methyl radical from the molecular ion gives a peak at  $m/z$  130 while the base peak at  $m/z$  74 may be formed by the loss of methyl radical from the ion at  $m/z$  89 which, in turn, may be formed by loss of a *tert*-butyl radical from  $m/z$  130 (figure 3.19; scheme 3.9). Further evidence to support the suggested structure of the compound is obtained when the Fenton reaction is carried out using  $d_3$ -acetaldehyde. The molecular ion  $m/z$  value increases by 9 units to 154 (figure 3.20) thus confirming the

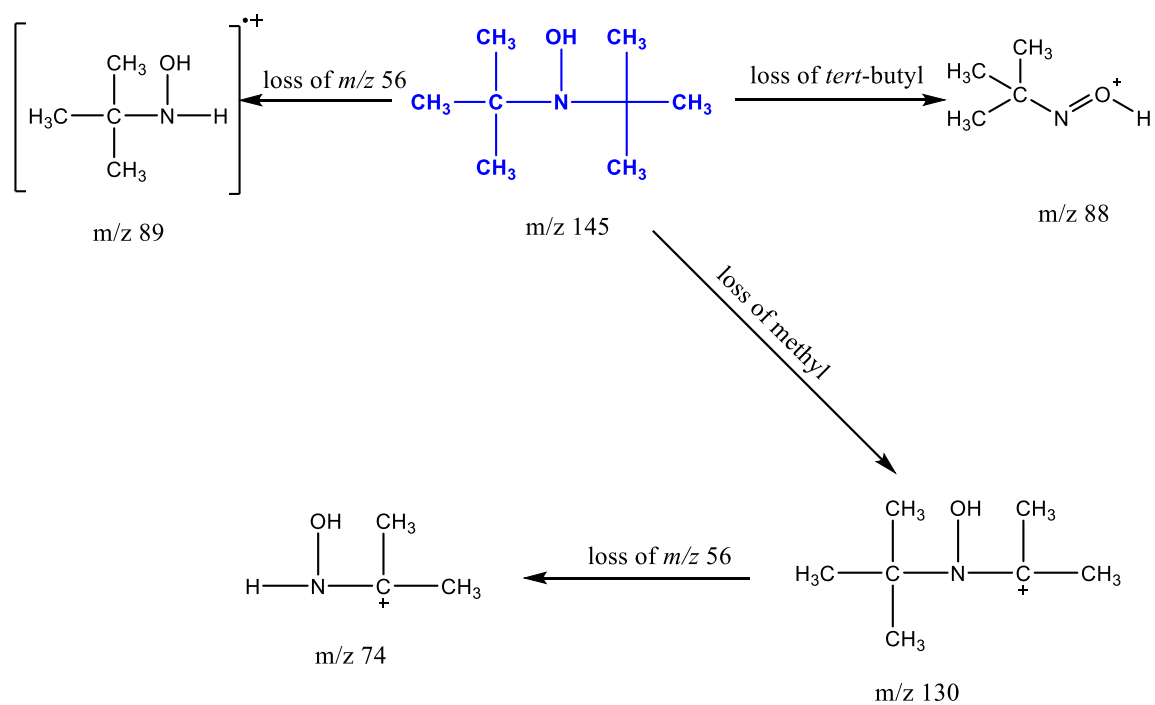
identity of adduct. Detection of di-*tert* butyl hydroxylamine while using different derivatives of PBN is summarised in table 3.4.



Scheme 3.7: Pathway of methyl adduct of *tert*-butylhydroaminoxyl formation from 2-methyl-2-nitrosopropane (MNP)

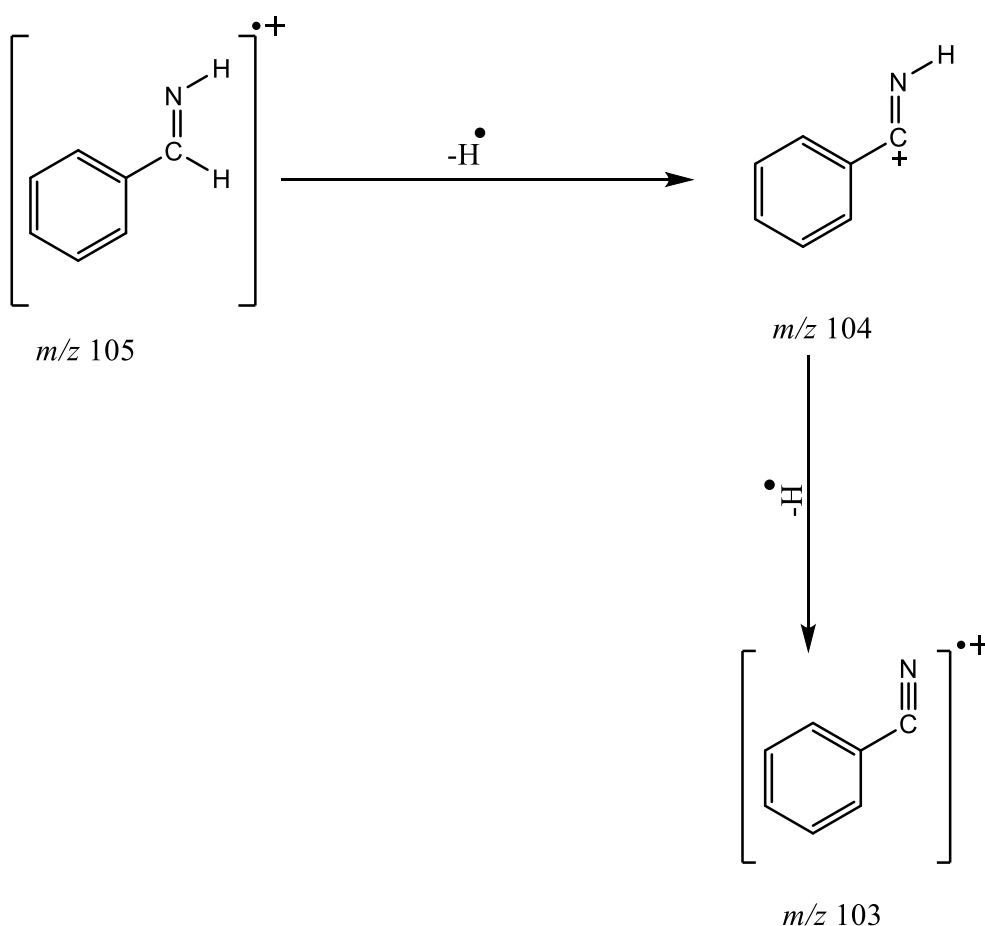


Scheme 3.8: Pathway of di-*tert*-butyl hydroxylamine formation from MNP



Scheme 3.9: Fragmentation pattern of di-*tert*-butyl hydroxylamine.

The peak retained at 2.22 minutes (shown in figure 3.1) is identified as phenyl methanimine with a molecular ion at  $m/z$  105 (figure 3.21). Loss of a hydrogen atom gives the base peak at  $m/z$  104, which further loses a hydrogen atom to generate a peak at  $m/z$  103 (scheme 3.10). The peak in the mass spectrum at  $m/z$  78 corresponds to the benzene radical cation and that at  $m/z$  77 to the  $C_6H_5^+$  cation. No methyl group is added to form this compound and thus experiments using  $d_3$ -acetaldehyde generated no changes in the mass spectrum. Experiments using  $d_6$ -PBN and other derivatives of PBN generated F-phenyl methanimine, Cl-phenyl methanimine and  $d_6$ -phenyl methanimine with molecular ions at  $m/z$  123, 140/142 and 111, respectively, when F-PBN, Cl-PBN and  $d_6$ -PBN were used. Retention times and identified adducts are summarised in table 3.5.



Scheme 3.10: Suggested pathway of phenyl methanimine fragmentation

An intense peak retained at 2.61 minutes (figure 3.1) is identified as benzaldehyde, which is a well known product of PBN degradation (Turnbull et al., 2001; Ebersson and Persson, 1998; Atamna, Paler-Martinez & Ames, 2000) The molecular ion was seen at  $m/z$  106 and base peak at  $m/z$  77 (figure 3.22). When different PBN derivatives were used in the Fenton reaction, the respective benzaldehyde derivatives i.e. Cl-benzaldehyde from Cl-PBN and F-benzaldehyde from F-PBN were detected, confirming the identity. Retention times &  $m/z$  values for molecular ions are summarised in table 3.6

A small peak retained at 5.22 minutes (figure 3.1) is identified as N-methoxy-1-phenylethanamine with a molecular ion at  $m/z$  151 (figure 3.23). Loss of a methyl radical gives a peak at  $m/z$  136 and dissociation of the molecular ion at the alpha carbon and nitrogen gave the base peak at  $m/z$  105, a fragment also formed from the breakdown of the molecular ion of the PBN dimethyl adduct (PBN-Me<sub>2</sub>). A possible mechanism of formation for this adduct is that, following the formation of PBN-Me<sub>2</sub>, as discussed earlier, 2-methyl propane (CH<sub>3</sub>CH(CH<sub>3</sub>)CH<sub>3</sub>) is lost. This reaction may occur in either the reaction mixture or within the injector port of the GC-MS. The identity of adduct was confirmed by using d<sub>3</sub>-acetaldehyde in the Fenton reaction. The molecular ion is clearly seen at  $m/z$  157 showing an increase of 6  $m/z$  units, confirming that two deuterium-methyl radicals have been trapped. Retention times and  $m/z$  values for the molecular ion, base peak and characteristic fragments are summarised in table 3.7.

Another small peak retained at 6.32 minutes (figure 3.1) is methoxy-(1-phenylethylidene)amine with a molecular ion at  $m/z$  149 (figure 3.25). Possibly, this is formed from the loss of 2-methyl-1-propene from PBN-Me<sub>2</sub>. The structure of molecular ion is presented in the mass spectrum in figure 3.25). Loss of a methoxy radical from the molecular ion gives a peak at  $m/z$  118 while other characteristic fragments are also seen at  $m/z$  105 & 77. When deuterated acetaldehyde is used in the Fenton system the molecular ion is detected at  $m/z$  155, an increase of 6  $m/z$  units, confirming the addition of two deuterium-methyl groups. Loss of OCD<sub>3</sub> from the molecular ion gives a fragment at  $m/z$  137. Retention times, molecular ion structures,  $m/z$  values of characteristic fragments, molecular ions and base peaks are summarised in table 3.8.

As discussed in the introduction, acetaldehyde is a primary metabolite of ethanol and considered as a potential carcinogen (Seitz and Stickel, 2007). The main objective of this research work was to develop a method for the detection of acetaldehyde. Thermal

desorption is a novel approach to detect spin trapped free radicals and the results presented here demonstrate the potential of this approach. Volatile PBN radical-adducts may potentially be used as biomarkers for the facile detection of acetaldehyde (see chapter 6 for further discussion).



## Chapter 4

Detection and analysis of spin-adducts from propanal and  
N-*tert*-Butyl- $\alpha$ -Phenylnitron (PBN) using Thermal  
Desorption-Gas Chromatography-Mass Spectrometry (TD-  
GC/MS)

## 4.1 Introduction

Free radicals may attack lipids especially polyunsaturated fatty acids (PUFAs) to start a chain reaction called lipid peroxidation (LPO). Lipid peroxidation is one of the most researched areas with the number of publications increased from 98 (1970-1974) to 13165 (2010-2013) (Ayala, Munoz & Arguelles, 2014), which shows the importance and scope of this process. LPO produces lipid hydroperoxides (LOOH) as a primary product while aldehydes like malondialdehyde (MDA), propanal (propionaldehyde), hexanal & 4-hydroxynonenal (4-HNE) can be formed as secondary products (Ayala, Munoz & Arguelles, 2014). There are literally hundreds of products formed during this process making it difficult to quantify them. This problem is made worse by the fact that they metabolise and are excreted at different rates. Nevertheless, they are still potentially very useful biomarkers for LPO (Niki, 2014). Oxidation of lipids may be responsible for the formation of toxic compounds which not only cause off-flavours to products but may also initiate different diseases like Alzheimer disease, Parkinson disease and Huntington disease (Reed, 2011; Shaker, 2006). Propanal and hexanal have been studied as secondary products of LPO and potentially may be used as indicators of the LPO in edible oils (Van Ruth, Roozen & Jansen, 2000).

Lipids can easily be oxidised by air so care should always be taken during sample handling to avoid artefactual oxidation (Niki, 2014). HPLC with various post column detection systems like UV spectrophotometry, chemiluminescence and mass spectrometry was used successfully for the detection of lipid hydroperoxides. Mass spectrometry is considered the best detection method but thermal instability in gas chromatograph is a disadvantage (Niki, 2014). Secondary oxidation products including aldehydes like propanal, hexanal and octanal have been evaluated by using proton transfer reaction-mass spectrometry (PTS-MS) as indicators of damage made by LPO in sunflower oil (Shaker, 2006). Pentafluorobenzyl (PFB) hydroxylamine was used to convert aldehydes into their PFB-oximes which can be detected easily by using GC-MS (Kawai, Takeda & Terao, 2007). Malondialdehyde (MDA) was detected successfully by using GC-MS with the suggestion that it is more sensitive than other methods (Liu *et al.* 1997).

One objective of this study is to spin trap the radicals produced by propanal in the Fenton reaction and detect the resulting adducts. PBN and its derivatives were used as spin trapping agents to make the radicals stable, which were further sampled and analysed by using TD-GC/MS.

## **4.2 Chromatograms**

Figure 4.1 shows the chromatogram produced following the introduction of propanal into the Fenton system containing the spin trap PBN. The Fenton reaction was carried out under standard conditions for five minutes then the reaction mixture (9.17 mL) was transferred into 40 mL vial and the headspace sampled (see section 2.4.2 for experimental procedure).

#### 4.2.1 Fenton reaction with PBN and propanal ( $\text{CH}_3\text{CH}_2\text{CHO}$ )

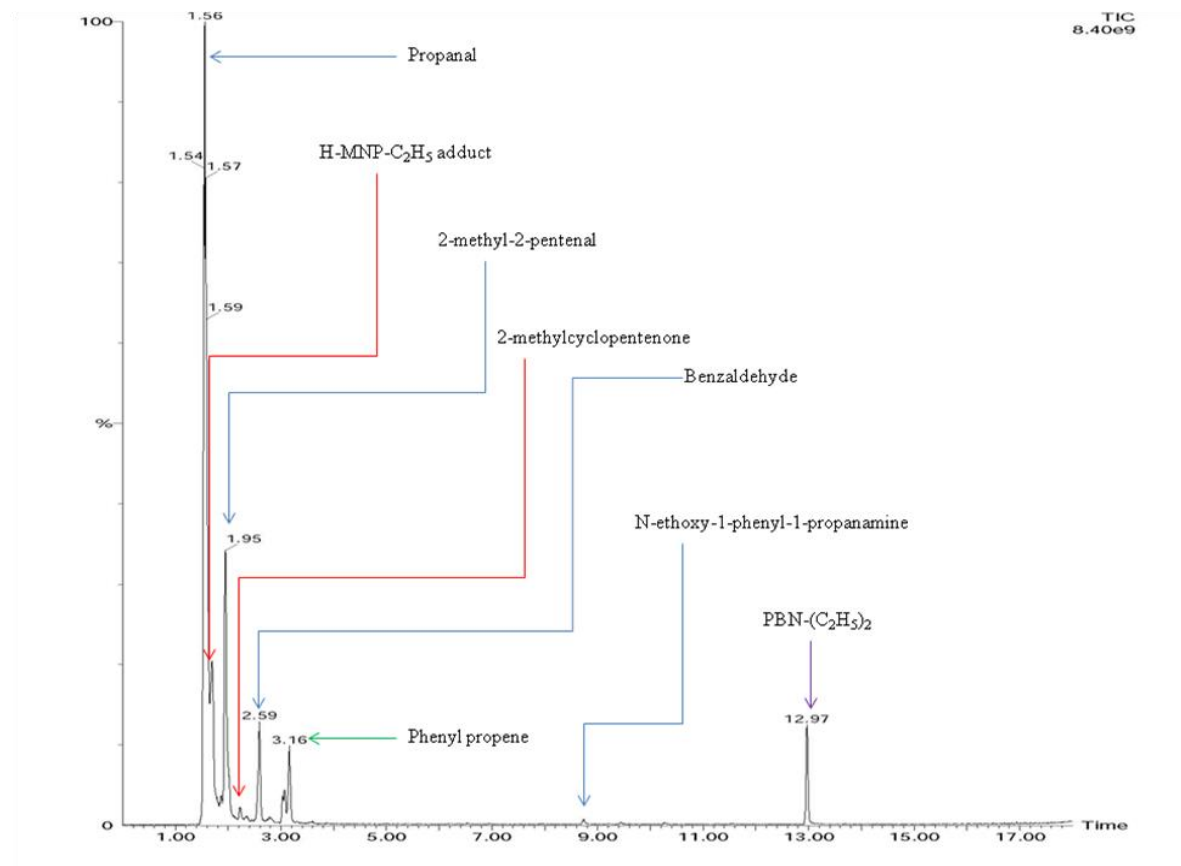


Figure 4.1: The total ion chromatogram (TIC) obtained from the headspace thermal desorption (TD)-GC-MS analysis of the Fenton reaction containing propanal and PBN.

Figure 4.1 shows the presence of peaks for the following compounds: unreacted propanal ( $R_t$  1.56 minutes); a hydrogen & ethyl adduct of MNP (H-MNP-C<sub>2</sub>H<sub>5</sub>) ( $R_t$  1.69 minutes); 2-methyl-2-pentenal ( $R_t$  1.95 minutes); 2-methylcyclopentenone ( $R_t$  2.23 minutes); benzaldehyde ( $R_t$  2.59 minutes); phenyl propene ( $R_t$  3.16 minutes); N-ethoxy-1-phenyl-1-propanamine ( $R_t$  8.74 minutes); and a di-ethyl adduct of the PBN (PBN-Et<sub>2</sub>) ( $R_t$  12.97 minutes). For a detailed analysis of electron ionisation-mass spectra (EI-MS) see sections 4.3 – 4.8.

## 4.2.2 Fenton reaction with PBN and d<sub>2</sub>-propanal (CH<sub>3</sub>CD<sub>2</sub>CHO)

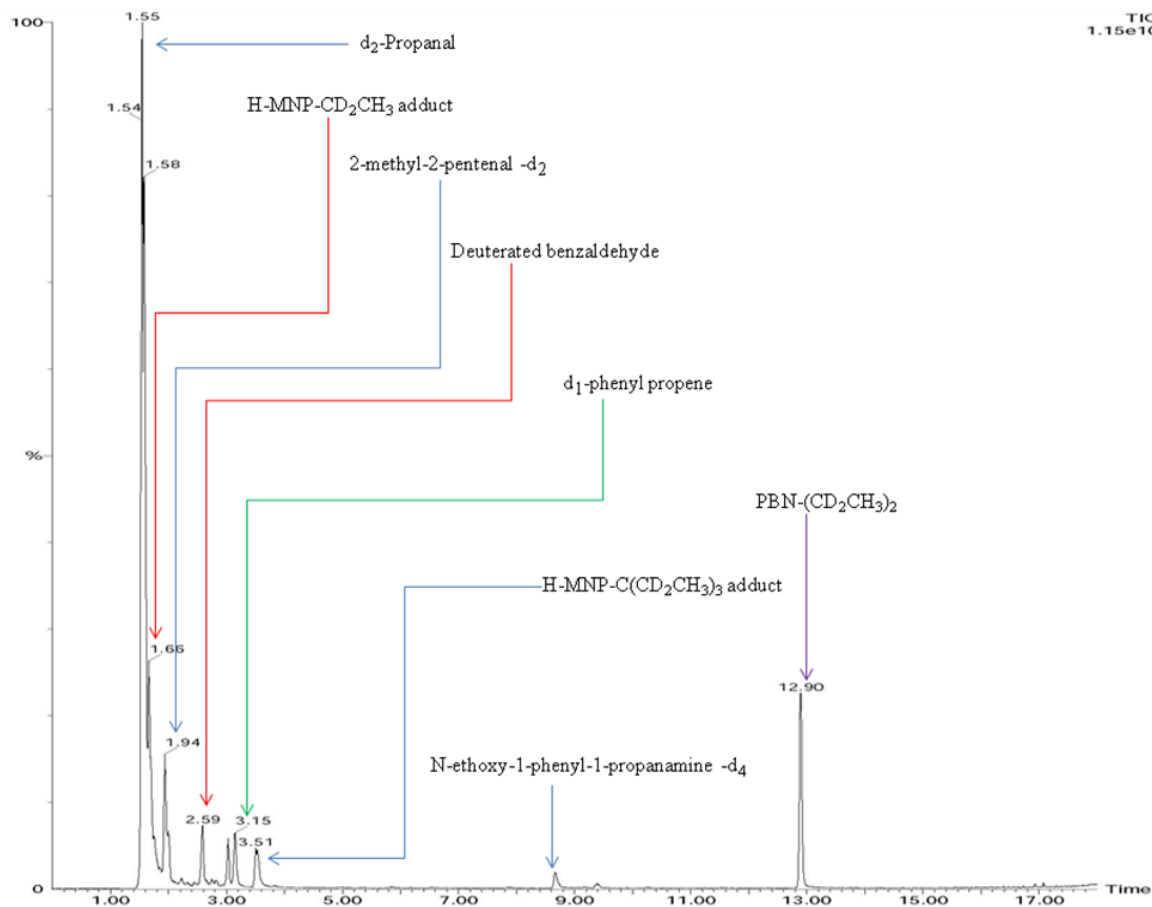


Figure 4.2: The total ion chromatogram (TIC) obtained from the headspace thermal desorption (TD)-GC-MS analysis of the Fenton reaction containing d<sub>2</sub>-propanal {(CH<sub>3</sub>CD<sub>2</sub>C(H)O)} and PBN.

Figure 4.2 shows the presence of peaks corresponding to the following compounds: unreacted d<sub>2</sub>-propanal (R<sub>t</sub> 1.55 minutes); a hydrogen & deuterium-ethyl adduct of MNP (H-MNP-CD<sub>2</sub>CH<sub>3</sub>) (R<sub>t</sub> 1.66 minutes); 2-methyl-2-pentenal-d<sub>2</sub> (R<sub>t</sub> 1.94 minutes); benzaldehyde (R<sub>t</sub> 2.59 minutes); d<sub>1</sub>-phenyl propene (R<sub>t</sub> 3.16 minutes); a hydrogen atom & d<sub>6</sub>-tert-ethyl adduct of MNP (H-MNP-(CD<sub>2</sub>CH<sub>3</sub>)<sub>3</sub>) (R<sub>t</sub> 3.51 minutes); N-ethoxy-1-phenyl-1-propanamine-d<sub>4</sub> (R<sub>t</sub> 8.66 minutes); and a di-deuterium-ethyl adduct of the PBN [PBN-(CD<sub>2</sub>CH<sub>3</sub>)<sub>2</sub>] (R<sub>t</sub> 12.97 minutes). For a detailed analysis of EI-mass spectra see sections 4.3 – 4.8.

### 4.2.3 Fenton reaction with $d_6$ -PBN and propanal

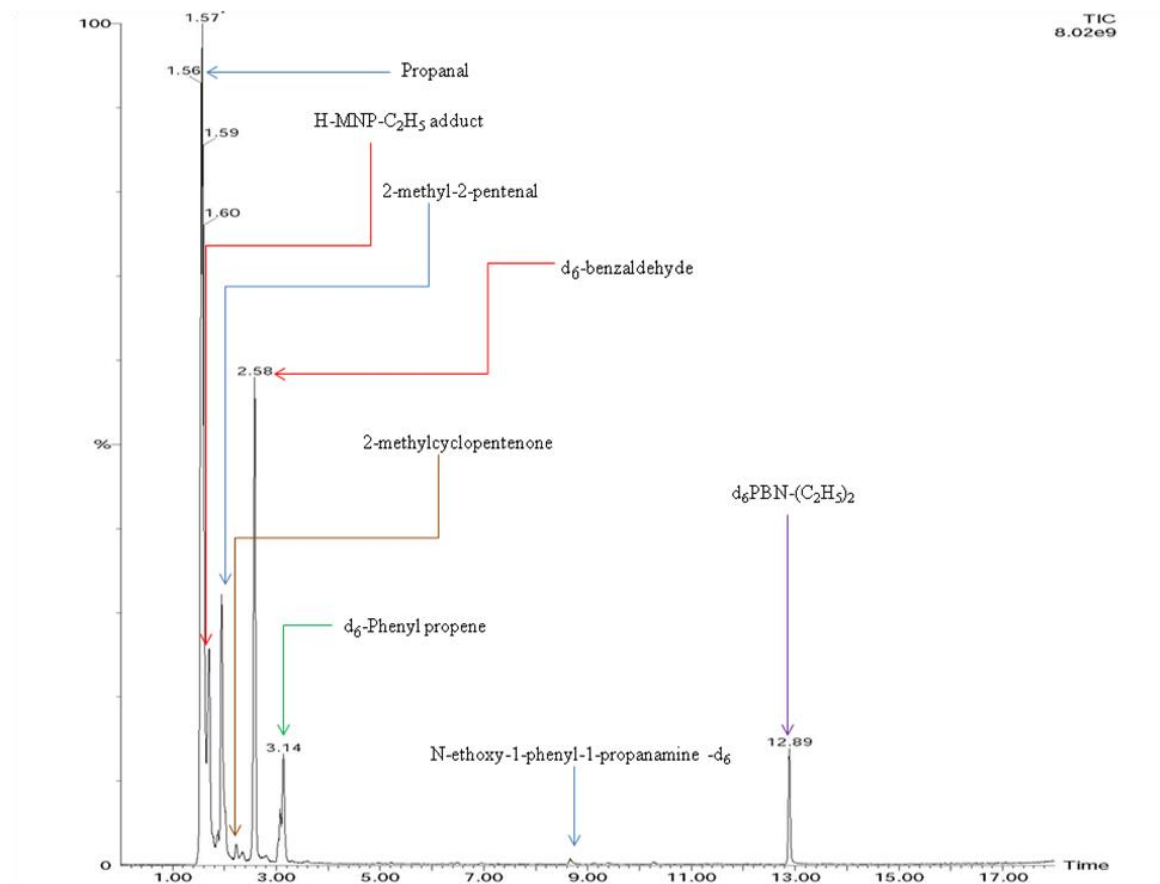


Figure 4.3: The total ion chromatogram (TIC) obtained from the headspace thermal desorption (TD)-GC-MS analysis of the Fenton reaction containing propanal and  $d_6$ -PBN.

Figure 4.3 shows the presence of peaks corresponding to the following compounds: propanal ( $R_t$  1.57 minutes), a hydrogen & ethyl adduct of MNP (H-MNP-C<sub>2</sub>H<sub>5</sub>) ( $R_t$  1.69 minutes); 2-methyl-2-pentenal ( $R_t$  1.95 minutes); 2-methylcyclopentenone ( $R_t$  2.23 minutes);  $d_6$ -benzaldehyde ( $R_t$  2.58 minutes);  $d_6$ -phenyl propene ( $R_t$  3.14 minutes);  $d_6$ -N-ethoxy-1-phenyl-1-propanamine ( $R_t$  8.66 minutes); and a di-ethyl adduct of the  $d_6$ -PBN ( $d_6$ PBN-Et<sub>2</sub>) ( $R_t$  12.97 minutes). For a detailed analysis of EI-mass spectra see sections 4.3 – 4.8.

#### 4.2.4 Fenton reaction with d<sub>6</sub>-PBN and d<sub>2</sub>-propanal (CH<sub>3</sub>CD<sub>2</sub>CHO)

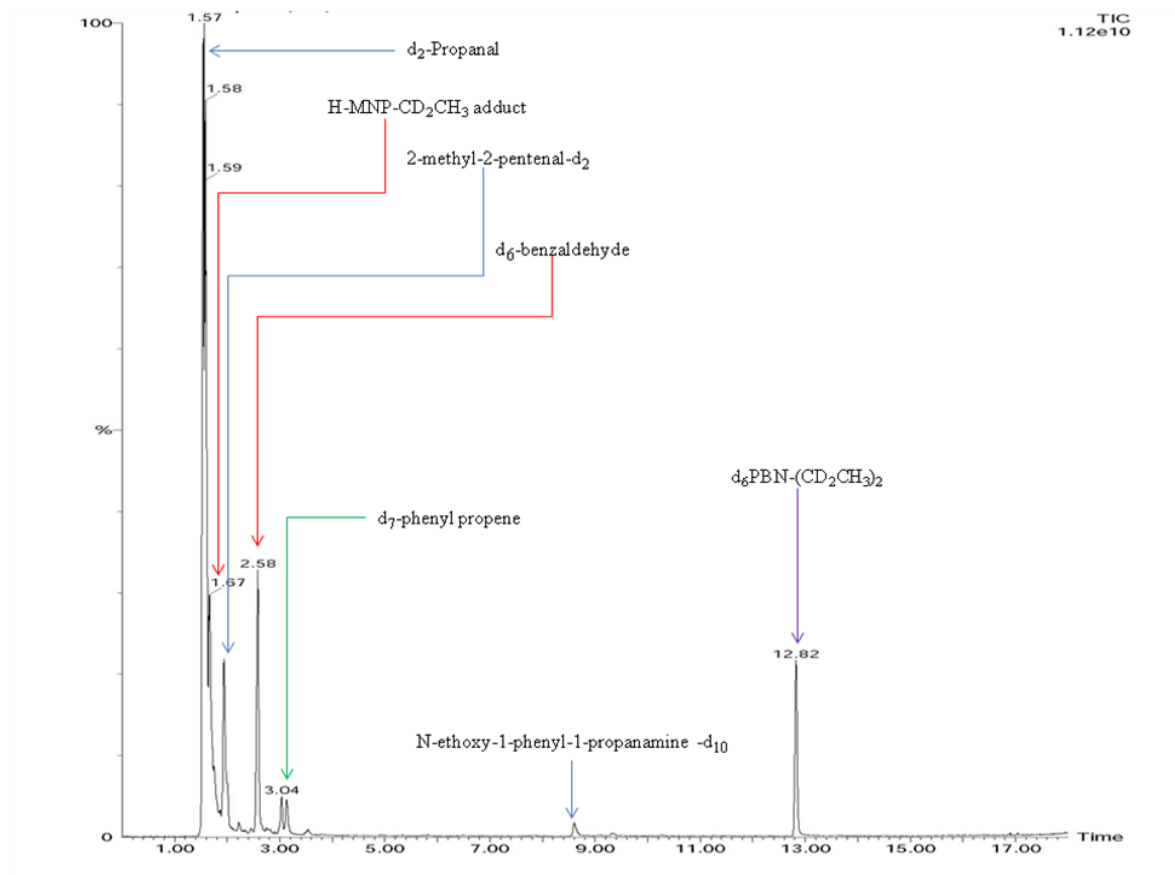


Figure 4.4: The total ion chromatogram (TIC) obtained from the headspace thermal desorption (TD)-GC-MS analysis of the Fenton reaction containing d<sub>2</sub>-propanal (CH<sub>3</sub>CD<sub>2</sub>CHO) and d<sub>6</sub>-PBN.

Figure 4.4 shows the presence of peaks corresponding to the following compounds: d<sub>2</sub>-propanal (R<sub>t</sub> 1.57 minutes); a hydrogen & CH<sub>3</sub>CD<sub>2</sub> adduct of MNP (H-MNP-CD<sub>2</sub>CH<sub>3</sub>) (R<sub>t</sub> 1.67 minutes); 2-methyl-2-pentenal-d<sub>2</sub> (R<sub>t</sub> 1.94 minutes); d<sub>6</sub>-benzaldehyde (R<sub>t</sub> 2.58 minutes); d<sub>7</sub>-phenyl propene (R<sub>t</sub> 3.14 minutes); d<sub>10</sub>-N-ethoxy-1-phenyl-1-propanamine (R<sub>t</sub> 8.66 minutes); and a di-deuteron ethyl adduct of the d<sub>6</sub>-PBN [d<sub>6</sub>-PBN-(CD<sub>2</sub>CH<sub>3</sub>)<sub>2</sub>] (R<sub>t</sub> 12.82 minutes). For a detailed analysis of EI-mass spectra see sections 4.3 – 4.8.

## 4.2.5 Fenton reaction with F-PBN and propanal

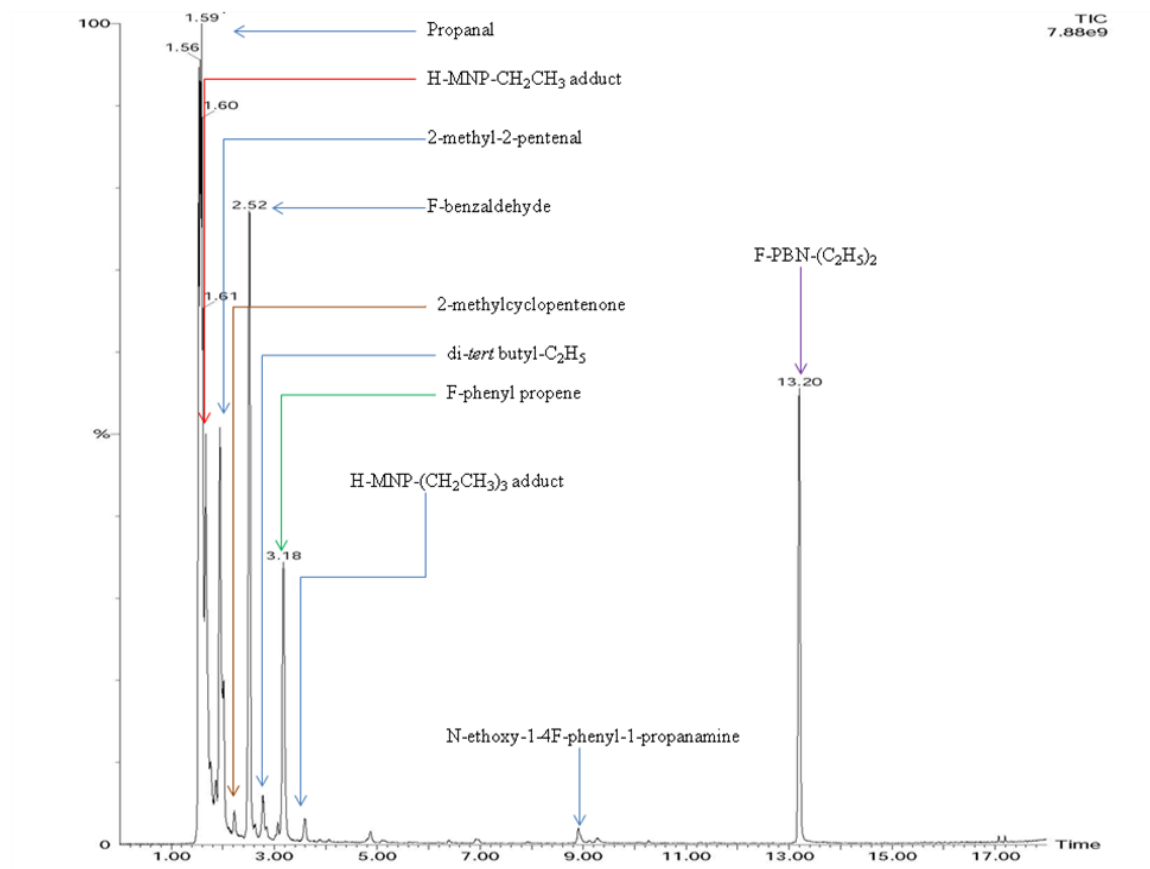


Figure 4.5: The total ion chromatogram (TIC) obtained from the headspace thermal desorption (TD)-GC-MS analysis of the Fenton reaction containing propanal and F-PBN.

Figure 4.5 shows the presence of peaks corresponding to the following compounds: propanal ( $R_t$  1.59 minutes); a hydrogen & ethyl adduct of MNP (H-MNP-C<sub>2</sub>H<sub>5</sub>) ( $R_t$  1.69 minutes); 2-methyl-2-pentenal ( $R_t$  1.95 minutes); 2-methylcyclopentenone ( $R_t$  2.23 minutes); F-benzaldehyde ( $R_t$  2.52 minutes); an ethyl adduct of di-*tert*-butyl ( $R_t$  2.77 minutes); F-phenyl propene ( $R_t$  3.18 minutes); a hydrogen atom & *tri*-ethyl adduct of MNP [H-MNP-(C<sub>2</sub>H<sub>5</sub>)<sub>3</sub>] ( $R_t$  3.59 minutes); N-ethoxy-1-4F-phenyl-1-propanamine ( $R_t$  8.90 minutes); and a di-ethyl adduct of the F-PBN (F-PBN-Et<sub>2</sub>) ( $R_t$  13.20 minutes). For a detailed analysis of EI-mass spectra see sections 4.3 – 4.8.



## 4.2.6 Fenton reaction with Cl-PBN and propanal

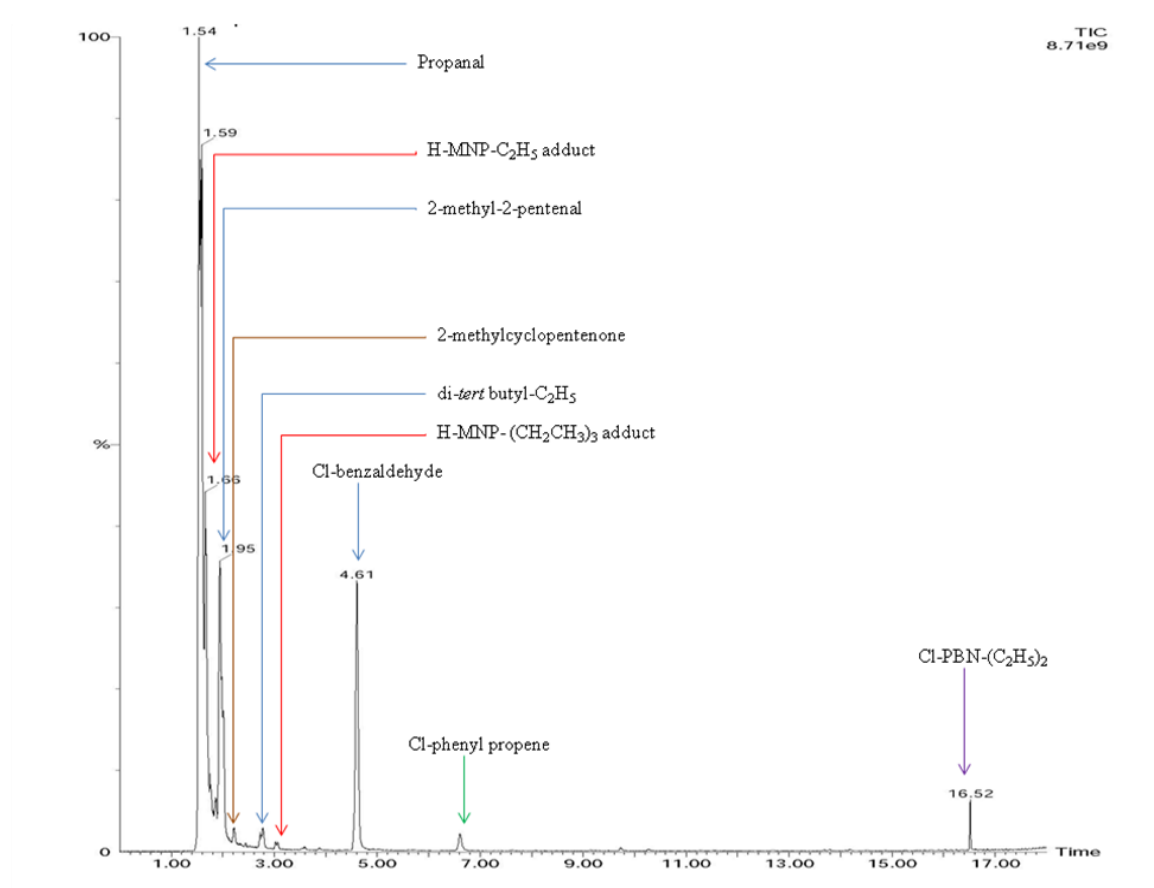


Figure 4.6: The total ion chromatogram (TIC) obtained from the headspace thermal desorption (TD)-GC-MS analysis of the Fenton reaction containing propanal and Cl-PBN.

Figure 4.6 shows the presence of peaks corresponding to the following compounds: propanal ( $R_t$  1.54 minutes); a hydrogen & ethyl adduct of MNP (H-MNP-C<sub>2</sub>H<sub>5</sub>) ( $R_t$  1.66 minutes); 2-methyl-2-pentenal ( $R_t$  1.95 minutes); 2-methylcyclopentenone ( $R_t$  2.23 minutes); an ethyl adduct of di-*tert*-butyl ( $R_t$  2.77 minutes), a hydrogen & *tri*-ethyl adduct of MNP [H-MNP-(C<sub>2</sub>H<sub>5</sub>)<sub>3</sub>] ( $R_t$  3.59 minutes); Cl-benzaldehyde ( $R_t$  4.61 minutes); Cl-phenyl propene ( $R_t$  6.61 minutes); and a di-ethyl adduct of the Cl-PBN (Cl-PBN-Et<sub>2</sub>) ( $R_t$  16.52 minutes). For a detailed analysis of EI-mass spectra see sections 4.3 – 4.8.

#### 4.2.7 Comparison chromatograms (control reactions versus the Fenton reaction; Rt 1-4 min)

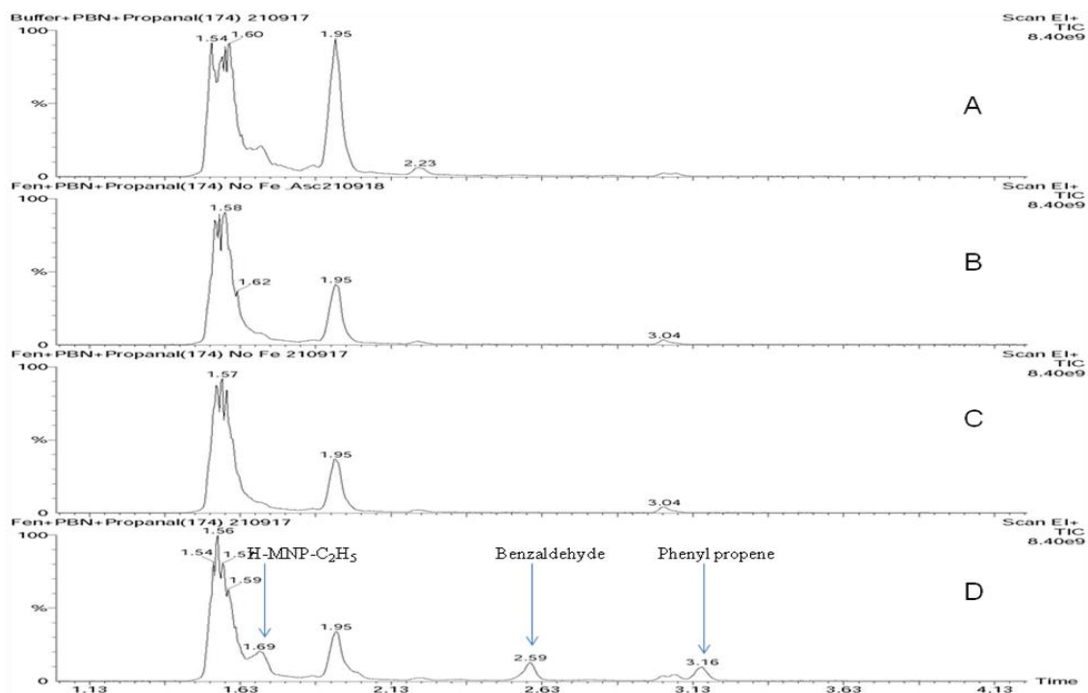


Figure 4.7: Comparison of chromatograms ( $R_t$  1-4 minutes). Chromatograms generated for control experiments whereby the headspace was extracted for a sample containing (A) phosphate buffer, propanal and spin trap. (B) All Fenton reagents (section 2.2.1) except iron and ascorbic acid. (C) All Fenton reagents (section 2.2.1) except iron. (D) The Fenton reaction (From top to bottom respectively).

There were six major peaks in the chromatogram when the Fenton reaction was carried out by using propanal and PBN. It can be seen clearly in above comparative chromatograms that the peaks at 1.56, 1.95, & 3.04 minutes are present in control reactions as well which is evident that either they are impurities or the products of non-radical mechanisms which are occurring alongside the Fenton reaction.

Peaks indicated with arrows ( $R_t$  1.69, 2.59 & 3.16 minutes) are the products of the Fenton reaction as they are present only when the Fenton reaction is carried out in the presence of propanal and PBN. The peak observed at 1.69 minutes is a hydrogen & ethyl adduct of MNP (H-MNP-C<sub>2</sub>H<sub>5</sub>) while the peak at 3.16 minutes corresponds to phenyl propene. The peak at 2.59 minutes corresponds to benzaldehyde, which is formed by the breakdown of PBN and has already been identified in chapter 3.

#### 4.2.8 Comparison chromatograms (control reactions versus the Fenton reaction; $R_t$ 4.19-14.19 min)

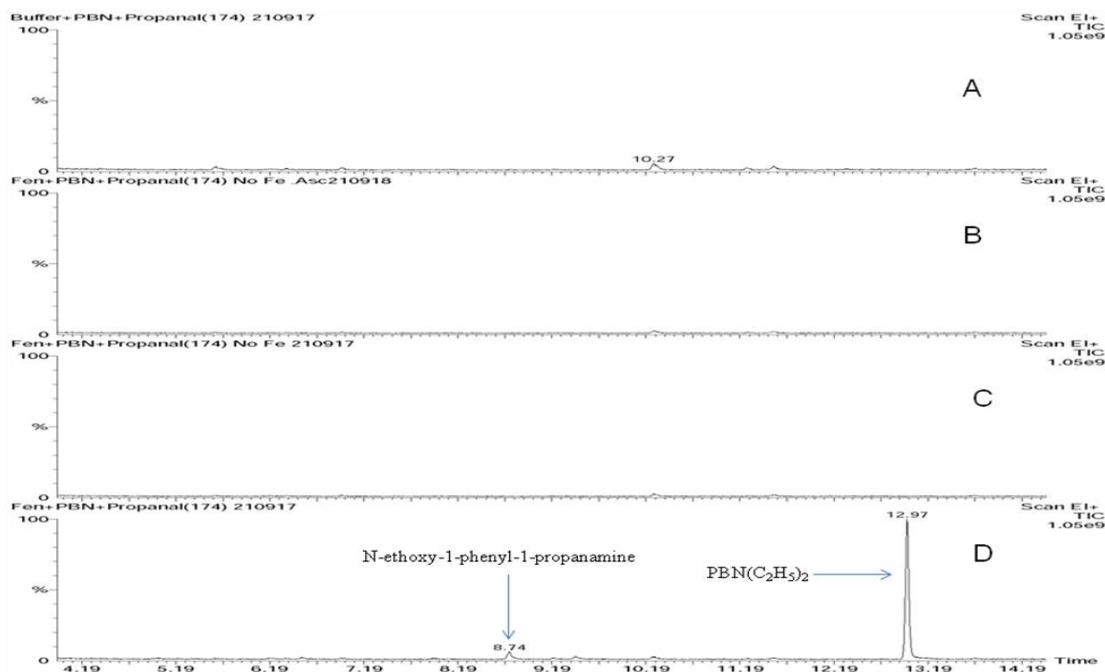


Figure 4.8: Comparison of chromatograms ( $R_t$  4.19-14.19 minutes). Chromatograms generated for control experiments whereby the headspace was extracted for a sample containing (A) phosphate buffer, propanal and spin trap. (B) All Fenton reagents (section 2.2.1) except iron and ascorbic acid. (C) All Fenton reagents (section 2.2.1) except iron. (D) The Fenton reaction (From top to bottom respectively).

Figure 4.8 shows two major peaks in a chromatogram when the Fenton reaction was carried out containing propanal and PBN spin trap. Both peaks ( $R_t$  8.74 & 12.97 minutes) are not present in any of the “control” experiments which confirms them as the products of the Fenton reaction.

The most intense peak at 12.97 minutes is a di-ethyl radical adduct of the PBN (PBN- $\text{Et}_2$ ). To best of our knowledge, this adduct has never been reported. For the confirmation of the adduct different experiments were performed which also identified characteristic fragments and fragmentation patterns within the EI-mass spectra. Since this is most significant adduct, confirming the successful trapping of ethyl radicals, its EI-mass spectrum will be discussed first in this chapter.

### 4.3 Electron ionisation mass spectra (EI-MS) of the di-ethyl adduct of PBN

#### 4.3.1 PBN(C<sub>2</sub>H<sub>5</sub>)<sub>2</sub> adduct

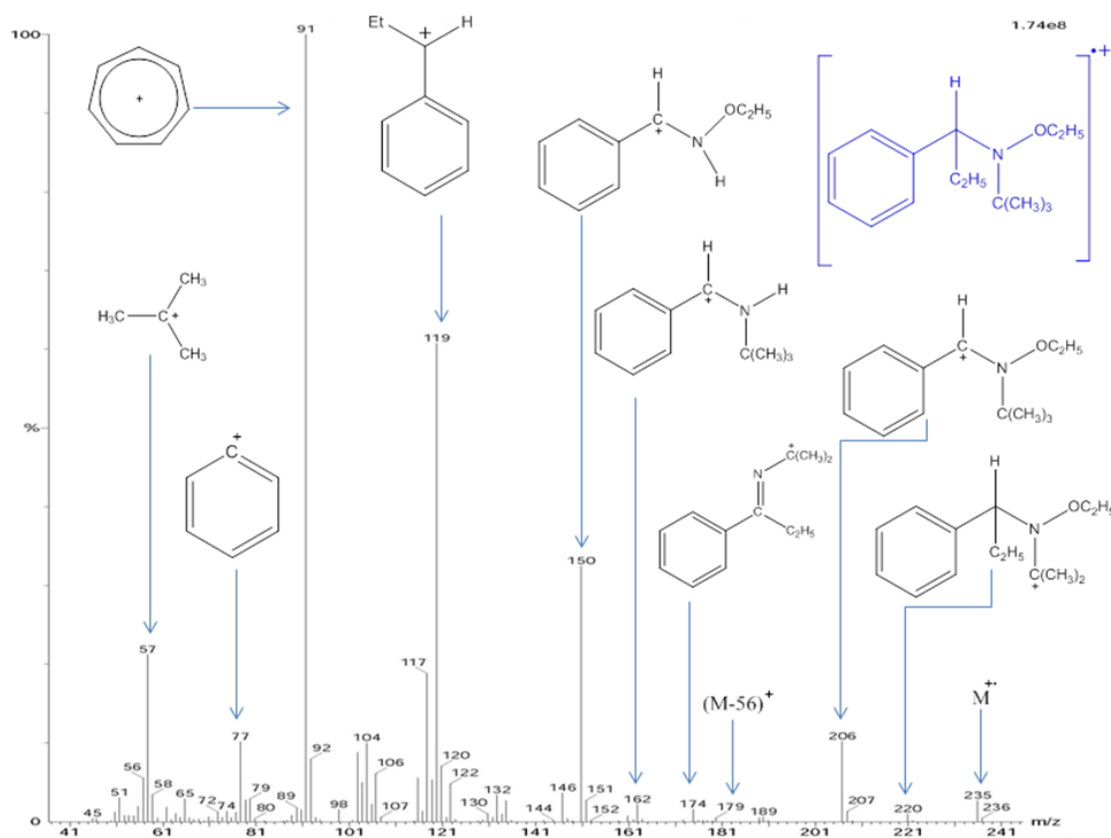
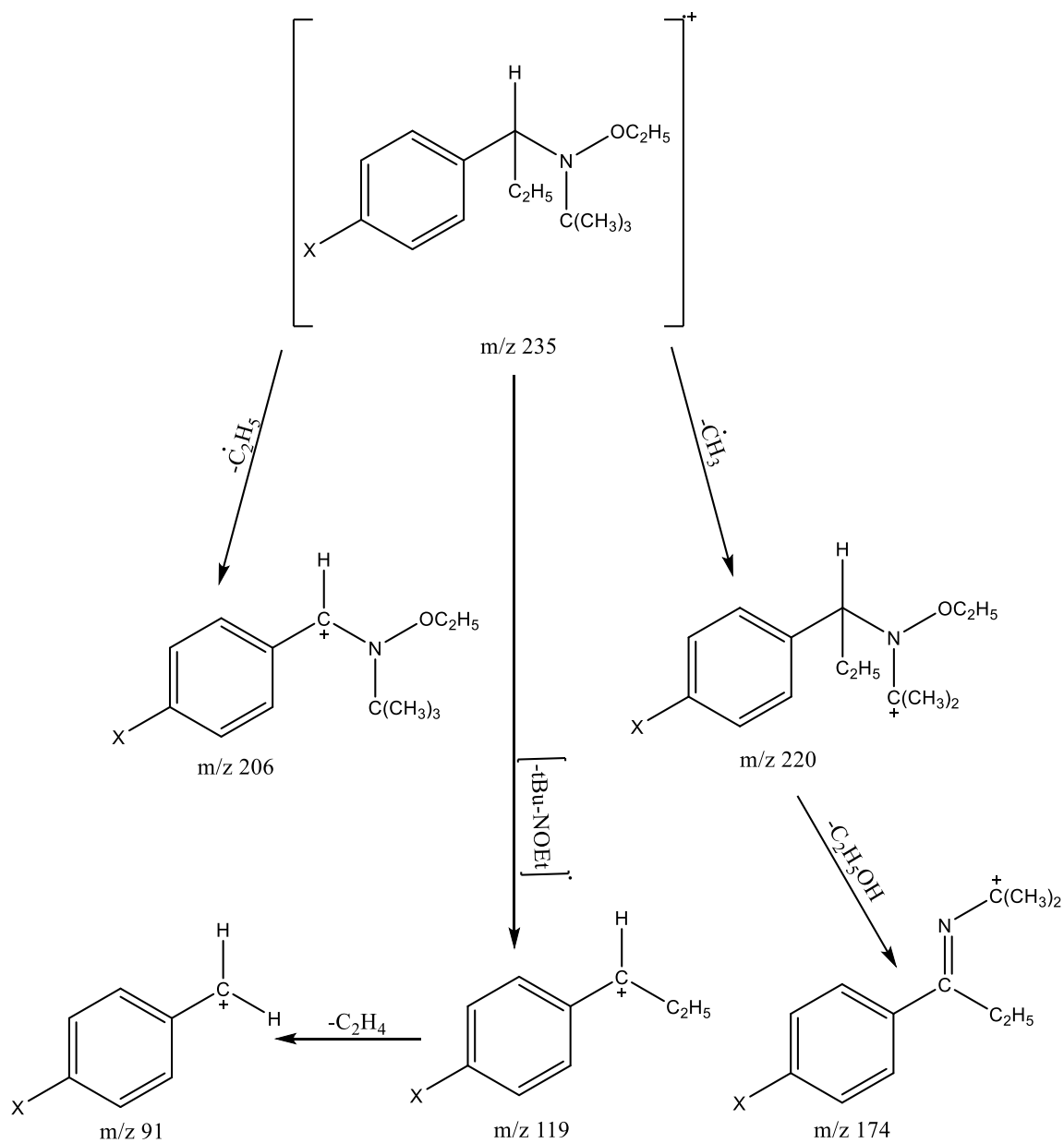


Figure 4.9: Electron ionisation (EI) mass spectrum of the peak at 12.97 minutes (figure 4.1) corresponding to a PBN-diethyl adduct  $\{(PBN-C_2H_5)_2\}$ . The structure given in the top right corner is that of the molecular ion ( $M^+$ ) of  $PBN(C_2H_5)_2$ , corresponding to the peak at  $m/z$  235.

The EI mass spectrum shown in figure 4.9 corresponds to the PBN di-ethyl radical adduct  $\{PBN(C_2H_5)_2\}$  with a molecular ion at  $m/z$  235. The fragment at  $m/z$  220 is formed by the loss of a methyl group from the <sup>t</sup>Bu group of the molecular ion while the loss of an ethyl group (from  $M^+$ ) gives a peak at  $m/z$  206. Loss of 2-methyl-1-propene (from  $M^+$ ) gives a weak peak at  $m/z$  179. Dissociation of the molecular ion between the alpha carbon and nitrogen gives the peak at  $m/z$  119; further break down leads to a phenyl cation peak at  $m/z$  77, whilst loss of ethene and rearrangement of the ion at  $m/z$  119 is the most likely mechanism for the formation of the base peak at  $m/z$  91 (which is a tropylium cation). The fragment at  $m/z$  57 corresponds to the *tert*-butyl cation and is a common fragment derived from the <sup>t</sup>Bu group of PBN adduct. A suggested fragmentation pathway for generation of the key ions is given in scheme 4.1.



Scheme 4.1: The fragmentation scheme for PBN-diethyl adduct (X is hydrogen for PBN, Chlorine for Cl-PBN and Fluorine for F-PBN)

### 4.3.2 PBN(CD<sub>2</sub>CH<sub>3</sub>)<sub>2</sub> adduct

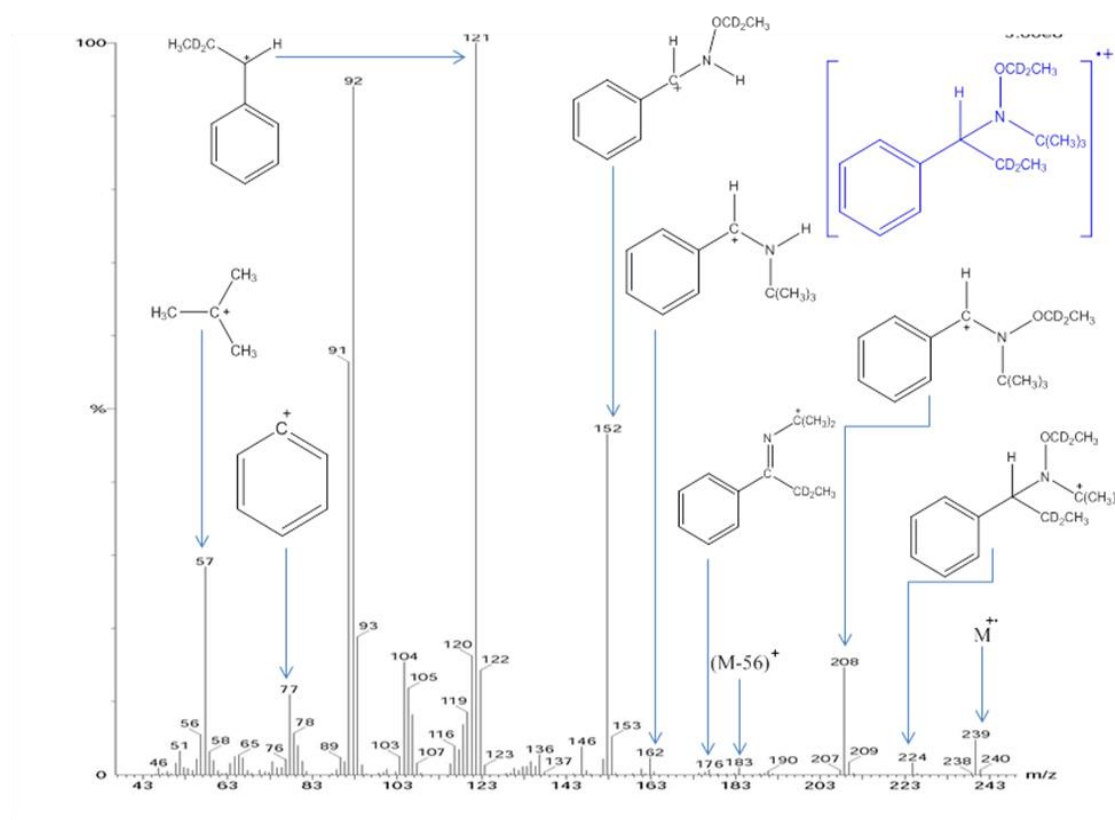


Figure 4.10: Electron ionisation (EI) mass spectrum of the peak at 12.90 minutes (figure 4.2) corresponding to the di-deuteron-ethyl adduct of PBN {PBN(CD<sub>2</sub>CH<sub>3</sub>)<sub>2</sub>}. The structure given in the top right corner is that of the molecular ion (M<sup>+</sup>) corresponding to the peak at *m/z* 239.

The EI mass spectrum shown in figure 4.10 corresponds to PBN(CD<sub>2</sub>CH<sub>3</sub>)<sub>2</sub> detected at 12.90 minutes when the reaction was carried out by using deuterated propanal (CH<sub>3</sub>CD<sub>2</sub>CHO) as a secondary source of radicals in the Fenton reaction system. The molecular ion can be clearly seen at *m/z* 239 (difference of 4 *m/z* units when compared to the molecular ion of PBN-Et<sub>2</sub>; figure 4.9) which confirms the trapping of two deuterone-ethyl (CD<sub>2</sub>CH<sub>3</sub>) radicals by PBN. The fragment at *m/z* 224 is formed by the loss of a methyl group (from the <sup>t</sup>Bu group of the molecular ion), whilst the loss of 2-methyl-1-propene (from M<sup>+</sup>) gives a peak at *m/z* 183. Dissociation of the molecular ion between alpha carbon and nitrogen generates the base peak at *m/z* 121 thus retaining one CD<sub>2</sub>CH<sub>3</sub> group; further break down leads to the phenyl cation peak at *m/z* 77, whilst loss of either C<sub>2</sub>D<sub>2</sub> or CDHCH<sub>2</sub> from the ion at *m/z* 121 gives a tropylium cation peaks at *m/z* 91 or 92, respectively (C<sub>7</sub>H<sub>7</sub><sup>+</sup> and C<sub>7</sub>DH<sub>6</sub><sup>+</sup>). The fragment at *m/z* 57 corresponds to the *tert*-butyl cation.

### 4.3.3 d<sub>6</sub>-PBN-(C<sub>2</sub>H<sub>5</sub>)<sub>2</sub> adduct

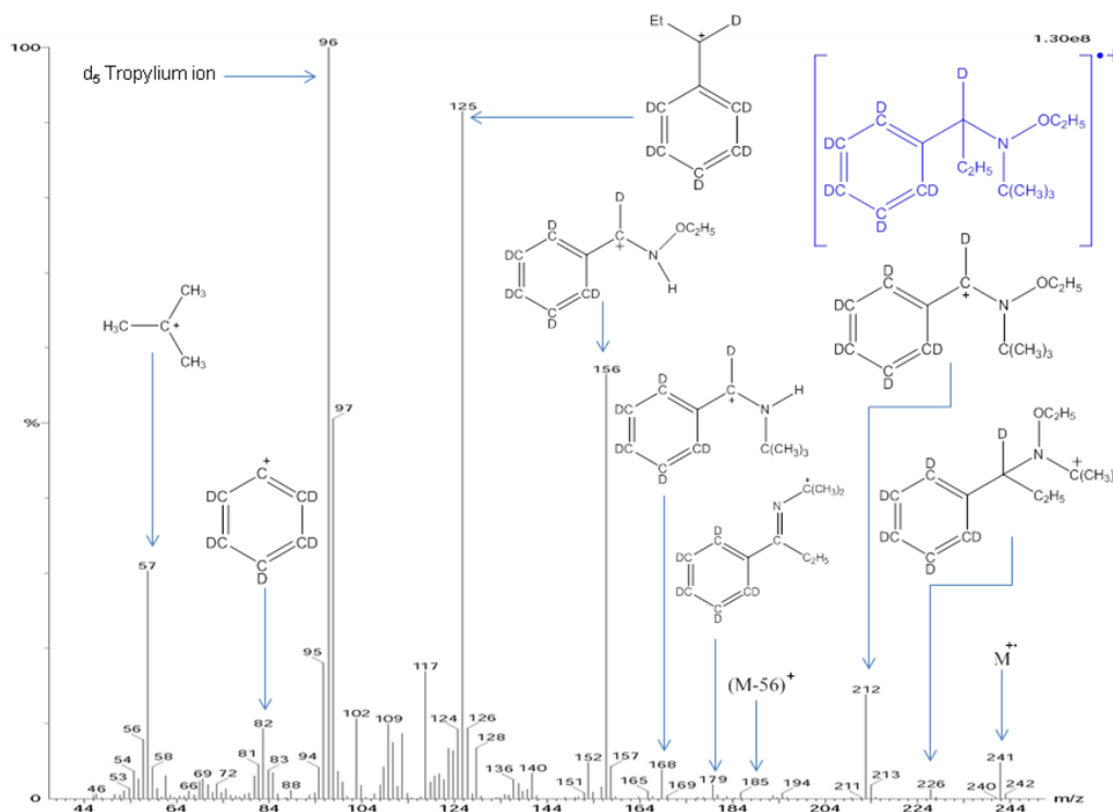


Figure 4.11: Electron ionisation (EI) mass spectrum of the peak at 12.89 minutes (figure 4.3) corresponding to d<sub>6</sub>-PBN(C<sub>2</sub>H<sub>5</sub>)<sub>2</sub>. The structure given in the top right corner is that of the molecular ion (M<sup>+</sup>) of d<sub>6</sub>-PBN(C<sub>2</sub>H<sub>5</sub>)<sub>2</sub>, corresponding to the peak at *m/z* 241.

The EI mass spectrum shown in figure 4.11 corresponds to d<sub>6</sub>-PBN(C<sub>2</sub>H<sub>5</sub>)<sub>2</sub>. The molecular ion can be clearly seen at *m/z* 241 when d<sub>6</sub>-PBN is used as the spin trapping agent. The *m/z* value for the molecular ion is 6 units higher than when non-deuterated PBN is used (figure 4.9), thus helping to confirm the identity of adduct and the trapping of two ethyl radicals. The fragment at *m/z* 226 is formed by the loss of a methyl group from the *tert*-butyl part of the molecular ion whilst the loss of 2-methyl-1-propene (from M<sup>+</sup>) gives a peak at *m/z* 185. Dissociation of the molecular ion between the alpha carbon and nitrogen atom gives the peak at *m/z* 125; further break down leads to a d<sub>5</sub>-phenyl cation peak at *m/z* 82, whilst loss of either C<sub>2</sub>DH or C<sub>2</sub>H<sub>2</sub> and rearrangement generates the base peak at *m/z* 96 (C<sub>7</sub>D<sub>5</sub>H<sub>2</sub><sup>+</sup>) and a peak at *m/z* 97 (C<sub>7</sub>D<sub>6</sub>H<sup>+</sup>), corresponding a d<sub>5</sub>- and d<sub>6</sub>-tropylium cations, respectively. The fragment at *m/z* 57 corresponds to the *tert*-butyl cation.

#### 4.3.4 $d_6\text{PBN}(\text{CD}_2\text{CH}_3)_2$ adduct

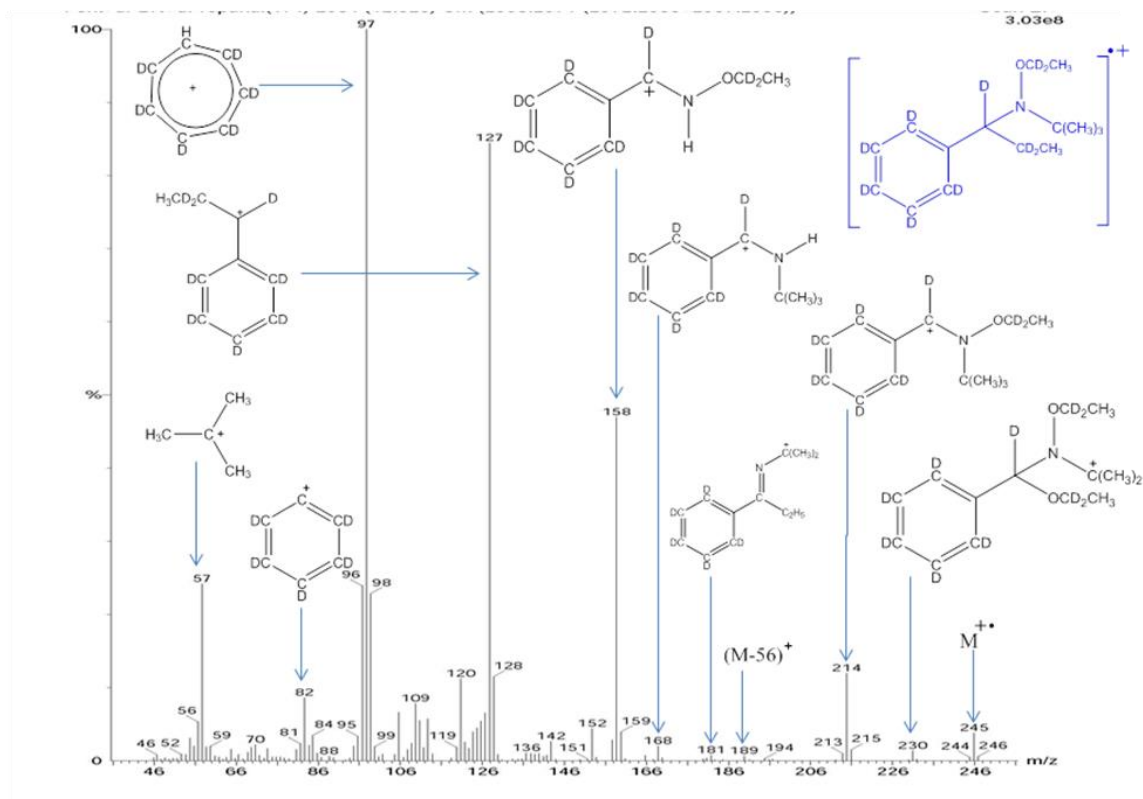


Figure 4.12: Electron ionisation (EI) mass spectrum of the peak at 12.82 minutes (figure 4.4) corresponding to  $d_6\text{-PBN}(\text{CD}_2\text{CH}_3)_2$ . The structure given in the top right corner is that of the molecular ion ( $\text{M}^+$ ) of  $d_6\text{-PBN}(\text{CD}_2\text{CH}_3)_2$ , corresponding to the peak at  $m/z$  245.

The EI mass spectrum shown in figure 4.12 corresponds to  $d_6\text{-PBN}(\text{CD}_2\text{CH}_3)_2$  with a molecular ion at  $m/z$  245. The molecular ion has shifted to  $m/z$  245 (a difference of 4  $m/z$  units) when compared to the molecular ion of  $d_6\text{-PBN}(\text{C}_2\text{H}_5)_2$  (figure 4.11). Thus confirms the identity of adduct i.e. trapping of two deuterium-ethyl ( $\text{CD}_2\text{CH}_3$ ) radicals by  $d_6\text{-PBN}$ . The fragment at  $m/z$  230 is formed by the loss of a methyl group (from the  $^t\text{Bu}$  group of the molecular ion), whilst the loss of 2-methyl-1-propene (from  $\text{M}^+$ ) gives a peak at  $m/z$  189. The peak at  $m/z$  214 is formed by the loss of a deuterated ethyl ( $\text{CH}_3\text{CD}_2$ ) group. Dissociation of the molecular ion between alpha carbon and nitrogen generates a peak at  $m/z$  127; further break down leads to a  $d_5$ -phenyl peak at  $m/z$  82, whilst loss of  $\text{CD}_2\text{H}_2$  and rearrangement gives a  $d_6$ -tropylium cation peak at  $m/z$  97 ( $\text{C}_7\text{D}_6\text{H}^+$ ). The fragment at  $m/z$  57 corresponds to the *tert*-butyl cation.



### 4.3.5 F-PBN-(C<sub>2</sub>H<sub>5</sub>)<sub>2</sub> adduct

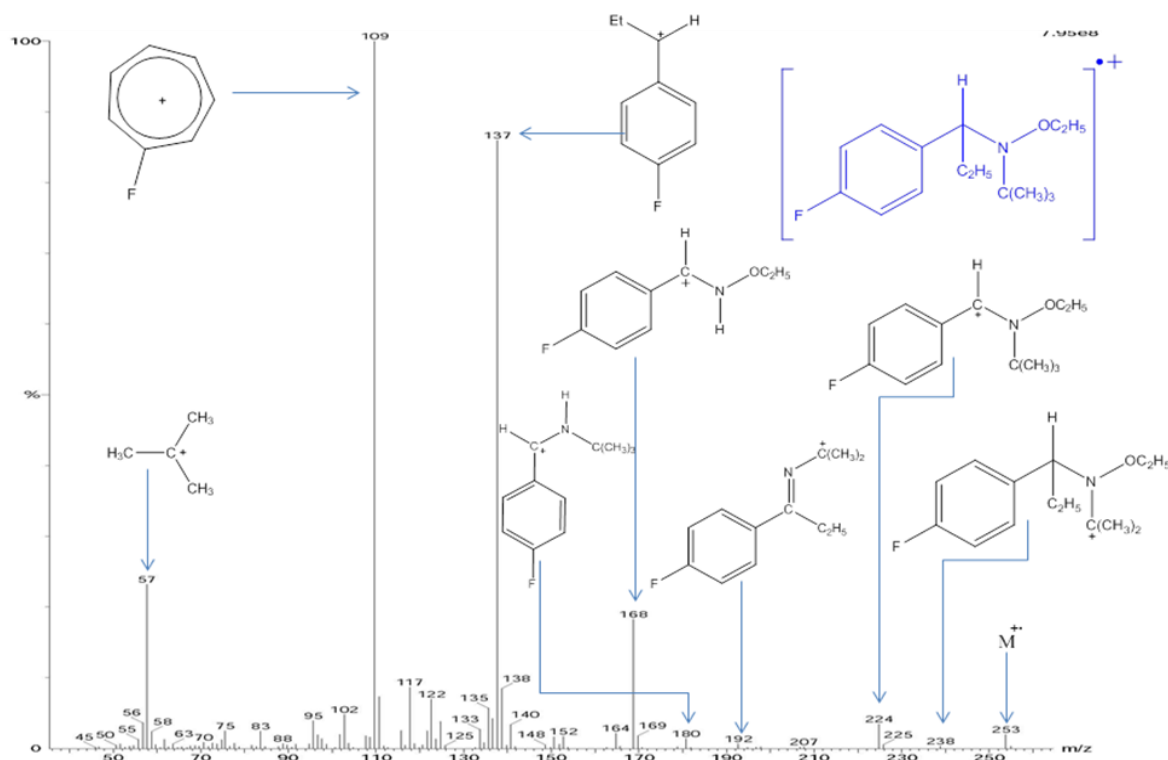


Figure 4.13: Electron ionisation (EI) mass spectrum of the peak at 13.20 minutes (figure 4.5) corresponding to F-PBN-diethyl adduct F-PBN-(C<sub>2</sub>H<sub>5</sub>)<sub>2</sub>. The structure given in the top right corner is that of the molecular ion (M<sup>++</sup>) of F-PBN-(C<sub>2</sub>H<sub>5</sub>)<sub>2</sub>, corresponding to the peak at *m/z* 253.

The EI mass spectrum shown in figure 4.13 corresponds to the F-PBN di-ethyl adduct {F-PBN-(C<sub>2</sub>H<sub>5</sub>)<sub>2</sub>} with a molecular ion at *m/z* 253 (a difference of 18 *m/z* units when compared to the molecular ion of PBN(C<sub>2</sub>H<sub>5</sub>)<sub>2</sub>; figure 4.9), thus confirming the identity of the di-ethyl adduct. The fragment at *m/z* 238 is formed by the loss of a methyl group from the <sup>t</sup>Bu group of the molecular ion, whilst a loss of an ethyl radical (from M<sup>++</sup>) generates the fragment at *m/z* 224. Dissociation of the molecular ion between the alpha carbon and nitrogen generates the peak at *m/z* 137; further break down leads to an F-phenyl cation peak at *m/z* 95, whilst loss of ethene and rearrangement gives the base peak at *m/z* 109 which is an F-tropylium cation (C<sub>7</sub>H<sub>6</sub>F<sup>+</sup>). The fragment at *m/z* 57 corresponds to the *tert*-butyl cation.

### 4.3.6 Cl-PBN-(C<sub>2</sub>H<sub>5</sub>)<sub>2</sub> adduct

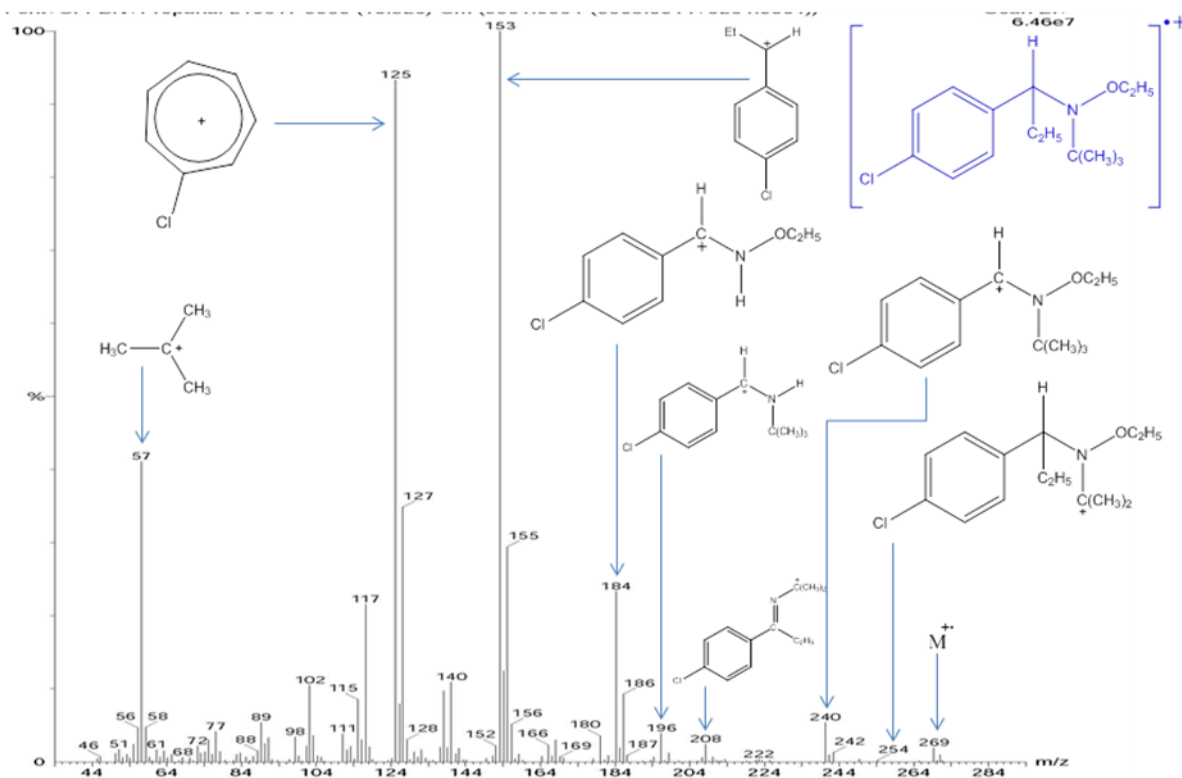


Figure 4.14: Electron ionisation (EI) mass spectrum of the peak at 16.52 minutes (figure 4.6) corresponding to Cl-PBN-diethyl adduct {Cl-PBN-(C<sub>2</sub>H<sub>5</sub>)<sub>2</sub>}. The structure given in the top right corner is that of the molecular ion (M<sup>+</sup>) of Cl-PBN(C<sub>2</sub>H<sub>5</sub>)<sub>2</sub>, corresponding to the peaks at *m/z* 269/271.

The EI mass spectrum shown in figure 4.14 corresponds to the Cl-PBN di-ethyl adduct {Cl-PBN(C<sub>2</sub>H<sub>5</sub>)<sub>2</sub>} with a molecular ion at *m/z* 269/271, depending upon which isotope of chlorine is present (<sup>35</sup>Cl or <sup>37</sup>Cl). This difference of 34/36 *m/z* units when compared to the molecular ion of PBN (figure 4.9) confirms the detection of the di-ethyl adduct. The fragment at *m/z* 254/256 is formed by the loss of a methyl radical (from the <sup>t</sup>Bu group of the molecular ion) and those at *m/z* 240/242 by the loss of ethyl group (from M<sup>+</sup>). Dissociation of the molecular ion between alpha carbon and nitrogen gives the base peak at *m/z* 153 (containing the <sup>35</sup>Cl isotope) and a peak at *m/z* 155 (containing the <sup>37</sup>Cl isotope); further break down leads to a low intensity Cl-phenyl cation peak at *m/z* 95, whilst loss of ethene and rearrangement gives a Cl-tropylium cation peaks (C<sub>7</sub>H<sub>6</sub>Cl<sup>+</sup>) at *m/z* 125 and 127. The fragment at *m/z* 57 corresponds to the *tert*-butyl cation.

Table 4.1: Summary of GC-MS data for the diethyl-adduct of PBN and its derivatives

| Spin adduct   | Retention time ( $R_t$ / minutes) | Molecular ion ( $m/z$ ) | Characteristics fragment peaks ( $m/z$ )  |
|---|-----------------------------------|-------------------------|---|
| PBN(C <sub>2</sub> H <sub>5</sub> ) <sub>2</sub>                  | 12.97                             | 235                     | 220, 206, 179, 174, 162, 150, 119, 77, 57 |
| PBN(CD <sub>2</sub> CH <sub>3</sub> ) <sub>2</sub>                | 12.90                             | 239                     | 224, 208, 183, 176, 162, 152, 121, 77, 57 |
| d <sub>6</sub> PBN(C <sub>2</sub> H <sub>5</sub> ) <sub>2</sub>   | 12.89                             | 241                     | 226, 212, 185, 179, 168, 156, 125, 82, 57 |
| d <sub>6</sub> PBN(CD <sub>2</sub> CH <sub>3</sub> ) <sub>2</sub> | 12.82                             | 245                     | 230, 214, 189, 181, 168, 158, 127, 82, 57 |
| F-PBN(C <sub>2</sub> H <sub>5</sub> ) <sub>2</sub>                | 13.20                             | 253                     | 238, 224, 192, 180, 168, 137, 57          |
| Cl-PBN(C <sub>2</sub> H <sub>5</sub> ) <sub>2</sub>               | 16.52                             | 241                     | 254, 240, 196, 184, 153, 77, 57           |

## 4.4 Electron ionisation mass spectra (EI-MS) of N-ethoxy-1-phenyl-1-propanamine

### 4.4.1 EI mass spectrum of N-ethoxy-1-phenyl-1-propanamine

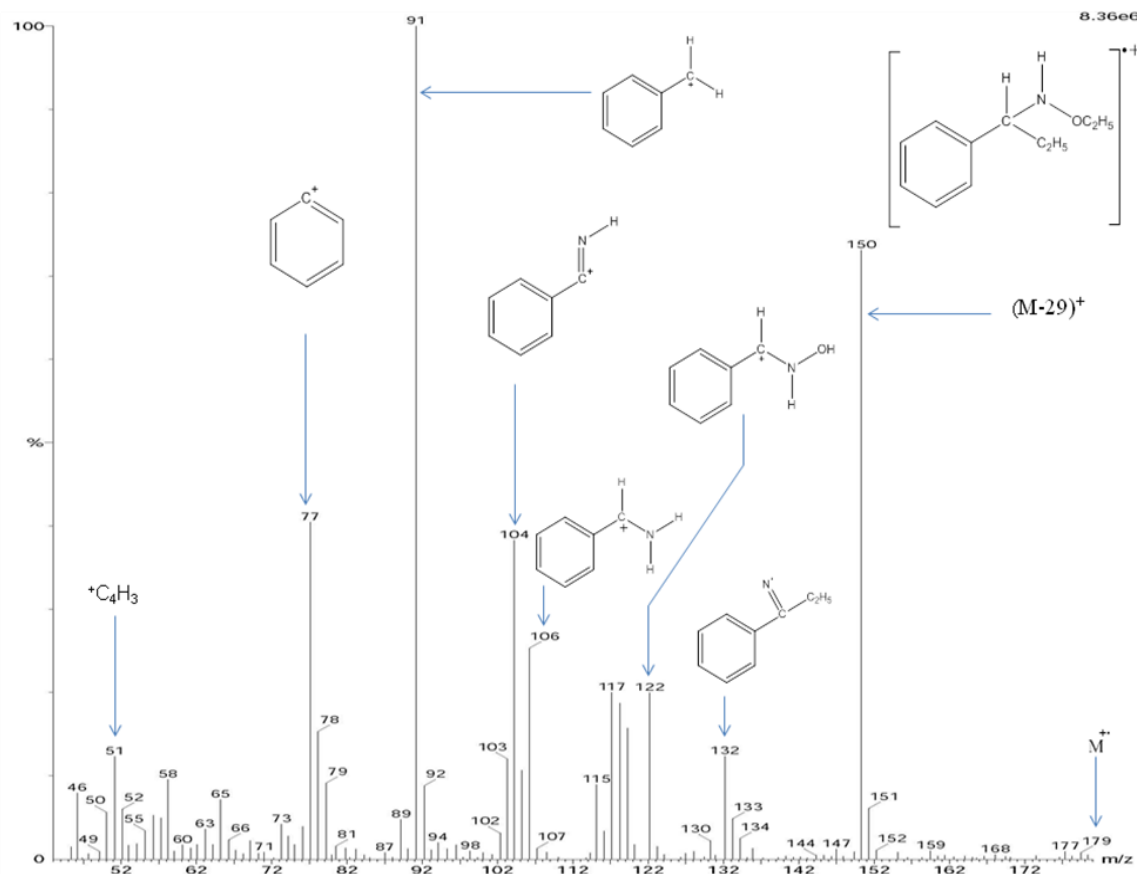


Figure 4.15: Electron ionisation (EI) mass spectrum of the peak at 8.74 minutes (figure 4.1) corresponding to N-Ethoxy-1-phenyl-1-propanamine. The structure given in the top right corner is that of the molecular ion ( $M^+$ ) corresponding to the peak at  $m/z$  179.

The EI mass spectrum shown in figure 4.15 corresponds to N-ethoxy-1-propanamine detected at 8.74 minutes. A weak peak at  $m/z$  179 corresponds to the molecular ion. The fragment at  $m/z$  150 is generated by the loss of an ethyl group from the molecular ion. It is not clear from the fragmentation pattern which of the ethyl groups is lost. The base peak at  $m/z$  91 is a tropylium cation ( $C_7H_7^+$ ) while the fragment at  $m/z$  57 corresponds to the *tert*-butyl cation.

#### 4.4.2 EI mass spectrum of N-ethoxy-1-phenyl-1-propanamine-d<sub>4</sub>

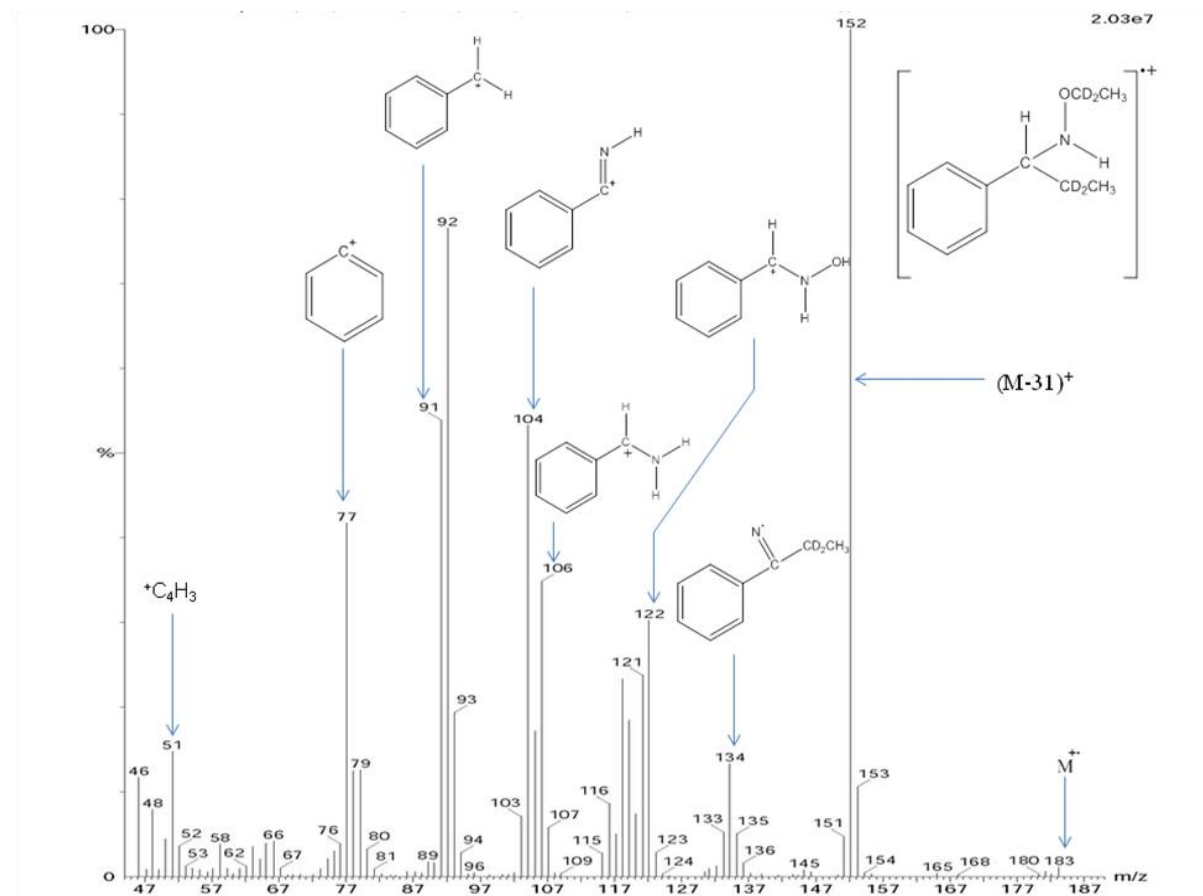


Figure 4.16: Electron ionisation (EI) mass spectrum of the peak at 8.66 minutes (figure 4.2) corresponding to N-ethoxy-1-phenyl-1-propanamine-d<sub>4</sub>. The structure given in the top right corner is that of the molecular ion (M<sup>+</sup>) corresponding to the peak at *m/z* 183.

The EI mass spectrum shown in figure 4.16 corresponds to N-ethoxy-1-phenyl-1-propanamine-d<sub>4</sub> (*R*<sub>t</sub> = 8.66 minutes) when the reaction was carried out using deuterated propanal (CH<sub>3</sub>CD<sub>2</sub>CHO) as a secondary source of free radicals in the Fenton reaction system. The molecular can be seen at *m/z* 183 (a difference of 4 *m/z* units when compared to the mass spectrum of non-deuterated propanal; figure 4.15) which confirms the trapping of two deuterium-ethyl (CH<sub>3</sub>CD<sub>2</sub>) radicals. The fragment at *m/z* 152 is generated by the loss of a CD<sub>2</sub>CH<sub>3</sub> group (31 *m/z* units) from the molecular ion, although it is not clear which of the two groups is lost. The peaks at *m/z* 91 and 92, respectively, correspond to the tropylium cation (C<sub>7</sub>H<sub>7</sub><sup>+</sup>) and d<sub>1</sub>-tropylium cation (C<sub>7</sub>H<sub>6</sub>D<sup>+</sup>). The fragment at *m/z* 57 is a *tert*-butyl cation.

#### 4.4.3 EI mass spectrum of N-ethoxy-1-phenyl-1-propanamine-d<sub>6</sub>

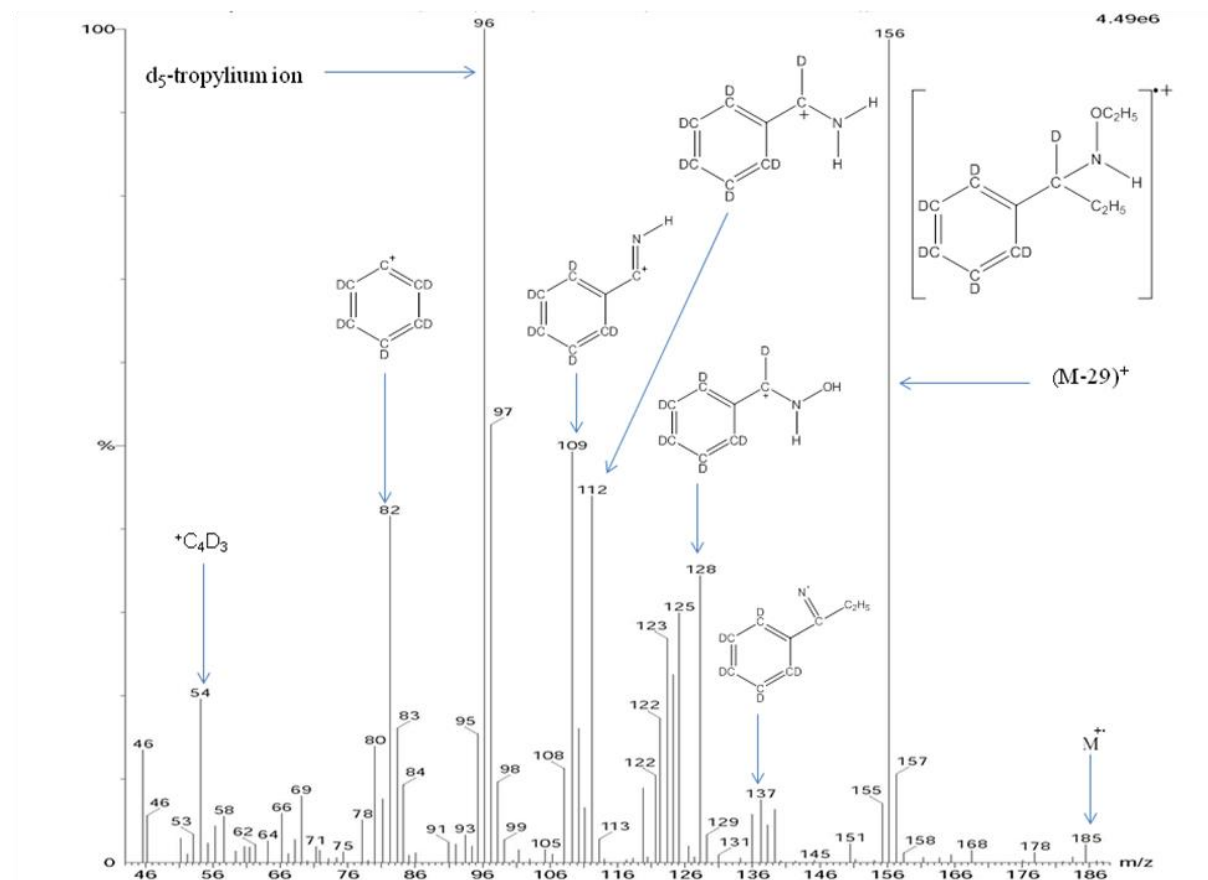


Figure 4.17: Electron ionisation (EI) mass spectrum of the peak at 8.66 minutes (figure 4.3) corresponding to N-ethoxy-1-phenyl-1-propanamine-d<sub>6</sub>. The structure given in the top right corner is that of the molecular ion (M<sup>+</sup>) corresponding to the peak at *m/z* 185.

The EI mass spectrum shown in figure 4.17 corresponds to N-ethoxy-1-phenyl-1-propanamine-d<sub>6</sub> (*R*<sub>t</sub> = 8.66 minutes) when the reaction was carried out using d<sub>6</sub>-PBN as the trapping agent in the Fenton reaction system. The molecular ion can be seen at *m/z* 185 (a difference of 6 *m/z* units when compared to the mass spectrum when PBN is used; figure 4.15) which confirms the formation of the adduct. The fragment at *m/z* 156 is generated by the loss of ethyl group (from M<sup>+</sup>). The base peak at *m/z* 96 and the peak at *m/z* 97 correspond to the d<sub>5</sub> and d<sub>6</sub> tropylium cations, respectively (C<sub>7</sub>H<sub>2</sub>D<sub>5</sub><sup>+</sup> and C<sub>7</sub>HD<sub>6</sub><sup>+</sup>). The fragment at *m/z* 82 corresponds to a d<sub>5</sub>-phenyl cation. The fragment at *m/z* 57 corresponds to the *tert*-butyl cation.

#### 4.4.4 EI mass spectrum of N-ethoxy-1-phenyl-1-propanamine-d<sub>10</sub>

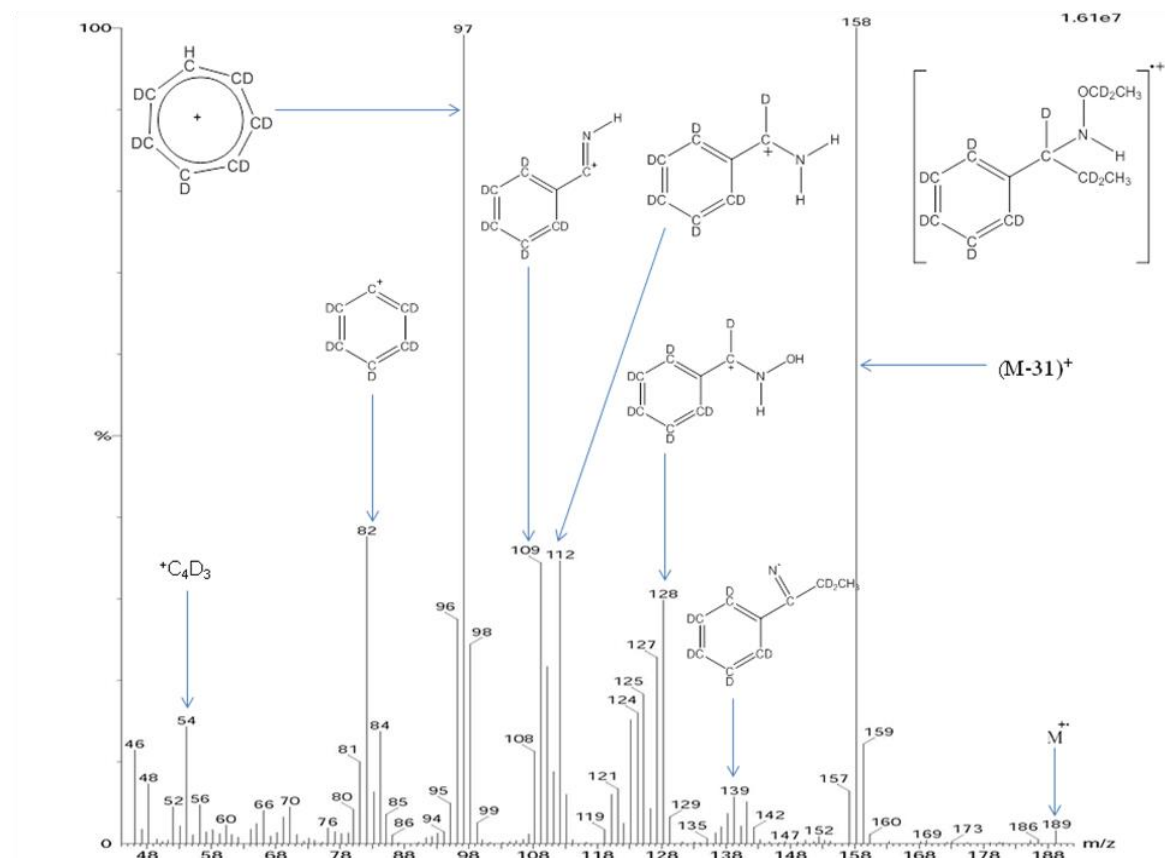


Figure 4.18: Electron ionisation (EI) mass spectrum of the peak at 8.60 minutes (figure 4.4) corresponding to N-ethoxy-1-phenyl-1-propanamine-d<sub>10</sub>. The structure given in the top right corner is that of the molecular ion (M<sup>+</sup>) corresponding to the peak at *m/z* 189.

The EI mass spectrum shown in figure 4.18 corresponds to N-ethoxy-1-phenyl-1-propanamine-d<sub>10</sub> (*R*<sub>t</sub> = 8.60 minutes) when the reaction was carried out using deuterated propanal (CH<sub>3</sub>CD<sub>2</sub>CHO) as a secondary source of radicals in the Fenton reaction system. The molecular ion can be seen at *m/z* 189 (a difference of 4 *m/z* units when compared to the mass spectrum of d<sub>6</sub>-PBN; figure 4.17) thus confirming the trapping of two deuterioethyl (CD<sub>2</sub>CH<sub>3</sub>) radicals. The fragment at *m/z* 158 is generated by the loss of deuterioethyl group (CD<sub>2</sub>CH<sub>3</sub>) from the molecular ion. The peak at *m/z* 97 corresponds to d<sub>6</sub>-tropylium cation (C<sub>7</sub>HD<sub>6</sub><sup>+</sup>) whilst the fragment at *m/z* 82 corresponds to a d<sub>5</sub>-phenyl cation. The fragment at *m/z* 57 corresponds to the *tert*-butyl cation.

#### 4.4.5 EI mass spectrum of N-ethoxy-1-fluorophenyl-1-propanamine

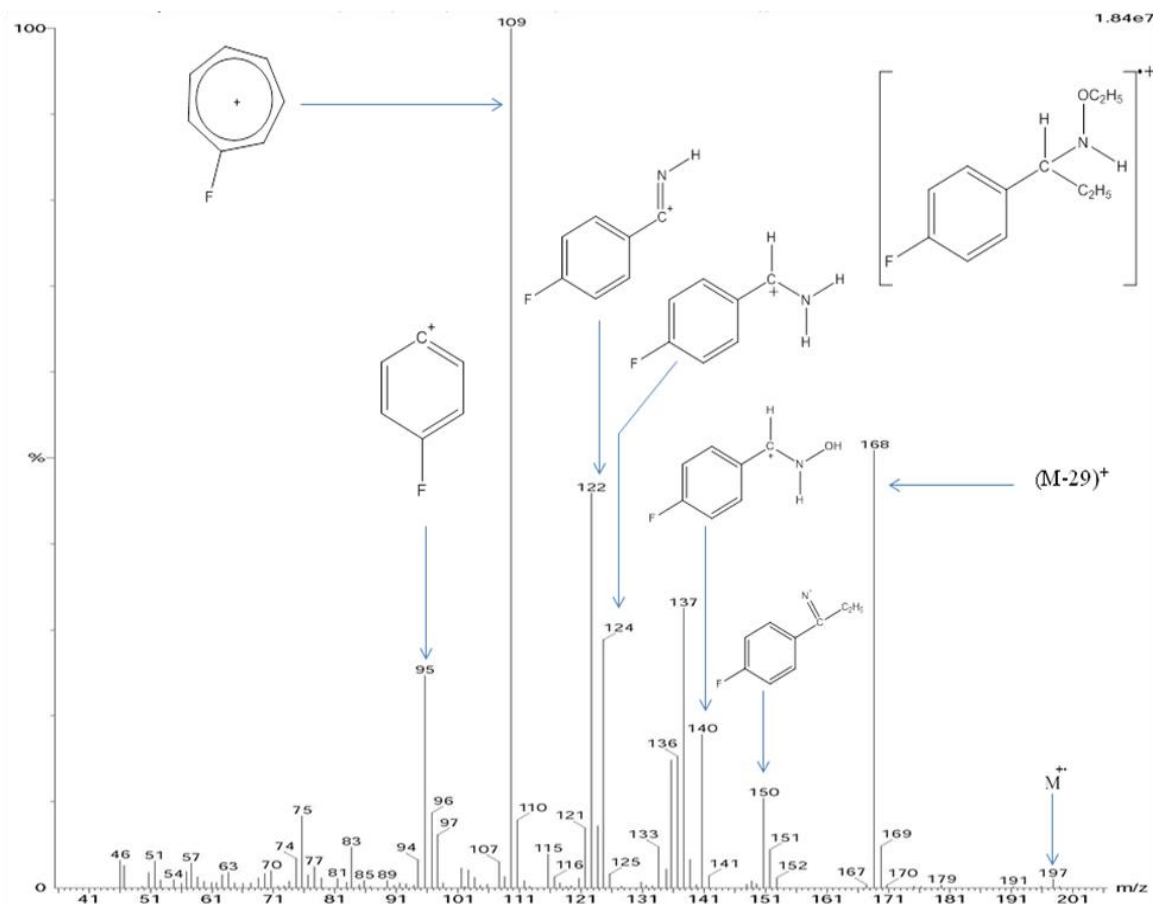
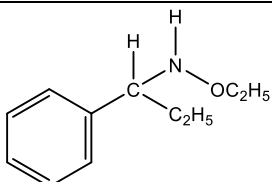
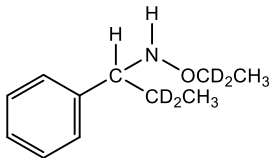
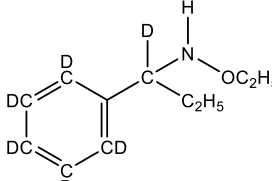
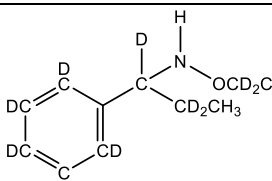
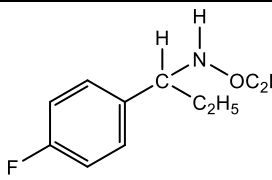


Figure 4.19: Electron ionisation (EI) mass spectrum of the peak at 8.90 minutes (figure 4.5) corresponding to N-ethoxy-1-fluorophenyl-1-propanamine. The structure given in the top right corner is that of the molecular ion ( $M^+$ ) corresponding to the peak at  $m/z$  197.

The EI mass spectrum shown in figure 4.19 corresponds to N-ethoxy-1-fluorophenyl-1-propanamine ( $R_t = 8.74$  minutes). The molecular ion can be seen at  $m/z$  197 (a difference of 18  $m/z$  units when compared to the molecular ion of N-ethoxy-1-phenyl-1-propanamine; figure 4.15), thus confirming the identity of the adduct. The fragment at  $m/z$  168 is generated by the loss of ethyl group (from  $M^+$ ). The base peak at  $m/z$  109 corresponds to F-tropylium cation ( $C_7H_6F^+$ ) while the fragment at  $m/z$  95 is an F-phenyl cation.



Table 4.2: Summary of GC-MS data for X-(N-ethoxy-1-phenylethanamine) where X is H for PBN, F for 4-FPBN, Cl for 4-CIPBN, when the reaction was carried out using PBN and its derivatives as trapping agents and propanal/deuterated (d<sub>2</sub>) propanal as a secondary source of free radicals.

| Reagents in the Fenton system                  | Identity  | Retention time (min) | Molecular ion ( <i>m/z</i> ) | Characteristics fragment peaks ( <i>m/z</i> ) |
|--|---|----------------------|------------------------------|---|
| PBN & propanal                                 |    | 8.74                 | 179                          | 150, 132, 122, 104, 91, 77, 51                |
| PBN & d <sub>2</sub> -propanal                 |   | 8.66                 | 183                          | 152, 134, 122, 104, 91, 77, 51                |
| d <sub>6</sub> -PBN & propanal                 |  | 8.66                 | 185                          | 156, 137, 128, 109, 96, 82, 54                |
| d <sub>6</sub> -PBN & d <sub>2</sub> -propanal |  | 8.60                 | 189                          | 158, 139, 128, 109, 97, 82, 54                |
| F-PBN & propionaldehyde                        |  | 8.90                 | 197                          | 168, 150, 140, 122, 109, 95, 51               |
| Cl-PBN & propionaldehyde                       |   | Not detected         |                              |   |

## 4.5 A hydrogen and ethyl adduct of MNP (H-MNP-C<sub>2</sub>H<sub>5</sub>)

### 4.5.1 EI mass spectrum of H-MNP-C<sub>2</sub>H<sub>5</sub> adduct

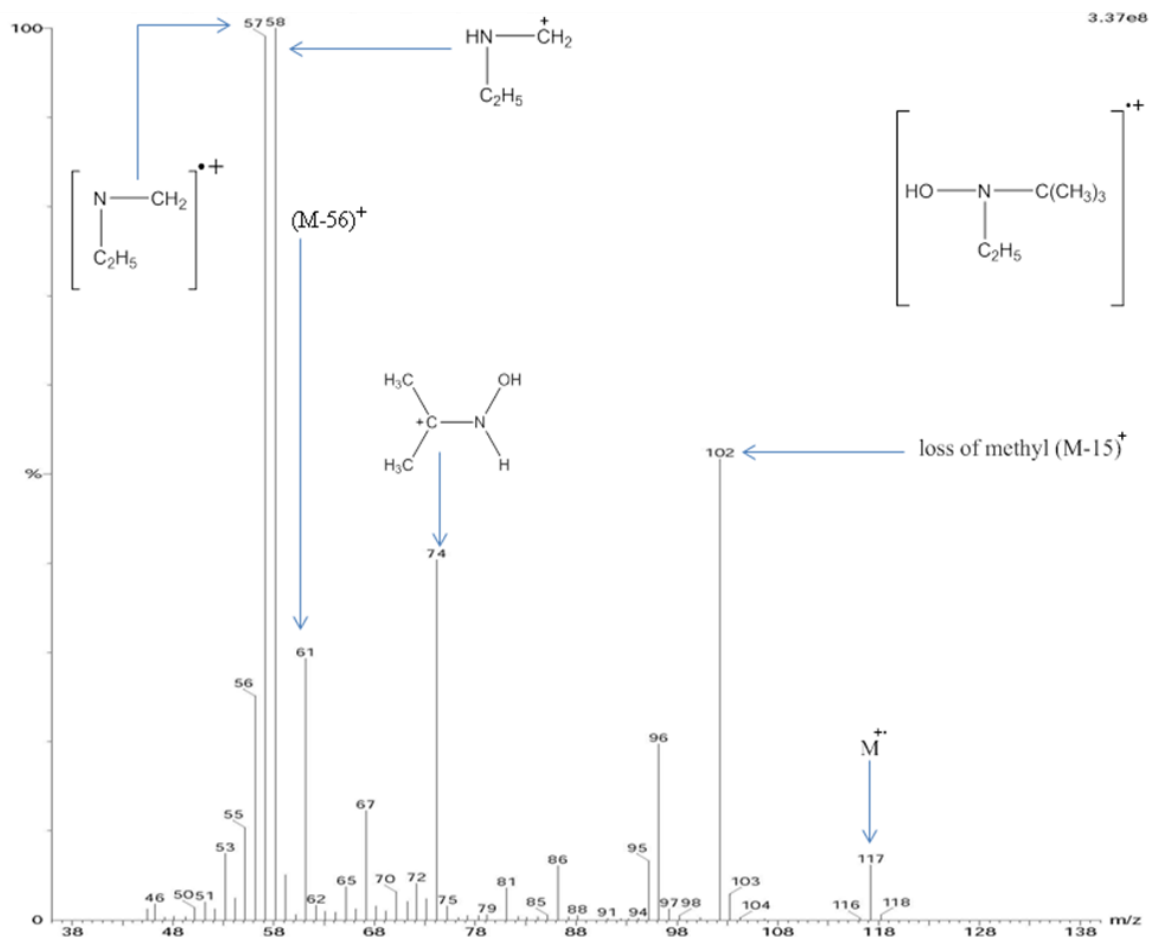


Figure 4.20: Electron ionisation (EI) mass spectrum of the peak at 1.69 minutes (figure 4.1) corresponding to a hydrogen & ethyl adduct of the MNP. The structure given in the top right corner is that of the molecular ion ( $M^+$ ) corresponding to the peak at  $m/z$  117.

The EI mass spectrum shown in figure 4.20 corresponds to a hydrogen and ethyl adduct of MNP (H-MNP-C<sub>2</sub>H<sub>5</sub>). The molecular ion can be seen at  $m/z$  117. The fragment at  $m/z$  102 is formed by the loss of methyl group from the molecular ion; further loss of ethene gives a peak at  $m/z$  74. The ion for the fragment at  $m/z$  57 is believed to be  $(\text{CH}_2\text{NC}_2\text{H}_5)^+$ .

## 4.5.2 EI mass spectrum of H-MNP-CD<sub>2</sub>CH<sub>3</sub> adduct

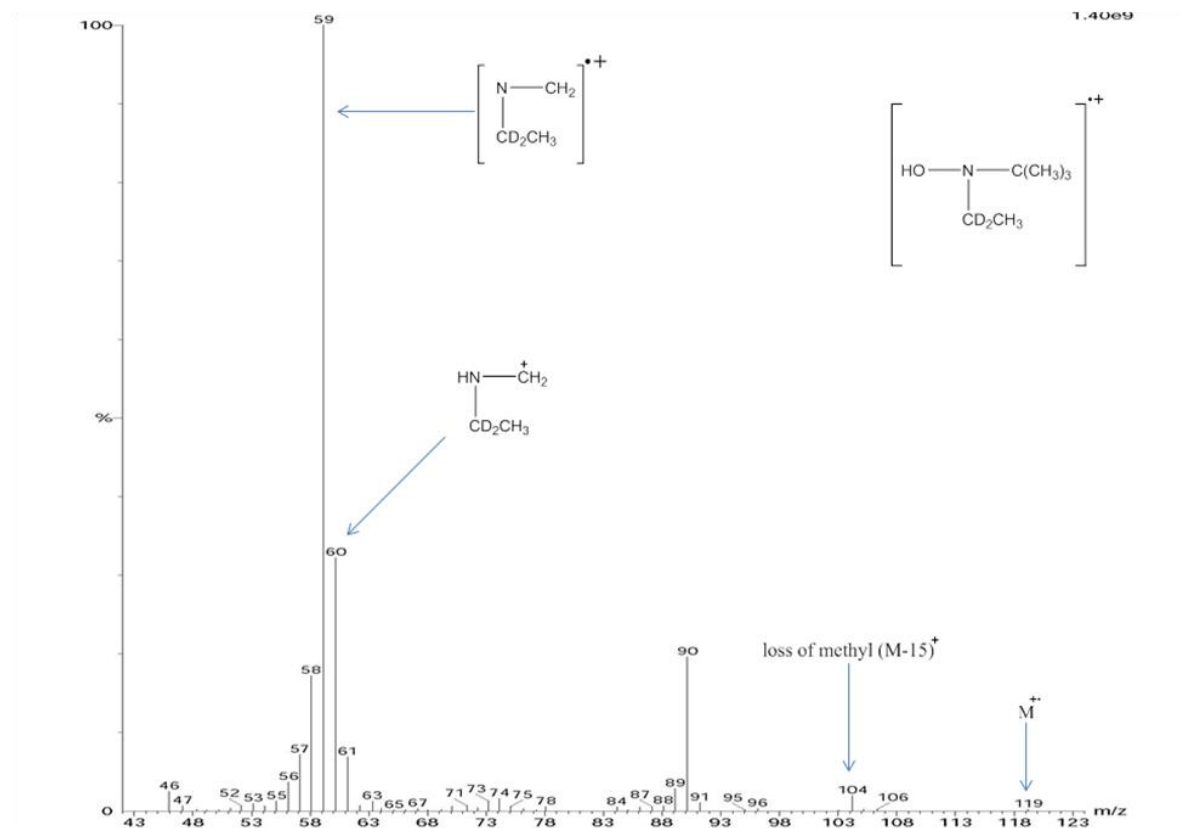


Figure 4.21: Electron ionisation (EI) mass spectrum of the peak at 1.66 minutes (figure 4.2) corresponding to a hydrogen & CH<sub>3</sub>CD<sub>2</sub> adduct of the MNP (H-MNP-CD<sub>2</sub>CH<sub>3</sub>). The structure given in the top right corner is that of the molecular ion (M<sup>+</sup>) corresponding to the peak at *m/z* 119.

The EI mass spectrum shown in Figure 4.21 corresponds to H-MNP-CD<sub>2</sub>CH<sub>3</sub> detected at *m/z* 119 when the reaction was carried out by using deuterated propanal (CH<sub>3</sub>CD<sub>2</sub>CHO) as a secondary source of radicals in the Fenton reaction system (a difference of 2 *m/z* units when compared to the molecular ion of H-MNP-C<sub>2</sub>H<sub>5</sub>; figure 4.20). This confirms the trapping of one deuterium-ethyl (CD<sub>2</sub>CH<sub>3</sub>) radical. As for the previous spectrum, the fragment at *m/z* 104 is formed by the loss of a methyl group (from the MNP part of the molecular ion). The ion at *m/z* 59 is believed to be (CH<sub>2</sub>NCD<sub>2</sub>CH<sub>3</sub>)<sup>+</sup>.

Table 4.3: Summary of GC-MS data for the hydrogen and ethyl adduct of MNP, formed when the reaction was carried out by using PBN and its derivatives as trapping agents and propanal/deuterated propanal as a secondary source of free radicals.

| Reactants in the Fenton system                 | Spin adduct                           | Retention time ( $R_t$ ) | Molecular ion ( $m/z$ ) | Characteristic fragment peaks ( $m/z$ ) |
|--|---------------------------------------|--------------------------|-------------------------|---|
| PBN & propanal                                 | H-MNP-C <sub>2</sub> H <sub>5</sub>   | 1.69                     | 117                     | 102, 74, 56, 57                         |
| PBN & d <sub>2</sub> -propanal                 | H-MNP-CD <sub>2</sub> CH <sub>3</sub> | 1.66                     | 119                     | 104, 90, 58, 59                         |
| d <sub>6</sub> -PBN & propanal                 | H-MNP-C <sub>2</sub> H <sub>5</sub>   | 1.70                     | 117                     | 102, 74, 56, 57                         |
| d <sub>6</sub> -PBN & d <sub>2</sub> -propanal | H-MNP-CD <sub>2</sub> CH <sub>3</sub> | 1.66                     | 119                     | 104, 90, 58, 59                         |
| F-PBN & propanal                               | H-MNP-C <sub>2</sub> H <sub>5</sub>   | 1.67                     | 117                     | 102, 74, 56, 57                         |
| Cl-PBN & propanal                              | H-MNP-C <sub>2</sub> H <sub>5</sub>   | 1.66                     | 117                     | 102, 74, 56, 57                         |

## 4.6 EI mass spectra of phenylpropene

### 4.6.1 Phenylpropene

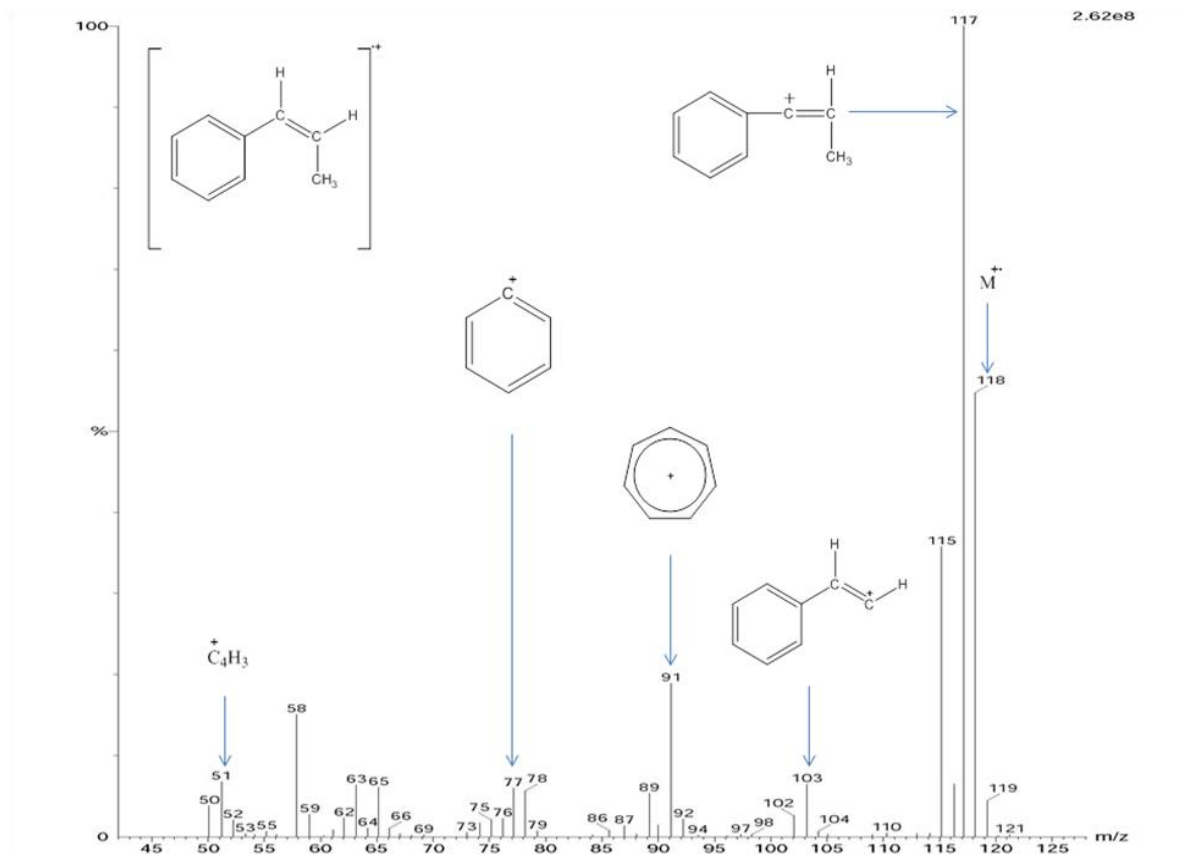


Figure 4.22: Electron ionisation (EI) mass spectrum of the peak at 3.16 minutes (figure 4.1) corresponding to phenylpropene. The structure given in the top left corner is that of the molecular ion ( $M^+$ ) corresponding to the peak at  $m/z$  118.

The EI mass spectrum shown in figure 4.22 corresponds to the phenylpropene with a molecular ion at  $m/z$  118. The fragment at  $m/z$  117 is formed by the loss of hydrogen from the molecular ion. The loss of methyl group from the molecular ion generates a fragment at  $m/z$  103. Other characteristics fragments are identified and shown in above figure.

## 4.6.2 d<sub>1</sub>-phenylpropene

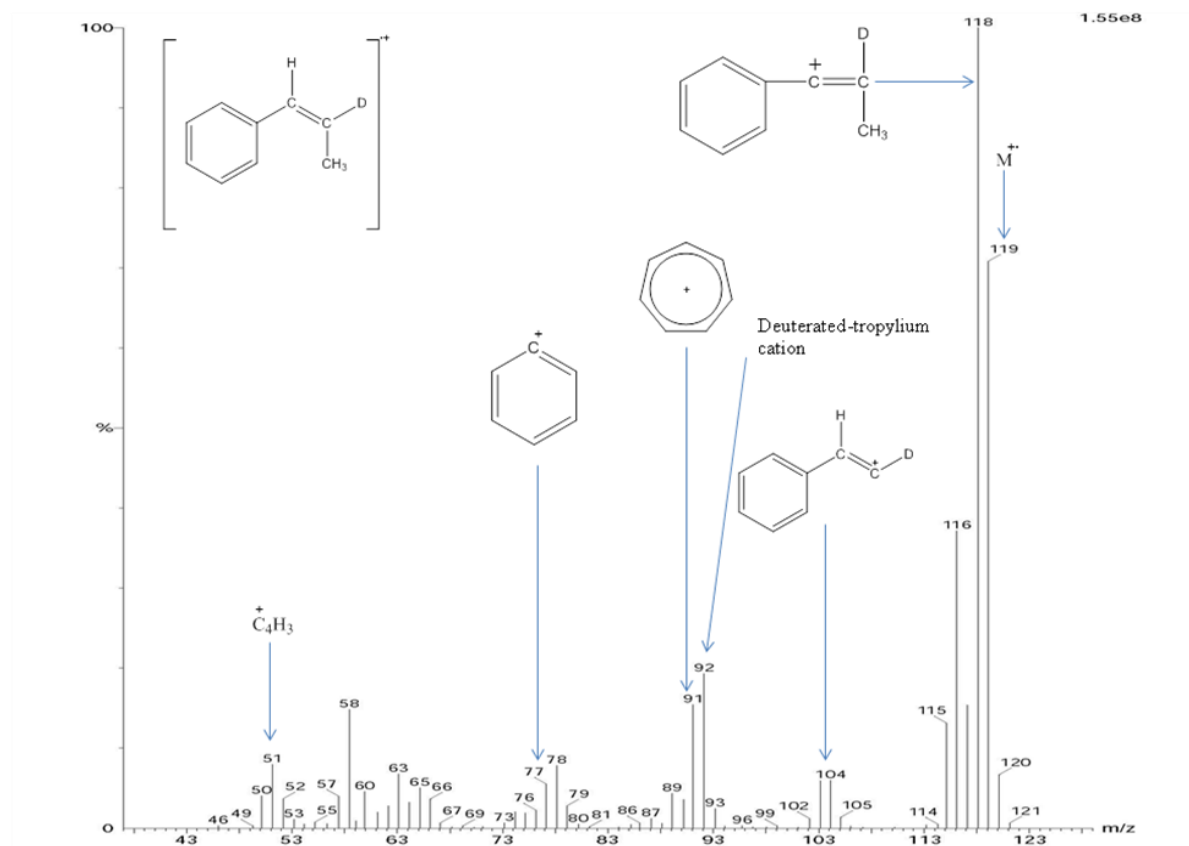
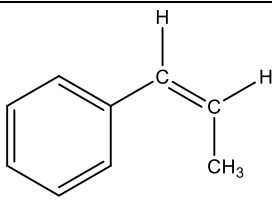
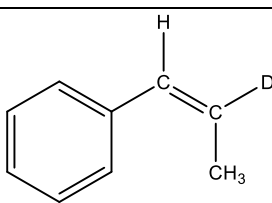
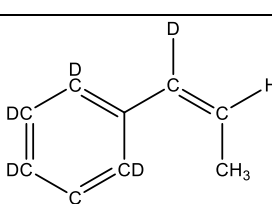
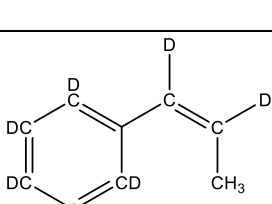
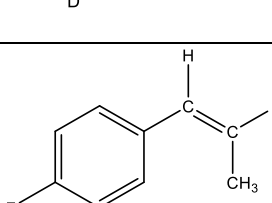
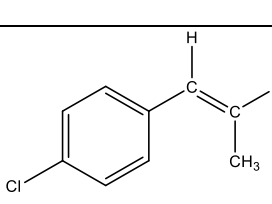


Figure 4.23: Electron ionisation (EI) mass spectrum of the peak at 3.15 minutes (figure 4.2) corresponding to d<sub>1</sub>-phenylpropene. The structure given in the top left corner is that of the molecular ion (M<sup>+</sup>) corresponding to the peak at *m/z* 119.

The EI mass spectrum shown in figure 4.23 corresponds to d<sub>1</sub>-phenylpropene (molecular ion appears at *m/z* 119) when the reaction was carried out by using deuterated propanal (CH<sub>3</sub>CD<sub>2</sub>CHO) as a secondary source of radicals in the Fenton reaction system. The fragment at *m/z* 118 is formed by the loss of hydrogen, whilst a loss of methyl group from the molecular ion generates a fragment at *m/z* 104. Other characteristic fragments are identified and their structures are shown in above figure.

Further experiments using other derivatives of PBN confirms the identity of adduct which is summarised in Table 4.4.

Table 4.4: Summary of GC-MS data for X-(phenylpropene) where X is hydrogen for PBN, F for 4-FPBN, Cl for 4-CIPBN, when the reaction was carried out by using PBN and its derivatives as trapping agents and propanal/deuterated propanal as a secondary source of free radicals.

| Reagents in the Fenton system                  | Identity  | Retention time (min) | Molecular ion ( $m/z$ ) | Characteristics fragment peaks ( $m/z$ )          |
|--|---|----------------------|-------------------------|---|
| PBN & propanal                                 |    | 3.16                 | 118                     | 117, 115, 103, 91, 77, 58, 51                     |
| PBN & d <sub>2</sub> -propanal                 |   | 3.15                 | 119                     | 118, 116, 104, 91, 77, 58, 51                     |
| d <sub>6</sub> -PBN & propanal                 |  | 3.14                 | 124                     | 123, 109, 96, 82, 61, 54                          |
| d <sub>6</sub> -PBN & d <sub>2</sub> -propanal |  | 3.14                 | 125                     | 124, 110, 96, 108, 82, 61, 54                     |
| F-PBN & propanal                               |  | 3.18                 | 136                     | 135, 133, 121, 109, 95                            |
| Cl-PBN & propanal                              |  | 6.61                 | 152/154                 | 151/149, 137/139, 125/127, 115/117, 89/91, 58, 51 |

## 4.7 Identification of extra peaks found with other derivatives of PBN:

### 4.7.1 EI mass spectrum of C<sub>2</sub>H<sub>5</sub>-MNP-*tert* butyl

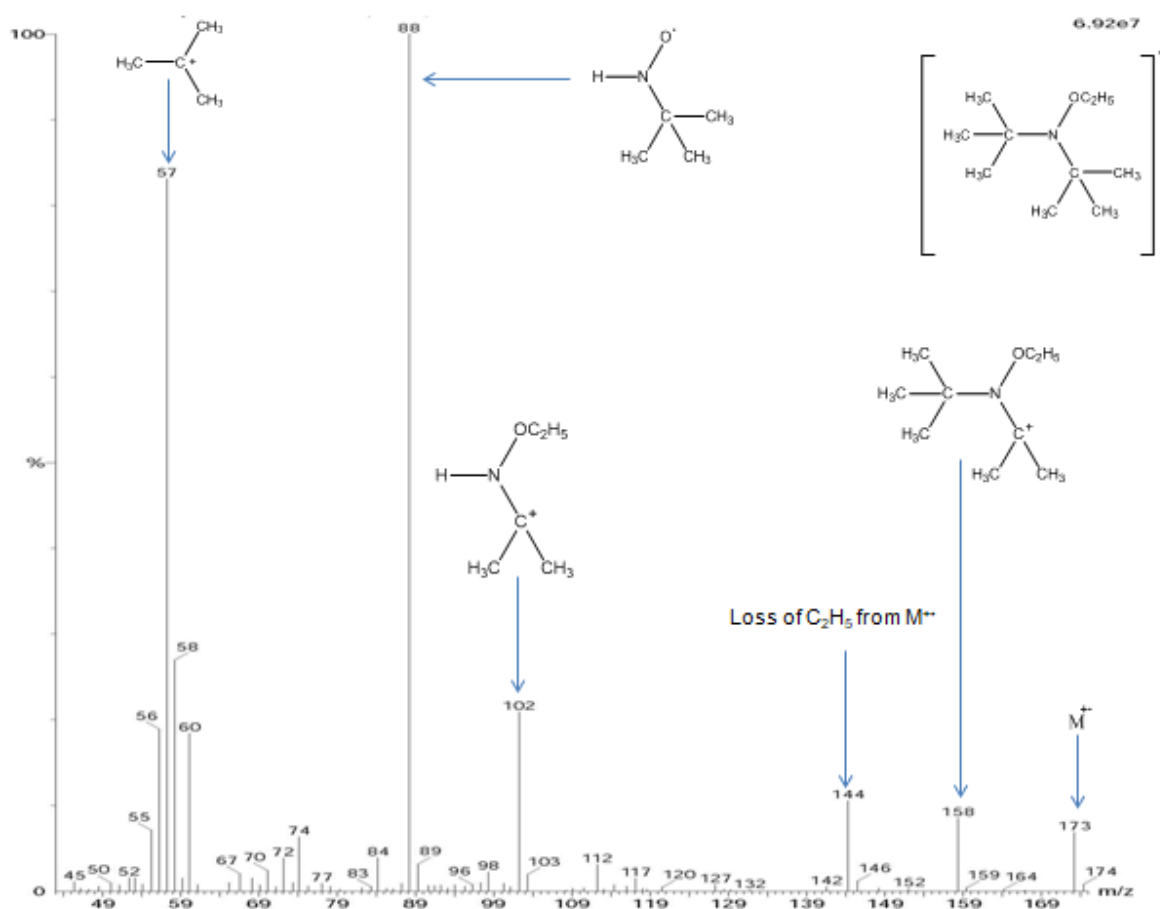


Figure 4.24: Electron ionisation (EI) mass spectrum of the peak at 2.77 minutes (figure 4.5 & 4.6) corresponding to an ethyl adduct of di-*tert*-butyl nitroxide (C<sub>2</sub>H<sub>5</sub>-MNP-*tert* butyl). The structure given in the top right corner is that of the molecular ion (M<sup>+</sup>) corresponding to the peak at *m/z* 173.

The EI mass spectrum shown in figure 4.24 corresponds to C<sub>2</sub>H<sub>5</sub>-MNP-*tert* butyl adduct detected at 2.77 minutes when the reaction was carried out by using F-PBN (figure 4.5) and Cl-PBN (figure 4.6) as spin trapping agents. The molecular ion can be seen clearly at *m/z* 173. The fragment at *m/z* 158 is generated by the loss of a methyl group from molecular ion, whilst loss of an ethyl group (from M<sup>+</sup>) gives a fragment at *m/z* 144. The fragment at *m/z* 102 is formed by the loss of 56 mass units from the fragment at *m/z* 158. The base peak at *m/z* 88 is formed by the loss of 56 mass units from *m/z* 144. The peak at *m/z* 57 corresponds to the *tert*-butyl cation.



## 4.7.2 Hydrogen & *tert*-ethyl adduct of MNP

### 4.7.2.1 EI mass spectrum of H-MNP-*tert* ethyl adduct

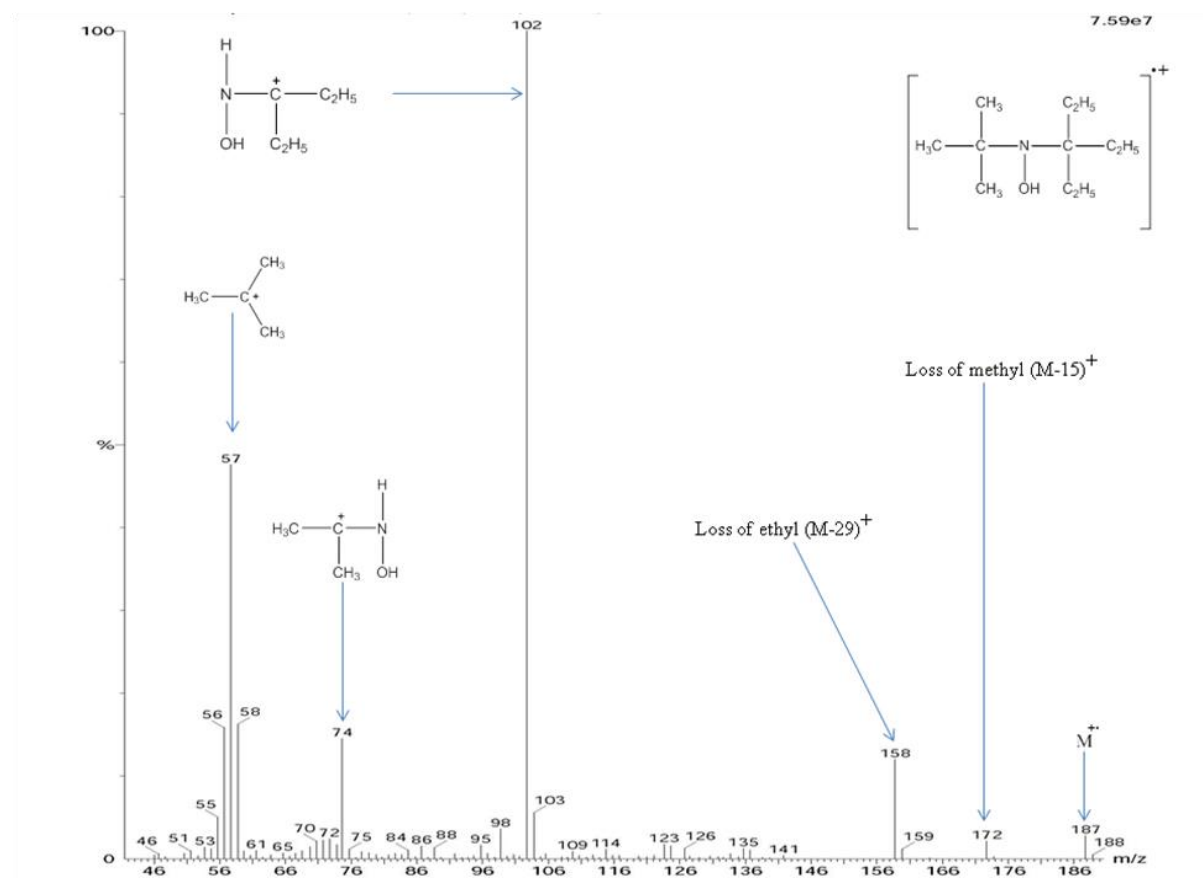


Figure 4.25: Electron ionisation (EI) mass spectrum of the peak at 3.59 minutes (figure 4.5) corresponding to hydrogen and a  $\text{CEt}_3$  adduct of MNP (H-MNP- $\text{CEt}_3$ ). The structure given in the top right corner is that of the molecular ion ( $M^+$ ) corresponding to the peak at  $m/z$  187.

The EI mass spectrum shown in figure 4.25 corresponds to H-MNP- $\text{CEt}_3$  adduct detected at 3.59 minutes when the reaction was carried out by using F-PBN (figure 4.5) as a spin trapping agent. The molecular ion can be seen clearly at  $m/z$  187. The fragment at  $m/z$  172 is generated by the loss of methyl group from the molecular ion, whilst loss of an ethyl group (from  $M^+$ ) gives a fragment at  $m/z$  158. The base peak at  $m/z$  102 is formed by the loss of 56 mass units ( $\text{H}_2\text{C}=\text{CMe}_2$ ) group from the fragment at  $m/z$  158. The peak at  $m/z$  57 corresponds to the *tert*-butyl cation.

#### 4.7.2.2 EI mass spectrum of H-MNP-*tert* ethyl-d<sub>6</sub> adduct

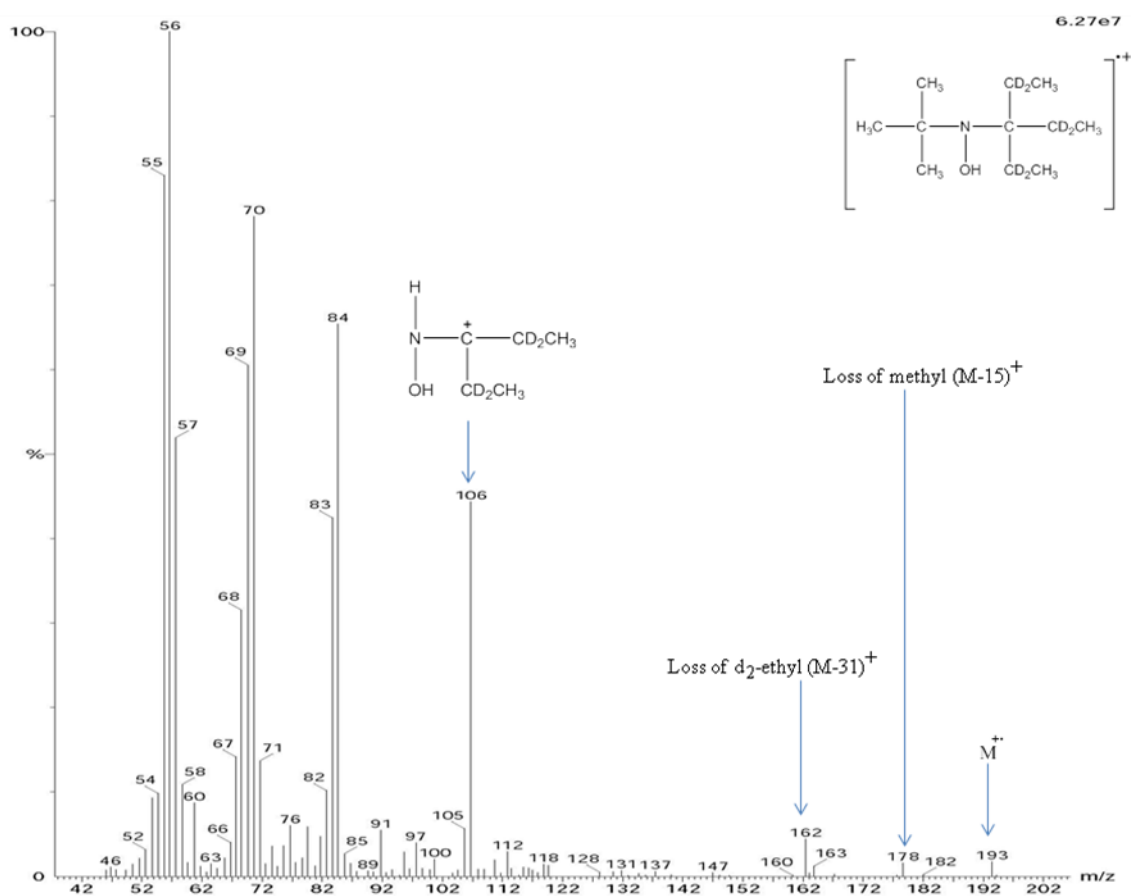


Figure 4.26: Electron ionisation (EI) mass spectrum of the peak at 3.51 minutes (figure 4.2) corresponding to a hydrogen and  $d_6$ - $\text{CET}_3$  adduct of MNP. The structure given in the top right corner is that of the molecular ion ( $M^{++}$ ) corresponding to the peak at  $m/z$  193.

The EI mass spectrum shown in figure 4.26 corresponds to  $\text{H-MNP-C}(\text{CD}_2\text{CH}_3)_3$  detected at 3.51 minutes when the reaction was carried out by using deuterated propanal ( $\text{CH}_3\text{CD}_2\text{CHO}$ ) as a secondary source of radicals in the Fenton reaction system (figure 4.2). The molecular ion can be clearly seen at  $m/z$  193 (a difference of 6  $m/z$  units when compared to the molecular ion of  $\text{H-MNP-C}(\text{C}_2\text{H}_5)_3$  (figure 4.25) which confirms the trapping of three deuterium-ethyl ( $^{\cdot}\text{CD}_2\text{CH}_3$ ) radicals and thus supporting the formation of suggested adduct. The fragment at  $m/z$  178 is generated by the loss of a methyl group from the molecular ion, whilst loss of a  $\text{CD}_2\text{CH}_3$  group (from  $M^{++}$ ) gives the fragment at  $m/z$  162. The fragment at  $m/z$  106 is formed by the loss of 56 mass units ( $\text{H}_2\text{C}=\text{CMe}_2$ ) from the fragment at  $m/z$  162.

## 4.8 Identification of other peaks (not derived from the Fenton reaction)

### 4.8.1 Propanal

EI mass spectrum of the peak (data not shown) retained at 1.56 minutes was searched in NIST library and been identified as unreacted propanal. Propanal is a volatile chemical and its presence in all controls as compared in figure 4.19 confirms that it is not a Fenton reaction derived peak.

#### 4.8.2.1 EI mass spectrum of 2-methyl-2-pentenal

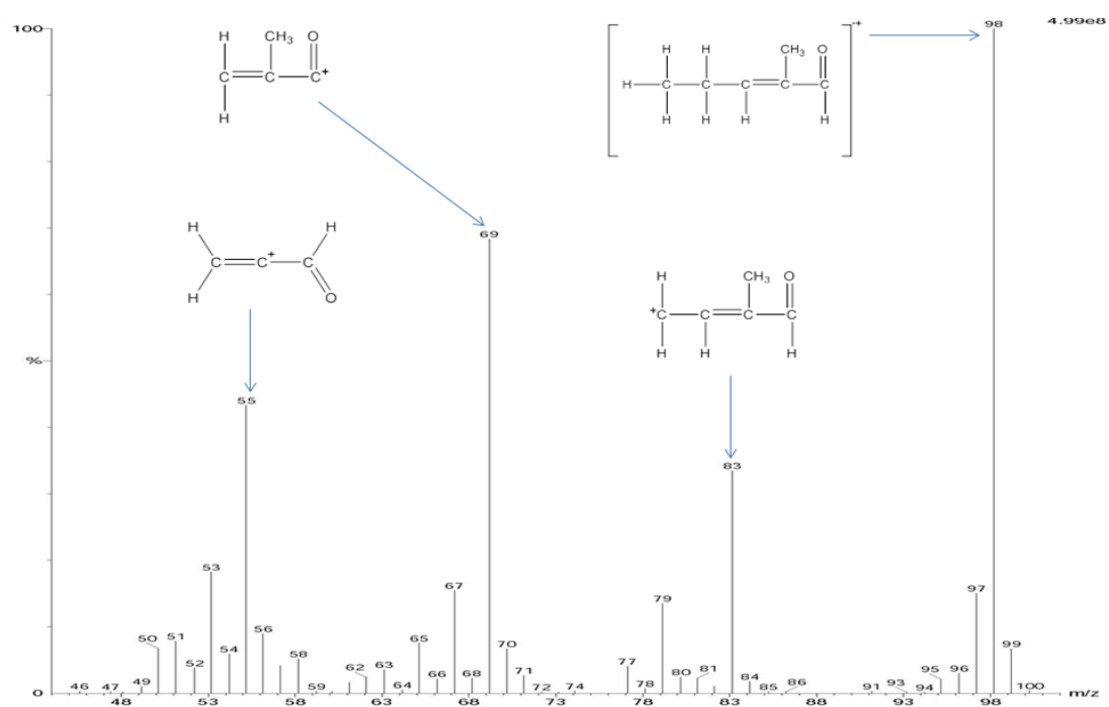


Figure 4.27: Electron ionisation (EI) mass spectrum of the peak at 1.95 minutes (figure 4.1) corresponding to 2-methyl-2-pentenal. The structure given in the top left corner is that of the molecular ion ( $M^{+\bullet}$ ) corresponding to the peak at  $m/z$  98.

The EI mass spectrum shown in figure 4.27 corresponds to 2-methyl-2-pentenal with a molecular ion at  $m/z$  98. The fragment at  $m/z$  83 is formed by the loss of a methyl group (from  $M^{+\bullet}$ ). The EI mass spectrum was searched in the NIST library and identified as 2-methyl-2-pentenal. Propanal can go under self-aldol condensation resulting in the formation of 2-methyl-2-pentenal. It is also present in all control reactions (figure 4.7) further demonstrating that it is formed by a non-Fenton pathway.

#### 4.8.2.2 EI mass spectrum of 2-methyl-2-pentenal (d<sub>2</sub>)

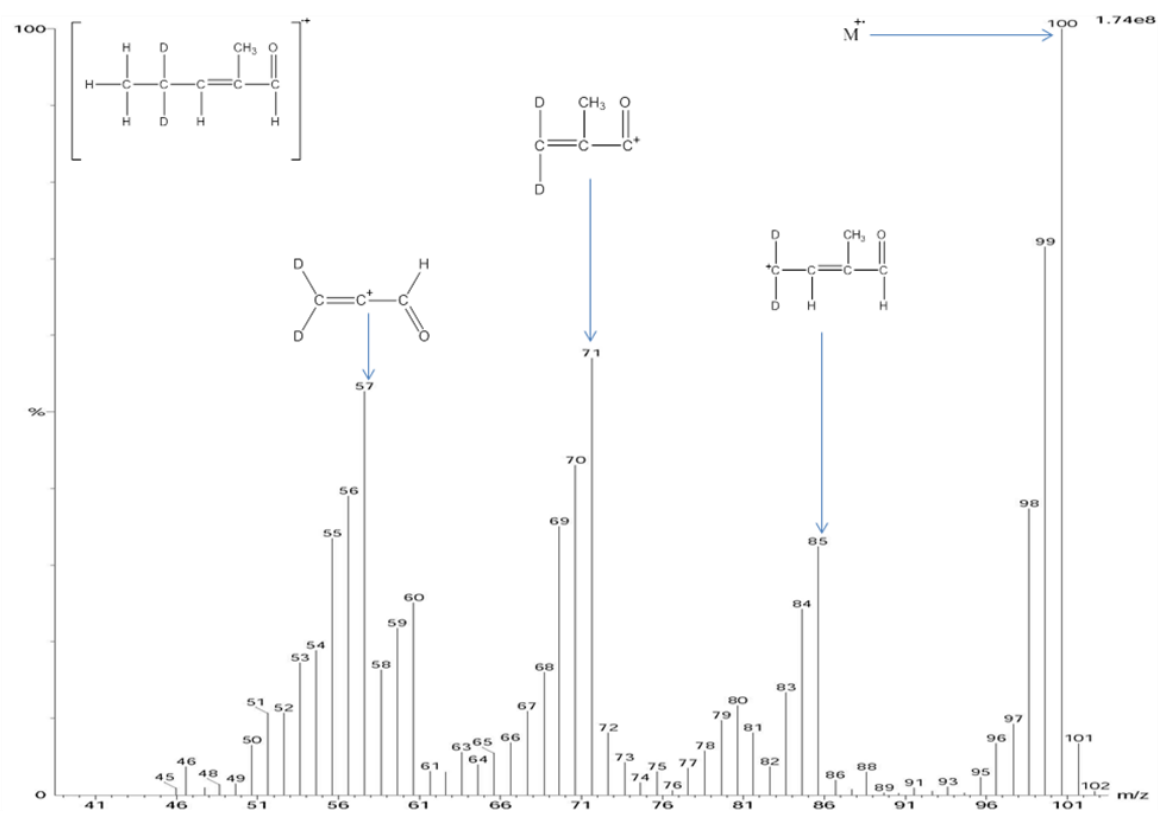


Figure 4.28: Electron ionisation (EI) mass spectrum of the peak at 1.94 minutes (figure 4.2) corresponding to 2-methyl-2-pentenal-d<sub>2</sub>. The structure given in the top left corner is that of the molecular ion (M<sup>+</sup>) corresponding to the peak at *m/z* 100.

The EI mass spectrum shown in figure 4.28 corresponds to 2-methyl-2-pentenal-d<sub>2</sub> with a molecular ion at *m/z* 100. The fragment at *m/z* 85 is formed by the loss of methyl group from the molecular ion. The mass spectrum supports the mechanism of self-aldol condensation (where two hydrogen atoms from carbon at position 2 and oxygen from another molecule of propanal are released to form a water molecule and 2-methyl-2-pentenal-d<sub>2</sub>). The fragmentation pattern also supports the formation of this compound.

### 4.8.3 EI mass spectrum of 2-methylcyclopentenone

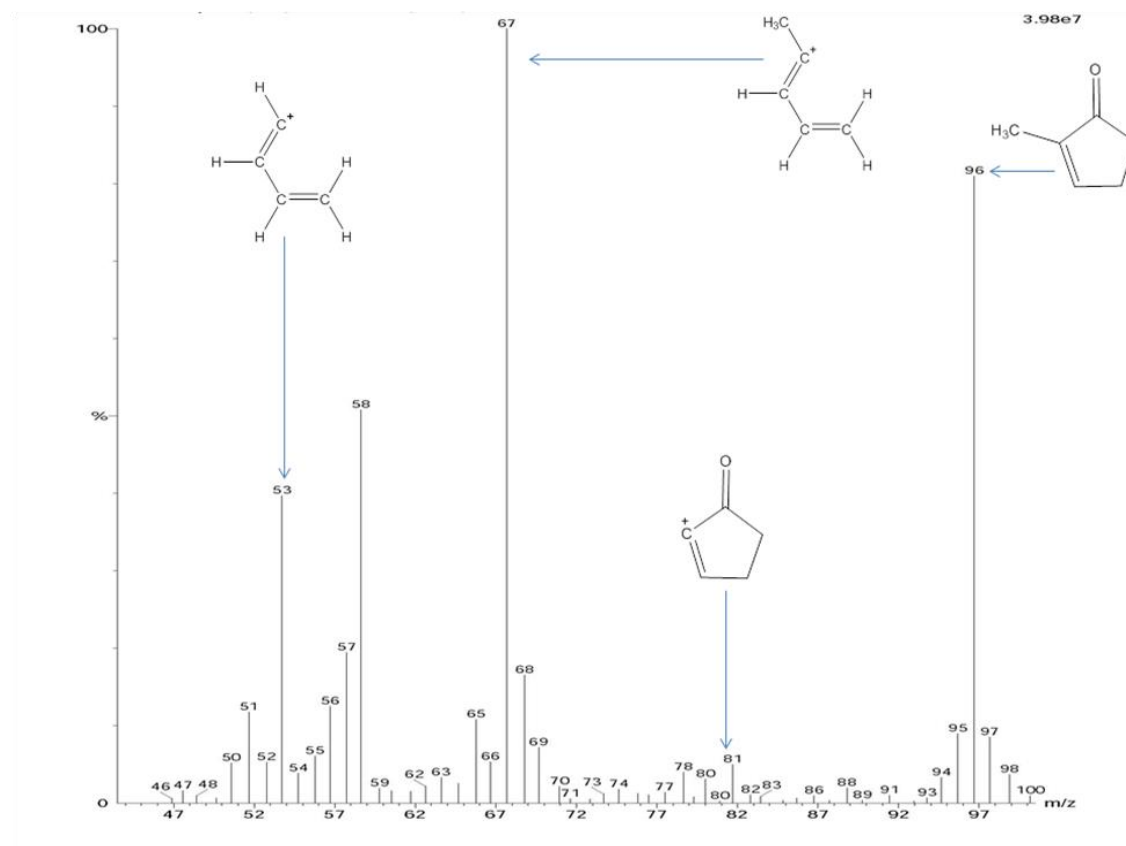
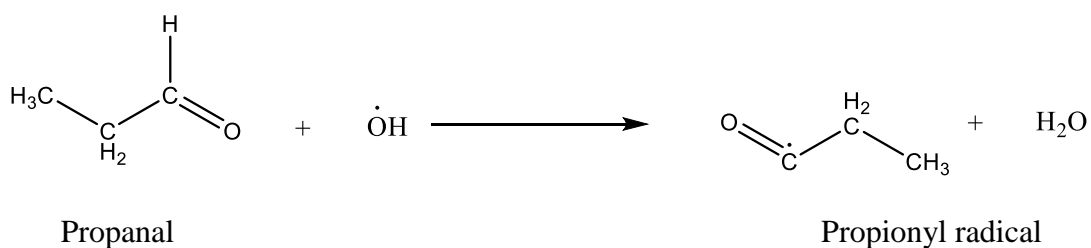


Figure 4.29: Electron ionisation (EI) mass spectrum of the peak at 2.23 minutes (figure 4.1) corresponding to 2-methylcyclopentenone, with a molecular ion peak at  $m/z$  96. It is present in all control reactions (figure 4.7) which demonstrates that it is not a product of the Fenton system. A NIST library search suggested it to be 2-methylcyclopentenoane. This identity was confirmed when analysis of a purchased standard was carried out (see Figure A3; appendix).

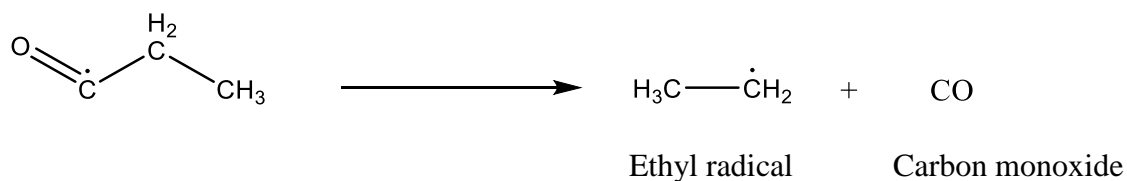
## 4.9 Discussion:

The aim of this series of experiments was to trap the free radicals generated from propanal by using the Fenton based chemistry, as explained in section 2.2.1. Propanal was used as a secondary source of free radicals, derived from hydroxyl radicals produced in the Fenton system (Scheme 4.2). PBN and its derivatives were then used as trapping agents to produce products stable enough to be sampled and analysed by using TD-GC-MS.

Step 1: Formation of propionyl radical from propanal



Step 2: Formation of ethyl radical from propionyl radical



Scheme 4.2: Formation of ethyl radicals from propanal. Formation of propionyl radical from propanal (step 1), which further breaks down to give ethyl radical (step 2).

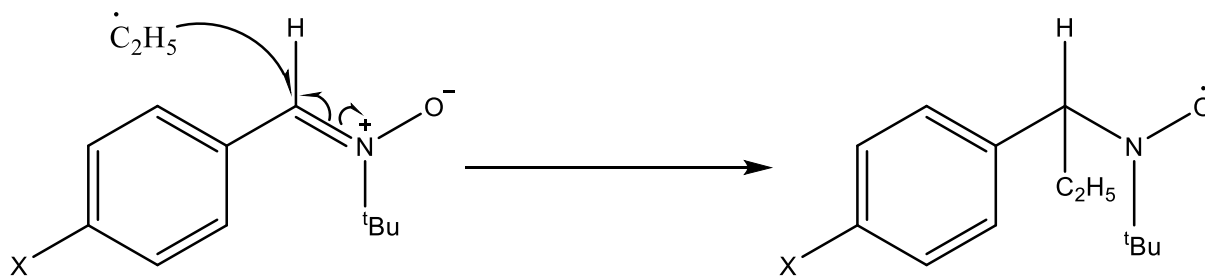
### 4.9.1 The Fenton reaction derived peaks

Five new peaks were observed when Fenton chemistry was used (with propanal as a secondary source of free radicals) as compared to control experiments (Figure 4.7 & 4.8). The most intense peak has been identified as a di-ethyl adduct. As described in chapter 3, the formation of a di-radical-adduct with PBN is a two-step process (Janzen *et al.*, 1985). Initially, an ethyl radical is trapped at the alpha carbon, converting the molecule into a nitroxide, which in turn traps another ethyl radical at the oxygen site and generates a stable di-ethyl species (scheme 4.3).

The mass spectrum in figure 4.9 clearly shows a molecular ion at  $m/z$  235 and a peak at  $m/z$  220 corresponding to loss of a methyl radical from the molecular ion. The methyl radical is lost from the <sup>t</sup>Bu group of PBN as indicated by experiments using d<sub>2</sub>-propanal (CH<sub>3</sub>CD<sub>2</sub>CHO) as the source of secondary radicals. One of the trapped ethyl groups may also be lost from alpha carbon which further loses 56 mass units (H<sub>2</sub>C=CMe<sub>2</sub>) to give a peak at  $m/z$  150. Loss of 2-methyl-1-propene from the molecular ion gives a fragment at  $m/z$  179. Dissociation of the molecular ion between the alpha carbon and nitrogen gives a peak at  $m/z$  119 (shown in scheme 4.1).

To confirm the source of the ethyl radicals, deuterated propanal was used in the Fenton system. Deuteron ethyl radicals (CH<sub>3</sub><sup>•</sup>CD<sub>2</sub>) were generated and then trapped by PBN to form a PBN(CD<sub>2</sub>CH<sub>3</sub>)<sub>2</sub> adduct (figure 4.10). The shift of 4  $m/z$  units clearly demonstrates that propanal is the source of the trapped ethyl radicals in the system. Furthermore, the identity of adduct was confirmed by using different combinations of spin trap and propanal/deuterated-propanal, summarised in table 4.1.

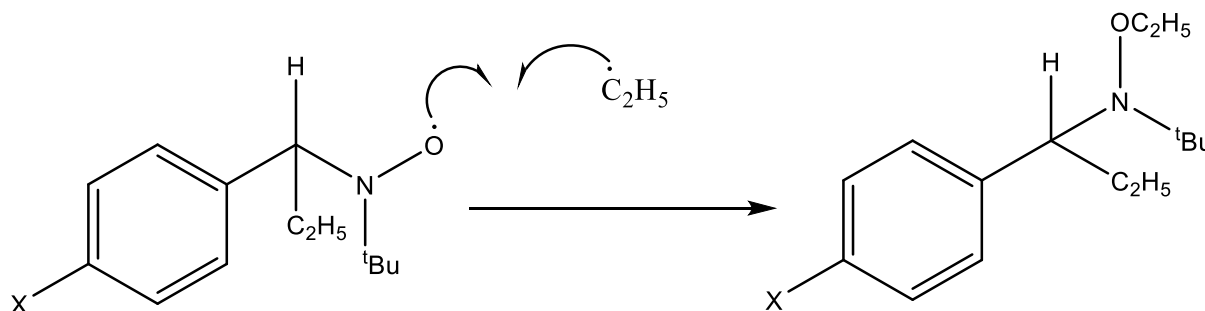
Step 1: Formation of a mono-ethyl adduct



PBN

PBN-mono-ethyl adduct

Step 2: Formation of di-ethyl adduct



PBN-mono-ethyl adduct

PBN-di-ethyl adduct

Scheme 4.3: Reaction mechanism for trapping ethyl radicals by PBN (or its derivatives) with the formation of a mono-ethyl adduct (step 1), and the addition of a second ethyl radical at the oxygen site to give a di-ethyl adduct (step 2). (X is H for PBN, F for F-PBN and Cl for Cl-PBN).

The chromatogram shown in figure 4.1 has a small peak retained at 8.74 minutes which has been identified as N-ethoxy-1-phenyl-1-propanamine. The suggested adduct is formed by trapping two ethyl radicals with a loss of 56 mass units ( $\text{H}_2\text{C}=\text{CMe}_2$ ) from PBN. The molecular ion can be seen at  $m/z$  179 (figure 4.15) which then loses an ethyl radical to give a peak at  $m/z$  150. The identity of adduct was confirmed by using  $\text{d}_2$ -



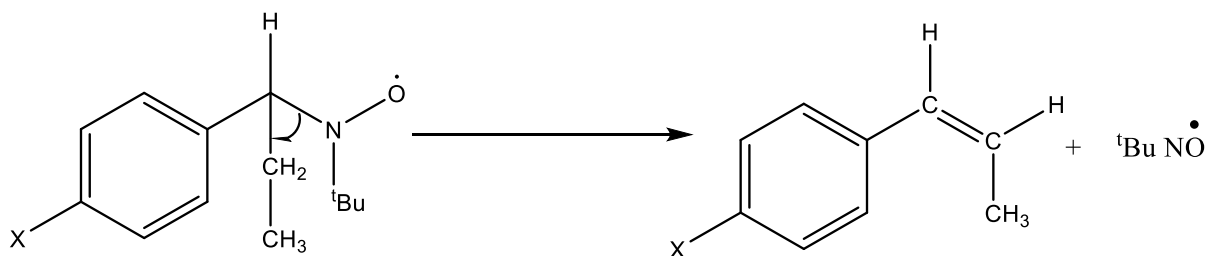
propanal in the Fenton reaction. The molecular ion is clearly seen at  $m/z$  183 showing an increase of 6  $m/z$  units, and thus confirming that two deuterium-ethyl radicals ( $\text{CH}_3\cdot\text{CD}_2$ ) have been trapped. Furthermore, the identity of the adduct was further supported by using different combinations of spin trap and propanal/deuterated propanal, summarised in table 4.2.

A peak retained at 1.69 minutes (figure 4.1) has been identified as an ethyl adduct of *tert*-butylhydroaminoxyl. Hydroxyl radical attack of PBN leads to the formation of 2-methyl-2-nitrosopropane (MNP) and benzaldehyde (Turnbull *et al.*, 2001). MNP is a known free radical spin trap which, in this study, may trap an ethyl radical and then the resulting nitroxide may be reduced to the hydroaminoxyl in the presence of ascorbate. The molecular ion of the adduct is seen at  $m/z$  117 (figure 4.20). In the corresponding experiment done by using  $\text{d}_2$ -propanal the  $m/z$  value of the molecular ion increases by 2 mass units to  $m/z$  119 (figure 4.21) confirming the addition of ethyl in the structure, summarised in table 4.3. The use of PBN derivatives demonstrates that the adduct no longer contains the benzene ring or alpha carbon, both of which are lost when the PBN is cleaved following hydroxyl radical addition. It is interesting to note that in the absence of both hydrogen peroxide and a secondary source of radicals from the “Fenton” system, MNP is still observed. This may be due to the presence of oxygen in the system, which can pick up an electron from  $\text{Fe}^{2+}$  to generate the superoxide radical. It is reasonable to suggest that superoxide radical addition to PBN may lead to the breakdown of PBN and thus formation of MNP and benzaldehyde.

Another peak retained at 2.59 minutes (figure 4.1) is identified as benzaldehyde, previously identified in chapter 3 (section 3.13). As explained above, benzaldehyde is formed from the free radical induced breakdown of the spin trapping agent (PBN or its derivatives).

The peak retained at 3.16 minutes (figure 4.1) is phenyl propene with a molecular ion at  $m/z$  118 (figure 4.22) which readily loses a hydrogen to generate a peak at  $m/z$  117 while a loss of methyl radical from the molecular ion gives a peak at  $m/z$  103. A possible mechanism is the breakdown of a mono-ethyl radical-adduct and formation of a double bond between the alpha carbon of PBN and carbon of ethyl, resulting in the formation of phenyl propene (scheme 4.4). Further evidence to support the suggested structure of the compound is obtained when the Fenton reaction is carried out using  $\text{d}_2$ -propanal. The

molecular ion value increases by 1  $m/z$  unit to  $m/z$  119 (figure 4.23), which follows the same fragmentation pattern. Furthermore, the identity of adduct was confirmed by using different combinations of spin trap and propanal/deuterated-propanal, summarised in table 4.4.



Scheme 4.4: Suggested mechanism of phenylpropene formation from the mono-ethyl adduct

The peak retained at 3.59 minutes (figure 4.5) is detected only when F-PBN is used as a spin trapping agent. It is identified as hydrogen and a  $\text{CET}_3$  adduct of MNP with a molecular ion at  $m/z$  187 (figure 4.25). The loss of a methyl group (from  $\text{M}^{+\bullet}$ ) generates a fragment at  $m/z$  172 while a loss of ethyl radical (from  $\text{M}^{+\bullet}$ ) gives a fragment at  $m/z$  158. The identity of adduct was confirmed by using  $\text{d}_2$ -propanal in the Fenton reaction. The molecular ion is clearly seen at  $m/z$  193 (figure 4.26) showing an increase of 6  $m/z$  units, confirming that three deuterium-ethyl radicals have been trapped.

A peak retained at 2.77 minutes was detected when the reaction was carried out by using either F-PBN (figure 4.5) or Cl-PBN (figure 4.6). The suggested compound is an ethyl adduct of di-*tert*-butyl nitroxide with a molecular ion at  $m/z$  173. Because of its presence in only two derivatives with similar information, it is not possible to confirm the identity of the adduct but its formation in two different derivatives of PBN i.e. Cl-PBN & F-PBN, confirms that the non-ring part of the spin trap is involved in its formation.

#### 4.9.2 Peaks not derived from the Fenton reaction

An intense peak seen at 1.56 minutes (figure 4.1) is identified as propanal. It is present in all non-Fenton derived reactions (figure 4.7) which confirms that it is not a product of the Fenton reaction. Its identity is confirmed through a NIST library search. Propanal is a known volatile organic compound which evaporates very easily (Curwin, Deddens & McKernan, 2015).

The peak retained at 1.95 minutes (figure 4.1 & 4.7) was identified as 2-methyl-2-pentenal through a NIST library search. Self-aldol condensation of propanal molecules can give 2-methyl-2-pentenal and a water molecule. The molecular ion can be seen clearly at  $m/z$  98 (figure 4.27). The identity of the compound was confirmed when deuterated propanal ( $d_2$ ) was used in the Fenton reaction, resulting in the formation of a molecular ion which is 2  $m/z$  units higher than when non-deuterated propanal was used, detected at  $m/z$  100 (figure 4.28).

A very small peak retained at 2.23 minutes (figure 4.1 & 4.7) is present in all non-Fenton derived reactions as well. It has been identified as 2-methylcyclopentenone when searched for in NIST library. Its presence in control reactions shows that it is not formed because of the Fenton free radical chemistry. This is most probably an impurity in a chemical used in the Fenton reaction.

Different aldehydes including propanal are identified as secondary products of LPO. Thiobarbituric acid (TBA) is the most common method used to detect aldehydes, whereby TBA and the sample are heated in an acid buffer and the resulting pink chromogen is measured. MDA is one of the lower molecular weight aldehydes formed by the decomposition of primary and secondary products of LPO, which can then be detected by using the TBA assay. Iron dependent reactions and radiation damage to nucleic acids, proteins and carbohydrates can also produce MDA, which is a limitation of the method in terms of measuring damage made by LPO (Liu *et al.* 1997). Furthermore, MDA can react with other compounds like sialic acid, amino pyridines and ribose. Thus, to measure MDA it is often derivatised with 2,4-dinitrophenylhydrazine (DNPH) before being separated by high performance liquid chromatography (HPLC) and measured by UV spectrophotometry (Cordis, Das & Riedel, 1998). As mentioned earlier in introduction chapter, mass spectrometry combined with HPLC may be used to identify the MDA from other products of oxidative stress (Cordis, Maulik & Das, 1995).

However, the derivatisation process is not only lengthy but complex as well. Other techniques used to identify small volatile organic compounds is gas chromatography coupled with mass spectrometric techniques like Proton transfer reaction mass spectrometry (Romano *et al.* 2015; Blake, Monks & Ellis, 2009) and selected ion flow tube mass spectrometry (Pysanenko, Spanel & Smith, 2009) but need of expensive instruments is a big drawback of these techniques.

The TD-GC-MS measurement of propanal radicals following spin trapping by PBN offers a potential alternative to the above-mentioned assays. Thermal desorption is a novel approach to detect spin trapped free radicals and the results presented here demonstrate the potential of this approach. Volatile PBN-adducts may be used as biomarkers for the facile detection of aldehydic products of LPO (see chapter 6 for further discussion).

## Chapter 5

### (Part 1)

Detection and analysis of spin-adducts from ethanal and 2,2,6,6-Tetramethylpiperidin-1-yl-oxy (TEMPO) using Thermal desorption - Gas Chromatography-Mass Spectrometry (TD-GC/MS)

## **5.1 Introduction`**

Ethanal (acetaldehyde) is a primary metabolite of ethanol and considered as a Class I carcinogen (Seitz and Stickel, 2007). Production routes, importance, damaging effects and detection of acetaldehyde are already discussed in the introduction to chapter 3.

As part of the current study, 2,2,6,6-Tetramethylpiperidin-1-yl-oxyl (TEMPO) and its derivatives were used as spin trapping agents to stabilise the free radicals and which were then further extracted from the headspace (HS) by two different approaches prior to analysis by GC-MS. To the best of our knowledge, these approaches have never been used to analyse radical adducts of TEMPO.

## **5.2 Chromatograms**

Figure 5.1 shows the chromatogram produced following the introduction of acetaldehyde into the Fenton system. Methyl radicals are primarily produced on reaction of hydroxyl radicals with the acetaldehyde (discussed in chapter 3) and these are then trapped by TEMPO. The Fenton reaction was carried out under standard conditions for five minutes with the sample mixture then transferred into a 40 mL vial and the headspace sampled (see section 2.4.2 for experimental procedure).

## 5.2.1 Fenton reaction with acetaldehyde and TEMPO

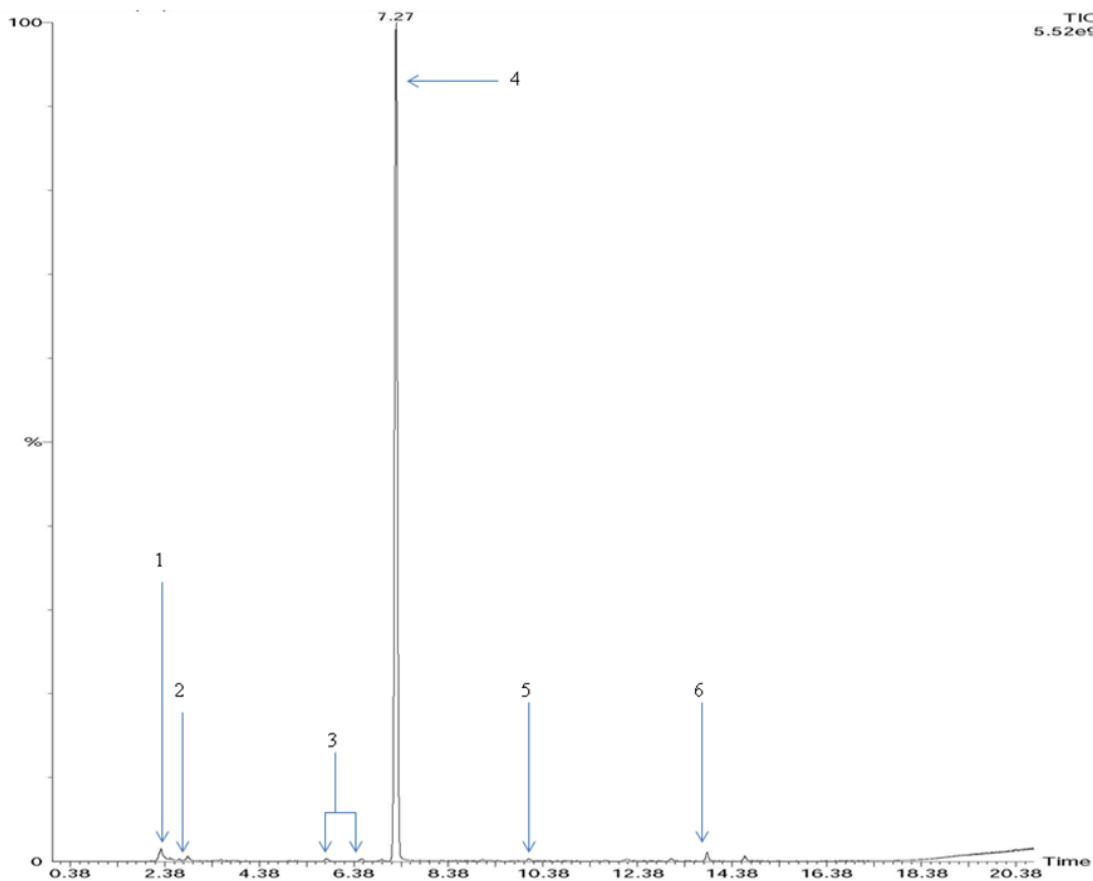


Figure 5.1: The total ion chromatogram (TIC) obtained from the headspace thermal desorption (TD)-GC-MS analysis of the Fenton reaction containing acetaldehyde and TEMPO showing a major peak at 7.27 minutes and several minor peaks.

Figure 5.1 shows the chromatogram following TD-GC-MS analysis of the Fenton reaction containing acetaldehyde and TEMPO with peaks corresponding to the following compounds of **1**) acetaldehyde ( $R_t$  2.31 minutes); **2**) paraldehyde ( $R_t$  2.86 minutes); **3**) 1-methoxy-2,2,6,6-tetramethyl-1,2,3,6-tetrahydropyridine (isomers at  $R_t$  5.80 & 6.54 minutes); **4**) TEMPO-CH<sub>3</sub> adduct ( $R_t$  7.27 minutes); **5**) 1-methoxy-2,2,4,6,6-pentamethylpiperidine ( $R_t$  10.07 minutes); **6**) TEMPO-*tert*-butyl adduct ( $R_t$  13.85 minutes). For a detailed analysis of EI-mass spectra see sections 5.3-5.8.

## 5.2.2 Fenton reaction with d<sub>3</sub>-acetaldehyde (CD<sub>3</sub>CHO) and TEMPO

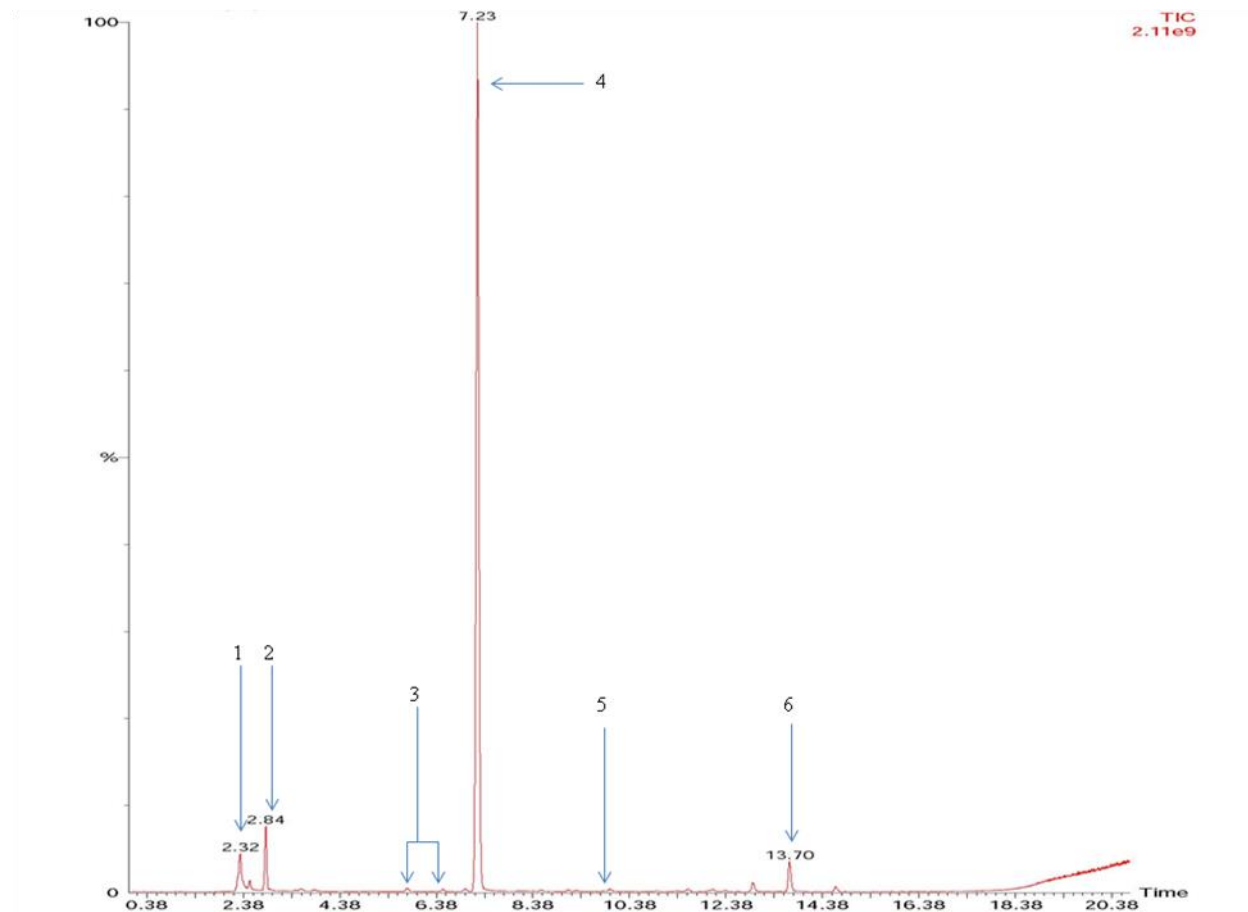


Figure 5.2: The total ion chromatogram (TIC) obtained from the headspace thermal desorption (TD)-GC-MS analysis of the Fenton reaction containing d<sub>3</sub>-acetaldehyde (CD<sub>3</sub>CHO) and TEMPO showing a major peak at 7.23 minutes and several minor peaks.

Figure 5.2 shows the chromatogram following TD-GC-MS analysis of the Fenton reaction containing d<sub>3</sub>-acetaldehyde and TEMPO with peaks corresponding to the following compounds: **1**) deuterated acetaldehyde (R<sub>t</sub> 2.31 minutes); **2**) deuterated paraldehyde-d<sub>9</sub> (R<sub>t</sub> 2.84 minutes); **3**) 1-(methoxy-d<sub>3</sub>)-2,2,6,6-tetramethyl-1,2,3,6-tetrahydropyridine (isomers at R<sub>t</sub> 5.17 & 6.52 minutes); **4**) TEMPO-CD<sub>3</sub> adduct (R<sub>t</sub> 7.23 minutes); **5**) 1-methoxy(d<sub>3</sub>)-2,2,6,6-tetramethyl-4-(methyl-d<sub>3</sub>)piperidine (R<sub>t</sub> 9.97 minutes); **6**) TEMPO-*tert*-butyl-d<sub>9</sub> adduct (R<sub>t</sub> 13.70 minutes). For a detailed analysis of EI-mass spectra see sections 5.3-5.8.



### 5.2.3 Fenton reaction with acetaldehyde and 4-methoxy-TEMPO

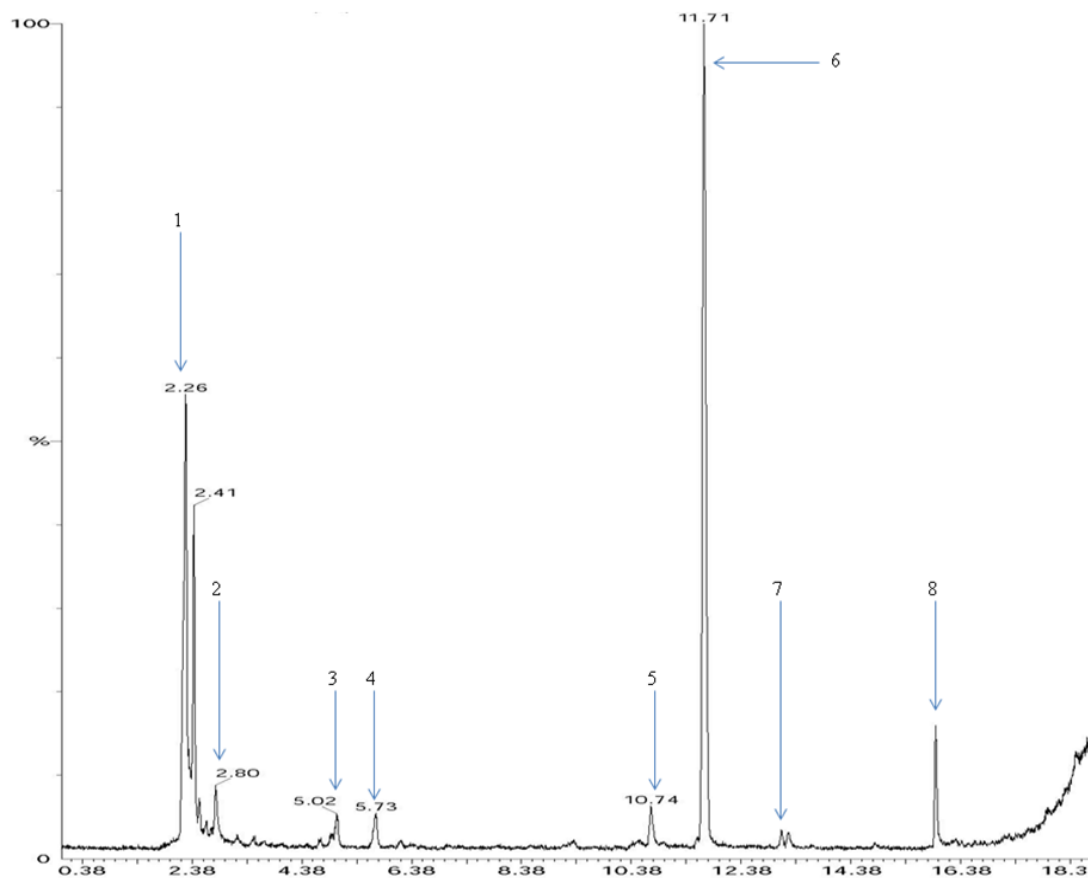


Figure 5.3: The total ion chromatogram (TIC) obtained from the headspace thermal desorption (TD)-GC-MS analysis of the Fenton reaction containing acetaldehyde and 4-methoxy-TEMPO showing major peaks at 11.71, 2.26 and 2.41 minutes.

Figure 5.3 shows the chromatogram following TD-GC-MS analysis of the Fenton reaction containing acetaldehyde and 4-methoxy-TEMPO with peaks corresponding to the following compounds: **1**) acetaldehyde ( $R_t$  2.31 minutes); **2**) paraldehyde ( $R_t$  2.86 minutes); **3**) 1,4-dimethoxy-2,6-dimethyl-1,4-dihydropyridine ( $R_t$  5.02 minutes); **4**) 1,4-dimethoxy-2,6-dimethyl-1,2-dihydropyridine ( $R_t$  5.73 minutes); **5**) an unidentified peak ( $R_t$  10.75 minutes) **6**)  $\text{CH}_3$  radical adduct of 4-methoxy-TEMPO (4- $\text{CH}_3\text{O}$ -TEMPO- $\text{CH}_3$ )  $R_t$  7.27 minutes); **7**) 1,4-dimethoxy-2,2-dimethyl-1,2-dihydropyridine ( $R_t$  13.11 minutes); **8**) 1,4-dimethoxy-2,2,6-trimethyl-1,2-dihydropyridine ( $R_t$  15.93 minutes). A comparison chromatogram (controls versus the Fenton reaction) is presented as figure A4 (appendix). For a detailed analysis of EI-mass spectra see sections 5.3-5.8.

## 5.2.4 Fenton reaction with acetaldehyde and 4-oxo-TEMPO

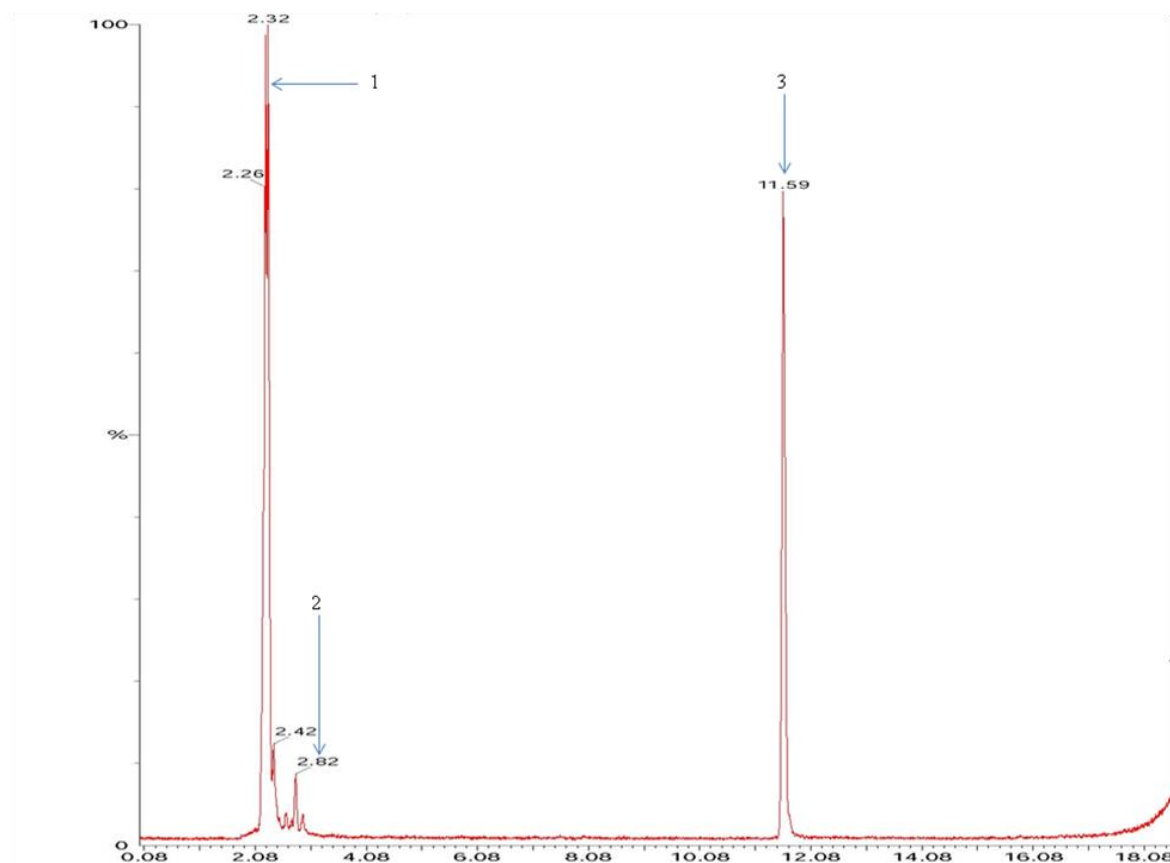


Figure 5.4: The total ion chromatogram (TIC) obtained from the headspace thermal desorption (TD)-GC-MS analysis of the Fenton reaction containing acetaldehyde and 4-oxo-TEMPO showing two major peaks at 2.32 (peak 1) and 11.59 minutes (peak 3) and one minor peak (2).

Figure 5.4 shows the chromatogram following TD-GC-MS analysis of the Fenton reaction containing acetaldehyde and 4-oxo-TEMPO with peaks corresponding to the following compounds: **1**) acetaldehyde ( $R_t$  2.32 minutes); **2**) paraldehyde ( $R_t$  2.82 minutes); **3**) 4-oxo-TEMPO-CH<sub>3</sub> adduct ( $R_t$  11.59 minutes). For a detailed analysis of EI-mass spectra see sections 5.3-5.8.

## 5.2.5 Comparison chromatograms (control reactions versus the Fenton reaction)

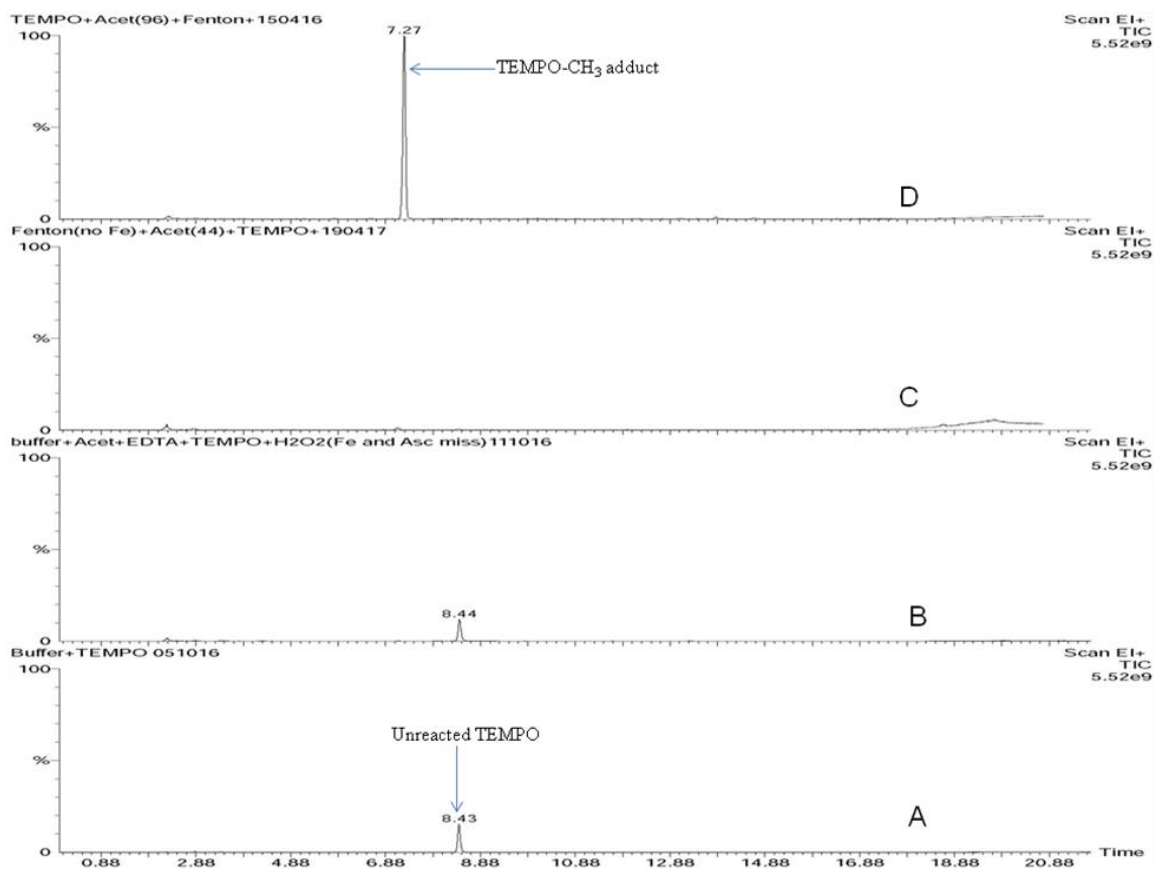


Figure 5.5: Comparison of chromatograms: Chromatograms generated for control experiments containing TEMPO (spin trap) and acetaldehyde (secondary source of radicals), whereby the headspace was extracted for a sample containing (A) phosphate buffer and spin trap, (B) All Fenton reagents (section 2.2.1) except iron and ascorbic acid, (C) All Fenton reagents (section 2.2.1) except iron, (D) The Fenton reaction (From bottom to top respectively).

There is a major peak in the chromatogram when the Fenton reaction was carried out containing acetaldehyde and TEMPO i.e. corresponding to TEMPO-CH<sub>3</sub> adduct (5.5; D). Peak at 8.43 minutes (5.5; A) corresponds to the unreacted TEMPO. For a detailed analysis of EI-mass spectra see sections 5.3-5.8.

## 5.3 Electron ionisation (EI) mass spectra of the methyl adduct of TEMPO and its derivatives

### 5.3.1 Methyl adduct of TEMPO (TEMPO-CH<sub>3</sub>)

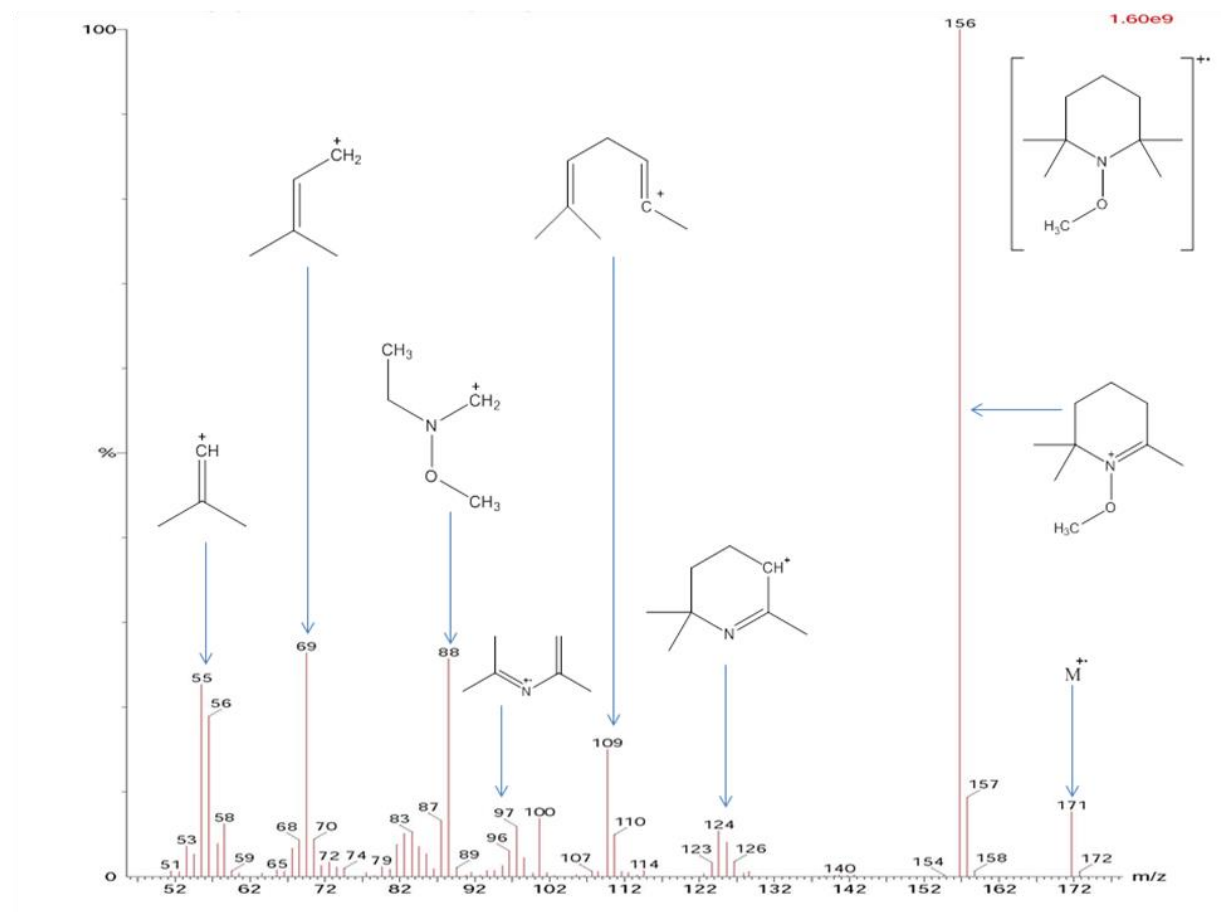
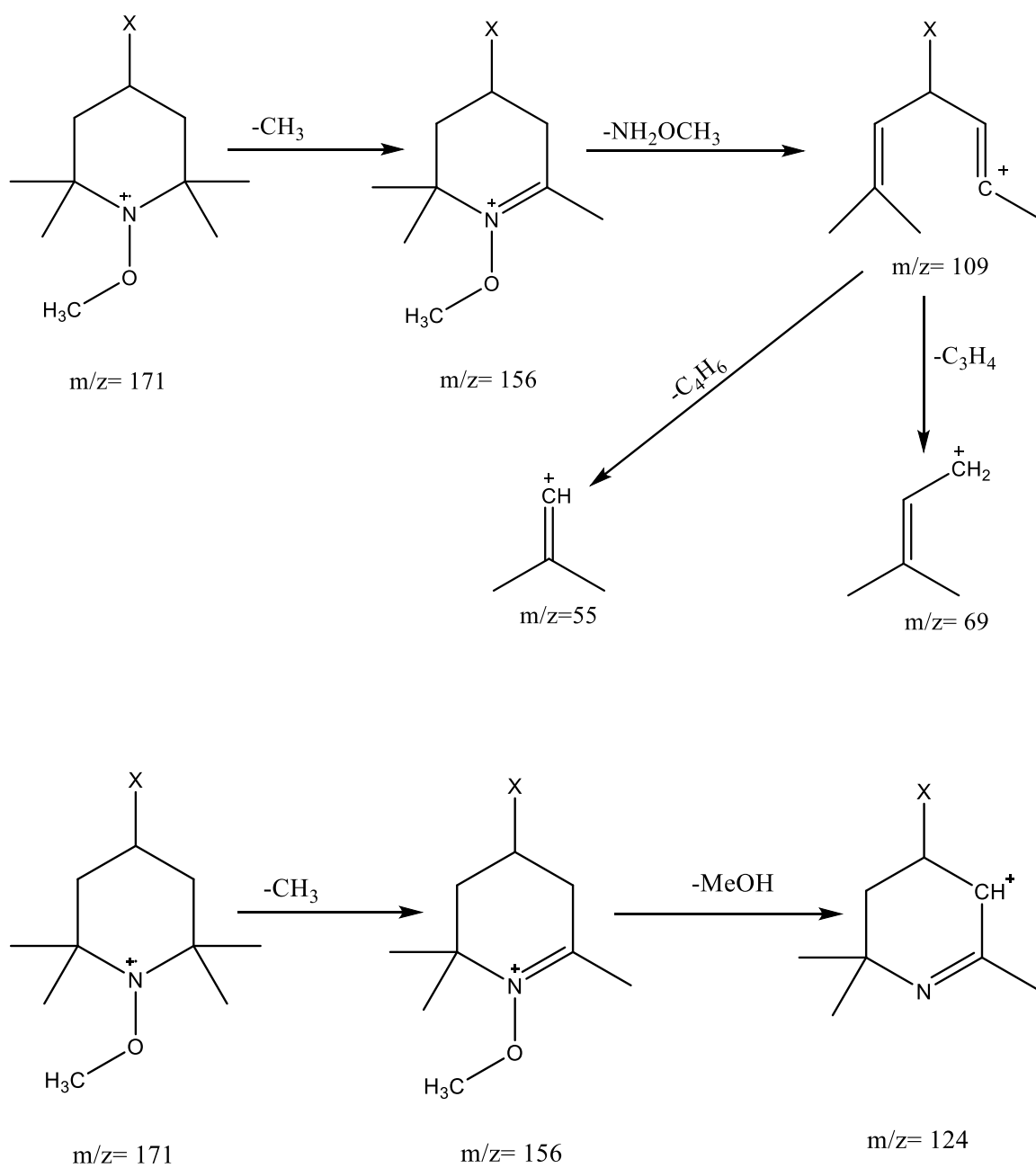


Figure 5.6: Electron ionisation (EI) mass spectrum of the peak at 7.27 minutes (figure 5.1) corresponding to TEMPO-CH<sub>3</sub>. The structure given in the top right corner is that of the molecular ion (M<sup>+</sup>) of TEMPO-CH<sub>3</sub>, corresponding to the peak at *m/z* 171.

The EI mass spectrum shown in figure 5.6 corresponds to the methyl adduct of TEMPO (TEMPO-CH<sub>3</sub>). The molecular ion can be seen at *m/z* 171 which may readily lose a methyl radical to give the base peak fragment at *m/z* 156. Further loss of methanol (CH<sub>3</sub>OH) gives a peak at *m/z* 124. Loss of NH<sub>2</sub>OCH<sub>3</sub> from the base peak fragment at *m/z* 156 generates a peak at *m/z* 109 (see schemes 5.1).



Scheme 5.1: Possible fragmentation pathways in the EI-MS source for TEMPO-CH<sub>3</sub> starting with the molecular ion.

### 5.3.2 TEMPO-CD<sub>3</sub> adduct

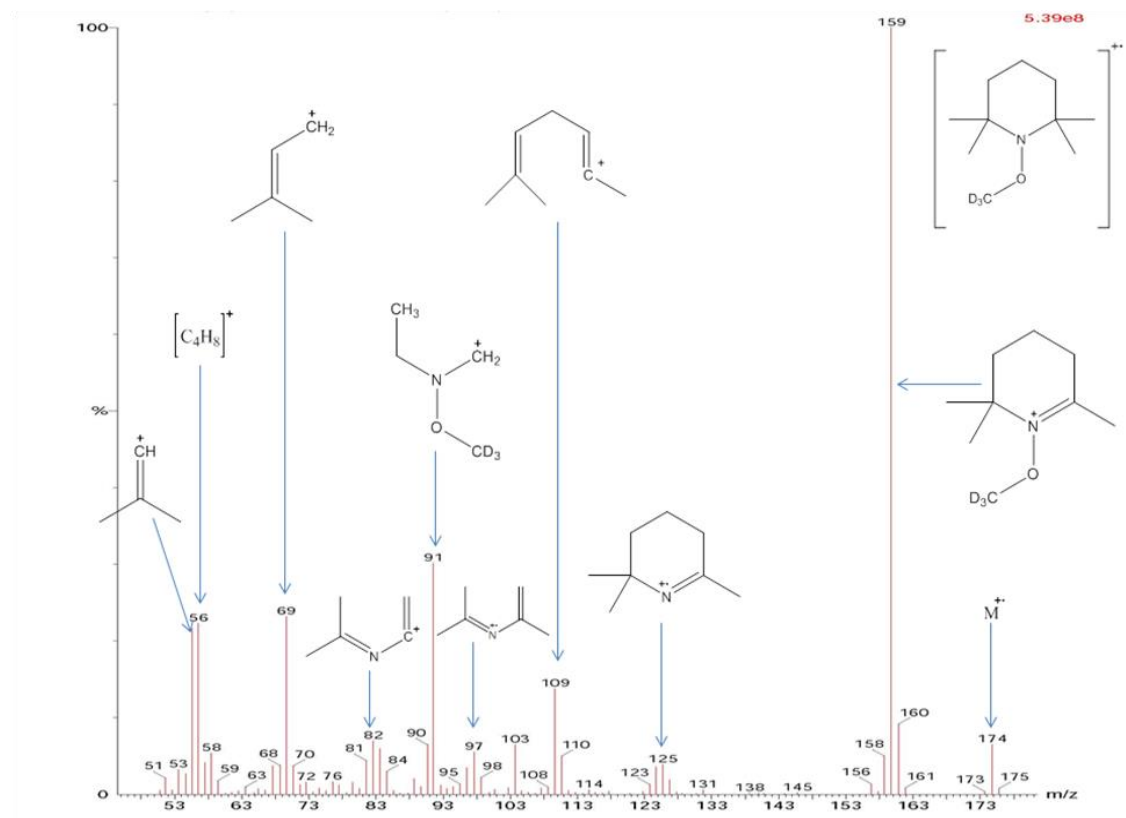


Figure 5.7: Electron ionisation (EI) mass spectrum of the peak at 7.23 minutes (figure 5.2) corresponding to the deuterium-methyl adduct of TEMPO (TEMPO-CD<sub>3</sub>). The structure given in the top right corner is that of the molecular ion (M<sup>+</sup>) of TEMPO-CD<sub>3</sub>, corresponding to the peak at *m/z* 174.

The EI mass spectrum shown in figure 5.7 corresponds to the CD<sub>3</sub> adduct of TEMPO (TEMPO-CD<sub>3</sub>), observed at 7.23 minutes when the reaction was carried out by using d<sub>3</sub>-acetaldehyde (the methyl hydrogen atoms replaced by deuterium) as a secondary source of radicals in the Fenton reaction system. The molecular ion can be seen at *m/z* 174 (a difference of 3 *m/z* units when compared to the molecular ion of TEMPO-CH<sub>3</sub>; figure 5.6) which confirms the trapping of a deuterium-methyl (<sup>•</sup>CD<sub>3</sub>) radical by TEMPO. The fragment at *m/z* 159, which is also the base peak, is formed by the loss of a methyl radical (from M<sup>+</sup>). Further loss of deuterium-methanol (CD<sub>3</sub>OH) gives a peak at *m/z* 124. The fragment at *m/z* 109 is formed by the loss of NH<sub>2</sub>OCD<sub>3</sub> from the base peak at *m/z* 159.

### 5.3.3 4-methoxy-TEMPO-CH<sub>3</sub> adduct

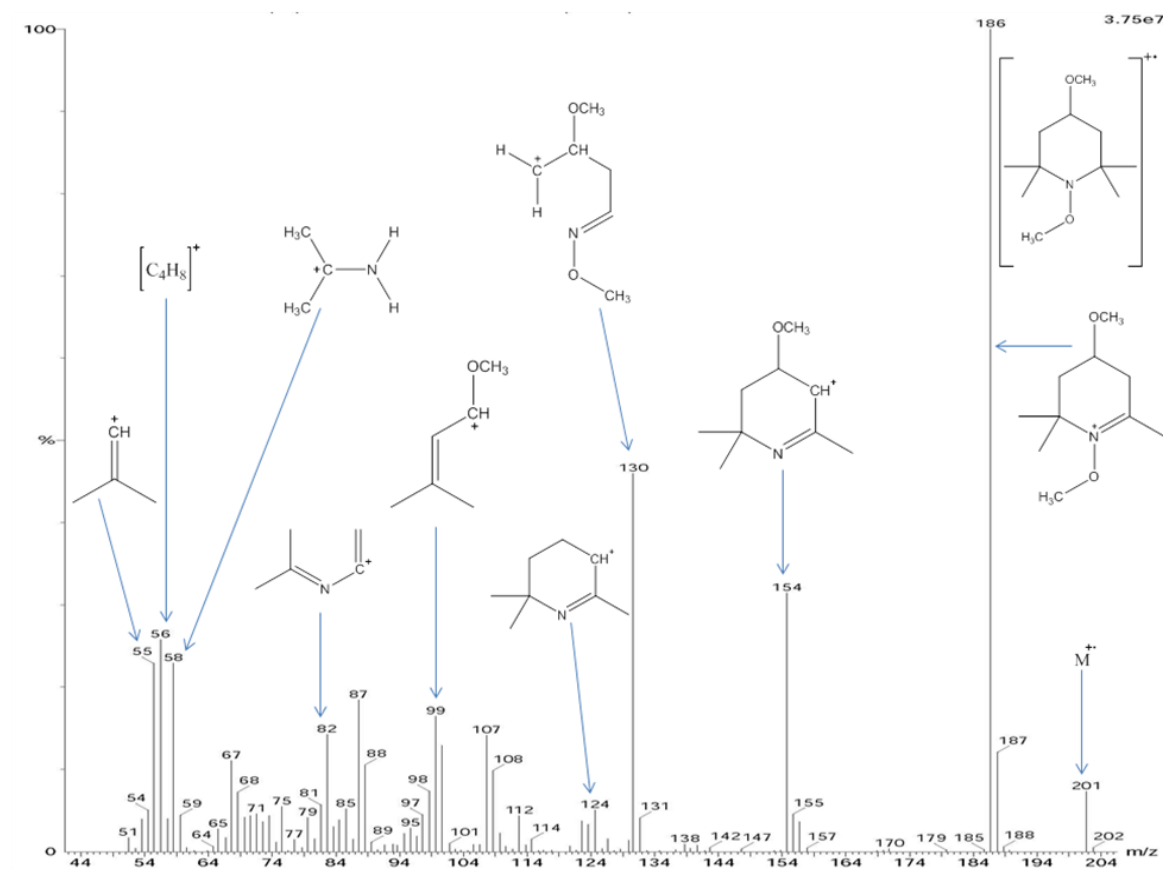


Figure 5.8: Electron ionisation (EI) mass spectrum of the peak at 11.71 minutes (figure 5.3) corresponding to 4-methoxy-TEMPO-CH<sub>3</sub>. The structure given in the top right corner is that of the molecular ion ( $M^{++}$ ) of 4-methoxy-TEMPO-CH<sub>3</sub>, corresponding to the peak at  $m/z$  201.

The EI mass spectrum shown in figure 5.8 corresponds to 4-methoxy-TEMPO-CH<sub>3</sub>. The molecular ion can be seen at  $m/z$  201. The  $m/z$  value for the molecular ion is 30 units higher than when TEMPO was used as the spin trapping agent, thus confirming the identity of the adduct and the trapping of a methyl radical. The fragment at  $m/z$  186 is formed by the loss of a methyl radical (from  $M^+$ ) which is also base peak. Further loss of methanol (CH<sub>3</sub>OH) gives a peak at  $m/z$  154. The fragment at  $m/z$  124 is formed by the loss of a methoxy group from the fragment at  $m/z$  154.

### 5.3.4 4-oxo-TEMPO-CH<sub>3</sub> adduct

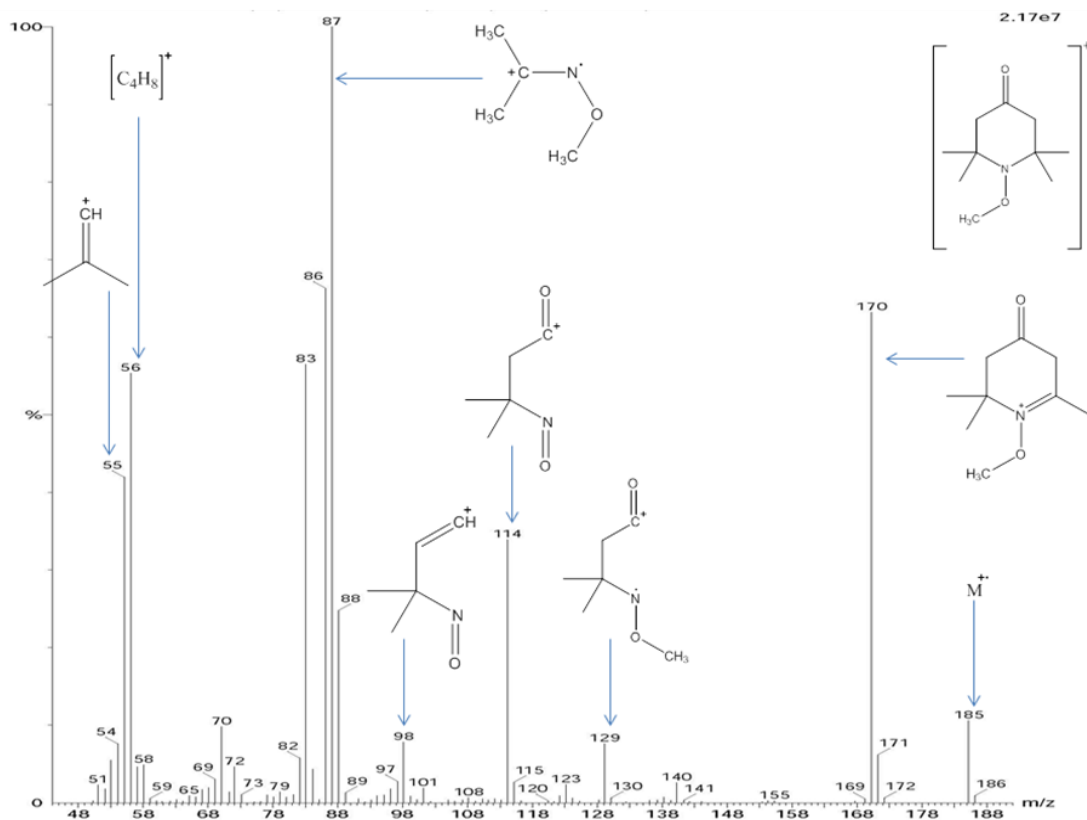


Figure 5.9: Electron ionisation (EI) mass spectrum of the peak at 11.59 minutes (figure 5.4) corresponding to 4-oxo-TEMPO-CH<sub>3</sub>. The structure given in the top right corner is that of the molecular ion (M<sup>+•</sup>) of 4-oxo-TEMPO-CH<sub>3</sub>, corresponding the peak *m/z* 185.

The EI mass spectrum shown in figure 5.9 corresponds to 4-oxo-TEMPO-CH<sub>3</sub>. The molecular ion can be seen at *m/z* 185. The *m/z* value for the molecular ion is 14 units higher than when TEMPO is used, thus confirming the identity of adduct and trapping of a methyl radical. The fragment at *m/z* 170 is formed by the loss of methyl (from M<sup>+•</sup>). Further fragmentation between the carbon next to hydrogen and the carbon attached to oxygen gives a fragment at *m/z* 129, The key GC-MS data for the methyl adduct of TEMPO and its derivatives is given in table 5.1.



Table 5.1: Summary of GC-MS data for the methyl adduct of TEMPO and its derivatives

| Spin adduct                     | Retention time (R <sub>t</sub> ) | Molecular ion ( <i>m/z</i> ) | Base peak ( <i>m/z</i> ) | Characteristic fragment peaks ( <i>m/z</i> ) |
|---------------------------------|----------------------------------|------------------------------|--------------------------|--|
| TEMPO-CH <sub>3</sub>           | 10.26                            | 171                          | 156                      | 124, 109, 97, 88, 69, 55                     |
| TEMPO-CD <sub>3</sub>           | 10.16                            | 174                          | 159                      | 124, 109, 97, 91, 69, 55                     |
| 4-methoxy-TEMPO-CH <sub>3</sub> | 10.19                            | 201                          | 186                      | 154, 130, 124, 99, 82, 55                    |
| 4-oxo-TEMPO-CH <sub>3</sub>     | 10.09                            | 185                          | 87                       | 129, 114, 98, 87, 69, 55                     |

## 5.4 Paraldehyde

The peak retained at 2.86 minutes is also present in non-Fenton control reactions (figure 5.1). A NIST library search identifies the peak as paraldehyde, which is not only a precursor of acetaldehyde but can also be formed by self-aldol condensation of acetaldehyde molecules in the presence of protons. The identity of the peak was confirmed when the Fenton reaction was carried out by using  $d_3$ -acetaldehyde. Three deuterated acetaldehyde- $d_3$  molecules combine stepwise to form deuterated paraldehyde, giving an increase of 9  $m/z$  units for molecular ion at  $m/z$  141 when compared to non-deuterated paraldehyde. The identification of the compound and formation pathway of paraldehyde is already explained in chapter 3 (section 3.12). Paraldehyde is also detected when PBN and its derivatives are used as spin trapping agents and acetaldehyde used as a secondary source of radicals in the Fenton reaction system (chapter 3).

## 5.5 Electron ionisation (EI) mass spectra of the methyl adduct of 2,2,6,6-tetramethyl-3,6-dihydropyridine

### 5.5.1 EI mass spectrum of 1-methoxy-2,2,6,6-tetramethyl-1,2,3,6-tetrahydropyridine

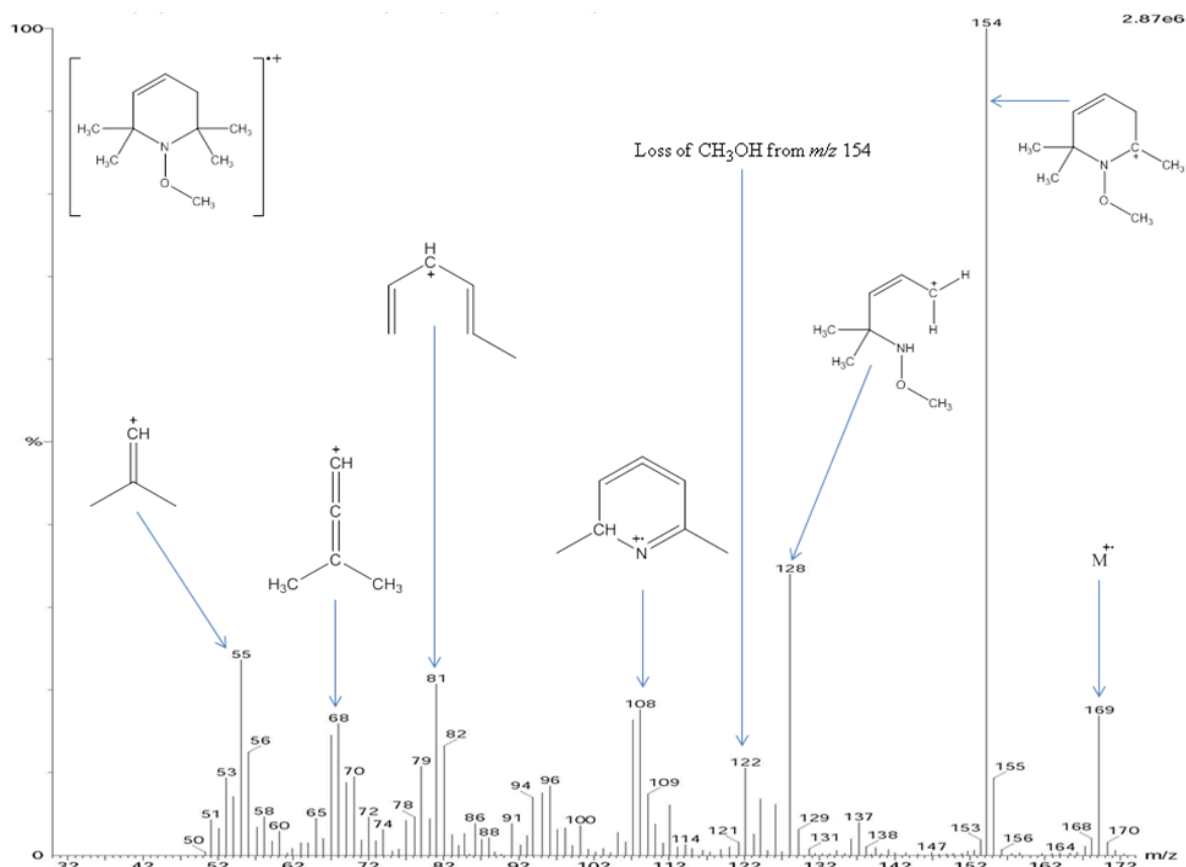
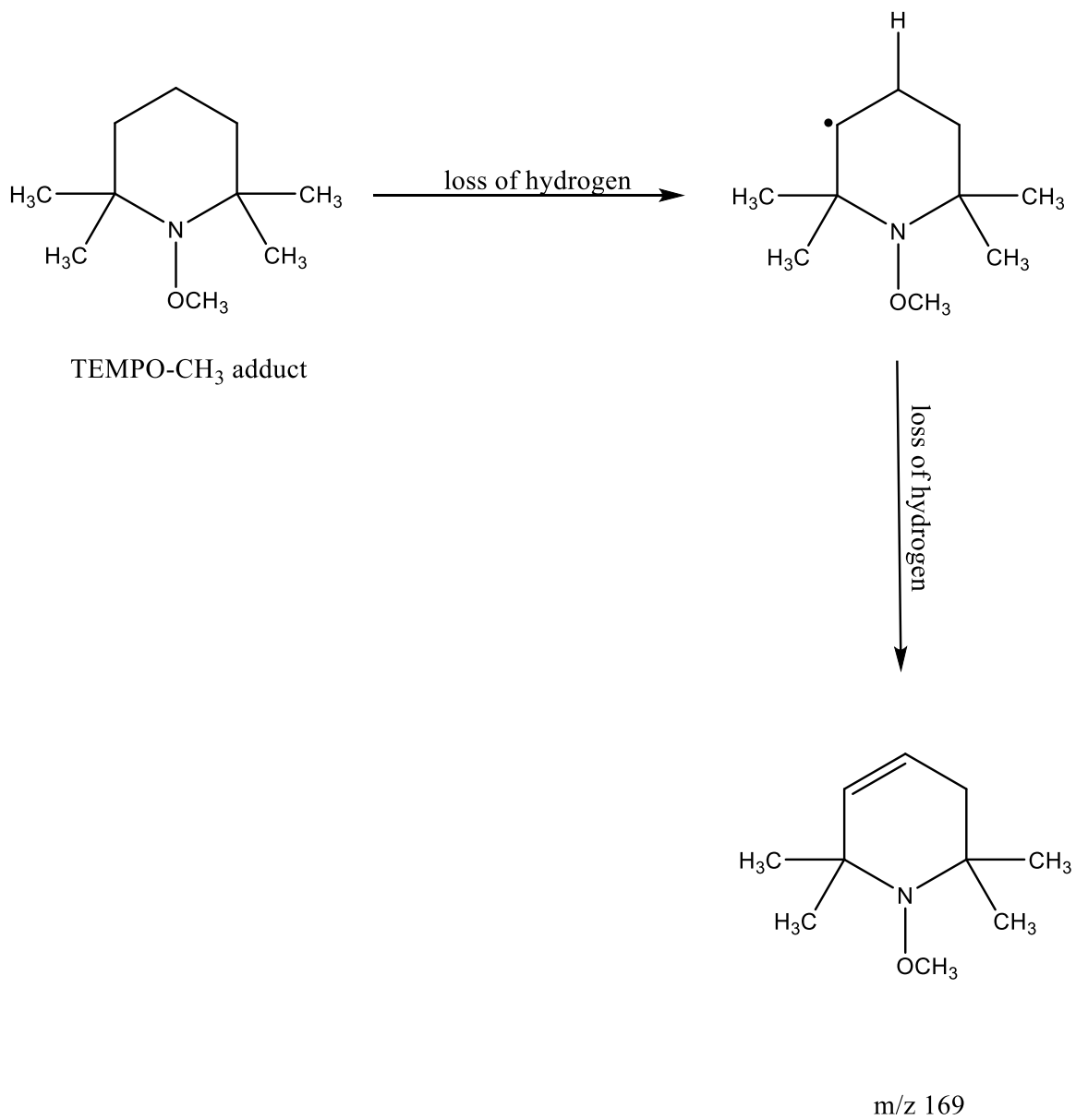


Figure 5.10: Electron ionisation (EI) mass spectrum of the peak at 6.55 minutes (figure 5.1) corresponding to 1-methoxy-2,2,6,6-tetramethyl-1,2,3,6-tetrahydropyridine. The structure given in the top right corner is that of the molecular ion ( $M^+$ ), corresponding to the peak at  $m/z$  169.

The EI mass spectrum shown in figure 5.10 corresponds to the methyl adduct of 2,2,6,6-tetramethyl-3,6-dihydropyridine. The pathway of 1-methoxy-2,2,6,6-tetramethyl-1,2,3,6-tetrahydropyridine formation is suggested in scheme 5.2. The molecular ion can be seen at  $m/z$  169 which readily loses a methyl radical to give the base peak at  $m/z$  154. Further loss of ethyne ( $C_2H_2$ ) gives a peak at  $m/z$  128, whilst the loss of methanol ( $CH_3OH$ ) generates a fragment at  $m/z$  122. A peak at  $m/z$  107 is formed by the loss of  $NH_2OCH_3$  from  $m/z$  154.



Scheme 5.2: A possible mechanism of 1-methoxy-2,2,6,6-tetramethyl-1,2,3,6-tetrahydropyridine formation

### 5.5.2 EI mass spectrum of 1-(methoxy-d<sub>3</sub>)-2,2,6,6-tetramethyl-1,2,3,6-tetrahydropyridine

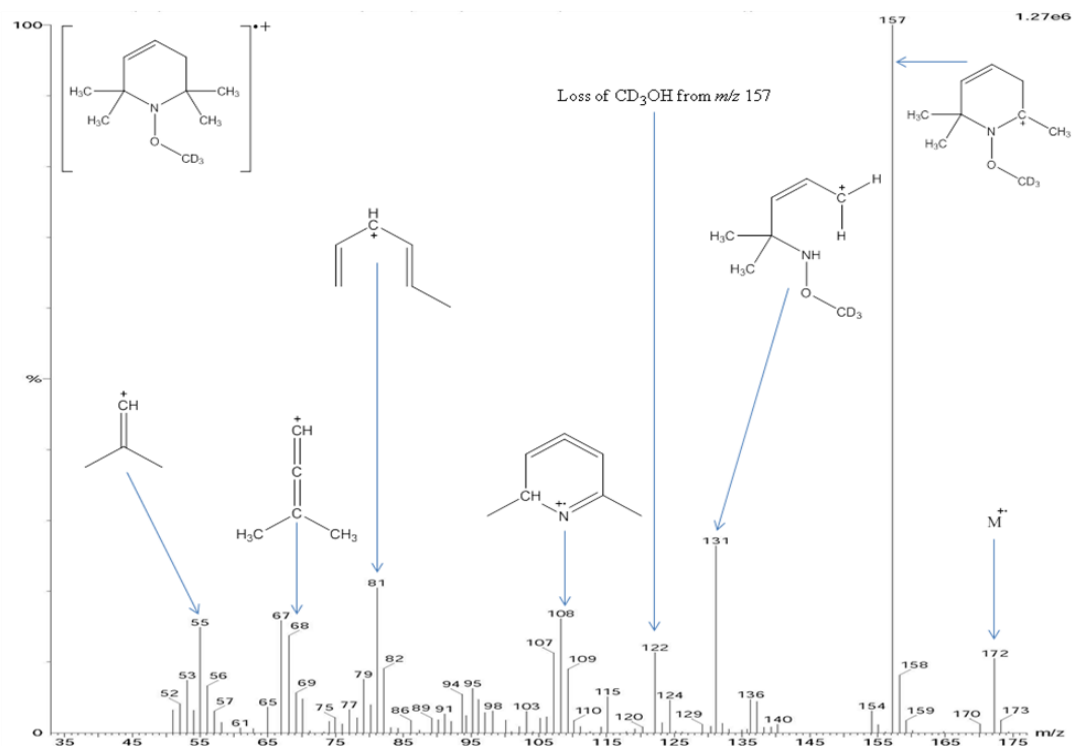


Figure 5.11: Electron ionisation (EI) mass spectrum of the peak at 6.52 minutes (figure 5.2) corresponding to 1-(methoxy-d<sub>3</sub>)-2,2,6,6-tetramethyl-1,2,3,6-tetrahydropyridine. The structure given in the top right corner is that of the molecular ion, corresponding to the peak at  $m/z$  172.

The EI mass spectrum shown in figure 5.11 corresponds to the CD<sub>3</sub> adduct of 2,2,6,6-tetramethyl-3,6-dihydropyridine observed at 6.52 minutes when the reaction was carried out by using d<sub>3</sub>-acetaldehyde (the methyl hydrogen atoms replaced by deuterium) as a secondary source of radicals in the Fenton reaction system. The molecular ion can be seen at  $m/z$  172 (a difference of 3  $m/z$  units when compared to the molecular ion of 1-methoxy-2,2,6,6-tetramethyl-1,2,3,6-tetrahydropyridine; figure 5.10), which confirms the trapping of one deuterium-methyl (<sup>•</sup>CD<sub>3</sub>) radical by 2,2,6,6-tetramethyl-3,6-dihydropyridine. The fragment at  $m/z$  157 (the base peak) is formed by the loss of a methyl radical from the molecular ion. Further loss of ethyne (C<sub>2</sub>H<sub>2</sub>) gives a peak at  $m/z$  131, whilst the loss of deuterium-methanol (CD<sub>3</sub>OH) generates a peak at  $m/z$  122. Further loss of methyl group with an addition of hydrogen gives a peak at  $m/z$  108, whilst the loss of NH<sub>2</sub>OCD<sub>3</sub> from  $m/z$  154 generates a peak at  $m/z$  107.

## 5.6 Electron ionisation mass spectra (EI-MS) of the *tert*-butyl adduct of TEMPO and its derivatives

### 5.6.1 TEMPO-*tert*-butyl adduct

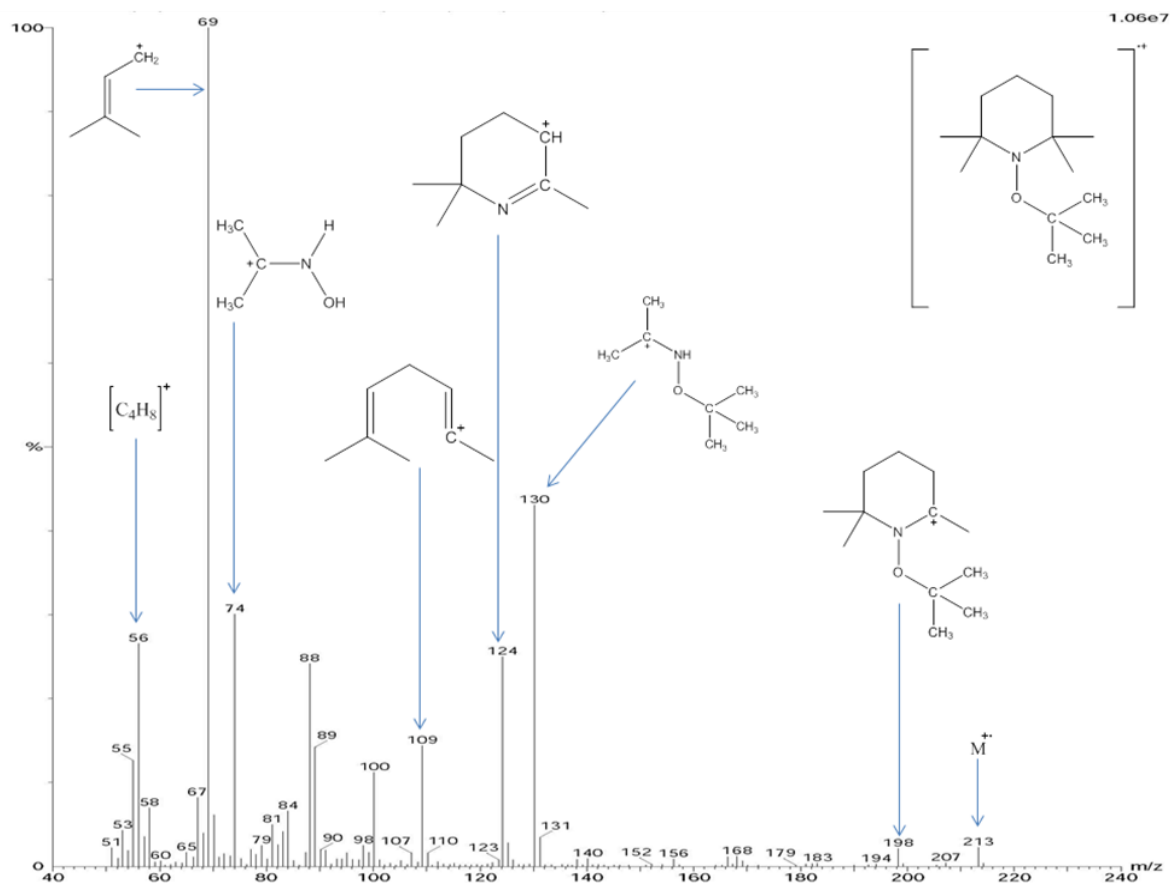


Figure 5.12: Electron ionisation (EI) mass spectrum of the peak at 13.85 minutes (figure 5.1) corresponding to TEMPO- $\text{C}(\text{CH}_3)_3$ . The structure given in the top right corner is that of the molecular ion ( $\text{M}^+$ ), corresponding to the peak at  $m/z$  213.

The EI mass spectrum shown in figure 5.12 corresponds to the *tert*-butyl adduct of TEMPO (TEMPO-*tert*-butyl). The loss of  $\text{C}(\text{CH}_3)_3\text{OH}$  from  $m/z$  198 gives a fragment at  $m/z$  124, whilst a loss of  $\text{NH}_2\text{OC}(\text{CH}_3)_3$  generates a peak at  $m/z$  109.

## 5.6.2 TEMPO-*tert*-butyl(d<sub>9</sub>) adduct

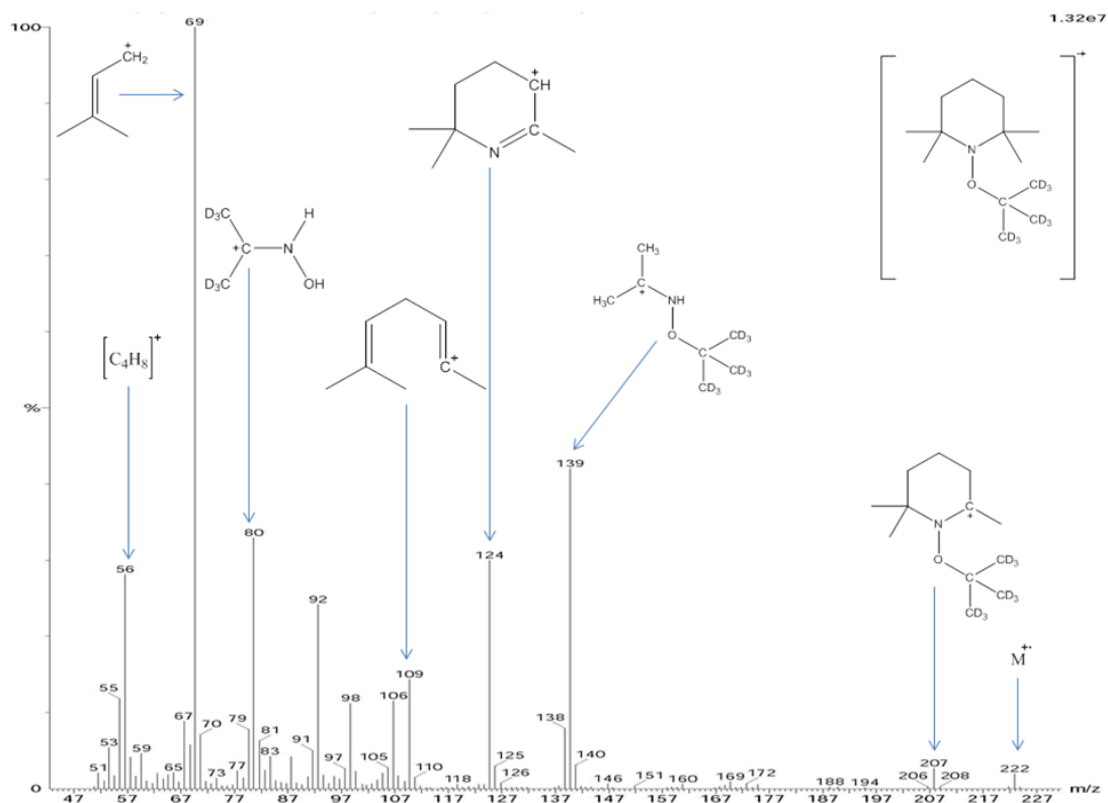


Figure 5.13: Electron ionisation (EI) mass spectrum of the peak at 13.70 minutes (figure 5.2) corresponding to TEMPO-C(CD<sub>3</sub>)<sub>3</sub>. The structure given in the top right corner is that of the molecular ion, corresponding to the peak at  $m/z$  222.

The EI mass spectrum shown in figure 5.13 corresponds to the d<sub>9</sub>-*tert*-butyl adduct of TEMPO observed at 13.70 minutes when the reaction was carried out by using d<sub>3</sub>-acetaldehyde as a secondary source of radicals in the Fenton reaction system. The molecular ion can be seen at  $m/z$  222 (a difference of 9  $m/z$  units when compared to the molecular ion of TEMPO-C(CH<sub>3</sub>)<sub>3</sub>; figure 5.12) which confirms the inclusion of three deuterium-methyl (CD<sub>3</sub>) groups in the compound. The fragment at  $m/z$  207 is formed by the loss of a methyl radical (from M<sup>+</sup>) which further loses C(CD<sub>3</sub>)<sub>3</sub>OH to give a fragment at  $m/z$  124. The loss of NH<sub>2</sub>OC(CD<sub>3</sub>)<sub>3</sub> from a fragment at  $m/z$  207 generates a peak at  $m/z$  109.

## 5.7 Electron ionisation (EI) mass spectra of the methyl adduct of 2,2,4,6,6-pentamethylpiperidine

### 5.7.1 EI-MS of 1-methoxy-2,2,4,6,6-pentamethylpiperidine

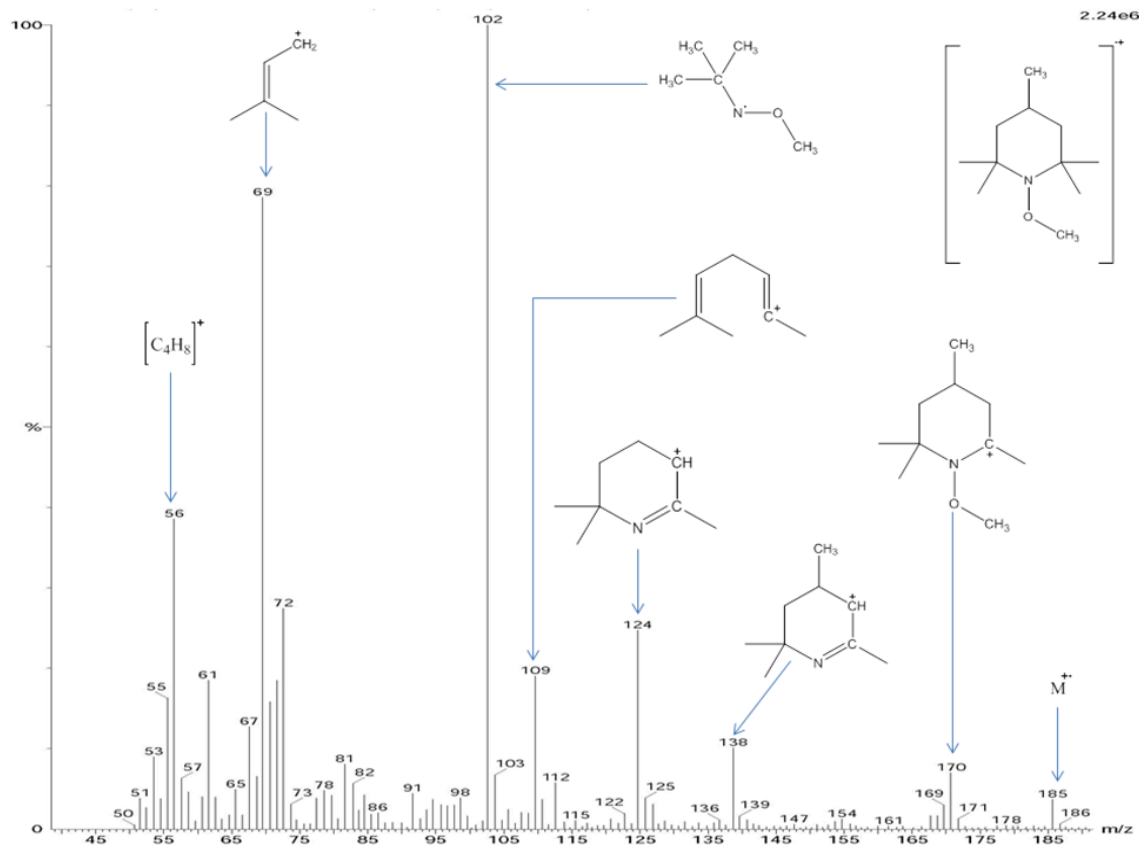


Figure 5.14: Electron ionisation (EI) mass spectrum of the peak at 10.07 minutes (figure 5.1) corresponding to a methyl adduct of 2,2,4,6,6-pentamethylpiperidine. The structure given in the top right corner is that of the molecular ion, corresponding to the peak at  $m/z$  185.

The EI mass spectrum shown in figure 5.14 corresponds to the 1-methoxy-2,2,4,6,6-pentamethylpiperidine. The fragment at  $m/z$  170 is formed by the loss of a methyl radical (from  $M^+$ ), which may then further lose  $CH_3OH$  to generate a fragment at  $m/z$  138. Further loss of methyl group with an addition of hydrogen gives a peak at  $m/z$  124.



### 5.7.2 EI mass spectrum of 1-(methoxy-d<sub>3</sub>)-2,2,6,6-tetramethyl-4-(methyl-d<sub>3</sub>) piperidine

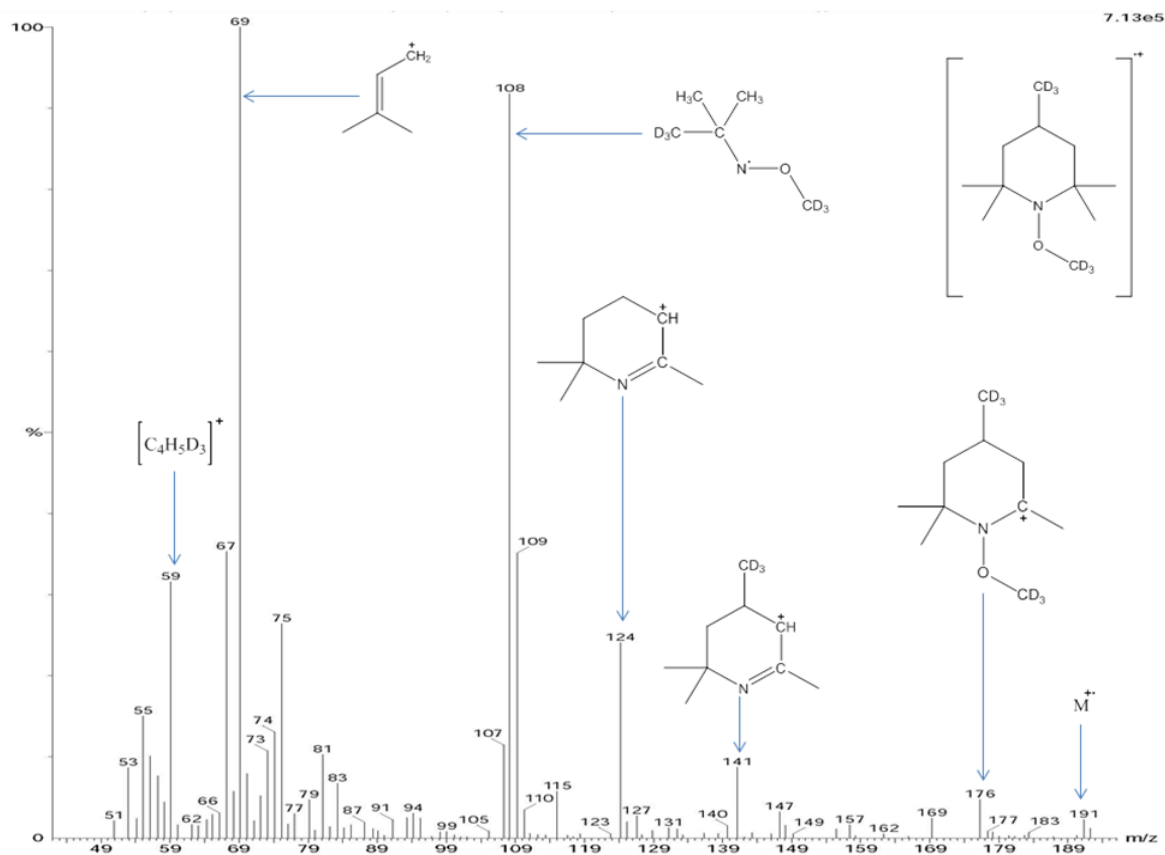


Figure 5.15: Electron ionisation (EI) mass spectrum of the peak at 9.97 minutes (figure 5.2) corresponding to the deuterio-methyl ( $\text{CD}_3$ ) adduct of 2,2,4-d<sub>3</sub>,6,6-pentamethylpiperidine. The structure given in the top right corner is that of the molecular ion, i.e. corresponding to the peak at  $m/z$  191.

The EI mass spectrum shown in Figure 5.15 corresponds to the 1-(methoxy-d<sub>3</sub>)-2,2,6,6-tetramethyl-4-(methyl-d<sub>3</sub>) piperidine observed at 9.97 minutes when the reaction was carried out by using d<sub>3</sub>-acetaldehyde as a secondary source of radicals in the Fenton system. The molecular ion can be seen at  $m/z$  191 (a difference of 6  $m/z$  units when compared to the non-deuterated adduct in figure 5.14, which confirms the trapping of two deuterio-methyl ( $\cdot\text{CD}_3$ ) radicals. The fragment at  $m/z$  176 is formed by the loss of a methyl radical (from  $\text{M}^+$ ) which further loses  $\text{CD}_3\text{OH}$  to generate a fragment at  $m/z$  141. Further loss of  $\text{CD}_3$  group from the ion at  $m/z$  141 with an addition of hydrogen gives a fragment at  $m/z$  124.

## 5.8 Identification of other peaks when for 4-methoxy-TEMPO is used as the trapping agent

### 5.8.1 EI mass spectrum of 1,4-dimethoxy-2,6-dimethyl-1,4-dihydropyridine

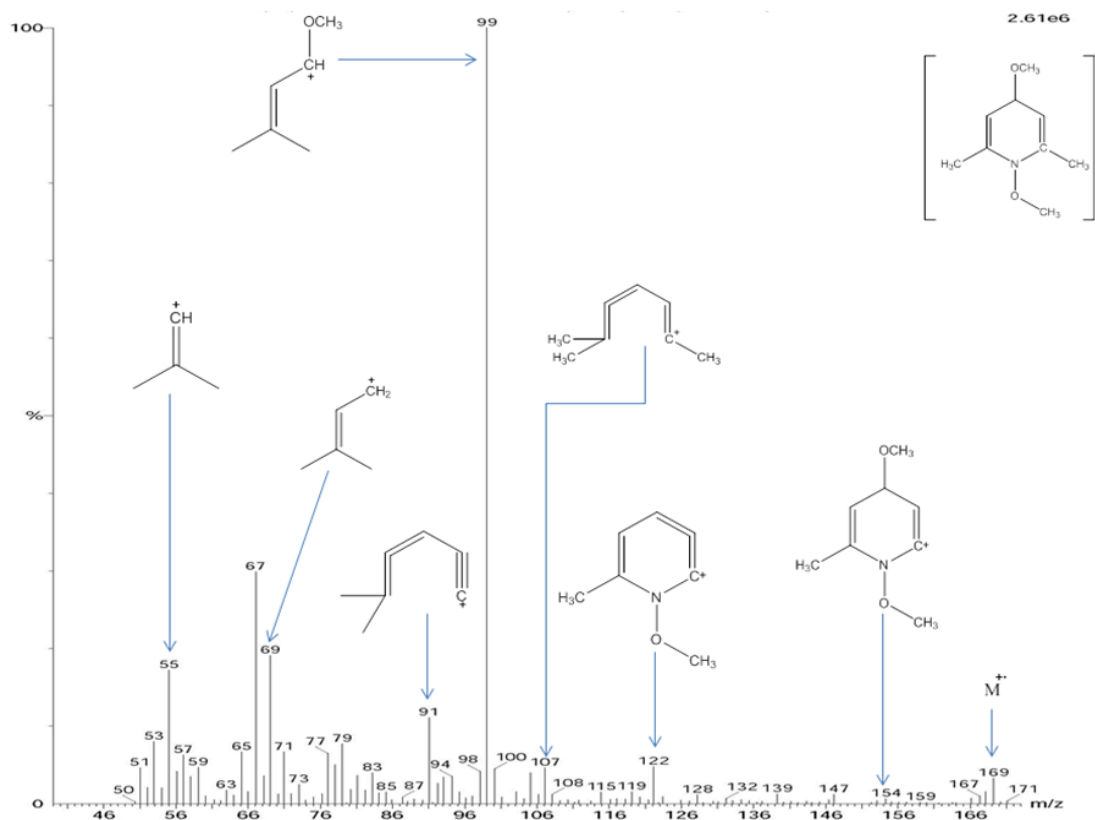


Figure 5.16: Electron ionisation (EI) mass spectrum of the peak at 5.02 minutes (figure 5.3) corresponding to 1,4-dimethoxy-2,6-dimethyl-1,4-dihydropyridine. The structure given in top right corner is that of the molecular ion ( $\text{M}^+$ ), corresponding to the peak at  $m/z$  169.

The EI mass spectrum shown in figure 5.16 corresponds to 1,4-dimethoxy-2,6-dimethyl-1,4-dihydropyridine. The fragment at  $m/z$  154 is formed by the loss of a methyl radical (from  $\text{M}^+$ ), which then further loses  $\text{CH}_3\text{OH}$  to generate a fragment at  $m/z$  122. Loss of a methyl group from the ion at  $m/z$  122 gives the fragment at  $m/z$  107.

### 5.8.2 EI mass spectrum of 1,4-dimethoxy-2,6-dimethyl-1,2-dihydropyridine

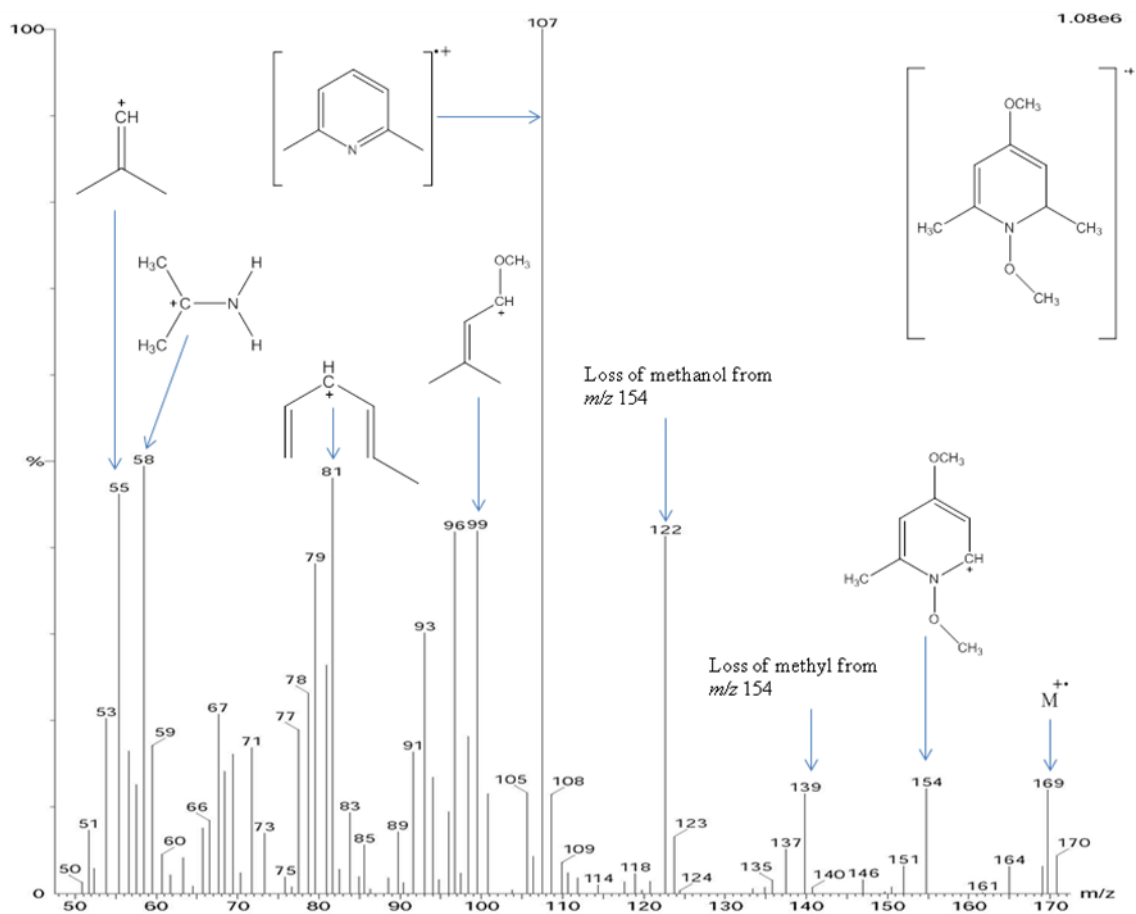


Figure 5.17: Electron ionisation (EI) mass spectrum of the peak at 5.74 minutes (figure 5.3) corresponding to 1,4-dimethoxy-2,6-dimethyl-1,2-dihydropyridine. The structure given in the top right corner is that of the molecular ion ( $M^+$ ), corresponding to the peak at  $m/z$  169.

The EI mass spectrum shown in figure 5.17 corresponds to 1,4-dimethoxy-2,6-dimethyl-1,2-dihydropyridine. The fragment at  $m/z$  154 is formed by the loss of a methyl group (from  $M^+$ ), which further loses  $CH_3OH$  to generate a fragment at  $m/z$  122. Further loss of a methyl group gives a fragment at  $m/z$  107. Structures of major ions are suggested which can be formed by the fragmentation of 1,4-dimethoxy-2,6-dimethyl-1,2-dihydropyridine.

### 5.8.3 EI mass spectrum of 1,4-dimethoxy-2,2-dimethyl-1,2-dihydropyridine (isomers)

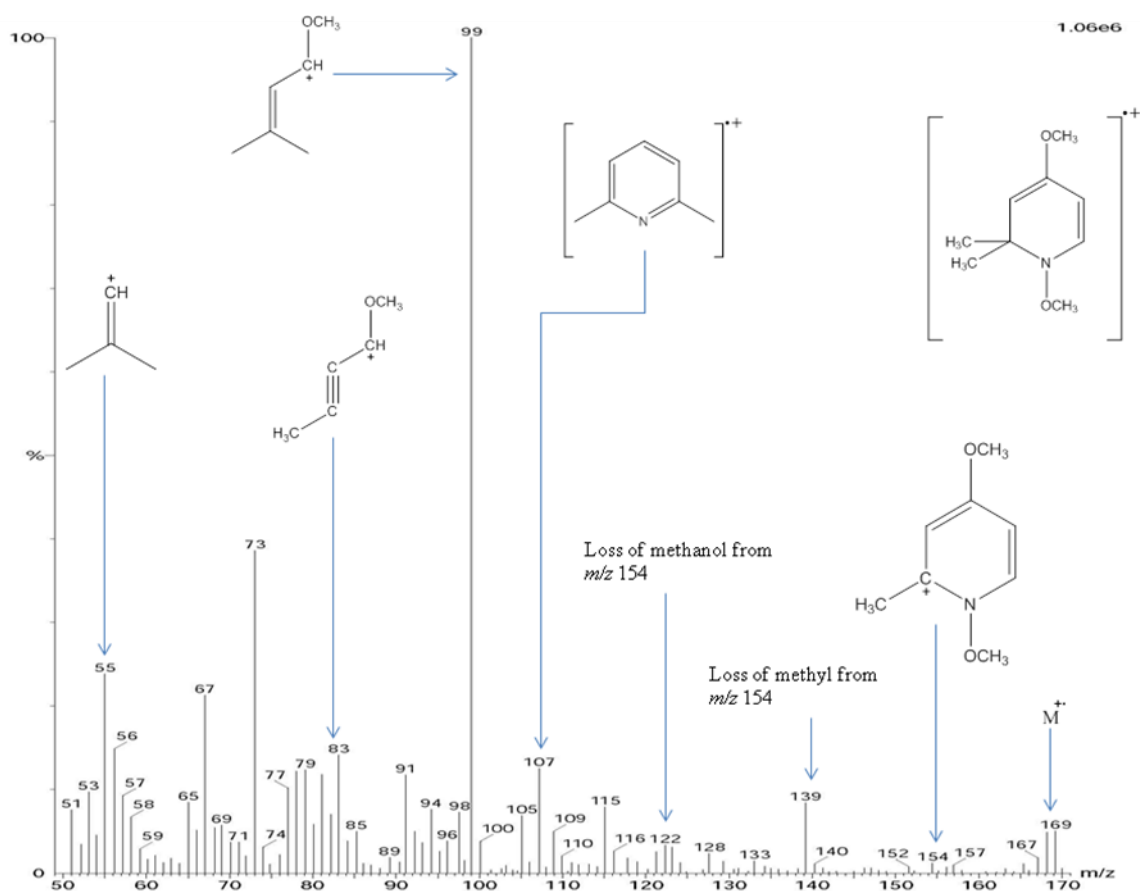


Figure 5.18: Electron ionisation (EI) mass spectrum of the peak at 13.11 minutes (figure 5.3) corresponding to 1,4-dimethoxy-2,2-dimethyl-1,2-dihydropyridine. The structure given in the top right corner is that of the molecular ion ( $M^+$ ), corresponding to the peak at  $m/z$  169.

The EI mass spectrum shown in figure 5.18 is believed to correspond to 1,4-dimethoxy-2,2-dimethyl-1,2-dihydropyridine. The fragment at  $m/z$  154 is formed by the loss of a methyl radical (from  $M^+$ ), which further loses  $CH_3OH$  to generate a fragment at  $m/z$  122. Further loss of a methyl group from the ion at  $m/z$  122 gives a fragment at  $m/z$  107. Suggested structures of major ions which can be formed by the fragmentation of 1,4-dimethoxy-2,6-dimethyl-1,2-dihydropyridine are given in above figure.

### 5.8.4 EI mass spectrum of 1,4-dimethoxy-2,2,6-trimethyl-1,2-dihydropyridine

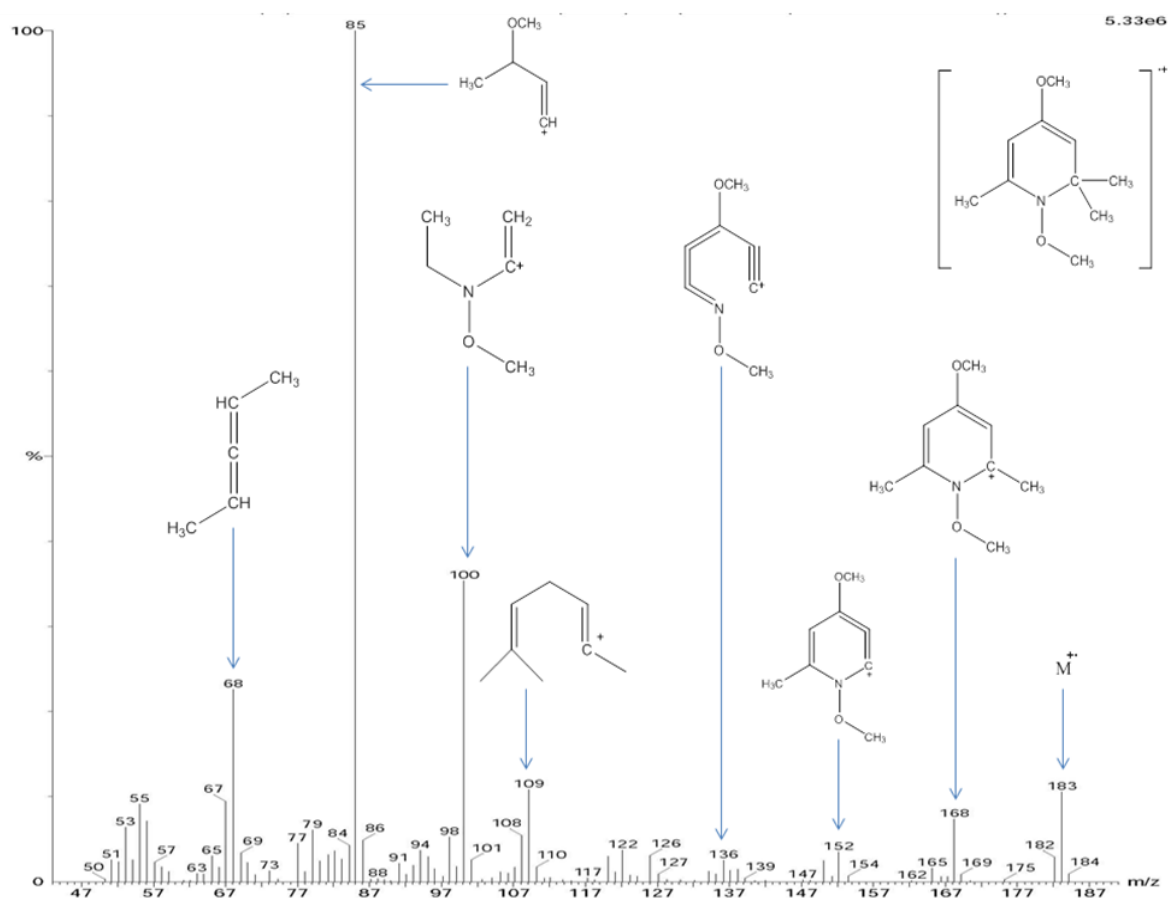


Figure 5.19: Electron ionisation (EI) mass spectrum of the peak at 15.93 minutes (figure 5.3) corresponding to 1,4-dimethoxy-2,2,6-trimethyl-1,2-dihydropyridine. The structure given in the top right corner is that of the molecular ion, corresponding to the peak at  $m/z$  183.

The EI mass spectrum shown in Figure 5.19 corresponds to 1,4-dimethoxy-2,2,6-trimethyl-1,2-dihydropyridine. The peak at  $m/z$  183 corresponds to the molecular ion. The fragment at  $m/z$  168 is formed by the loss of a methyl radical (from  $M^+$ ), which further loses methane to generate a fragment at  $m/z$  152. A similar pathway (loss of methane) is followed in the formation of the fragment at  $m/z$  136. Structures of major fragments are suggested in figure 5.19.

## Chapter 5

### (Part 2)

Detection and analysis of spin-adducts from ethanal and  
TEMPO by using Solid phase microextraction-Gas  
Chromatography-Mass Spectrometry (SPME-GC/MS)

## 5.9 Chromatograms

### 5.9.1 Fenton reaction with acetaldehyde and TEMPO

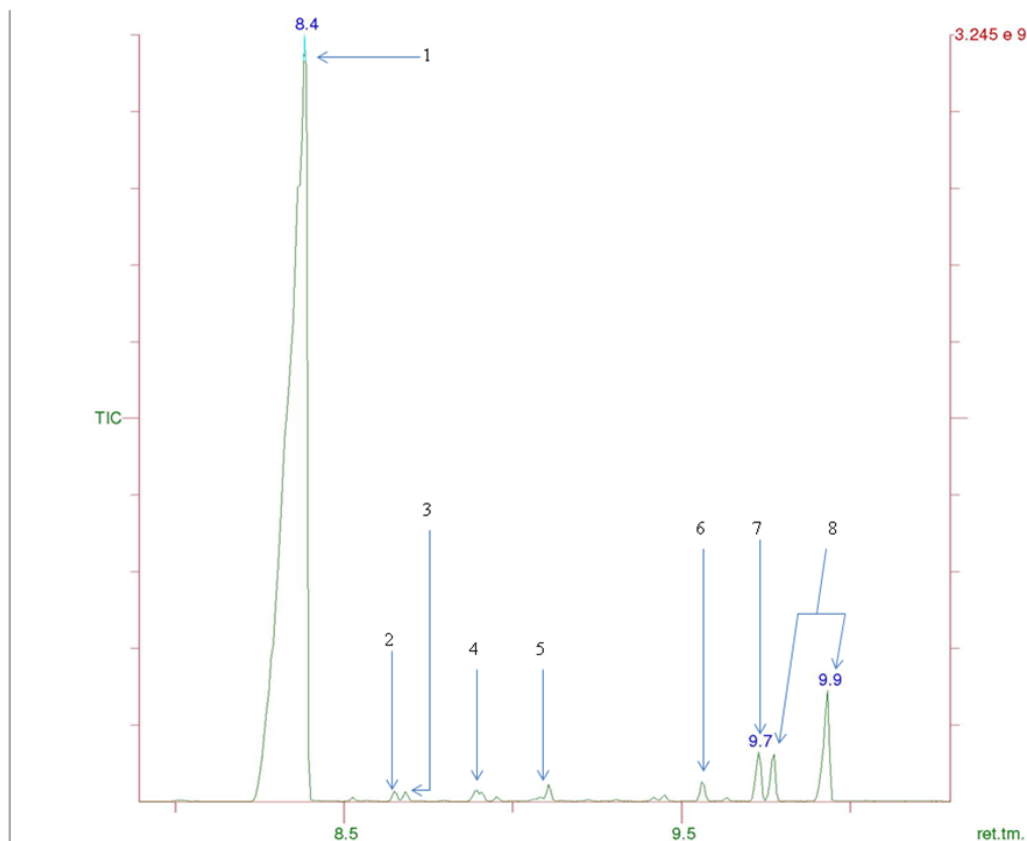


Figure 5.20: The total ion chromatogram (TIC) obtained from the headspace solid phase microextraction (SPME)-GC-MS analysis of the Fenton reaction containing acetaldehyde and TEMPO.

Figure 5.20 shows the chromatogram following SPME-GC-MS analysis of the Fenton reaction containing acetaldehyde and TEMPO with peaks corresponding to the following compounds: **1**) CH<sub>3</sub> adduct of TEMPO (R<sub>t</sub> 8.4 minutes); **2**) 1-methoxy-2,2,6-trimethyl-2,3,4,5-*ter*trahydropyridin-1-ium (R<sub>t</sub> 8.6 minutes); **3**) unreacted TEMPO (R<sub>t</sub> 8.7 minutes); **4**) 2,6-Dimethyl-1,5-heptadiene (R<sub>t</sub> 8.9 minutes); **5**) 1-methoxy-2,2,4,6,6-pentamethylpiperidine (R<sub>t</sub> 9.1 minutes); **6**) 1-(1-methoxy-2,2,6-trimethylpiperidin-4-yl) ethan-1-one (R<sub>t</sub> 9.5 minutes); **7**) acetyl adduct of TEMPO (R<sub>t</sub> 9.7 minutes); **8**) TEMPO-*tert*-butyl adduct (R<sub>t</sub> 9.9 minutes).

## 5.9.2 Fenton reaction with d<sub>3</sub>-acetaldehyde and TEMPO

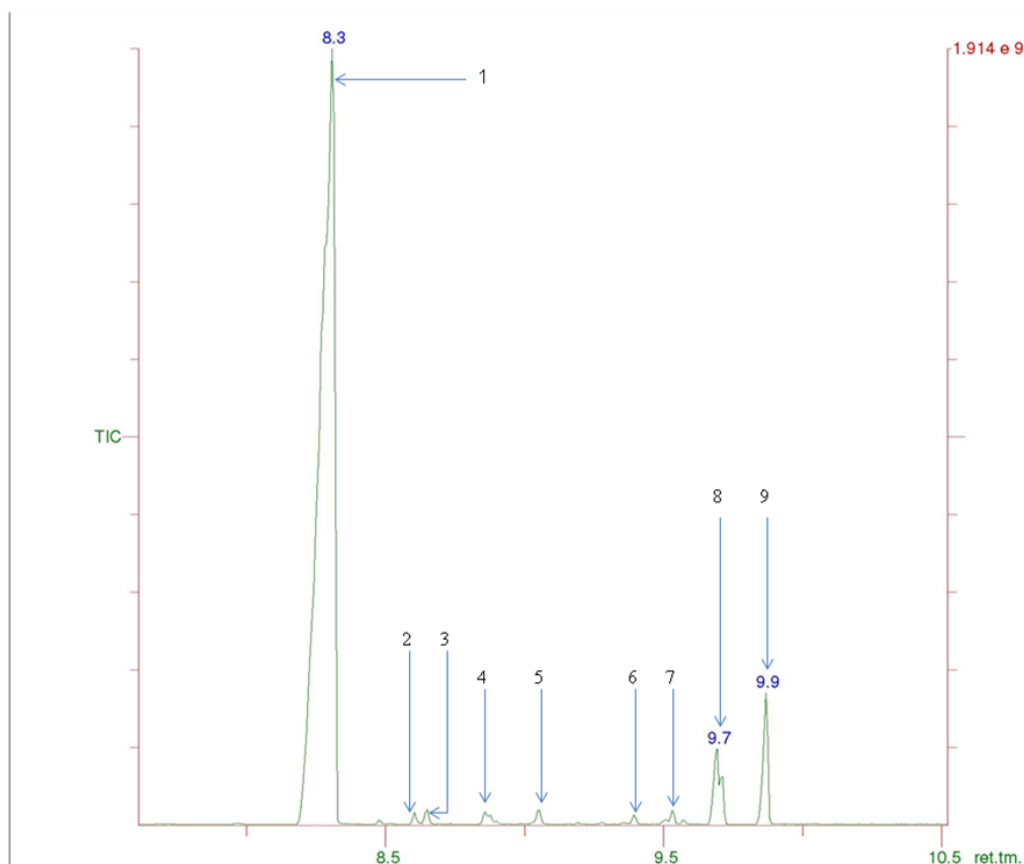


Figure 5.21: The total ion chromatogram (TIC) obtained from the headspace solid phase microextraction (SPME)-GC-MS analysis of the Fenton reaction containing d<sub>3</sub>-acetaldehyde and TEMPO.

Figure 5.21 shows the chromatogram following SPME-GC-MS analysis of the Fenton reaction containing d<sub>3</sub>-acetaldehyde and TEMPO with peaks corresponding to the following compound: **1**) the CD<sub>3</sub> adduct of TEMPO (R<sub>t</sub> 8.3 minutes); **2**) 1-(methoxy-d<sub>3</sub>)-2,2,6-trimethyl-2,3,4,5-*tetra*hydropyridin-1-ium (R<sub>t</sub> 8.6 minutes); **3**) unreacted TEMPO (R<sub>t</sub> 8.7 minutes); **4**) 2,6-dimethyl-1,5-heptadiene (R<sub>t</sub> 8.9 minutes); **5**); 1-(methoxy-d<sub>3</sub>)-2,2,4,6,6-tetramethyl-4-(methyl-d<sub>3</sub>) piperidine (R<sub>t</sub> 9.1 minutes); **6**- 1-(1-methoxy-d<sub>3</sub>)-2,2,6-trimethylpiperidin-4-yl) ethan-1-one-d<sub>3</sub> (R<sub>t</sub> 9.5 minutes); **7**); an unidentified impurity (R<sub>t</sub> 9.5 minutes); **8**) an acetyl-d<sub>3</sub> adduct of TEMPO (R<sub>t</sub> 9.7 minutes); **9**- TEMPO-*tert*-butyl-d<sub>9</sub> adduct (R<sub>t</sub> 9.9 minutes).



### 5.9.3 Fenton reaction with acetaldehyde and 4-methoxy-TEMPO

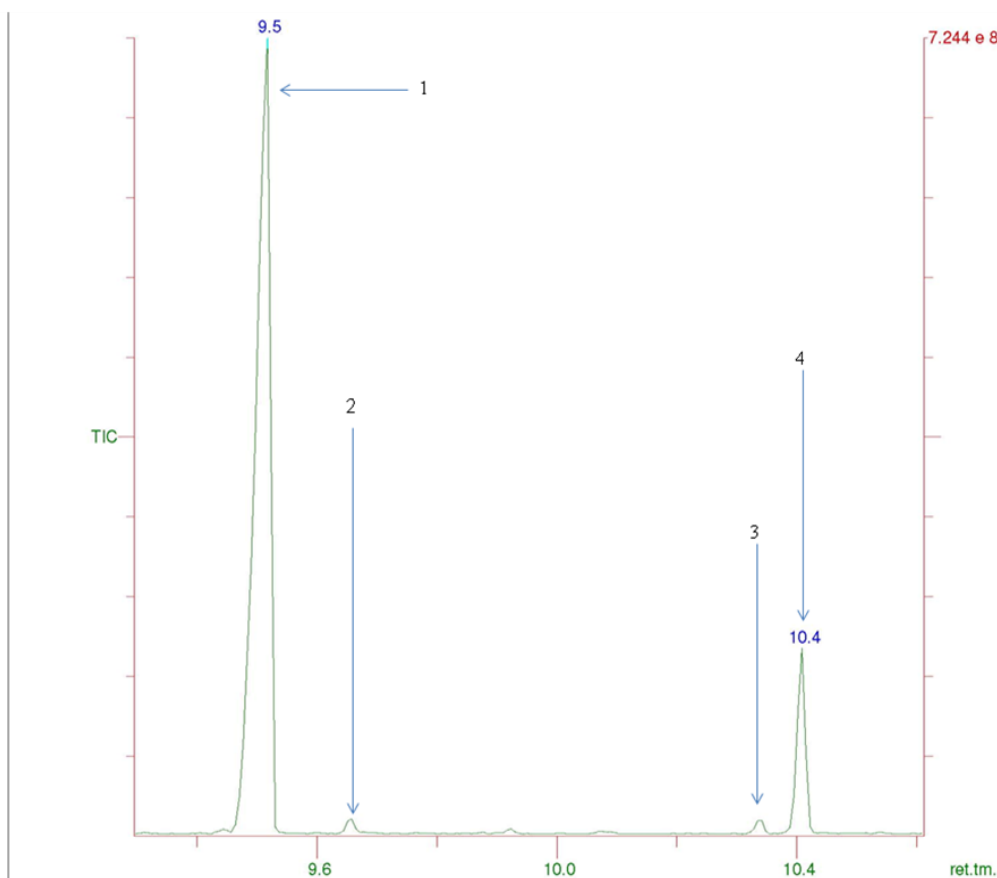


Figure 5.22: The total ion chromatogram (TIC) obtained from the headspace solid phase microextraction (SPME)-GC-MS analysis of the Fenton reaction containing acetaldehyde and 4-methoxy-TEMPO.

Figure 5.22 shows the chromatogram following SPME-GC-MS analysis of the Fenton reaction containing acetaldehyde and 4-methoxy-TEMPO with peaks corresponding to the following compounds: **1**) a CH<sub>3</sub> adduct of methoxy-TEMPO (R<sub>t</sub> 9.5 minutes); **2**) unreacted 4-methoxy-TEMPO spin trap (R<sub>t</sub> 9.7 minutes); **3**) an acetyl adduct of methoxy-TEMPO (R<sub>t</sub> 10.3 minutes); **4**) a *tert*-butyl adduct of methoxy-TEMPO (R<sub>t</sub> 10.4 minutes).

### 5.9.4 Fenton reaction with acetaldehyde and 4-oxo-TEMPO

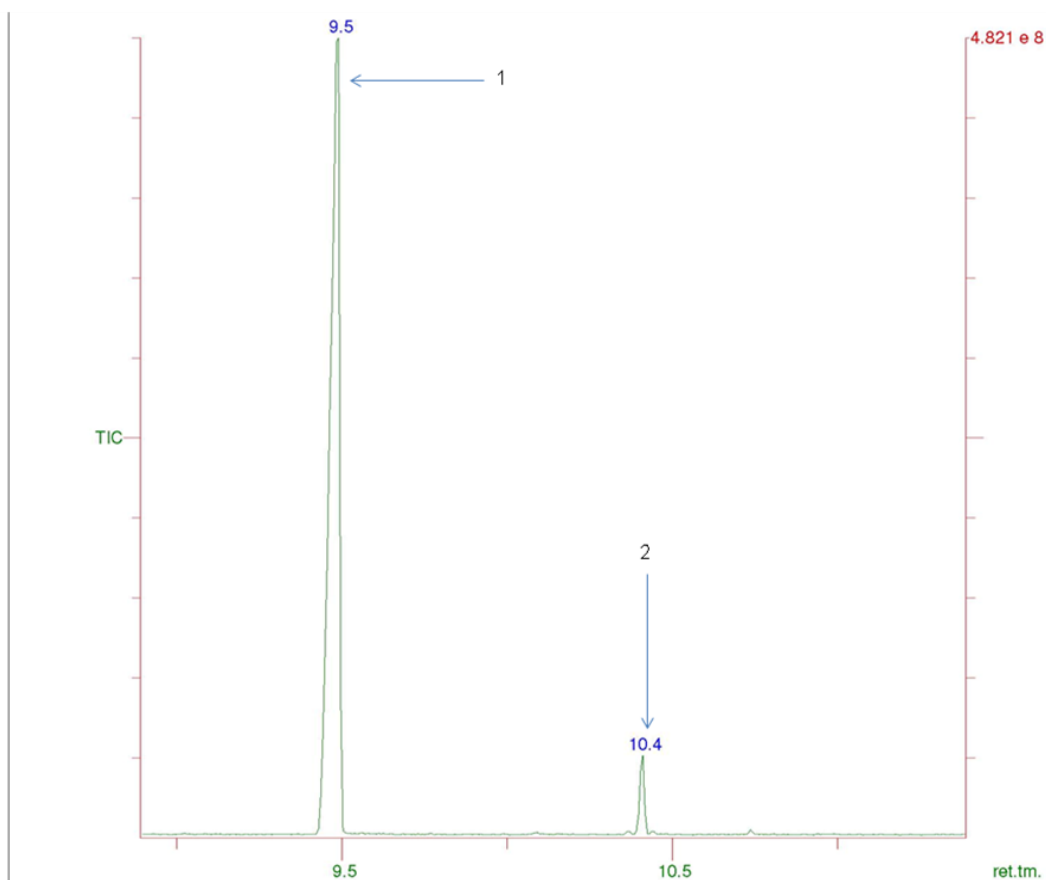


Figure 5.23: The total ion chromatogram (TIC) obtained from the headspace solid phase microextraction (SPME)-GC-MS analysis of the Fenton reaction containing acetaldehyde and 4-oxo-TEMPO.

Figure 5.23 shows the chromatogram following SPME-GC-MS analysis of the Fenton reaction containing acetaldehyde and 4-oxo-TEMPO with peaks corresponding to the following compounds: **1**) a CH<sub>3</sub> adduct of 4-oxo-TEMPO (R<sub>t</sub> 9.5 minutes); **2**) a 4-oxo-TEMPO-*tert*-butyl adduct (R<sub>t</sub> 10.4 minutes).

### **5.10 Detection and analysis of methyl radical adducts.**

The most intense peak in all chromatograms (figure 5.20-5.23) is that of the methyl adduct of TEMPO and its derivatives. The relevant mass spectra of the methyl adduct of TEMPO and its derivatives are the same as described earlier in section 5.3 when the sampling and analysis was done by using the TD-GC-MS approach.

### **5.11 Methyl adduct of 2,2,4,6,6-pentamethylpiperidine**

The methyl adduct of 2,2,4,6,6-pentamethylpiperidine was identified previously when using TD-GC-MS as the sampling and analysis technique (for relevant mass spectra of the adduct see earlier in this chapter (section 5.7)). The identity of adduct was confirmed in this study when  $d_3$ -acetaldehyde was used as a secondary source of radicals in the Fenton reaction system. The molecular ion shifted position in the EI-mass spectrum by 6  $m/z$  units, thus confirming the addition of 2 deuterium-methyl ( $^2CD_3$ ) radicals (figure 5.15).

### **5.12 Detection and analysis of a *tert*-butyl adduct of TEMPO and its derivatives**

A *tert*-butyl adduct of TEMPO and its derivatives is detected when sampling is carried out using SPME-GC/MS. This adduct is detected by TD-GC-MS when TEMPO is used as a spin trapping agent (see chapter 5, part 1). The relevant mass spectra for the adduct are exactly the same as described earlier in this chapter (section 5.6) when the sampling and analysis was done by using thermal desorption TD-GC-MS. Interestingly, it is detected with not only TEMPO but with all of its derivatives, which not only confirms the identity of the adduct but also helps in the understanding of the fragmentation pattern. GC-MS data for the identification of the *tert*-butyl adduct of TEMPO and its derivatives is summarised in table 5.2

Table 5.2: Summary of GC-MS data for the *tert*-butyl adduct of TEMPO and its derivatives when the analysis was carried out by SPME-GC-MS

| Spin adduct                         | Retention time( $R_t$ ) | Molecular ion ( $m/z$ ) | Characteristics fragment peaks ( $m/z$ ) |
|-------------------------------------|-------------------------|-------------------------|--|
| TEMPO- <i>tert</i> -butyl           | 9.9                     | 213                     | 198, 130, 124, 109, 88, 74, 69, 56       |
| TEMPO- <i>tert</i> -butyl- $d_9$    | 9.7                     | 222                     | 207, 139, 109, 80, 69, 56                |
| 4-methoxy-TEMPO- <i>tert</i> -butyl | 10.4                    | 243                     | 228, 139, 130, 99, 88, 69, 56            |
| 4-oxo-TEMPO- <i>tert</i> -butyl     | 10.4                    | 227                     | 212, 170, 139, 130, 88, 69, 56           |

## 5.13 Electron ionisation (EI) mass spectra of the acetyl adduct of TEMPO and its derivatives

### 5.13.1 TEMPO-COCH<sub>3</sub> adduct

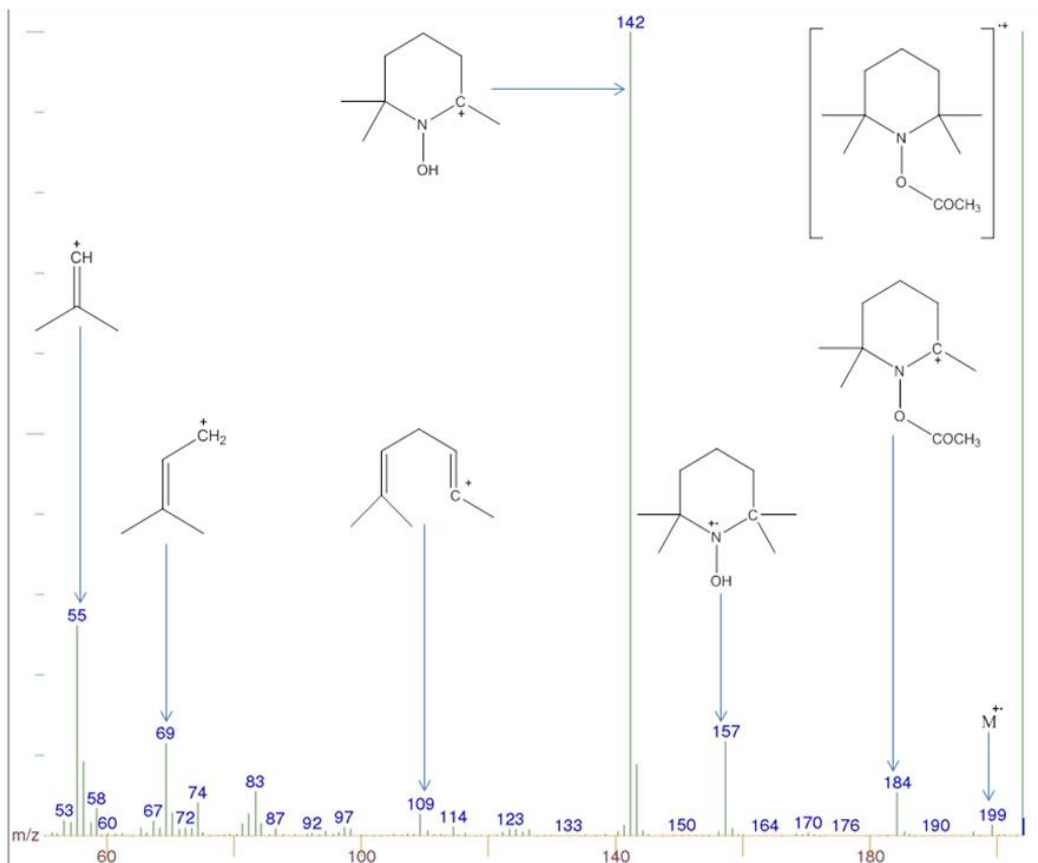


Figure 5.24: Electron ionisation (EI) mass spectrum of the peak at 9.7 minutes (figure 5.20) corresponding to TEMPO-COCH<sub>3</sub>. The structure given in the top right corner is that of the molecular ion (M<sup>+</sup>), corresponding to the peak at *m/z* 199.

The EI mass spectrum shown in figure 5.24 corresponds to the acetyl adduct of TEMPO (TEMPO-COCH<sub>3</sub>). The peak at *m/z* 199 corresponds to the molecular ion. The fragment at *m/z* 184 is formed by the loss of a methyl radical (from M<sup>+</sup>). The base peak at *m/z* 142 is formed by the loss of methyl group from a peak at *m/z* 157. Other characteristic fragments of TEMPO can be seen at *m/z* 109, 69 and 55.

### 5.13.2 TEMPO-COCD<sub>3</sub> adduct

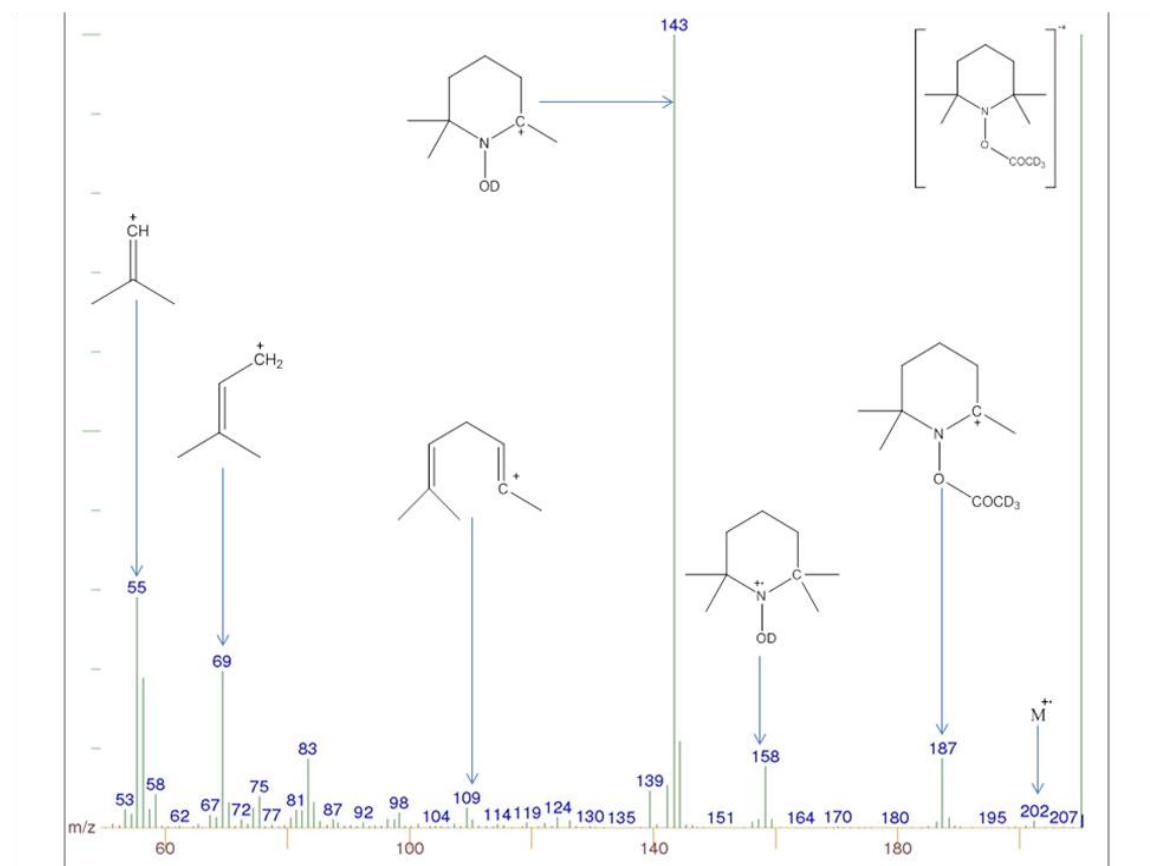


Figure 5.25: Electron ionisation (EI) mass spectrum of the peak at 9.7 minutes (figure 5.21) corresponding to TEMPO-COCD<sub>3</sub>. The structure given in the top right corner is that of the molecular ion, corresponding to the peak at  $m/z$  202.

The EI mass spectrum shown in figure 5.25 corresponds to the d<sub>3</sub>-acetyl adduct of TEMPO (TEMPO-COCD<sub>3</sub>) observed at 9.7 minutes when the reaction was carried out by using d<sub>3</sub>-acetaldehyde as a secondary source of radicals in the Fenton system. The molecular ion can be seen clearly at  $m/z$  202 (a difference of 3  $m/z$  units when compared to the molecular ion of TEMPO-COCH<sub>3</sub>; figure 5.24) which confirms the trapping of a d<sub>3</sub>-acetyl radical by TEMPO. The fragment at  $m/z$  187 is formed by the loss of a methyl group (from M<sup>+</sup>). The loss of a methyl group from the fragment at  $m/z$  158 gives a peak at  $m/z$  143. Other characteristic fragments of TEMPO can be seen at  $m/z$  109, 69 and 55. The GC-MS data for this adduct is summarised in table 5.3.

Table 5.3: Summary of GC-MS data for the acetyl adduct of TEMPO and its derivatives when the analysis was carried using SPME-GC-MS.

| Spin adduct            | Retention time ( $R_t$ ) | Molecular ion ( $m/z$ ) | Characteristic fragment peaks ( $m/z$ ) |
|------------------------|--------------------------|-------------------------|---|
| TEMPO-acetyl           | 9.7                      | 199                     | 184, 157, 142, 109, 83, 69, 55          |
| TEMPO-acetyl( $d_3$ )  | 9.7                      | 202                     | 187, 158, 143, 124, 109, 83, 69, 56     |
| 4-methoxy-TEMPO-acetyl | 10.3                     | 229                     | 214, 186, 142, 109, 88, 69, 56          |

## 5.14 Electron ionisation (EI) mass spectra of a methyl adduct of 2,2,6-trimethyl-2,3,4,5-tetrahydropyridin-1-ium

### 5.14.1 EI mass spectrum of 1-methoxy-2,2,6-trimethyl-2,3,4,5-tetrahydropyridin-1-ium

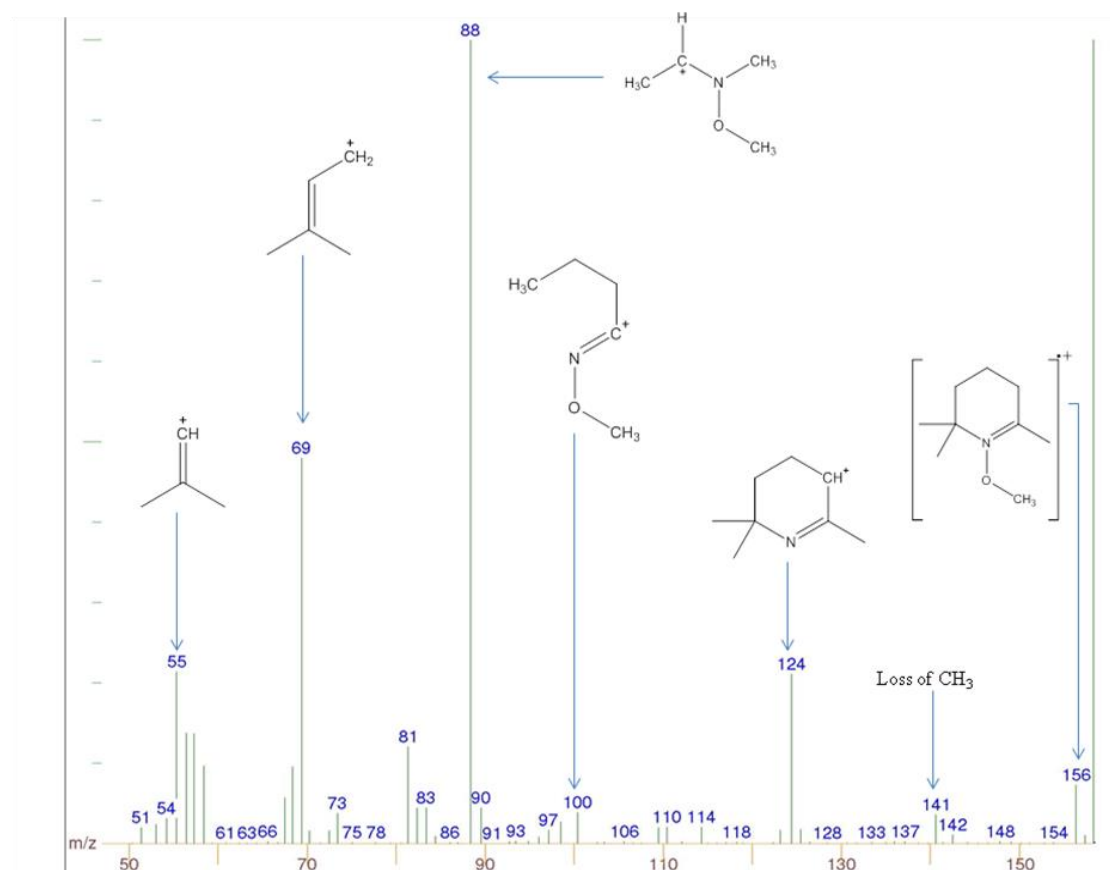


Figure 5.26: Electron ionisation (EI) mass spectrum of the peak at 8.6 minutes (figure 5.20) corresponding to the 2,2,6-trimethyl-2,3,4,5-tetrahydropyridin-1-ium. The molecular ion can be seen at  $m/z$  156.

Figure 5.26 shows the EI-MS for the peak observed at 8.6 minutes. It may correspond to a methyl adduct of 2,2,6-trimethyl-2,3,4,5-tetrahydropyridin-1-ium with a molecular ion at  $m/z$  156. The molecular ion may lose a methyl group to give the fragment at  $m/z$  141, whilst the loss of CH<sub>3</sub>OH (from M<sup>+</sup>) generates a fragment at  $m/z$  124. Although the fragmentation pathway needs further investigation the structure for the base peak at  $m/z$  88 is supported when using d<sub>3</sub>-acetaldehyde (figure 5.27). Characteristic fragments of TEMPO can be seen at  $m/z$  69 and 55.



### 5.14.2 EI mass spectrum of 1-(methoxy-d<sub>3</sub>)-2,2,6-trimethyl-2,3,4,5-tetrahydropyridin-1-ium

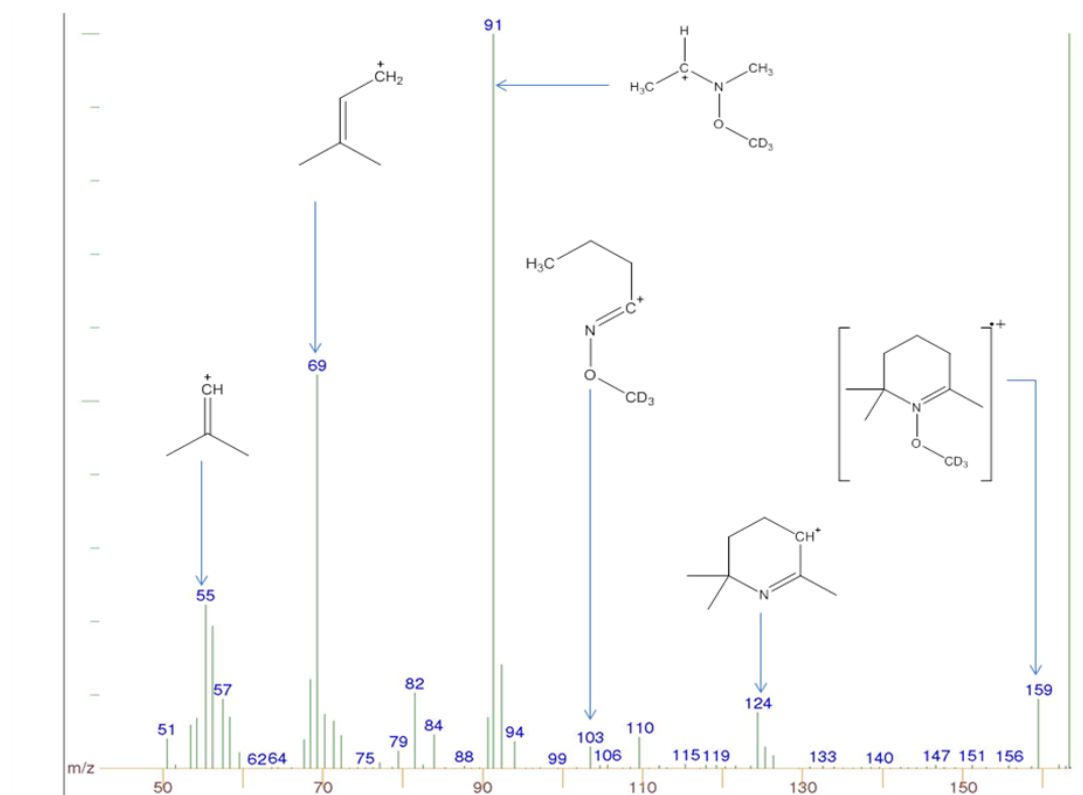


Figure 5.27: Electron ionisation (EI) mass spectrum of the peak at 8.5 minutes (figure 5.21) corresponding to 1-(methoxy-d<sub>3</sub>)-2,2,6-trimethyl-2,3,4,5-tetrahydropyridin-1-ium. The molecular ion can be seen at  $m/z$  159.

The EI mass spectrum shown in figure 5.27 is believed to correspond to 1-(methoxy-d<sub>3</sub>)-2,2,6-trimethyl-2,3,4,5-tetrahydropyridin-1-ium observed at 8.5 minutes when the reaction is carried out by using d<sub>3</sub>-acetaldehyde as a secondary source of radicals in the Fenton system. The molecular ion can be seen clearly at  $m/z$  159 (a difference of 3  $m/z$  units when compared to the molecular ion of 2,2,6-trimethyl-2,3,4,5-tetrahydropyridin-1-ium; figure 5.26) which confirms the trapping of a  $\cdot\text{CD}_3$  radical. A peak expected at  $m/z$  144 (loss of methyl group) was not detected but a fragment at  $m/z$  124 can clearly be seen which is most probably formed by the loss of  $\text{CD}_3\text{OH}$  from the molecular ion. Characteristic fragments of TEMPO can be seen at  $m/z$  69 and 55 while the suggested structure for the base peak at  $m/z$  91 clearly correlates with that suggested for the base peak in figure 5.26, when the reaction was carried out by using acetaldehyde.

## 5.15 Electron ionisation mass spectrum of 2,6-dimethyl-1,5-heptadiene

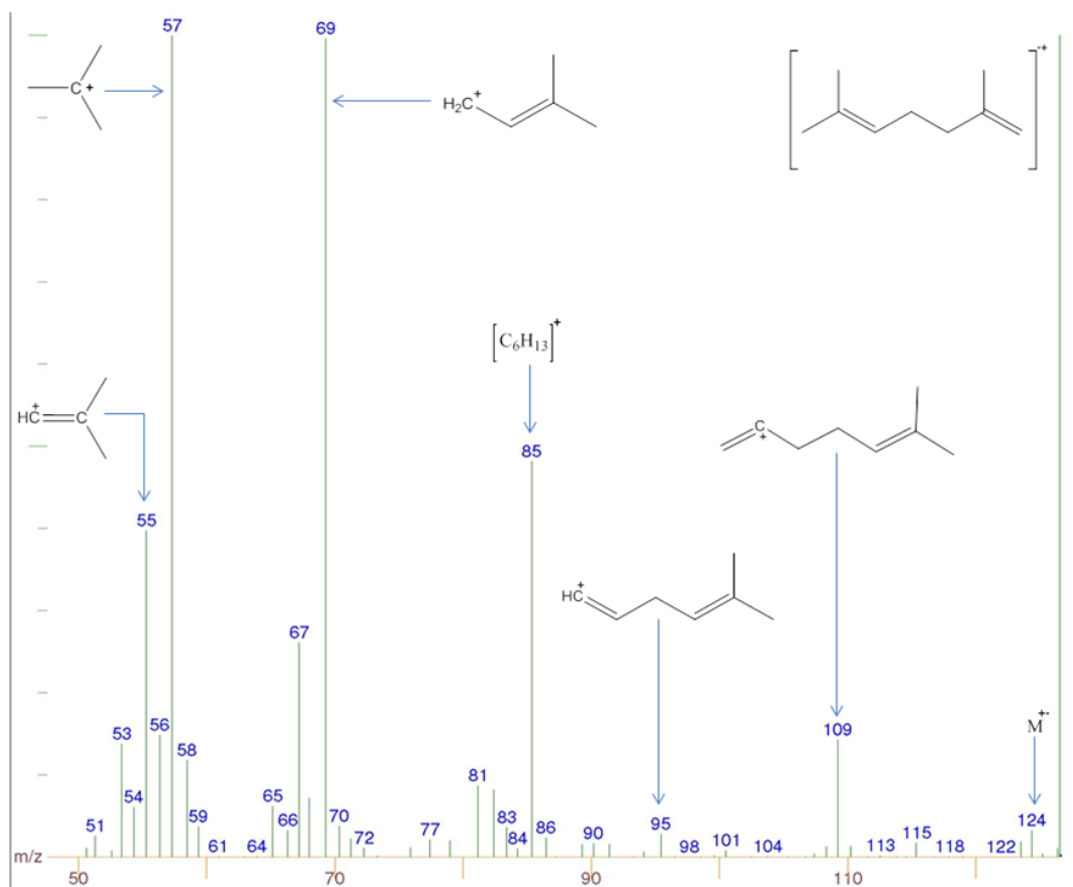


Figure 5.28: Electron ionisation (EI) mass spectrum of the peak at 8.9 minutes (figure 5.20 & 5.21) corresponding to 2,6-dimethyl-1,5-heptadiene. The structure given in the top right corner is that of the molecular ion, corresponding to the peak at  $m/z$  124.

The EI mass spectrum shown in figure corresponds to 2,6-dimethyl-1,5-heptadiene. The molecular ion can be seen at  $m/z$  124. This may lose a methyl group to generate a fragment at  $m/z$  109. Further loss of  $C_2H_4$  generates a fragment  $m/z$  85.

## 5.16 Electron ionisation (EI) mass spectrum of methyl and acetyl adduct of 2,2,6-trimethylpiperidine.

### 5.16.1 EI mass spectrum of 1-(1-methoxy-2,2,6-trimethylpiperidin-4-yl) ethan-1-one

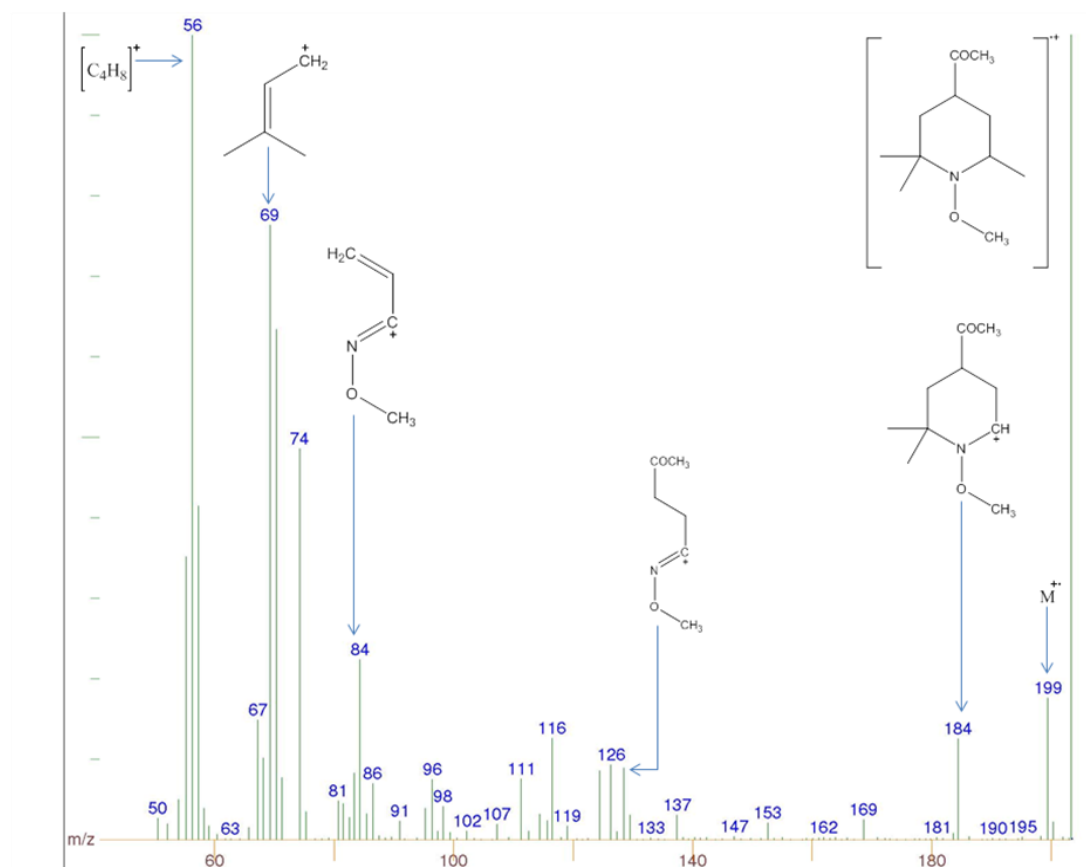


Figure 5.29: Electron ionisation (EI) mass spectrum of the peak at 9.5 minutes (figure 5.20) corresponding to a methyl and acetyl adduct of 2,2,6-trimethylpiperidine. The structure given in the top right corner is that of the molecular ion, corresponding to the peak at  $m/z$  199.

The suggested structure for the peak observed at 9.5 minutes is shown in the top right corner of the mass spectrum. It is believed to correspond to a methyl & acetyl adduct of 2,2,6-trimethylpiperidine with a molecular ion at  $m/z$  199. The fragment at  $m/z$  184 is formed by the loss of a methyl radical from the molecular ion. Although the fragmentation pathway needs further investigation the structures of major fragments at  $m/z$  84 and 128 are suggested (figure 5.30). The peaks at  $m/z$  55 and  $m/z$  69 are characteristic of TEMPO derivatives.

### 5.16.2 EI mass spectrum of 1-(1-(methoxy-d<sub>3</sub>)-2,2,6-trimethylpiperidin-4-yl)ethan-1-one-2,2,2-d<sub>3</sub>

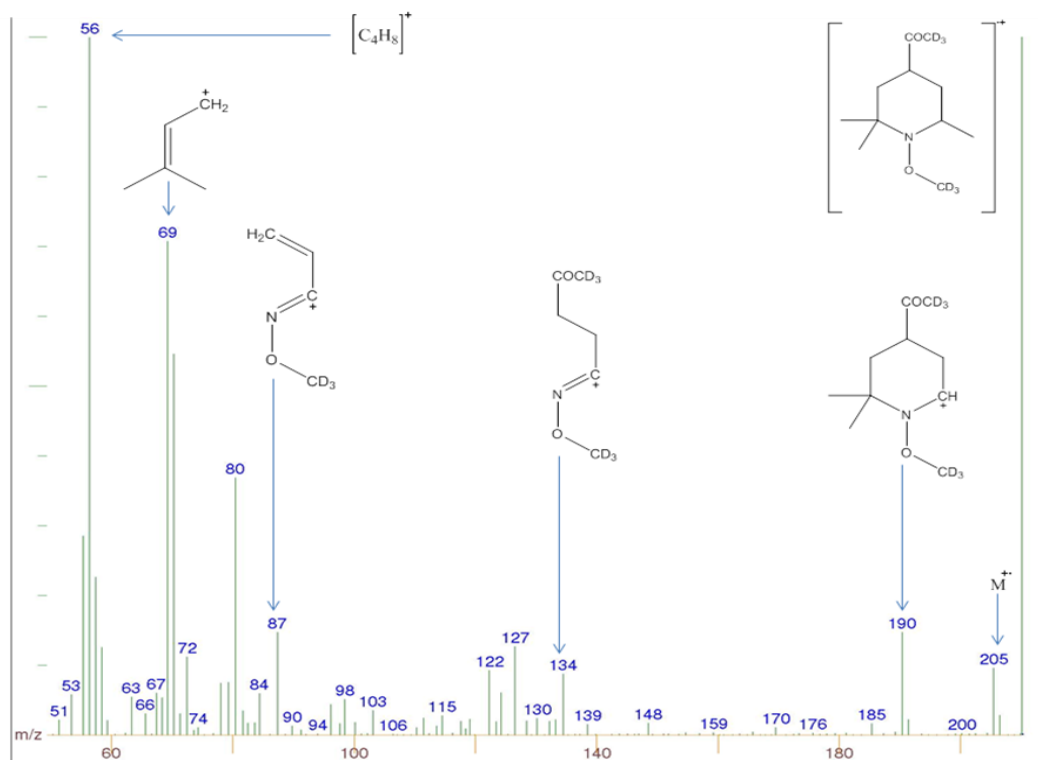


Figure 5.30: Electron ionisation (EI) mass spectrum of the peak at 9.4 minutes (figure 5.21) corresponding to a deuterio-methyl ( $\cdot\text{CD}_3$ ) and a deuterio-acetyl ( $\cdot\text{COCD}_3$ ) adduct of 2,2,6-trimethylpiperidine. The structure given in the top right corner is that of the molecular ion, corresponding to the peak at  $m/z$  205.

The EI mass spectrum shown in figure 5.30 corresponds to 1-(1-(methoxy-d<sub>3</sub>)-2,2,6-trimethylpiperidin-4-yl)ethan-1-one-2,2,2-d<sub>3</sub> when the reaction is carried out by using d<sub>3</sub>-acetaldehyde as a secondary source of radicals in the Fenton system. The molecular ion can be seen clearly at  $m/z$  205 (a difference of 6  $m/z$  units when compared to the molecular ion in figure 5.29) which confirms the trapping of two  $\text{CD}_3$  groups (believed to be  $\text{CD}_3$  and  $\text{COCD}_3$ ). Comparing the mass spectrum to the one for non-deuterated acetaldehyde, the structure for the molecular ion is suggested as shown in top right corner of the above figure. The fragment at  $m/z$  190 is formed by the loss of methyl radical from the molecular ion. Although the fragmentation pathway needs further investigation suggested structures for major fragments at  $m/z$  134 and 87 are given in figure 5.30. The peaks at  $m/z$  55 and  $m/z$  69 are characteristic of TEMPO derivatives.

## 5.17 Electron ionisation mass spectrum of unreacted TEMPO

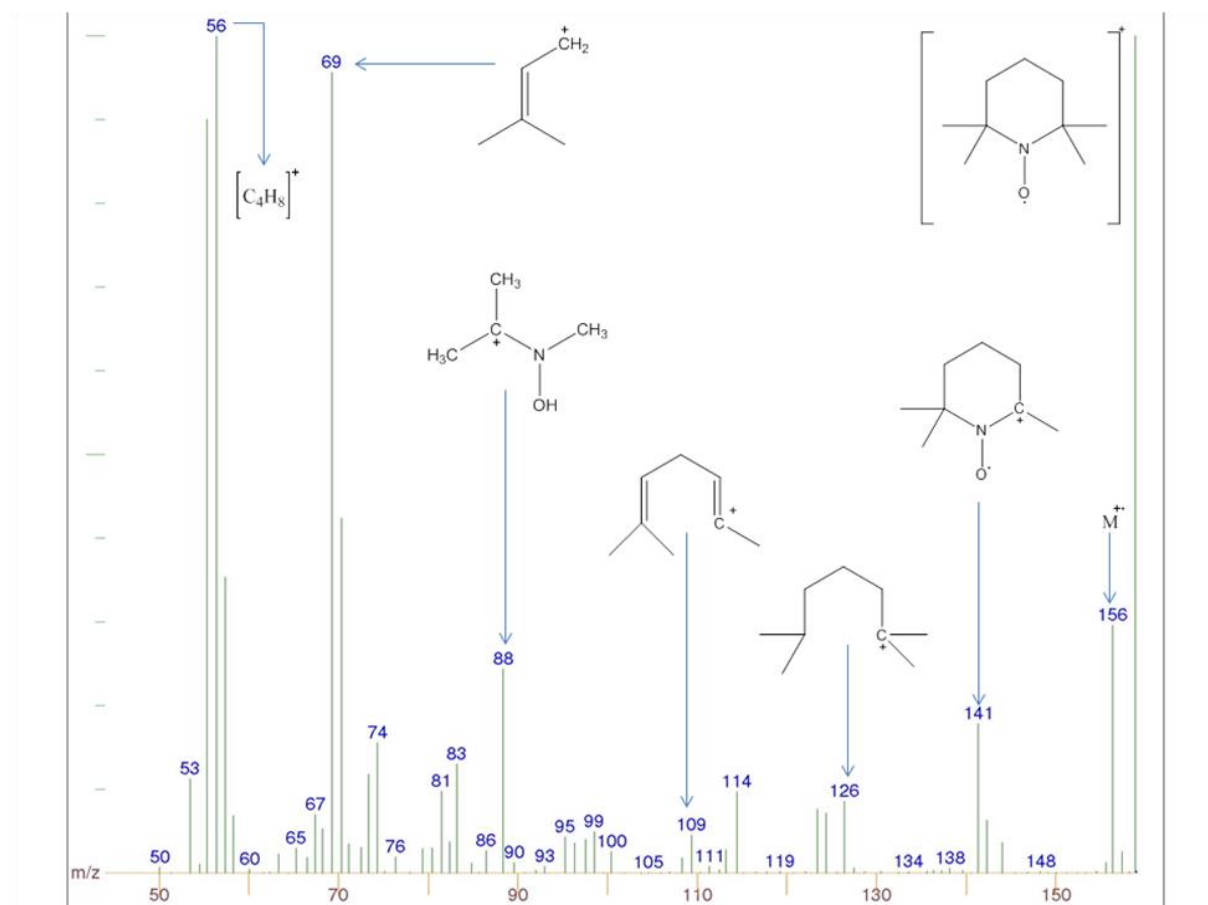


Figure 5.31: Electron ionisation (EI) mass spectrum of the peak at 8.7 minutes (figure 5.20) corresponding to unreacted TEMPO. The structure given in the top right corner is that of the molecular ion ( $M^+$ ), corresponding to the peak at  $m/z$  156.

The EI mass spectrum shown in Figure 5.31 corresponds to the unreacted TEMPO. The molecular ion can be seen at  $m/z$  156 which may lose a methyl radical to give a fragment at  $m/z$  141. Further loss of a methyl group gives a fragment at  $m/z$  126. Characteristic fragments of TEMPO can be seen at  $m/z$  109, 69 and 55.

## 5.18 Discussion

In the current study, the Fenton reaction was used to generate hydroxyl radicals which may then react with acetaldehyde (a secondary source of free radicals) to produce acetyl radicals, which further decompose into methyl radicals by decarbonylation (Nakao *et al.*, 2000), already explained in chapter 3. The secondary radicals (mainly methyl and acetyl) then react with TEMPO to produce stable radical adducts which may be extracted from the headspace by TD or SPME and analysed by using GC-MS.

The chromatogram obtained (figure 5.1) for the Fenton reaction containing acetaldehyde shows an intense peak retained at 7.27 minutes and the corresponding mass spectrum (figure 5.6) shows a molecular ion at  $m/z$  171 for the methyl adduct of TEMPO. For confirmation and interpretation of the mass spectrum, other derivatives of TEMPO i.e. 4-methoxy-TEMPO and 4-oxo-TEMPO were used in the Fenton reaction as spin-trapping agents and both derivatives showed intense methyl adduct peaks in the TIC with similar fragmentation patterns. To confirm the identity and source of the methyl radical, deuterated acetaldehyde was used in the reaction. Deuterated acetaldehyde generated  $^{\bullet}\text{CD}_3$  radicals which were then trapped by TEMPO to form a TEMPO- $\text{CD}_3$  adduct showing the shift of 3 mass units from  $m/z$  171 to 174 and thus confirming acetaldehyde as the source of the free radicals (figure 5.7).

The methyl adduct peak was absent when control reactions were carried out (figure 5.5), which means the Fenton reaction is responsible for the production of methyl radicals (when hydroxyl radicals attack acetaldehyde as explained in chapter 3, scheme 3.3).

A small peak retained at 13.85 minutes (figure 5.1) corresponds to a TEMPO-*tert*-butyl adduct which has not previously been observed, to the best of our knowledge. An addition of  $m/z$  57 units to TEMPO produces a molecular ion at  $m/z$  213 units. The loss of methyl radical (from  $\text{M}^{\bullet}$ ) produces an ion at  $m/z$  198, whilst a loss of  $m/z$  57 from the molecular ion generates a peak at  $m/z$  156. A similar fragmentation pattern is observed with both methyl and acetyl adducts. To confirm the identity of the *tert*-butyl adduct of TEMPO, the Fenton reaction was carried out by using  $\text{d}_3$ -acetaldehyde. A small peak retained at 13.70 minutes (figure 5.2) corresponds to TEMPO-deuterated *tert*-butyl- $\text{d}_9$  adduct. The  $m/z$  value of the molecular ion increases by 9 units to  $m/z$  222, thus confirming the addition of a *tert*-butyl group (figure 5.13). The generation of *tert*-butyl radical is not fully understood but there is one study which suggests the production of

*tert*-butyl radical when iso-butane is attacked by methyl radicals (Anastasi, 1983), but their generation in the Fenton system needs further investigation.

The *tert*-butyl adduct is not detected with any of the TEMPO derivatives when TD extraction approach is used. Interestingly, this adduct is detected not only with TEMPO but also with its other derivatives when SPME is used as a sampling approach, which not only confirms the identity of the adduct but also helps in understanding its fragmentation pathway. Confirmation of the fragmentation pathway of this adduct needs further investigation, possibly by using isotopically labelled TEMPO & its other derivatives and by using other analytical techniques.

Two very small peaks retained at 5.80 & 6.54 minutes (figure 5.1) may be isomers of a methyl adduct of 2,2,6,6-tetramethyl-3,6-dihydropyridine. A possible mechanism of suggested adduct formation from TEMPO-CH<sub>3</sub> is shown in scheme 5.2. It is believed that methyl adduct of TEMPO breaks down in two steps successively losing hydrogen in each step to generate the suggested adduct with molecular ion at  $m/z$  169, which loses methyl radical to give a fragment at  $m/z$  154. Further loss with the ring opening generates the fragment at  $m/z$  128, whilst the loss of CH<sub>3</sub>OH gives a fragment at  $m/z$  122. To confirm the identity of the adduct, the Fenton reaction was carried out by using d<sub>3</sub>-acetaldehyde which shows two small peaks at 5.17 & 6.52 minutes (figure 5.2). The corresponding mass spectrum (figure 5.11) shows a shift of 3  $m/z$  units thus confirming the addition of a <sup>13</sup>C<sub>3</sub> radical. The molecular ion can be seen clearly at  $m/z$  172. This may readily lose a methyl radical to give a fragment at  $m/z$  157. Further loss ring opening give a fragment at  $m/z$  131, whilst the loss of CD<sub>3</sub>OH generates a fragment at  $m/z$  122. Further loss of methyl from this fragment with an addition of hydrogen gives a fragment at  $m/z$  108 (figure 5.11).

A very small peak retained at 10.07 minutes may be a methyl adduct of 2,2,4,6,6-pentamethylpiperidine. As discussed earlier, TEMPO can give different structures because of its internal re-arrangement reactions.

It is suggested that a TEMPO-CH<sub>3</sub> adduct traps another methyl radical by replacing an hydrogen to give 1-methoxy-2,2,4,6,6-pentamethylpiperidine (methyl adduct of 2,2,4,6,6-pentamethylpiperidine). The molecular ion can be seen at  $m/z$  185 which may then lose a methyl radical to give a fragment at  $m/z$  170. Loss of CH<sub>3</sub>OH from  $m/z$  170 generates a peak at  $m/z$  138. Then further loss of methyl group with an addition of

hydrogen gives a fragment at  $m/z$  124. Other fragments characteristic of TEMPO and its derivatives are seen at  $m/z$  109, 69 and 56. Structures of all major fragments are shown in the corresponding mass spectrum (figure 5.14). To confirm the identity of this adduct, the Fenton reaction was carried out using  $d_3$ -acetaldehyde. A small peak observed at 9.97 minutes (figure 5.2) corresponds to the deuterated version of the adduct. The  $m/z$  value of the molecular ion increases by 6 units to  $m/z$  191, thus confirming the addition of two  $^1CD_3$  radicals (figure 5.15). This adduct was also detected when sampling was carried out using SPME approach. No other derivatives of TEMPO appeared to show this adduct with either of the extraction techniques.

The chromatogram (figure 5.20) shows a small peak retained at 9.7 minutes and the corresponding mass spectrum (figure 5.24) shows a strong peak for molecular ion at  $m/z$  199, corresponding to an acetyl adduct of TEMPO. For confirmation of the adduct and interpretation of the MS, derivatives of TEMPO were used in the Fenton reaction. Acetyl radicals were successfully trapped by 4-methoxy-TEMPO where molecular ion can be seen at  $m/z$  229. Acetyl radicals were not observed when the reaction was carried out with 4-oxo-TEMPO. To confirm the identity and source of the acetyl radicals, deuterated acetaldehyde was used in the Fenton reaction. Deuterated acetaldehyde generates the  $CD_3C^*O$  radical which is then trapped by TEMPO to form a TEMPO-acetyl adduct showing a shift of 3 mass units from  $m/z$  199 to 202, thus confirming the acetaldehyde as a source of acetyl radicals (figure 5.25).

Nakao and his colleagues also detected acetyl radicals by trapping with DMPO & POBN whilst studying the metabolism of acetaldehyde (Nakao *et al.*, 2000). They successfully detected the methyl and acetyl adducts of the POBN and DMPO by using EPR spectroscopy. In another study, acetyl radicals were detected as PBN-acetyl adducts when the Fenton reaction was carried out by using acetaldehyde as secondary source of radicals (Castro, Costantini and Castro, 2009).

### **5.18.1 Possible fragmentation pathways of radical adducts**

The fragmentation pathway of nitroxide spin traps is neither simple nor easy to interpret because of the inner rearrangement in the structure of the spin trap. One mechanism which could fit with different fragments is the following one: cation radical is generated



in the ion source when an electron is lost by the nitrogen atom. The presence of peaks for TEMPO-CH<sub>3</sub> at  $m/z$  171 (molecular ion) and  $m/z$  156 (obtained after demethylation of the molecular ion) can be explained by this mechanism. The ion at  $m/z$  156, after an electronic arrangement, abstracts a proton-linked to the carbon beta to the nitrogen, resulting in the ejection of a methanol molecule (loss of 32 mass units) resulting in the production of a cyclic piperidine cation ( $m/z$  124) with a charge on the carbon atom (scheme 5.1). This fragmentation pattern follows the one observed for TEMPO breakdown by other groups (Morrison and Davies, 1970; Smith *et al.*, 2000).

Another possible fragmentation pattern for TEMPO-CH<sub>3</sub> is shown in scheme 5.1. Loss of a methyl radical from adduct molecule molecular ion will form the peak at  $m/z$  156. Further loss of NH<sub>2</sub>OCH<sub>3</sub> will result in the formation of the peak at  $m/z$  109. Further loss of C<sub>3</sub>H<sub>4</sub> and C<sub>4</sub>H<sub>6</sub> may form the peaks at  $m/z$  69 and  $m/z$  55 respectively. Both peaks at  $m/z$  55 and  $m/z$  69 appear in many of the mass spectra of TEMPO and its derivatives. In the case of <sup>13</sup>C<sub>3</sub>D<sub>3</sub> trapping, the initial loss of methyl results in the formation of the base peak at  $m/z$  159, as shown in scheme 4.4. Further loss of NH<sub>2</sub>OCD<sub>3</sub> forms a peak at  $m/z$  109. Subsequent fragmentation follows a similar pattern to that of the methyl adduct, as explained in scheme 5.1 (Morrison and Davies, 1970; Smith *et al.*, 2000). Most of the ions produced during the fragmentation of the acetyl adduct are similar to ions produced during the fragmentation of the methyl adduct, which suggests a similar fragmentation pattern.

This study demonstrates that solvent free approaches may be used for indirect detection of the hydroxyl radicals and to study the breakdown of acetaldehyde, which is a product of ethanol metabolism (Zhang *et al.*, 2004). Furthermore, solvent-free extraction approaches have the advantage of no direct contact with reactants in the Fenton mixture, which are sometimes damaging for the GC columns.

## Chapter 6

### Conclusions and future work

## 6.1 Summary and Conclusions

The Fenton reaction is one of the most studied biochemical reactions. It generates hydroxyl radicals which can be damaging to different constituents of the cell. Hydroxyl radicals are short-lived with a half-life of  $10^{-9}$  seconds, making them very hard to detect. They can react with organic molecules to produce other radicals and possibly initiate a chain reaction which is even more destructive to the living body (Dalle-Donne *et al.*, 2006). Free radicals may trigger different diseases, which include neurodegenerative diseases like Parkinson's or Alzheimer's (Nikolaou, 2012; Uttara *et al.*, 2009), rheumatoid arthritis, diabetes and asthma (Lee, Koo & Min, 2004).

Spin trapping is a technique used to trap free radicals. Spin traps are chemical compounds which react with free radicals to produce comparatively stable radical adducts which can be measured by using different analytical techniques (Halliwell & Gutteridge, 2015). EPR spectroscopy is commonly used for the detection of free radicals but it is not easy to identify them because of similar EPR signals irrespective of the radical being trapped. The cost of coupling EPR spectroscopy with MS is quite high and hence not available in most laboratories. Other techniques like LC/MS, GC-MS, NMR (Valery *et al.*, 2011) and MALDI-TOF-MS (Podmore *et al.*, 2013) may be used for the detection and identification of spin trapped free radicals.

The main objective of the present research work was to use GC-MS for the separation and identification of spin trapped free radicals following TD or SPME sampling of the headspace as solvent free extraction approaches. To the best of our knowledge, this is a completely novel approach to the identification of spin trapped free radicals. Hydroxyl radicals can react with secondary source of free radicals (ethanal and propanal in this project) to produce more stable radicals, which may then react with spin trapping agents (PBN and its derivatives/ TEMPO and its derivatives) to produce stable radical adducts. These adducts may then be extracted and analysed/identified using GC-MS, for methodology see chapter 2. Solvent free sampling has an advantage over traditional extraction using an organic solvent in that it leaves much "cleaner" samples e.g. if not fully removed prior to entry into the GC, the Fenton reagents can heavily contaminate the GC inlet and column. In addition, the solvent free extraction approach is less laborious and time efficient.

In chapter 3, acetaldehyde was used as a secondary source of free radicals and PBN and its derivatives as trapping agents. Acetaldehyde present in the Fenton reaction was readily attacked by the hydroxyl radicals to produce methyl radicals which were then trapped by PBN & its derivatives to produce stable radical adducts. These adducts were extracted, separated and analysed by TD-GC-MS as a novel approach to study the spin trapped free radicals. PBN traps a radical at its  $\alpha$ -carbon site to give a nitroxide, which may then further trap a radical at the oxygen (unpaired electron on the nitroxide is delocalised between the nitrogen and oxygen atoms). Methyl radicals are generated in abundance and readily trapped by PBN to give a di-methyl adduct with a molecular ion at  $m/z$  207. Although the PBN-dimethyl adduct is the most intense peak in the chromatogram, other peaks were also observed that are clearly formed via Fenton chemistry.

To confirm acetaldehyde as the source of free radicals and to confirm the identity of the di-methyl adduct,  $d_3$ -acetaldehyde was used in the Fenton reaction. The chromatogram (figure 3.2) shows an intense peak at 10.16 minutes. The EI mass spectrum of the peak shows a molecular ion at  $m/z$  213, which is 6  $m/z$  units higher than the corresponding mass spectrum for the non-deuterated dimethyl adduct of PBN, clearly demonstrating the addition of 2  $^1CD_3$  radicals and thus confirming the identity of the adduct. Furthermore, when deuterated PBN ( $d_6$ -PBN) is used as the trapping agent with non-deuterated acetaldehyde (and then separately with  $d_3$ -acetaldehyde) molecular ions at  $m/z$  213 and  $m/z$  219, respectively, are observed, which not only confirms the identity of the adduct but helps to identify the fragments and pattern of fragmentation.

Another small peak retained at 8.52 minutes (figure 3.1) is identified as a methyl & hydrogen adduct of PBN with a molecular ion at  $m/z$  193, formed by a similar pathway as of di-methyl adduct; a hydrogen is trapped at the alpha carbon site which then readily traps methyl radical to give a stable adduct. The identity of the adduct was confirmed when the Fenton reaction was carried out by using  $d_3$ -acetaldehyde. The molecular ion has moved from  $m/z$  193 to  $m/z$  196 confirming the addition of 3 deuterium atoms ( $^1CD_3$ ). Further experiments using  $d_6$ -PBN in the presence of acetaldehyde or  $d_3$ -acetaldehyde & other derivatives of PBN also provided evidence to confirm the identity of the adduct.

A strong peak retained at 2.61 minutes is identified as benzaldehyde with its characteristic fragmentation pattern. Benzaldehyde is a known product of PBN breakdown (Turnbull *et al.*, 2001; Kotake and Janzen 1991).

Two very small peaks at 15.91 & 16.25 minutes were identified as isomers of 2,3-diphenylbutane with a molecular ion at  $m/z$  210. The adduct is most probably formed in the Fenton system although mechanism of its formation needs further investigation. These peaks were absent in control reactions which also support the evidence as they are formed from Fenton-based chemistry. To confirm the identity of the adduct, the Fenton reaction was carried out by using  $d_3$ -acetaldehyde. The molecular ion shifted by 6 units to  $m/z$  216 thus demonstrating the addition of two  $^1CD_3$ . A further experiment with  $d_6$ -PBN gave a molecular ion at  $m/z$  222 providing further evidence of the suggested structure.

From these results, it can be concluded that acetaldehyde, when used as a secondary source of free radicals, produces methyl radicals which may then be trapped by PBN and its derivatives to give volatile radical adducts. These adducts may be extracted very easily using a solvent free approach and detected by using GC-MS. In many studies, only one biomarker of oxidative stress is often used which may not be indicative of the condition as one product may be formed by different pathways. During this study, different products, which may be potential biomarkers of oxidative stress, have been successfully identified and characterised. These products may be particularly useful as “fingerprint” markers of lipid peroxidation, and possibly more reliable than using only one biomarker. Moreover, headspace sampling is not only time efficient but cost effective as well.

To confirm the effectiveness of the developed method, propanal was used as a secondary source of free radicals in the Fenton reaction. Propanal produced ethyl radicals when attacked by hydroxyl radicals. Ethyl radicals were spin trapped by PBN to produce a PBN-diethyl adduct with a molecular ion at  $m/z$  235. To confirm the identity of adduct, deuterated propanal ( $CH_3CD_2CHO$ ) was used in the Fenton reaction. The resulting strong adduct peak (figure 4.2) confirmed the identity of the adduct by showing the shift of 4  $m/z$ . This confirmed the addition of two ethyl radicals to PBN with the molecular ion at  $m/z$  239.

Another very small peak retained at 8.74 minutes (figure 4.1) is identified as N-ethoxy-1-phenyl-1-propanamine. It is not present in any of the control reaction experiments which shows that it is formed via Fenton chemistry. An experiment using d<sub>2</sub>-propanal helped to confirm its identity. Further experiments using other derivatives of PBN as spin traps helped to elucidate the structure of the fragments.

Alongside these two major products, three other peaks, including benzaldehyde, were identified and fully characterised in chapter 4. These results are promising as all major peaks are identified and clearly demonstrate that the developed method may be used effectively for the identification of radical adducts.

In chapter 5, TEMPO & its derivatives were used as spin trapping agents to identify acetaldehyde derived radical adducts by using two different sampling approaches, i.e. TD and SPME. A very strong peak for the TEMPO-CH<sub>3</sub> adduct (molecular ion at  $m/z$  171) was detected when the headspace (HS) was extracted and analysed using TD-GC-MS. To confirm the identity and acetaldehyde as the source of methyl radicals, d<sub>3</sub>-acetaldehyde was used in the Fenton reaction. The molecular ion was seen  $m/z$  174, showing an increase of 3 mass units and thus confirming acetaldehyde as the source of methyl radicals. Further experiments using other derivatives of TEMPO not only confirmed the identity of adduct but also helped to deduce the structure of different fragments.

A very small peak at 13.85 minutes (figure 5.1) is identified as a *tert*-butyl adduct of TEMPO with a molecular ion at  $m/z$  213. The identity of adduct was confirmed when the reaction was carried out by using d<sub>3</sub>-acetaldehyde. The molecular ion showed an increase of 9  $m/z$  units (seen at  $m/z$  222) thus supporting the suggestion of *tert*-butyl addition to TEMPO.

The small peak at 10.07 minutes may be a methyl adduct of 2,2,4,6,6-pentamethylpiperidine with a molecular ion at  $m/z$  185. The identity of this adduct is supported by experiments carried out by using d<sub>3</sub>-acetaldehyde. The molecular ion increases to  $m/z$  191, clearly showing the addition of two methyl radicals. Although it has not been confirmed, the site of addition for the second methyl radical has been suggested and is supported by the fragmentation pattern.

An acetyl adduct was detected when extraction was carried out using the SPME approach. The TEMPO-COCH<sub>3</sub> adduct was observed with a molecular ion at  $m/z$  199 and its identity confirmed when the reaction was carried out using d<sub>3</sub>-acetaldehyde. The molecular ion at  $m/z$  202 shows an increase of 3  $m/z$  thus confirming the detection of acetyl adduct.

Another very small peak at 6.55 minutes is identified as 1-methoxy-2,2,6,6-tetramethyl-1,2,3,6-tetrahydropyridine. A possible mechanism is that methyl adduct of TEMPO loses two hydrogen atoms (a two-step process) to generate suggested adduct. Extra peaks in the chromatogram are detected when the reaction is carried out using 4-methoxy-TEMPO as a trapping agent. Although the structures of these adducts are suggested, their identity is less certain as they are detected with only one spin trap.

## 6.2 Areas of future study

Other chromatographic techniques like liquid chromatography coupled with mass spectrometry can also be used to identify adducts formed during the current project. The most important finding of the work is the successful trapping of methyl and ethyl radicals. Structure and formation of newly suggested adducts can be analysed by using other techniques like NMR.

During the current project, deuterated propanal (CH<sub>3</sub>CD<sub>2</sub>CHO) was used for the confirmation of adducts. In future experiments, other forms of deuterated propanal i.e. CD<sub>3</sub>CH<sub>2</sub>CHO, CD<sub>3</sub>CD<sub>2</sub>CHO and CD<sub>3</sub>CD<sub>2</sub>CDO might be useful for the better understanding of the reaction mechanism, breakdown of propanal and formation of different adducts. This will also help to understand the fragmentation pattern of molecular ion for different adducts. Carbon labelled (<sup>13</sup>C) ethanal and propanal can also be used in future studies which might add something new about formation and fragmentation pattern of spin adducts.

Although the possible mechanism of formation & fragmentation pattern for some new adducts are suggested but it will be worth using perdeuterated TEMPO for a detailed study. This will be of great help to elucidate the structure of different fragments which in turn will be helpful to understand the fragmentation pattern.

After successful *in vitro* studies and characterisation of adducts from acetaldehyde by using two different classes of spin traps, it will be worthwhile to do PBN and TEMPO dose response studies on a different type of cells. In a second phase, it is suggested to study cell lines under oxidative stress (with PBN or TEMPO) and formation of different adducts (characterised during the current project) can be focused which can potentially be used as a biomarker fingerprint for the oxidative stress.



## References

- Abe, K., Suezawa, H., Hirota, M. and Ishii, T. (1984) 'Mass spectrometric determination of spin adducts of hydroxyl and aryl free radicals', *Journal of the Chemical Society, Perkin Transactions* 2(1), 29-34.
- Agelopoulos, N.J and Pickett, J.H. (1998) 'Headspace analysis in chemical ecology: effects of different sampling methods on ratios of volatile compounds present in headspace samples', *J Chem Ecol*, 24, 1161-1171.
- Aikens, J. and Dix, T. (1991) 'Perhydroxyl radical (HOO<sup>•</sup>) initiated lipid peroxidation. The role of fatty acid hydroperoxides', *J. Biol. Chem*, 266(23), 15091-15098.
- Alam, Z.I., Jenner, A., Daniel, S.E., Lees, A.J., Cairns, N., Marsden, C.D., Jenner, P. and Halliwell, B. (1997) 'Oxidative DNA damage in the parkinsonian brain: An apparent selective increase in 8- hydroxyguanine levels in substantia nigra', *Journal of Neurochemistry*, 69(3), 1196-1203.
- Al-Dalaen, S.M. and Al-Qtaitat, A.I. (2014) 'Oxidative stress versus antioxidants', *American Journal of Bioscience and Bioengineering*, 2(5), 60-71.
- Alessio, H.M. and Blasi, E.R. (1997) 'Physical activity as a natural antioxidant booster and its effect on a healthy lifestyle', *Res. Q. Exerc. Sport*, 68 (4), 292-302.
- Alpendurada, M.D. (2000), 'Solid-phase microextraction: a promising technique for sample preparation in environmental analysis', *Journal of Chromatography A*, 889,3-14.
- Anastasi, C. (1983) 'Study of methyl-isobutane reaction in the range  $478 < T/K < 560$ ', *J. Chem. Soc., Faraday Trans*, 79, 741-747.
- Areias, F.M., Rego, A.C., Oliveira, C.R. and Seabra, R.M. (2001) 'Antioxidant effect of flavonoids after ascorbate/Fe<sup>2+</sup>-induced oxidative stress in cultured retinal cells<sup>1</sup>', *Biochemical Pharmacology*, 62(1), 111-118.
- Arlt, S., Beisiegel, U. and Kontush, A. (2002) 'Lipid per- oxidation in neurodegeneration: New insights into Alz- heimer's disease', *Current Opinion in Lipidology*, 13(3), 289- 294.

- Aslan, M. and Ozben, T. (2004) 'Reactive Oxygen and Nitrogen Species in Alzheimer's Disease', *Current Alzheimer Research*, 1(2), 111-119.
- Atamna, H., Paler-Martinez, A. and Ames, B.N. (2000) 'N-t-Butyl Hydroxylamine, a Hydrolysis product of  $\alpha$ -Phenyl-N-t-butyl Nitron, Is More Potent in Delaying Senescence in Human Lung Fibroblasts', *The Journal of Biological Chemistry*, 275, 6741-6748.
- Attri, P., Kim, Y.H., Park, D.H., Hong, Y.J., Uhm, H.S., Fridman, A. and Choi, E.H. (2015) 'Generation mechanism of hydroxyl radical species and its lifetime prediction during the plasma-initiated ultraviolet (UV) photolysis', *Scientific Reports*, 5(9332), 1-8.
- Ayala, A., Munoz, M.F. and Arguelles, S. (2014) 'Lipid peroxidation: production, metabolism and signaling mechanisms of malondialdehyde and 4-hydroxyl-2-nonenal', *Oxidative Medicine and Cellular Longevity*, 1-31.
- Bagchi, K. and Puri, S. (1998) 'Free radicals and antioxidants in health and disease', *Eastern Mediterranean Health Journal*, 4(2), 350-360.
- Baltussen, E., Cramers, C.A. and Sandra, P.J. (2002) 'Sorptive sample preparation- a review', *Anal. Bioanal Chem*, 373(1-2), 3-22.
- Bandebuche, S. and R Melinkeri, R. (2011) 'Oxidative Stress and Antioxidant Status in Patients of Ovarian Cancer', *Biomedical research*, 22(2), 193-197.
- Baradaran, A., Nasri, H., Nematbakhsh, M. and Rafieian-Kopaei, M. (2014) 'Antioxidant activity and preventive effect of aqueous leaf extract of Aloe Vera on gentamicin-induced nephrotoxicity in male Wistar rats', *Clin Ter*, 165(1), 7-11.
- Barciszewski, J., Siboska, G.E, Pedersen, B.O. and Rattan, S.I. (1997) 'Furfural, a Precursor of the Cytokinin Hormone Kinetin, and Base Propenals Are Formed by Hydroxyl Radical Damage of DNA', *Biochemical and Biophysical Research Communications*, 238(2), 317 - 319.

- Barrera, G. (2012) 'Oxidative Stress and Lipid Peroxidation Products in Cancer Progression and Therapy', *Oncology*, 1-21.
- Barrington, J.W., Lindsay, P., James, D., Smith, S. and Roberts, A. (1996) 'Selenium deficiency and miscarriage: A possible link?', *British Journal of Obstetrics and Gynaecology*, 103(2), 130- 132.
- Basu, A.K. and Marnett, L.J. (1983) 'Unequivocal demonstration that malonaldehyde is a mutagen', *Carcinogenesis*, 4(3), 331-333.
- Battaglia, S., den Hertog, H., Timmers, M.C., Lazeroms, S.P., Vignola, A.M., Rabe, K.F., Bellia, V., Hiemstra, P.S. and Sterk, P.J. (2005) 'Small airways function and molecular markers in exhaled air in mild asthma', *Thorax*, 60(8), 639-644.
- Beckman, K.B. and volka, B.N. (1998) 'The free radical theory of ageing matures', *Physiol Rev*, 78(2), 547-581.
- Beevi, S., Rasheed, M.H., and Geetha, A. (2004) 'Evaluation of Oxidative Stress and Nitric Oxide Levels in Patients with Oral Cavity Cancer', *Japanese Journal of Clinical Oncology*, 34(7), 379-385.
- Bekhit, A.A., Hopkins, D.L., Fahri, F.T. and Ponnampalam, E.N. (2013) 'Oxidative Processes in Muscle Systems and Fresh Meat: Sources, Markers, and Remedies', *Comprehensive reviews in food science and food safety*, 12(5), 565-597.
- Beranek, J. and Kubatova, A. (2008) 'Evaluation of solid-phase microextraction methods for determination of trace concentration aldehydes in aqueous solution', *Journal of Chromatography A*, 1209 (1-2), 44-54.
- Bergendi, L., Benes, L., Durackova, Z. and Ferencik, M. (1999) 'Chemistry, physiology and pathology of free radicals', *Life Sci*, 65(18-19), 1865-1874
- Bergh, V.D., Vanhees, I., De Boer, R., Compemolle, F. and Vinckier, C. (2000) 'Identification of the oxidation products of the reaction between  $\alpha$ -pinene and hydroxyl radicals by gas and high-performance liquid chromatography with mass spectrometric detection', *Journal of Chromatography A*, 896(1-2), 135 – 148.

- Berliner, L.J., Khramtsov, V., Clanton, T. and Fujii, H. (2002) 'NMR and MRI spin trapping: using NMR to learn about free radicals', *Current topics in biophysics*, 26(1), 21-27.
- Bhattacharya, S., Ahmed, K.K.M. and Chakraborty, S. (2011) 'Free Radicals Cardiovascular Diseases: An Update', *Free Radicals and Antioxidants*, 1(1), 17-22.
- Blake, R.S., Monks, P.S. and Ellis, A.M. (2009) 'Proton-Transfer Reaction Mass Spectrometry', *Chemical Reviews*, 109(3), 861-896.
- Blum, K. and Payne, J. (1991) 'The Biochemistry of Alcoholism: Early Clues' In *Alcohol and the Addictive Brain* (pp. 102-105). NYC: The Free Press.
- Blumberg, L.M. (2012) 'Theory of Gas chromatography' In *Gas Chromatography*, Chapter 2 (pp. 19-78). Elsevier.
- Bocci, V. and Valacchi, G. (2013) 'Free radicals and antioxidants: How to re-establish redox homeostasis in chronic disease', *Current Medicinal Chemistry*, 20(27), 3397-3415.
- Bojko, B., Cudjoe, E., Gómez-Ríos, G.A., Gorynski, K., Jiang, R., Reyes-Garcés, N. and Risticvic, S. (2012) 'SPME – Quo vadis?', *Analytica Chimica Acta*, 750, 132–151.
- Bojko, B., Vuckovic, D. and Cudjoe, E. (2011) 'Determination of tranexamic acid concentration by solid phase microextraction and liquid chromatography-tandem mass spectrometry: first step to in vivo analysis', *Journal of Chromatography B*, 879(32), 3781-3787.
- Britigan, B. E., Cohen, M. S. and Rosen, G. M. (1987) 'Detection of the production of oxygen-centered free radicals by human neutrophils using spin trapping techniques: a critical perspective', *J Leukoc Biol*, 41(4), 349-62.
- Bryant, R. and McClung, A. (2011) 'Volatile profiles of aromatic and non-aromatic rice cultivars using SPME/GC-MS', *Food Chemistry*, 124 (2), 501–513.

- Buettner, G.R. (1993) 'The spin trapping of superoxide and hydroxyl free radicals with DMPO (5,5-Dimethylpyrroline-N-oxide): More about iron', *Free Radical Research Communications*, 19(1), S79-S87.
- Burkitt, M.J. and Mason, R.P. (1991) 'Direct evidence for in vivo hydroxyl-radical generation in experimental iron overload: An ESR spin-trapping investigation', *Proc Natl Acad Sci*, 88(19), 8440-8444.
- Buszewski, B., Szultka, M., Olszowy, P., Bocian, S. and Ligor, T. (2011) 'A novel approach to the rapid determination of amoxicillin in human plasma by solid phase microextraction and liquid chromatography', *Analyst*, 136(12), 2635-2642.
- Cacho, J.I., Campillo, N., Vinas, P. and Hernandez-Cordoba, M. (2016) 'Gas chromatography-mass spectrometry using microvial insert thermal desorption for the determination of BTEX in edible oils', *RSC Advances*, 6(25), 20886-20891.
- Cadet, J., Douki, T., Gasparutto, D. and Ravanat, J.L. (2003) 'Oxidative damage to DNA: formation, measurement and biochemical features', *Mutation Research/Fundamental and Molecular Mechanisms of Mutagenesis*, 531(1), 5-23.
- Callan, B., Walsh, K. and Dowding, P. (1993) 'Industrial hygiene VOC measurement interference', *Chemistry and Industry*, 5, 250-252.
- Cancilla, D.A. and Quehee, S.S. (1992) 'O-(2,3,4,5,6-Pentafluorophenyl)methylhydroxylamine hydrochloride: a versatile reagent for the determination of carbonyl-containing compounds', *Journal of Chromatography A*, 627(1-2), 1-16.
- Cantin, A.M., North, S.L., Fells, G.A., Hubbard, R.C. and Crystal, R.G. (1987) 'Oxidant-mediated epithelial cell injury in idiopathic pulmonary fibrosis', *Journal of Clinical Investigation*, 79(6), 1665-1673.
- Caris, J.A., Chaves, A.R. and Queiroz, M.E.C. (2012) 'Evaluation of solid-phase microextraction using a polythiophene film and liquid chromatography with spectrophotometric detection for the determination of antidepressants in plasma samples', *Journal of Brazilian Chemical Society*, 23(1), 57-64.

- Carney, J.M., Starke-Reed, P.E., Oliver, C.N., Landum, R.W., Cheng, M.S. and Wu, J.F. (1991) 'Reversal of age-related increase in brain protein oxidation, decrease in enzyme activity, and loss in temporal and spatial memory by chronic administration of the spin-trapping compound N-tert-butyl-alpha-phenylnitron', *Proc Natl Acad Sci U S A*, 88(9), 3633-3636.
- Caro, A. and Puntarulo, S. (1996) 'Effect of in vivo iron supplementation on oxygen radical production by soybean roots', *Biochim Biophys Acta*, 1291(3), 245-51.
- Carr, A.C., Zhu, B.Z. and Frei, B. (2000) 'Potential antiatherogenic mechanisms of ascorbate (vitamin C) and alpha-tocopherol (vitamin E)', *Circ Res*, 87(5), 349-354.
- Carter, J.F., Sleeman, R. and Parry, J. (2003) 'The distribution of controlled drugs on banknotes via counting machines', *Forensic Sci Int*, 132(2), 106-112.
- Castro, G.D., Costantini, M.H. and Castro, J.A. (2009) 'Rat ventral prostate xanthine oxidase-mediated metabolism of acetaldehyde to acetyl radical', *Hum Exp Toxicol*, 28(4), 203-208.
- Castro, J.A. and Castro, G.D. (2002) 'Hydroxyl and 1-hydroxyethyl radical detection by spin trapping and GC-MS', *Methods Mol Biol*, 186, 89-99.
- Chamulitrat, W., Jordan, S.J., Mason, R.P., Saito, K. and Cutler, R.G. (1993) 'Nitric oxide formation during light-induced decomposition of phenyl N-tert-butyl nitron', *Journal of Biological Chemistry*, 268(16), 11520-11527.
- Chance, B., Sies, H. and Boveris, A. (1979) 'Hydroperoxide metabolism in mammalian organs', *Physiological Reviews*, 59(3), 527-605.
- Chen, G., Bray, T.M., Janzen, E.G. and McCay, P.B. (1990) 'Excretion, metabolism and tissue distribution of a spin trapping agent,  $\alpha$ -phenyl-N-tert-butyl-nitron (PBN) in rats', *Free Radical Research*, 9(3-6), 317-323.

- Chen, H., Ying, J., Huang, J. and Liao, L. (2009) 'Dispersive liquid-liquid microextraction followed by high-performance liquid chromatography as an efficient and sensitive technique for simultaneous determination of chloramphenicol and thiamphenicol in honey', *Analytica Chimica Acta*, 632(1), 80-85.
- Cheng-Ping, X., Yong, L. & Min-Jian, L. (2011) 'Thermal desorption-Gas Chromatography/Mass Spectrometric analysis of volatile organic compounds emitted from automobile chair in thermal condition', *Chinese Journal of Analytical Chemistry*, 39(2), 265-268.
- Christian, G.D. (1994) "Chromatographic methods" in Christian, G.C. *Analytical Chemistry* (pp. 505-561), New York: John Wiley & Sons.
- Chromedia.org, (2015). Introduction to Capillary GC injection techniques. - Introduction to Capillary GC injection techniques. - Chromedia. Available at: <http://www.chromedia.org/chromedia?waxtrapp=w1qdcDsHqnOxmOIIecClBwFjE&subNav=rwhpbjDsHqnOxmOIIecClBwFjEQ> [accessed: 06/07/2015]
- Chrysostomou, V., Rezanian, F., Trounce, I.A. and Crowston, J.G. (2013) 'Oxidative stress and mitochondrial dysfunction in glaucoma', *Curr Opin Pharmacol*, 13(1), 12-15.
- Cohen, L.H. and Gusev, A.I. (2002) 'Small molecule analysis by MALDI mass spectrometry', *Anal Bioanal Chem*, 373, 571-586.
- Conger, A.D. and Fairchild, L.M. (1952) 'Breakage of chromosomes by oxygen', *Proceedings of the National Academy of Sciences of the USA*, 38, 289-299.
- Cordis, G.A., Das, D.K. and Riedel, W. (1998) 'High-performance liquid chromatographic peak identification of 2,4-dinitrophenylhydrazine derivatives of lipid peroxidation aldehydes by photodiode array detection', *Journal of Chromatography A*, 798(1), 117-123.
- Cordis, G.A., Maulik, N. and Das, D.K. (1995) 'Detection of oxidative stress in heart by estimating the dinitrophenylhydrazine derivative of malonaldehyde', *Journal of Molecular and Cellular Cardiology*, 27(8), 1645-1653.



- Cui, H., Kong, Y. and Zang, H. (2012) 'Oxidative Stress, Mitochondrial Dysfunction, and Ageing', *J Signal Transduct*, 1-13.
- Curwin, B.D., Deddens, J.A. and McKernan, L.T. (2015) 'Flavoring exposure in food manufacturing', *Journal of exposure science & environmental epidemiology*, 25(3), 324-333.
- Czapski, G. (1984) 'Reaction of  $\cdot OH$ ', in P, Lester (Ed.) *Methods in Enzymology*, Academic Press: Vol. 105, 209-215.
- Dalle-Donne, I., Rossi, R., Colombo, R., Giustarini, D. and Milzani, A. (2006) 'Biomarkers of oxidative damage in human disease', *Clin Chem*, 52, 601-623.
- Dandona. P., Thusu. K., Cook. S., Snyder. B., Makowski. J., Armstrong. D. and Nicotera, T. (1996) 'Oxidative DNA damage diabetes mellitus', *Lancet*, 347(8999), 444-445.
- Dasgupta, A. and Klein, K. (2014) 'Role of Oxidative Stress in Neurodegenerative Diseases and Other Diseases Related to Ageing', *Antioxidants in Food, Vitamins and Supplements*, 167-184.
- Dauchet, L., Amouyel, P. and Dallongeville, J. (2009) 'Fruits, vegetables and coronary heart disease', *Nat Rev Cardiol*, 6(9), 599-608.
- Davies, M.J. (2016a) 'Detection and characterisation of radicals using electron paramagnetic resonance (EPR) spin trapping and related methods', *Methods*, 109, 21-30.
- Davies, M.J. (2016b) 'Protein oxidation and peroxidation', *Biochemical Journal*, 473(7), 805-825.
- DeGraff, W.G., Krishna, M.C., Kaufman, D. and Mitchell, J.B. (1992a) 'Nitroxide-mediated protection against X-ray and neocarzinostatin-induced DNA damage', *Free Radic Biol Med*, 13(5), 479-487.

- Degraff, W.G., Krishna, M.C., Russo, A. and Mitchell, J.B. (1992b) 'Antimutagenicity of a low molecular weight superoxide dismutase mimic against oxidative mutagens', *Environmental and Molecular Mutagenesis*, 19(1), 21-26.
- De Grey, A.D.N.J. (2002) 'H<sub>2</sub>O: the forgotten radical', *DNA Cell Biol*, 21(4), 251-257.
- Deitrich, R., Zimatkin, S. and Pronko, S. (2006) 'Oxidation of ethanol in the brain and its consequences', *Alcohol Research & Health*, 29(4), 266-273.
- Deng, C. and Zhang, X. (2004) 'A simple, rapid and sensitive method for determination of aldehydes in human blood by gas chromatography/mass spectrometry and solid-phase microextraction with on-fiber derivatisation', *Rapid Communications in Mass Spectrometry*, 18(15), 1715-120.
- Devasagayam, T.P., Tilak, J.C., Bloor, K.K., Sane, K.S., Ghaskadbi, S.S. and Lele, R.D. (2004) 'Free radicals and antioxidants in human health: Current status and future prospects', *Journal of the Association of Physicians of India*, 52, 794-804.
- Dhalla, N.S., Temsah, R.M. and Netticadan, T. (2000) 'Role of oxidative stress in cardiovascular diseases', *J Hypertens*, 18(6), 655-673.
- Dietz, C., Sanz, J. and Camara, C. (2006) 'Recent developments in solid-phase microextraction coatings and related techniques', *Journal of Chromatography A*, 1103(2), 183-192.
- Dikalov, S.I. and Mason, R.P. (2001) 'Spin trapping of polyunsaturated fatty acid-derived peroxy radicals: reassignment to alkoxy radical adducts', *Free Radical Biology and Medicine*, 30(2), 187-197.
- Diniz, B.S., Mendes-Silva, A.P., Silva, L.B., Bertola, L., Vieira, M.C., Ferreira, J.D., and Kapczinski, F. (2018) 'Oxidative stress markers imbalance in late-life depression', *Journal of Psychiatric Research*, 102, 29-33.
- Dizdaroglu, M. (1991) 'Chemical determination of free radical-induced damage to DNA', *Free Radic Biol Med*, 10(3-4), 225-42.

- Dizdaroglu, M. and Jaruga, P. (2012) 'Mechanisms of free radical-induced damage to DNA', *Free Radical Research*, 46(4), 382-419.
- Dong, Y., Lu, N. and Cole, R. B. (2013) 'Analysis of the volatile organic compounds in Cinnamomum cassia bark by direct sample introduction thermal desorption gas chromatography–mass spectrometry', *Journal of Essential Oil Research*, 25(6), 458-463.
- Dreissigacker, U., Suchy, M.T., Maassen, N. and Tsikas, D. (2010) 'Human plasma concentrations of malondialdehyde (MDA) and the F<sub>2</sub>-isoprostane 15(S)-8-iso-PGF<sub>2</sub> may be markedly compromised by hemolysis: Evidence by GC-MS/MS and potential analytical and biological ramifications', *Clinical Biochemistry*, 43(1), 159-167.
- Droge, W. (2002) 'Free radicals in the physiological control of cell function', *Physiol Rev*, 82(1), 47-95.
- Durackova, Z. (2010) 'Some current insights into oxidative stress', *Physiol Res*, 59, 459-469.
- Eberson, L. and Persson, O. (1998) "Spin adducts from the reaction between N-phenyl- $\alpha$ -tert-butyl nitron (PBN) and activated olefins. A facile pathway converting PBN into 2-methyl-2-nitrosopropane (MNP)", *Acta Chemica Scandinavica*, 52, 1081-1095.
- Edenberg, H. J. (2007) 'The genetics of alcohol metabolism: Role of alcohol dehydrogenase and aldehyde dehydrogenase variants', *Alcohol Research & Health*, 30(1), 5–13.
- Eggink, M., Wijtmans, M., Ekkebus, R., Lingeman, H., Deesch, I.J., Kool, J., Niessen, W.M. and Irth, H. (2008) 'Development of a selective ESI-MS derivatisation reagent: synthesis and optimization for the analysis of aldehydes in biological mixtures', *Anal Chem*, 80(23), 9042-9051.
- Eggink, M., Wijtmans, M., Kretschmer, A., Kool, J., Lingeman, H., De Esch, I.J.P., Niessen, W.M.A. and Irth, H. (2010) 'Targeted LC-MS derivatisation for aldehydes and carboxylic acids with a new derivatisation agent 4-APEBA', *Analytical and Bioanalytical Chemistry*, 397(2), 665-675.

- El-Samahy, M., Adly, A.A., El-Gindi, H.D. and El-Ghaffar, H.H. (2009) 'The relation between oxidative stress and adhesion molecules in Egyptian children and adolescents with type1 diabetes mellitus', *Egypt. J. Pediatric Allergy Immunol.*, 7(1), 65-77.
- Enoiu, M., Wellman, M., Leroy, P., Ziegler, J.M., Mitrea, N. and Siest, G. (2000) 'Gas and liquid chromatography-mass spectrometry of aldehydic products from lipid peroxidation', *Analisis*, 28(4), 285-290.
- Environmental protection agency (2000) "Acetaldehyde", on the EPA website <<https://www.epa.gov/sites/production/files/2016-09/documents/acetaldehyde.pdf>> [accessed on 26/06/18]
- Eruslanov, E. and Kusmartsev, S. (2009) *Identification of ROS Using Oxidised DCFDA and Flow-Cytometry*. In D. Armstrong (Ed.), *Advanced Protocols in Oxidative Stress II* (pp. 57-72). Totowa, NJ: Humana Press.
- Erzsebet, F., Dumtru, C.M., Ibolya, F. and Daniela-Lucia, M. (2016) 'Is the oxidative stress really a disease?', *Acta Medica Marisiensis*, 62(1), 112-120.
- Ferger, B., Eberjardt, O., Teismann, P., deGroote, C. and Schulz, J.B. (1999) 'Malonate induced generation of reactive oxygen species in rat strium depends on dopamine release but not on NMDA receptor activation', *Journal of Neurochemistry*, 73(3), 1329-1332.
- Fiamegos, Y.C. and Stalikas, C.D. (2007) 'Theoretical analysis and experimental evaluation of headspace in-drop derivatisation single-drop microextraction using aldehydes as model analytes', *Analytica Chimica Acta*, 599(1), 76-83.
- Floyd, R.A. and Carney, J.M. (1992) 'Free radical damage to protein and DNA: mechanisms involved and relevant observations on brain undergoing oxidative stress', *Ann Neurol*, 32, 22-27.
- Floyd, R.A., Kopke, R.D., Choi, C.H., Foster, S.B., Doblaz, S. and Towner, R.A. (2008) 'Nitrones as Therapeutics', *Free Radical Biology & Medicine*, 45(10), 1361-1374.

- Forbes, T.P., Staymates, M. and Sisco, E. (2017) 'Broad spectrum infrared thermal desorption of wipe-based explosive and narcotic samples for trace mass spectrometric detection', *Analyst*, 142(16), 3002-3010.
- Fraga, C.G., Shigenaga, M.K., Park, J. W., Deagan, P. and Ames, B.N. (1990) 'Oxidative damage to DNA during ageing : 8-hydroxy-2- deoxy-guanosine in rat organ DNA and urine', *Proc Natl Acad Sci USA*, 87, 4533-4537.
- Fuchs, P., Loeseken, C., Schubert, J. K. and Miekisch, W. (2010) 'Breath gas aldehydes as biomarkers of lung cancer', *Int J Cancer*, 126(11), 2663-2670.
- Galkin, A.A., Grinberg, O.Y., Dubinskii, A.A., Din, N.N., Krymov, V.N., Kurochkin, V.I., Lebedev, Y.S., Oranskii, L.G. and Shuvalov, V.F. (1997) 'EPR spectrometry in 2-mm range for chemical research', *Instrum, Experim. Tech*, 20(4), pp. 1229-1233.
- Georgieff, K.K. (1966) 'Spontaneous polymerization of acetaldehyde to polyacetaldehyde at close to dry- ice temperature', *Applied Polymer Science*, 10(9), 1305-1313.
- Ghafourifar, P. and Cadenas, E. (2005) 'Mitochondrial nitric oxide synthase', *Trends Pharmacol. Sci*, 26(4), 190-195.
- Ghulam, M., Yeni, E., Kocyigit, A., Taskin, A., Savas, M., Ciftci, H. and Altunkol, A. (2011) 'Sperm DNA damage and seminal oxidative status after shock-wave lithotripsy for distal ureteral stones', *Fertility and Sterility*, 96(5), 1087-1090.
- Gil, L., Siems, W., Mazurek, B., Gross, J., Schroeder, P., Voss, P. and Grune, T. (2006) 'Age-associated analysis of oxidative stress parameters in human plasma and erythrocytes', *Free Radical Research*, 40(5), 495-505.
- Goldring, C., Casini, A.F., Maellaro, E., Del Bello, B. and Comporti, M. (1993) 'Determination of 4-hydroxynonenal by high-performance liquid chromatography with electrochemical detection', *Lipids*, 28(2), 141-145.

- Gordon, S.M., Szidon, J.P., Krotoszynski, B.K., Gibbons, R.D. and O'Neill, H.J. (1985) 'Volatile organic compounds in exhaled air from patients with lung cancer', *Clinical Chemistry*, 31(8), 1278-1282.
- Grabowska-Polanowska, B., Faber, J., Skowron, M., Miarka, P., Pietrzycka, A., Śliwka, I. and Amann, A. (2013) 'Detection of potential chronic kidney disease markers in breath using gas chromatography with mass-spectral detection coupled with thermal desorption method', *Journal of Chromatography A*, 1301, 179-189.
- Griglione, A., Liberto, E., Cordero, C., Bressanello, D., Cagliero, C., Rubiolo, P. and Sgorbini, B. (2015) 'High-quality Italian rice cultivars: Chemical indices of ageing and aroma quality', *Food Chemistry*, 172, 305–313.
- Grob, K. (1997) 'Carrier gases for GC', on the *Restek* website <[http://www.restek.com/Technical-Resources/Technical\\_Library/Editorial/editorial\\_A017](http://www.restek.com/Technical-Resources/Technical_Library/Editorial/editorial_A017)> [accessed: 04/07/2018]
- Grote, A.A. and Kennedy, E.R. (2002) 'Workplace monitoring for volatile organic compounds using thermal desorption-gas chromatography-mass spectrometry', *J Environ Monit*, 4(5), 679-684.
- Gupta, K.R., Kumar Patel, A., Kumari, R., Chugh, S., Srivastava, C., Mehra, S. and Sharma, A. (2012) 'Interactions between Oxidative Stress, Lipid Profile and Antioxidants in Breast Cancer: A Case Control Study', *Asian Pacific Journal of Cancer Prevention*, 13(12), 6295-6298.
- Guzzi, R. and Bartucci, R. (2015) 'Electron spin resonance of spin-labeled assemblies and proteins', *Archives of Biochemistry and Biophysics*, 580, 102-111.
- Hakim, M., Broza, Y.Y., Barash, O., Peled, N., Phillips, M., Amann, A. and Haick, H. (2012) 'Volatile organic compounds of lung cancer and possible biochemical pathways', *Chemical Reviews*, 112(11), 5949-5966.
- Halliwell, B. and Gutteridge, J. (1989). *Free Radicals in Biology and Medicine*. 2nd ed. Oxford: The Clarendon Press.

- Halliwell, B. (1994) 'Free radicals and antioxidants: A personal view', *Nutrition Reviews*, 52(8 pt 1), 253-265.
- Halliwell, B. (1996) 'Antioxidants in Human Health and Disease', *Annual Review of Nutrition*, 16(1), 33-50.
- Halliwell, B. (2001a) 'Role of Free Radicals in the Neurodegenerative Diseases', *Drugs & Ageing*, 18(9), 685-716.
- Halliwell, B. (2001b). *Free Radicals and Other Reactive Species in Disease*. eLS. John Wiley & Sons, Ltd.
- Halliwell, B. and Gutteridge, J. (2007). *Free Radicals in Biology and Medicine*, (4th edition), United States: Oxford University Press.
- Halliwell, B. and Gutteridge, J. (2015). *Free radicals in biology and medicine*, (5<sup>th</sup> edition), Oxford University Press Inc.
- Hashir, M.A., Stecher, G., Rania, B., Kasemosook, S., Blassnig, B., Feuerstein, I., Abel, G., Popp, M., Bobleter, O. and Bonn, G.K. (2007) 'Identification of carbohydrates by matrix-free material-enhanced laser desorption/ionisation mass spectrometry', *Rapid Communication in Mass Spectrometry*, 21, 2759-2769.
- Hebestreit, M (2011), Monitoring Ambient Air by TD and GC/MS on Markes website {[https://www.agilent.com/cs/library/slidepresentation/public/Hebestreit\\_TD\\_AmbientAir.pdf](https://www.agilent.com/cs/library/slidepresentation/public/Hebestreit_TD_AmbientAir.pdf)} [accessed: 07/03/18]
- Heilek, G.M. and Noller, H.F. (1996) 'Site-directed hydroxyl radical probing of the rRNA neighborhood of ribosomal protein S5', *Science*, 272(5268), 1659-1662.
- Herman, D. (1957) 'Prolongation of the normal life span by radiation protection chemicals', *J Gerontol*, 12(3), 257-263.
- Hideg, K., Kálai, T. and Sár, C.P. (2005) 'Recent results in chemistry and biology of nitroxides', *Journal of Heterocyclic Chemistry*, 42(3), 437-450.

- Hietala, J., Tuomi, H., Latvala, J., Anttila, P. and Niemelä, O. (2006) 'IgAs Against Acetaldehyde-Modified Red Cell Protein as a Marker of Ethanol Consumption in Male Alcoholic Subjects, Moderate Drinkers, and Abstainers', *Alcoholism*, 30(10), 1693-1698.
- Hill, W., Miessner, H. and Öhlmann, G. (1989) 'Fourier transform infrared study of the adsorption and of reactions of acetaldehyde on dispersed silica', *J. Chem. Soc., Faraday Trans. 1*, 85(3), 691-697.
- Hinton, R. and Janzen, E. (1992), 'Synthesis and characterization of phenyl-substituted C-phenyl-n-tert-butyl nitrones and some of their radical adducts', *J. Org. Chem*, 57(9), 2646-2651.
- Hipolito, L., Sanchez, M.J., Polache, A. and Granero, L. (2007) 'Brain metabolism of ethanol and alcoholism: An update', *Current Drug Metabolism*, 8(7), 716-726.
- Ho, E., Galougahi, K., Liu., C. and Bhindi, R. (2013) ' Biological markers of oxidative stress: Application to cardiovascular research and practice', *Redox Biology*, 1(1), 483-491.
- Höhn, A., Jung, T. and Grune, T. (2014) 'Pathophysiological importance of aggregated damaged proteins', *Free Radical Biology and Medicine*, 71, 70-89.
- Holley, A.E. and Cheeseman, K.H. (1993) 'Measuring free radical reactions in vivo', *British Medical Bulletin*. 49(3), 494-505.
- Hoshino, Y. and Mishima, M. (2008) 'Antioxidants and redox signalling redox-based therapeutics for lung diseases', *Antioxid Redox Signal*, 10, 701-704.
- Hu, L. and Chen, D.Y. (2009) 'Application of headspace solid phase microextraction for study of noncovalent interaction of borneol with human serum albumin', *Acta Pharmacologica Sinica*, 30(14), 1573-1576.
- Huang, X. (2003) 'Iron overload and its association with cancer risk in humans: evidence for iron as a carcinogenic metal', *Mutat Res*, 533(1-2), 153-171.



- Huilian, M., Jing, J., Yun, L. and Chen, J. (2017) 'Target and non-target screening of volatile organic compounds in industrial exhaust gas using thermal desorption-gas chromatography-mass spectrometry', *Chinese Journal of Chromatography*, 35(10), 1094-1099.
- Imlay, J.A. (2003) 'Pathways of Oxidative Damage', *Annual Review of Microbiology*, 57, 395-418.
- Inoue, M., Sato, E.F., Nishikawa, M., Park, A.M., Kira, Y., Imada, I. and Utsumi, K. (2003) 'Mitochondrial generation of reactive oxygen species and its role in aerobic life', *Curr. Med. Chem*, 10(23), 2495-2505.
- Ireland, J.C. and Valinieks, J. (1992) 'Rapid measurement of aqueous hydroxyl radical concentrations in steady-state •OH flux systems', *Chemosphere*, 25(3), 383-396.
- Iwahashi, H., Nishizaki, K. and Takagi, I. (2002) 'Detection of the radical and reduced forms of  $\alpha$ - (4- pyridyl 1- oxide)- N- tert- butylnitron/pentyl radical adduct formed on reaction of an oxidised linoleic acid with ferrous ions using high performance liquid chromatography with electrochemical detection', *Journal of Separation Science*, 25(9), 601-607.
- Iwahashi, H., Parker, C.E., Mason, R.P. and Tomer, K.B. (1990) 'Radical identification by liquid chromatography/thermospray mass spectrometry', *Rapid Communications in Mass Spectrometry*, 4(9), 352-354.
- Iwahashi, H., Parker, C.E., Mason, R.P. and Tomer, K.B. (1991) "Radical adducts of nitrosobenzene and 2-methyl-2-nitrosopropane with 12,13-epoxylinoleic acid radical, 12,13-epoxylinolenic acid radical and 14,15-epoxyarachidonic acid radical", *Biochemical Journal*, 276(2), 447-453.
- Izzotti, A., Bagnis, A. and Sacca, S.C. (2006) 'The role of oxidative stress in glaucoma', *Mutation Res*, 612(2), 105-114.
- Jackson, A.L. and Loeb, L.A. (2001) 'The contribution of endogenous sources of DNA damage to the multiple mutations in cancer', *Mutation Research - Fundamental and Molecular Mechanisms of Mutagenesis*, 477(1-2), 7-21.

- Janzen, E.J. and Blackburn, B.J. (1968) 'Detection and identification of short-lived free radicals by an electron spin resonance trapping technique', *J. Am. Chem. Soc.*, 90(21), 5909-5910.
- Janzen, E.G. (1971) 'Spin trapping', *Acc. Chem. Res.*, 4(1), 31-40.
- Janzen, E.G., Krygsman, P.H. and Haire, D.L. (1988) 'The application of gas chromatographic/mass spectrometric techniques to spin trapping. Conversion of  $\alpha$ -phenyl N-tert-butyl nitron (PBN) spin adducts to stable trimethylsilylated derivatives', *Biological Mass Spectrometry*, 15(2), 111-116.
- Janzen, E.G., Krygsman, P.H., Lindsay, D.A. and Haire, D.L. (1990) "Detection of Alkyl, Alkoxy, and Alkylperoxy Radicals from the Thermolysis of Azobis(isobutyronitrile) by ESR /Spin Trapping. Evidence for Double Spin Adducts from Liquid-Phase Chromatography and Mass Spectroscopy", *J. Am. Chem. Soc.*, 112(23), 8279-8284.
- Janzen, E.G. and Nutter, D.E. (1998) 'Spin trapping chemistry of Iminyl free radicals', *Magnetic Resonance in Chemistry*, 35(2), 131-140.
- Janzen, E.G., Weber, J.R., Haire, D.L. and Fung, D.M. (1985) 'Gas Chromatography - Mass Spectroscopy (GC/MS) of Single and Double Spin Adducts of PBN and the Hydroxylamines of Corresponding Structure', *Analytical Letters*, 18(14), 1749-1757.
- Jelen, H.H., Majcher, M. and Dziadas, M. (2012) 'Microextraction techniques in the analysis of food flavour compounds: a review', *Analitica Chimica Acta*, 738, 13-26.
- Jenkins, C.A., Murphy, D.M., Rowlands, C.C. and Egerton, T.A. (1997) 'EPR study of spin-trapped free radical intermediates formed in the heterogeneously-assisted photodecomposition of acetaldehyde', *Journal of the Chemical Society, Perkin Transactions*, 2(12), 2479-2486.
- Jenuwain, T. and Allis, C.D. (2001) 'Translating the histone code', *Science*, 293(5532), 1074-1080.

- Jerzykiewicz, M., Ćwieląg-Piasecka, I., Witwicki, M. and Jeziński, A. (2011) 'α-Tocopherol impact on oxy-radical induced free radical decomposition of DMSO: Spin trapping EPR and theoretical studies', *Chemical Physics*, 383(1), 27-34.
- Jin, K. (2010) 'Modern Biological Theories of Ageing', *Ageing Dis*, 1(2), 72-74.
- Jing, Z., Hao-Yang, W. and Yin-Long, G. (2005) 'Amino Acids Analysis by MALDI Mass Spectrometry Using Carbon Nanotube as Matrix', *Chinese Journal of Chemistry*, 23, 185-189.
- Johansen, J.S., Harris, A.K., Rychly, D.J. and Ergul, A. (2005) 'Oxidative stress and the use of antioxidants in diabetes: Linking basic science to clinical practice', *Cardiovasc. Diabetol.*, 4(5), 1-11.
- Jones, G.P. (2000) 'Evaluation of a Fully Automated Thermal Desorption Device for the Headspace Screening of Fire Debris', *Canadian Society of Forensic Science Journal*, 33(2), pages 55-60.
- Juillet, Y., Dubois, C., Bintein, F., Dissard, J. and Bossee, A. (2014) 'Development and validation of a sensitive thermal desorption-gas chromatography-mass spectrometry (TD-GC-MS) method for the determination of phosgene in air samples', *Anal Bioanal Chem*, 406(21), 5137-5145.
- Juricic, M.A., Berríos-Cárcamo, P.A., Acevedo, M.L., Israel, Y., Almodóvar, I. and Cassels, B.K. (2012). 'Salsolinolandisosalsolinol:condensation products of acetaldehyde and dopamine. Separation of their enantiomers in the presence of a large excess of dopamine', *J.Pharm. Biomed.Anal*, 63, 170–174.
- Kálai, T., Kuppusamy, M.L., Balog, M., Selvendiran, K., Rivera, B.K., Kuppusamy, P. and Hideg, K. (2011) 'Synthesis of N-substituted 3,5-bis(arylidene)-4-piperidones with high antitumor and antioxidant activity', *J. Med.Chem*, 54(15), 5414–5421.
- Kanno, T., Nakamura, K., Ikai, H., Kikuchi, K., Sasaki, K. and Niwano, Y. (2012) 'Literature review of the role of hydroxyl radicals in chemically-induced mutagenicity and carcinogenicity for the risk assessment of a disinfection system utilizing

- photolysis of hydrogen peroxide', *Journal of Clinical Biochemistry and Nutrition*, 51(1), 9-14.
- Kataoka, H. (2010) 'Recent developments and applications of microextraction techniques in drug analysis', *Analytical and Bioanalytical Chemistry*, 396 (1), 339-364.
- Kato, S., Burke, P.J., Koch, T.H. and Bierbaum, V.M. (2001) 'Formalehyde in human cancer cells: Detection by preconcentration-chemical ionisation mass spectrometry', *Analytical Chemistry*, 73(13), 2992-2997.
- Kaur, J., Kukreja, S., Kaur, A., Malhotra, N. and Kaur, A. (2012) 'The oxidative stress in cataract patients', *J Clin Diagn Res*, 6(10), 1629-1632.
- Kawai, Y., Takeda, S. and Terao, J. (2007) 'Lipodemic analysis for lipid peroxidation-derived aldehydes using gas chromatography-mass spectrometry', *Chem Res Toxicol*, 20(1), 99-107.
- Kennedy, C.H., Hatch, G.E., Slade, R. and Mason, R.P. (1992) 'Application of the EPR spin-trapping technique to the detection of radicals produced in vivo during inhalation exposure of rats to ozone', *Toxicol Appl Pharmacol*, 114(1), 41-46.
- Khan, M.A., Tania, M., Zhang, D. and Chen, H. (2010) 'Antioxidant enzymes and cancer', *Chinese Journal of Cancer Research*, 22(2), 87-92.
- Khanna, J.M. and Israel, Y. (1980) 'Ethanolmetabolism', *Int.Rev Physiol*, 21, 275-315.
- Khramtsov, V., Berliner, L.J. and Clanton, T.L. (1999) 'NMR spin trapping: Detection of free radical reactions using a phosphorus- containing nitrene spin trap', *Magnetic Resonance in Medicine*, 42(2), 228-234.
- Khramtsov, V. and Clanton, T.L. (2011) 'NMR Spin Trapping: Insight into the Hidden Life of Free Radical Adducts', *Applied Magnetic Resonance*, 41(2), 305-323.
- Kim, J.K., Kim, Y.J., Fillmore, J.J., Chen, Y., Moore, I., Lee, J. and Shulman, G.I. (2001) 'Prevention of fat-induced insulin resistance by salicylate', *The Journal of Clinical Investigation*, 108(3), 437-446.

- Kirkbride, K.P., Klass, G. and Pigou, P.E. (1998) 'Application of solid-phase microextraction to the recovery of organic explosives', *J. Forensic Sci*, 43(1), 76-81.
- Kissner, R., Nauser, T., Bugnon, P., Lye, P.G. and Koppenol, W.H. (1997) 'Formation and Properties of Peroxynitrite as Studied by Laser Flash Photolysis, High-Pressure Stopped-Flow Technique, and Pulse Radiolysis', *Chemical Research in Toxicology*, 10(11), 1285-1292.
- Klaunig, J.E., Kamendulis, L.M. (2004) 'The role of oxidative stress in carcinogenesis', *Annual Review of Pharmacology and Toxicology*, 44, 239-267.
- Klaunig, J.E., Xu, Y., Bachowski, S. and Jiang, J. (1997). *Free Radical Toxicology*. K.B. Wallace, London: Taylor and Francis.
- Klaunig, J.E., Xu, Y., Isenberg, J.S., Bachowski, S., Kolaja, K.L., Jiang, J., Stevenson, D.E., Walborg Jr., E.F. (1998) 'The role of oxidative stress in chemical carcinogenesis', *Environmental Health Perspectives*, 106(1), 289-295.
- Koenig, A., Bügler, J., Kirsch, D., Köhler, F. and Weyermann, C. (2014) 'Ink Dating Using Thermal Desorption and Gas Chromatography/Mass Spectrometry: Comparison of Results Obtained in Two Laboratories', *Journal of Forensic Sciences*, 60(S1), S152-S161.
- Koning, S.D., Janssen, H. and Brinkman, U. (2009) 'Modern Methods of Sample Preparation for GC Analysis', *Chromatographia*, 69, S33-S78.
- Kotake, Y. and Janzen, E. (1991) 'Decay and fate of the hydroxyl radical adduct of alpha-phenyl-n-tert-butyl nitron in aqueous media', *J. Am. Chem. Soc.*, 113(25), 9503-9506.
- Kristensson, J. and Widen, M. (1987) '*Development and evaluation of a diffusive sampler for measurements of anaesthetic gases*' In Diffusive sampling – an alternative approach to workplace air monitoring (Eds.) (pp. 423–426), RSC Publication.

- Krogh, M., Grefslie, H. and Rasmussen, K.E. (1997) 'Solvent-modified solid-phase microextraction for the determination of diazepam in human plasma samples by capillary gas chromatography', *Journal of Chromatography B*, 689(2), 357-364.
- Kuanglin, Y., Liqiong, L., Xiayi, Z., Xiaohua, X. and Yujuan, C. (2013) 'Progress of sample preparation techniques in gas chromatographic analysis', *Chinese Journal of Chromatography*, 31(7), 634-639.
- Kushch, I., Schwarz, K., Schwenter, L., Baumann, B., Dzien, A., Schmid, A. and Amann, A. (2008) 'Compounds enhanced in a mass spectrometric profile of smokers, exhaled breath versus non-smokers as determined in a pilot study using PTR-MS', *J Breath Res*, 2(2).
- Kumar, H., Lim, H.W., More, S.V., Kim, B.W., Koppula, S., Kim, I.S. and Choi, D.K. (2012) 'The role of free radicals in the ageing brain and Parkinson's disease: convergence and parallelism', *Int J Mol Sci*, 13(8), 10478-10504.
- Kuroda, S., Tsuchidate, R., Smith, M.L., Maples, K.R. and Siesjo, B.K. (1999) 'Neuroprotective effects of a novel nitrone, NXY-059, after transient focal cerebral ischemia in the rat', *J Cereb Blood Flow Metab*, 19(7), 778-787.
- Lagercrantz, C. (1971) 'Spin trapping of some short-lived radicals by the nitroxides method', *J. Phys. Chem*, 75, 3466-3475.
- Laguerre, M., Mestres, C., Davrieux, F., Ringuet, J. and Boulanger, R. (2007) 'Rapid discrimination of scented rice by solid-phase microextraction, mass spectrometry, and multivariate analysis used as a mass sensor', *Journal of Agricultural and Food Chemistry*, 55 (4), 1077-1083.
- Lam, M.A., Pattison, D.I., Bottle, S.E., Keddie, D J. and Davies, M.J. (2008) 'Nitric oxide and nitroxides can act as efficient scavengers of protein-derived free radicals', *Chem. Res. Toxicol*, 21(11), 2111-2119.
- Lee, H.S., Lee, H.J., Yu, H.J., Ju do, W., Kim, Y., Kim, C.T. and Suh, H.J. (2011) 'A comparison between high hydrostatic pressure extraction and heat extraction of

- ginsenosides from ginseng (*Panax ginseng* CA Meyer)', *J Sci Food Agric*, 91(8), 1466-1473.
- Lee, J., Koo, N. and Min, D.B. (2004) 'Reactive Oxygen Species, Ageing, and Antioxidative Nutraceuticals', *Comprehensive Reviews in Food Science and Food Safety*, 3(1), 21-33.
- Lemarechal, H., Allanore, Y., Chenevier-Gobeaux, C., Ekindjian, O.G., Kahan, A. and Borderie, D. (2006) 'High redox thioredoxin but low thioredoxin reductase activities in the serum of patients with rheumatoid arthritis', *Clinica Chimica Acta*, 367(1-2), 156-161.
- Lemire, J.A., Harrison, J.J. and Turner, R.J. (2013) 'Antimicrobial activity of metals: mechanisms, molecular targets and applications', *Nat Rev Micro*, 11(6), 371-384.
- Li, F., Arimura, H., Suzuki, K., Shiraishi, J., Li, Q., Abe, H., Engelmann, R., Sone, S., Macmahon, H. and Doi, K. (2005a) 'Computer-aided detection of peripheral lung cancers missed at CT: ROC analyses without and with localization', *Radiology*, 237(2), 648-690.
- Li, H., Cui, S., Wang, S., Jiang, X., Zhang, S., Zhang, R. and Sun, X. (2015) 'Ultrasensitive UPLC–MS/MS method for analysis of etheno-DNA adducts in human white blood cells', *Free Radical Research*, 49(9), 1049-1054.
- Li, J., Wuliji, O., Li, W., Jiang, Z. and Ghanbari, H.A. (2013) 'Oxidative stress and neurodegenerative disorders', *Int. J. Mol. Sci*, 14 (12), 24438-24475.
- Li, N., Deng, C., Yin, X., Yao, N., Shen, X. and Zhang, X. (2005b) 'Gas chromatography-mass spectrometric analysis of hexanal and heptanal in human blood by headspace single-drop microextraction with droplet derivatisation', *Analytical Biochemistry*, 342(2), 318-326.
- Li, X. (2010) 'EPA method 524 for determination of VOCs in drinking water using Agilent 5975TLTM GC MSD with static headspace' on the EPA website <<http://hpst.cz/sites/default/files/attachments/5990-6442en-epa-method-524->

[determination-vocs-drinking-water-using-agilent-5975t-ltm-gc-msd-static.pdf](#)>

[accessed on 03/07/18].

Li, Y., Liu, K. and Chen, F. (2016) 'Effect of selenium enrichment on the quality of germinated brown rice during storage', *Food Chemistry*, 207, 20–26.

Life sciences mass spectrometry facility. (2008) 'Gas chromatography mass spectrometry GC/MS', Retrieved 3rd May 2015, from <<http://www.bris.ac.uk/nerclsmsf/techniques/gcms.html>> [accessed on 5/7/18]

Likhtenshtein, G., Yamauchi, J., Nakatsuji, S., Smirnov, A.I. and Tamura, R. (2008) '*Nitroxides: applications in chemistry, biomedicine, and materials Science*', Wiley-VCH, Weinheim, Germany.

Lili, L., Xu, H., Song, D., Cui, Y., Hu, S. and Zhang, G. (2010) 'Analysis of volatile aldehyde biomarkers in human blood by derivatisation and dispersive liquid-liquid microextraction based on solidification of floating organic droplet method by high performance liquid chromatography', *Journal of Chromatography A*, 1217(16), 2365-2370.

Lin, W.W. and Karin, M. (2007) 'A cytokine-mediated link between innate immunity, inflammation, and cancer', *J. Clin. Invest.*, 117(5), 1175-1183.

Lindholm, P.C., Knuutinen, J.S., Ahkola, H.S.J. and Herve, S.H. (2014) 'Analysis of trace Pharmaceuticals and related compounds in municipal waste waters by pre-concentration, chromatography, derivatisation and separation methods, Analysis of Pharmaceuticals', *BioResources*, 9(2), 3688-3732.

Lipinski, B. (2011) 'Hydroxyl radical and its scavengers in health and disease', *Oxidative Medicine and Cellular Longevity*, 1-9.

Liu, J., Yeo, H. C., Doniger, S.J. and Ames, B.N. (1997) 'Assay of aldehydes from lipid peroxidation: gas chromatography-mass spectrometry compared to thiobarbituric acid', *Anal Biochem*, 245(2), 161-166.



- Liu, Y., Liu, X., Zhong, F., Tian, R., Zhang, K., Zhang, X. and Li, T. (2011) 'Comparative study of phenolic compounds and antioxidant activity in different species of cherries', *Journal of Food Science*, 76(4), C633-C638.
- Loft, S., Poulsen, H.E. (1996) 'Cancer risk and oxidative DNA damage in man', *Journal of Molecular Medicine*, 74(6), 297-312.
- Lona-Ramirez, F.J., Gonzalez-Alatorre, G., Rico-Ramírez, V., Perez-Perez, M.C. and Castrejón-González, E.O. (2016) 'Gas chromatography/mass spectrometry for the determination of nitrosamines in red wine', *Food Chemistry*, 196, 1131–1136.
- Looi, M. L., Zailani Hatta Mohd Dali, A., Md Ali, S., Wan Ngah, W.Z. and Mohd Yusof, Y. (2008) 'Oxidative damage and antioxidant status in patients with cervical intraepithelial neoplasia and carcinoma of the cervix', *European Journal of Cancer Prevention*, 17(6), 555-560.
- Lord, H. and Pawliszyn, J. (2000) 'Evolution of solid-phase microextraction technology', *J. Chromatogr. A*, 885, 153-193.
- Lowe, F. (2014). *Biomarkers of Oxidative Stress*. In I. Laher (Ed.), *Systems Biology of Free Radicals and Antioxidants* (pp. 65-87). Berlin, Heidelberg: Springer Berlin Heidelberg.
- Łuczaj, W., Gindzienska-Sieskiewicz, E., Jarocka-Karpowicz, I., Andrisic, L., Sierakowski, S., Zarkovic, N., Waeg, G. and Skrzydlewska, E. (2016) 'The onset of lipid peroxidation in rheumatoid arthritis: consequences and monitoring', *Free Radical Research*, 50(3), 304-313.
- Luks-Betlej, K., Popp, P., Janoszka, B. and Paschke, H. (2001) 'Solid phase microextraction of phthalates from water', *J. Chromatogr A*, 938 (1-2), 93-101.
- Luo, F., Wu, Z., Tao, P. and Cong, Y. (2009) 'Preparation by low temperature nonthermal plasma of graphite fiber and its characteristics for solid-phase microextraction', *Analytica Chimica Acta*, 631(1), 62-68.

- Lushchak, V. (2014) 'Free radicals, reactive oxygen species, oxidative stress and its classification', *Chem Biol Interact*, 224, 164-175.
- Lykkesfeldt, J. (2012) 'Ascorbate and dehydroascorbic acid as biomarkers of oxidative stress: validity of clinical data depends on vacutainer system used', *Nutrition Research*, 32(1), 66-69.
- Makino, K., Moriya, F. Hatano, H. (1985) 'Separation of free radicals by high-performance liquid chromatography with electron spin resonance detection', *Journal of Chromatography*, 332, 71-106.
- Makker, K., Agarwal, A. and Sharma, R. (2009) 'Oxidative stress and male infertility', *Indian Journal of Medical Research*, 129(4), 357-367.
- Marrocco, I., Altieri, F. and Peluso, I. (2017) 'Measurement and clinical significance of biomarkers of oxidative stress in humans', *Oxidative medicine and cellular longevity*, 1-33.
- Mastaloudis, A., Leonard, S.W. and Traber, M.G. (2001) 'Oxidative stress in athletes during extreme endurance exercise', *Free Radic Biol Med*, 31(7), 911-922.
- Mateen, S., Moin, S., Khan, A.Q., Zafar, A. and Fatima, N. (2016) 'Increased reactive oxygen species formation and oxidative stress in rheumatoid arthritis', *PLoS One*, 11, 1-15.
- Mattson, M.P. (2004) 'Metal-catalyzed disruption of membrane protein and lipid signaling in the pathogenesis of neurodegenerative disorders', *Ann N Y Acad Sci*, 1012, 37-50.
- Maynard, S, M., Schurman, S.H., Harboe, C., De Souza-Pinto, N.C. and Bohr, V.A. (2009) 'Base excision repair of oxidative DNA damage and association with cancer and ageing', *Carcinogenesis*, 30(1), 2-10.
- McConnell, H. M. (1976). *Spin Labeling: Theory and Applications*. Berliner, L., editor. New York: Academic Press.

- McIntyre, T.M. and Hazen, S.L. (2010) 'Lipid Oxidation and Cardiovascular Disease: Introduction to a Review Series', *Circulation research*, 107, 1167-1169.
- McMillan, J.A. (1961) 'Electron Paramagnetic Resonance of free radicals', *Journal of chemical education*, 38(9), 438-440.
- Melin, V., Henriquez, A., Freer, J. and Contreras, D. (2015) 'Reactivity of catecholamine driven Fenton reaction and its relationship with iron (III) speciation', *Redox report*, 20(2), 89-96.
- Menezo, Y.J.R., Silvestris, E., Dale, B. and Elder, K. (2016) 'Oxidative stress and alterations in DNA methylation: two sides of the same coin in reproduction', *Reproductive biomedicine online*, 33(6), 668-683.
- Merkle, S., Kleeberg, K.K. and Fritsche, J. (2015) 'Recent Developments and Application of Solid Phase Microextraction (SPME) in Food and Environmental Analysis: A Review', *Chromatography*, 2, 293-381.
- Mezey, E. (1976) 'Ethanol metabolism and ethanol-druginteractions', *Biochem.Pharmacol*, 25, 869-875.
- Mikami, N., Takahashi, N., Yamada, H. and Miyamoto, J. (1985) 'Separation and identification of short lived free radicals formed by photolysis of the pyrethroid insecticide fenvalerate', *Pesticide Science*, 16(2), 101-112.
- Milevoj Kopčinović, L., Domijan, A.M., Posavac, K., Čepelak, I., Žanić Grubišić, T. and Rumora, L. (2016) 'Systemic redox imbalance in stable chronic obstructive pulmonary disease', *Biomarkers*, 21(8), 692-698.
- Miller, D.M., Buettner, G.R., and Aust, S.D. (1990) 'Transition metals as catalysts of autoxidation reactions', *Free Radic. Biol. Med.*, 8(1), 95-108.
- Mishra, S.S. (2016) 'Detection and analysis of spin trapped radical adduct by using a phenyl-*tert*-butyl nitron (PBN) derivatives and GC/MS', *PhD*. UK: University of Salford.

- Mistry, P., Najim, N., Purdie, A. and Podmore, I. (2008) 'Indirect detection of hydroxyl radicals using spin trapping and gas chromatography-mass spectrometry', *Journal of Chemical Research*, 7, 395-397.
- Mitchell, J.B., Samuni, A., Krishna, M.C., DeGraff, W.G., Ahn, M.S., Samuni, U. and Russo, A. (1990) 'Biologically active metal-independent superoxide dismutase mimics', *Biochemistry*, 29(11), 2802-2807.
- Miura, Y., Utsumi, H. and Hamada, A. (1993) 'Antioxidant activity of nitroxide radicals in lipid peroxidation of rat liver microsomes', *Archives of Biochemistry and Biophysics*, 300(1), 148-156.
- Miyajima, T. and Kotake, Y. (1995) 'Spin Trapping Agent, Phenyl N-tertbutyl Nitron (PBN) Inhibits Induction of Nitric Oxide Synthase in Endotoxin-Induced Shock in Mice', *Biochemical and Biophysical Research Communications*, 215(1), 114-121.
- Mizukami, S., Ichimura, R., Kemmochi, S., Wang, L., Taniai, E., Mitsumori, K. and Shibutani, M. (2010) 'Tumor promotion by copper-overloading and its enhancement by excess iron accumulation involving oxidative stress responses in the early stage of a rat two-stage hepatocarcinogenesis model', *Chem Biol Interact*, 185(3), 189-201.
- Moinfar, S. and Hosseini, M.R.M. (2009) 'Development of dispersive liquid-liquid microextraction method for the analysis of organophosphorus pesticides in tea', *Journal of Hazardous Materials*, 169(1-3), 907-911.
- Monteleone, M., Naccarato, A., Sindona, G. and Tagarelli, A. (2012) 'A rapid and sensitive assay of perfluorocarboxylic acids in aqueous matrices by headspace solid phase microextraction-gas chromatography-triple quadrupole mass spectrometry', *Journal of Chromatography A*, 1251, 160-168.
- Montine, T.J., Beal, M.F., Robertson, D., Cudkowicz, M.E., Biaggioni, I., O'Donnell, H., Zackert, W.E., Robers, L.J. and Morrow, J.D. (1999) 'Cerebrospinal fluid F<sub>2</sub>-isoprostanes are elevated in Huntington's disease', *Neurology*, 52(5), 1104-1105.

- Montuschi, P., Ciabattoni, G., Paredi, P., Pantelidis, P., du Bois, R.M. (1998) '8-Isoprostane as a biomarker of oxidative stress in interstitial lung diseases', *American Journal of Respiratory and Critical Care Medicine*, 158, 1524-1527.
- Morrison, A. and Davies, A. P. (1970) 'Mass spectrometry of piperidine nitroxides- A class of stable free radicals', *Organic Mass Spectrometry*, 3, 353-366.
- Murano, N., Ishizaki, M., Sato, S., Fukuda, Y., Takahashi, H. (2008) 'Corneal Endothelial Cell Damage by Free Radicals Associated With Ultrasound Oscillation', *Arch Ophthalmol*, 126(6), 816-821.
- Musarrat, J., Arezina-Wilson, J. and Wani, A.A. (1996) 'Prognostic and aetiological relevance of 8-hydroxyguanosine in human breast carcinogenesis', *Eur. J. Cancer*, 32A(7), 1209-1214.
- Musshoff, F. (2002) 'Chromatographic methods for the determination of markers of chronic and acute alcohol consumption', *Journal of Chromatography B*, 781(1), 457-480.
- Naccarato, A., Gionfriddo, E., Sindona, G. and Tagarelli, A. (2014) 'Simultaneous determination of benzothiazoles, benzotriazoles and benzosulfonamides by solid phase microextraction-gas chromatography-triple quadrupole mass spectrometry in environmental aqueous matrices and human urine', *Journal of Chromatography A*, 1338, 164-173.
- Naccarato, A. and Pawliszyn, J. (2016) 'Matrix compatible solid phase microextraction coating, a greener approach to sample preparation in vegetable matrices', *Food Chemistry*, 206, 67-73.
- Nakamura, T. and Lipton, S.A. (2007) 'Molecular mechanisms of nitrosative stress-mediated protein misfolding in neurodegenerative diseases', *Cellular and Molecular Life Sciences*, 64(13), 1609-1620.
- Nakao, L., Kadiiska, M., Mason, R., Grijalba, M. and Augusto, O. (2000) 'Metabolism of acetaldehyde to methyl and acetyl radicals: *in vitro* and *in vivo* electron paramagnetic resonance spin-trapping studies', *Free Radic Biol*, 29(8), 721-729.

- Nakao, L.S., Ouchi, D. and Augusto, O. (1999) 'Oxidation of acetaldehyde by peroxy nitrite and hydrogen Peroxide/Iron(II). Production Of acetate, formate, and methyl radicals', *Chem Res Toxicology*, 12(10), 1010-1018.
- Nasri, H. and Rafieian-Kopaei, M. (2014) 'Protective effects of herbal antioxidants on diabetic kidney disease', *J Res Med Sci*, 19(1), 82–83.
- Natarajan, K., Mathialagan Gokila, D., Raghavan, S. and Shanmugam, N. (2015) 'The advanced lipoxidation end product precursor malondialdehyde induces IL-17E expression and skews lymphocytes to the Th17 subset', *Cellular and Molecular Biology Letters*, 20(4), 647-662.
- Negre-Salvayre, A., Auge, N., Ayala, V., Basaga, H., Boada, J., Brenke, R. and Zarkovic, N. (2010) 'Pathological aspects of lipid peroxidation', *Free Radical Research*, 44(10), 1125-1171.
- Nerin, C., Salafranca, J., Aznar, M. and Batlle, R. (2009) 'Critical review on recent developments in solventless techniques for extraction of analytes', *Anal Bioanal Chem*. 393, 809-833.
- Niki, E. (2014) 'Biomarkers of lipid peroxidation in clinical material', *Biochimica et Biophysica Acta (BBA) - General Subjects*, 1840(2), 809-817.
- Niki, E. (2018) 'Oxidant-Specific Biomarkers of Oxidative Stress. Association with Atherosclerosis and Implication for Antioxidant Effects', *Free Radical Biology and Medicine*, In Press, Accepted manuscript. <https://doi.org/10.1016/j.freeradbiomed.2018.04.001>
- Nikolova, G. (2012) 'Oxidative stress and Parkinson disease', *Trakia Journal of Sciences*, 10(1), 92-100.
- Ortiz de Montellano, P.R., Augusto, O., Viola, F. and Kunze, K.L. (1983) 'Carbon radicals in the metabolism of alkyl hydrazines', *Journal of Biological Chemistry*, 258(14), 8623-8629.
- Paakkari, I. and Lindsberg, P. (1995) 'Nitric oxide in the central nervous system', *Annals of Medicine*, 27(3), 369-377.

- Panchenko, A., Dilger, H., Kerres, J., Hein, M., Ullrich, A., Kaz, T. and Roduner, E. (2004) 'In-situ spin trap electron paramagnetic resonance study of fuel cell processes', *Physical Chemistry Chemical Physics*, 6(11), 2891-2894.
- Parker, C.E., Iwahashi, H. and Tomer, K.B. (1991) 'Spin-trapped radicals: determination by LC-TSP-MS and LC-ESI-MS', *Journal of the American Society for Mass Spectrometry*, 2(5), 413 – 418.
- Patel, R.P., McAndrew, J., Sellak, H., White, C.R., Jo, H., Freeman, B.A. and Darley-Usmar, V.M. (1999) 'Biological aspects of reactive nitrogen species', *Biochim Biophys Acta*, 1411(2-3), 385-400.
- Penalver, A., Pocurull, E., Borrull, F. and Marce, R.M. (1999) 'Trends in solid-phase microextraction for determining organic pollutants in environmental samples', *TrAC Trends in Analytical Chemistry*, 18, 557-568.
- Pena-Pereira, F., Kloskowski, A. and Namiesnik, J. (2015) 'Perspectives on the replacement of harmful organic solvents in analytical methodologies: A framework toward the implementation of a generation of eco-friendly alternatives', *Green Chemistry*, 17 (7), 3687–3705.
- Perry, G., Nunomura, A., Hirai, K., Zhu, X., Prez, M. and Avila, J. (2002) 'Is oxidative damage the fundamental pathogenic mechanism of Alzheimer's and other neurodegenerative diseases?', *Free Radical Biology and Medicine*, 33(11), 1475-1479.
- Petersen, A.B., Gniadecki, R., Vicanova, J., Thorn, T. and Wulf, H.C. (2000) 'Hydrogen peroxide is responsible for UVA-induced DNA damage measured by alkaline comet assay in HaCaT keratinocytes', *J Photochem Photobiol B*, 59(1-3), 123-131.
- Pham-Huy, L. A., He, H. and Pham-Huy, C. (2008) 'Free Radicals, Antioxidants in Disease and Health', *International Journal of Biomedical Science : IJBS*, 4(2), 89-96.
- Phillips, M. (1992) 'Breath tests in medicine', *Sci Am*, 267(1), 74-79.

- Phull, A., Nasir, B., Haq, I. and Kim, S.J. (2018) 'Oxidative stress, consequences and ROS mediated cellular signaling in rheumatoid arthritis', *Chemico-Biological Interactions*, 281, 121-136.
- Pillai, A.K.K.V., Gautam, K., Jain, A. and Verma, K.K. (2009) 'Headspace in-drop derivatisation of carbonyl compounds for their analysis by high-performance liquid chromatography-diode array detection', *Analytical Chimica Acta*, 632(2), 208-215.
- Plant, N. and Keen, C. (2007) 'Application of Thermal Desorption to Occupational Exposure Monitoring' on the PerkinElmer website [http://www.perkinelmer.co.uk/lab-solutions/resources/docs/APP\\_IndustrialHygieneMonitoringbyTD.pdf](http://www.perkinelmer.co.uk/lab-solutions/resources/docs/APP_IndustrialHygieneMonitoringbyTD.pdf) [accessed: 07/03/18]
- Podhaisky, H.P., Abate, A., Polte, T., Oberle, S. and Schröder, H. (1997) 'Aspirin protects endothelial cells from oxidative stress – possible synergism with vitamin E', *FEBS Letters*, 417(3), 349-351.
- Podmore, I., Cunliffe, L. and Heshmati, M. (2013) 'Rapid detection of free radicals using spin trapping and MALDI-TOF mass spectrometry', *Journal of chemical research*, 37(1), 45-47.
- Poli, G., Leonarduzzi, G., Biasi, F. and Chiarotto, E. (2004) 'Oxidative stress and cell signalling', *Curr Med Chem*, 11(9), 1163-1182.
- Potts, R.J., Newbury, C.J., Smith, G., Notarianni, L.J. and Jefferies, T.M. (1999) 'Sperm chromatin damage associated with male smoking', *Mutation Research*, 423(1-2), 103-111.
- Powell, S.R. and Hall, D. (1990) 'Use of salicylate as a probe for .OH formation in isolated ischemic rat hearts', *Free Radic Biol Med*, 9(2), 133-141.
- Poyton, R.O., Ball, K.A. and Castello, P.R. (2009) 'Mitochondrial generation of free radicals and hypoxic signalling', *Trends in Endocrinology and Metabolism*. 20(7), 332-340.
- Pragst, F. (2007) 'Application of solid-phase microextraction in analytical toxicology', *Analytical and Bioanalytical Chemistry*, 388(7), 339-364.



- Proctor, P.H and Reynolds, E.S. (1984) 'Free radicals and diseases in man', *Physiological Chemistry and Physics and Medical NMR*, 16, 175-195.
- Psillakis, E. and Kalogerakis, N. (2001) 'Solid-phase microextraction versus single drop microextraction for the analysis of nitroaromatic explosives in water samples', *J. Chromatogr, A*, 938 (1-2), 113-120.
- Pyo, S.H., Hedström, M., Lundmark, S., Rehnberg, N. and Hatti-Kaul, R. (2011) 'Self- and Cross-Aldol Condensation of Propanal Catalyzed by Anion-Exchange Resins in Aqueous Media', *Organic Process Research & Development*, 15(3), 631-637.
- Pysanenko, A., Španěl, P. and Smith, D. (2009) 'Analysis of the isobaric compounds propanol, acetic acid and methyl formate in humid air and breath by selected ion flow tube mass spectrometry, SIFT-MS', *International Journal of Mass Spectrometry*, 285(1), 42-48.
- Quertemont, E. and Didone, V. (2006) 'Role of acetaldehyde in mediating the pharmacological and behavioral effects of alcohol', *Alcohol Research & Health*, 29(4), 258-265.
- Rabaud, N.E., Ebeler, S.E., Ashbaugh, L.L. and Flocchini, R.G. (2002) 'The Application of Thermal Desorption GC/MS with Simultaneous Olfactory Evaluation for the Characterization and Quantification of Odor Compounds from a Dairy', *Journal of Agricultural and Food Chemistry*, 50(18), 5139-5145.
- Rahal, A., Kumar, A., Singh, V., Yadav, B., Tiwari, R., Chakaraborty, S. and Dhama, K. (2014) 'Oxidative stress, Prooxidants and Antioxidants: The Interplay', *BioMed Research international*, 1-19.
- Rahman, I. (2003) 'Oxidative stress, chromatin remodeling and gene transcription in inflammation and chronic lung diseases', *Journal of Biochemistry and Molecular Biology*, 36(1), 95-109.
- Rahman, T., Hosen, I., Islam, M.M.T. and Shekhar, H.U. (2012) 'Oxidative stress and human health', *Advances in Bioscience and Biotechnology*, 3, 997-1019.

- Rajabi, A. A., Yamini, Y., Faraji, M. and Seidi, S. (2013) 'Solid-phase microextraction based on cetyltrimethylammonium of antidepressants from biological fluids', *Medicinal Chemistry Research*, 22(4), 1570-1577.
- Ras, M.R., Marce, R.M. and Borrull, F. (2009) 'Characterization of ozone precursor volatile organic compounds in urban atmospheres and around the petrochemical industry in the Tarragona region', *Sci Total Environ*, 407(14), 4312-4319.
- Rattan, S.I.S. (2006) 'Theories of biological ageing: Genes, proteins, and free radicals', *Free Radical Research*, 40(12), 1230-1238.
- Rawlinson, C., Martin, S., Frosina, J. and Wright, C. (2017) 'Chemical characterisation of aerosols emitted by electronic cigarettes using thermal desorption–gas chromatography–time of flight mass spectrometry', *Journal of Chromatography A*, 1497, 144-154.
- Reed, T.T. (2011) 'Lipid peroxidation and neurodegenerative disease', *Free Radical Biology and Medicine*, 21(7), 1302-1319.
- Rendon-Ramirez, A. (2014) 'Alcoholism: Common and oxidative damage biomarkers', *J Clin Toxicol*, 1-8.
- Reuter, S., Gupta, S.C., Chaturvedi, M.M. and Aggarwal, B.B. (2010) 'Oxidative stress, inflammation, and cancer: How are they linked?', *Free Radic Biol Med*, 49(11), 1603-1616.
- Rezaee, M., Assadi, Y., Milani hosseini, M.R., Aghaee, E., Ahmadi, F. and Berijani, S. (2006) 'Determination of organic compounds in water using dispersive liquid-liquid microextraction', *Journal of Chromatography A*, 1116(1-2), 1-9.
- Rezaee, M., Yamini, Y. and Faraji, M. (2010) 'Evolution of dispersive liquid-liquid microextraction method', *Journal of Chromatography A*, 1217(16), 2342-2357.

- Rezaei, F., Bidari, A., Birjandi, A.P., Milani hosseini, M.R. and Assadi, Y. (2008) 'Development of a dispersive liquid-liquid microextraction method for the determination of polychlorinated biphenyls in water', *Journal of Hazardous Materials*, 158(2-3), 621-627.
- Reznick, A.Z. and Packer, L. (1994) 'Oxidative damage to proteins: spectrophotometric method for carbonyl assay', *Methods Enzymol*, 233, 357-363.
- Riley, P.A. (1994) 'Free radicals in biology: oxidative stress and the effects of ionizing radiation', *Int J Radiat Biol*, 65, 27-33.
- Romano, A., Capozzi, V., Spano, G. and Biasioli, F. (2015) 'Proton transfer reaction–mass spectrometry: online and rapid determination of volatile organic compounds of microbial origin', *Applied Microbiology and Biotechnology*, 99(9), 3787-3795.
- Rosen, G.M. and Rauckman, E.J. (1981) 'Spin trapping of free radicals during hepatic microsomal lipid peroxidation', *Proc Natl Acad Sci*, 78(12), 7346-7349.
- Rosselin, M., Tuccio, B., Pério, P., Villamena, F.A., Fabre, P.L. and Durand, G. (2016) 'Electrochemical and Spin-Trapping Properties of para-substituted  $\alpha$ -Phenyl-N-tert-butyl Nitrones', *Electrochimica Acta*, 193, 231-239.
- Ruan, E.D., Aalhus, J.L., Juárez, M. and Sabik, H. (2015) 'Analysis of Volatile and Flavor Compounds in Grilled Lean Beef by Stir Bar Sorptive Extraction and Thermal Desorption—Gas Chromatography Mass Spectrometry', *Food Analytical Methods*, 8(2), 363-370.
- Saito, K. and Cutler, R.G. (1995) 'Nitron spin-traps release nitric oxide reaction with reactive oxygen species: Possible mechanism of biological activity'. *Oxidative Stress and Ageing*, Basel, Birkhäuser Basel, 379-386.
- Samuni, A., Mitchell, J.B., DeGraff, W., Krishna, C.M., Samuni, U. and Russo, A. (1991) 'Nitroxide SOD-mimics: modes of action', *Free Radic Res Commun*, 12–13(Pt 1), 187–194.

- Samuni, A., Samuni, A. and Swartz, H.M. (1989) 'The cellular induced decay of DMPO spin adducts of  $\cdot\text{OH}$  and  $\cdot\text{O}_2$ ', *Free Radic Biol Med*, 6(2), 179-183.
- Sarma, A.D., Mallick, A.R. and Ghosh, A.K. (2010) 'Free radicals and their role in different clinical conditions: An overview', *International Journal of Pharma Sciences and Research*, 1(3), 185-192.
- Saugstad, O.D. (2000) 'Therapy in free radical disease in the newborn', *Current Obstetrics and Gynaecology*, 10(2), 103-108.
- Savareear, B., Brokl, M., Wright, C. and Focant, J.F. (2017) 'Thermal desorption comprehensive two-dimensional gas chromatography coupled to time of flight mass spectrometry for vapour phase mainstream tobacco smoke analysis', *Journal of Chromatography A*, 1525, 126-137.
- Schacker, M., Foth, H., Schluter, J. and Kahl, R. (1991) 'Oxidation of tris to one-carbon compounds in a radical-producing model system, in microsomes, in hepatocytes and in rats', *Free Radic Res Commun*, 11(6), 339-347.
- Schlatter, J., Chiadmi, F., Gandon, V. and Chariot, P. (2014) 'Simultaneous determination of methanol, acetaldehyde, acetone, and ethanol in human blood by gas chromatography with flame ionisation detection', *Human & Experimental Toxicology*, 33(1), 74-80.
- Schmarr, H.J., Postouridis, T., Ganb, S., Sang, W., Kopp, B., Bokuz, U. and Fischer, U. (2008) 'Analysis of carbonyl compounds via headspace solid-phase microextraction with on-fiber derivatisation and gas chromatographic-ion trap tandem mass spectrometric determination of their O-(2,3,4,5,6-pentafluorobenzyl)oxime derivatives', *Analytica Chimica Acta*, 617(1-2), 119-131.
- Schmidt, E. (1997) 'Fatty acids and risk of coronary heart disease', *Danish Medical Bulletin*, 44(1), 1-22.
- Schmidt, K. and Podmore, I. (2015) 'Current Challenges in Volatile Organic Compounds Analysis as Potential Biomarkers of Cancer', *Journal of Biomarkers*, 1-16.

- Seitz, H.K. and Becker, P. (2007) 'Alcohol metabolism and cancer risk', *Alcohol Research & Health*, 30(1), 38–47.
- Seitz, H.K. and Stickel, F. (2007) 'Molecular mechanisms of alcohol-mediated carcinogenesis', *Nature Reviews Cancer*, 7(8), 599-612.
- Seppanen, C.M. and Csallany, A.S. (2001) 'Simultaneous determination of lipophilic aldehydes by high-performance liquid chromatography in vegetable oil', *Journal of the American Oil Chemists' Society*, 78(12), 1253-1260.
- Shaker, E.S. (2006) 'Antioxidative effect of extracts from red grape seed and peel on lipid oxidation in oils of sunflower', *LWT - Food Science and Technology*, 39(8), 883-892.
- Sharma, S., Shrivastav, A. and Shrivastav, B.R. (2014) 'Clinical evidences of oxidative stress as a biomarker in various types of cancer: A review', *International Journal of Pharmaceutical Sciences and Research*, 5(3), 657-665.
- Shenker, N. and Flanagan, M. (2012) 'Intragenic DNA methylation: implications of this epigenetic mechanism for cancer research', *British Journal of Cancer*, 106, 248-253.
- Shigenaga, M.K., Hagen, T.M. and Ames, B.N. (1994) 'Oxidative damage and mitochondrial decay in ageing' *Proceedings of the National Academy of Sciences of the USA*, 91(23), 10771-10778.
- Shin, H.S. (2009) 'Determination of malondialdehyde in human blood by headspace-solid phase micro-extraction gas chromatography-mass spectrometry after derivatisation with 2,2,2-trifluoroethylhydrazine', *Journal of Chromatography B: Analytical technologies in the Biomedical and Life Sciences*, 877(29), 3707-3711.
- Shu, Y., Wu, X., Tong, X., Wang, X., Chang, Z., Mao, Y., Chen, X., Sun, J., Wang, Z., Hong, Z., Zhu, L., Zhu, C., Chen, J., Liang, Y., Shao, H. and Shao, Y.W. (2017) 'Circulating Tumor DNA Mutation Profiling by Targeted Next Generation Sequencing Provides Guidance for Personalized Treatments in Multiple Cancer Types', *Scientific Reports*, 7(583), 1-11.

- Sies, H. (1985). 'Oxidative stress: Introductory Remarks' In *Oxidative Stress* (pp 1-7). London: Academic Press.
- Sies, H. (1991) 'Oxidative stress: from basic research to clinical application', *Am J Med*, 91(3c), 31s-38s.
- Simm, A. and Bromme, H. (2005) 'Reactive oxygen species (ROS) and ageing: Do we need them- can we measure them-should we block them?', *Signal Transduction*, 5, 115-125.
- Simonian, N.A. and Coyle, J.T. (1996) 'Oxidative stress in neurodegenerative diseases', *Annu Rev Pharmacol Toxicol*, 36, 83-106.
- Sipowicz, M.A., Chomarat, P., Diwan, B.A., Anver, M.A., Awasthi, Y.C., Ward, J.M., Rice, J.M., Kasprzak, K.S., Wild, C.P. and Anderson, L.M. (1997) 'Increased oxidative DNA damage and hepatocyte over expression of specific cytochrome P450 isoforms in hepatitis of mice infected with helicobacter hepaticus', *Am J Pathol*, 151(4), 933-941.
- Sivanandham, V. (2011) 'Free radicals in health and diseases, A mini review', *Pharmacologyonline 1*, 1062-1077.
- Smith, C.D., Bartley, J.P., Bottle, S.E., Micallef, A.S. and Reid, D.A. (2000) 'Electrospray ionisation mass spectrometry of stable nitroxides free radicals and two isoindoline nitroxides dimers', *Journal of Mass Spectrometry*, 35, 607-611.
- Somogyi, A., Rosta, K., Pusztai, P., Tulassay, Z and Nagy, Z. (2007) 'Antioxidant measurements', *Physiological Measurement*, 28(4), R41.
- Sosa, V., Molinéa, T., Somozaa, R., Paciuccib, R., Kondohc, H. and Leonart, M.E. (2013) 'Oxidative stress and cancer: An overview', *Ageing Research Reviews*, 12(1), 376-390.
- Soule, B.P., Hyodo, F., Matsumoto, K., Simone, N.L., Cook, J.A., Krishna, M.C. and Mitchell, J.B. (2007) 'The chemistry and biology of nitroxide compounds', *Free Radic Biol Med*, 42(11), 1632-1650.

- Sousa, B.C., Pitt, A.R. and Spickett, C.M. (2017) 'Chemistry and analysis of HNE and other prominent carbonyl-containing lipid oxidation compounds', *Free Radical Biology and Medicine*, 111, 294-308.
- Spietelun, A., Pilarczyk, M., Kloskowski, A. and Namiesnik, J. (2010) 'Current trends in solid-phase microextraction (SPME) fibre coatings', *Chem Soc Rev*, 39(11), 4524-4537.
- Spulber, M., and Schlick, S. (2010) 'Using Cyclodextrins to Encapsulate Oxygen-Centered and Carbon-Centered Radical Adducts: The Case of DMPO, PBN, and MNP Spin Traps', *The Journal of Physical Chemistry A*, 114(21), 6217-6225.
- Stadtman, E.R. and Levine, R.L. (2003) 'Free radical-mediated oxidation of free amino acids and amino acid residues in proteins', *Amino Acids*, 25(3), 207-218.
- Stashenko, E.E., Puertas, M.A., Salgar, W., Delgado, W. and Martínez, J.R. (2000) 'Solid-phase microextraction with on-fibre derivatisation applied to the analysis of volatile carbonyl compounds', *Journal of Chromatography A*, 886(1-2), 175-181.
- Steinberg, D. (1997) 'Low density lipoprotein oxidation and its pathological significance', *The Journal of Biological Chemistry*, 272(34), 20963-20966.
- Ste-Marie, L., Boismenu, D., Vachon, L. and Montgomery, J. (1996) 'Evaluation of sodium 4-hydroxybenzoate as hydroxyl radical trap using gas chromatography-mass spectrometry and high-performance liquid chromatography with electrochemical detection', *Anal Biochem*, 241(1), 67-74.
- Steven, Q.Y., Yi, X. and Yan, G. (2012) 'Combination of Spin trapping, LC/ESR and LC/MS technique in characterization of PUFA-derived free radicals in lipid peroxidation', *Acta Biophysica sinica*, 28(5), 355-372.
- Stolze, K., Udilova, N. and Nohl, H. (2000) 'Lipid radicals: properties and detection by spin trapping', *Acta biochimica Polonica*, 47(4), 923-930.
- Storz, P. (2005) 'Reactive oxygen species in tumour progression', *Frontiers in biosciences*, 10(2), 1881-1896.

- Suezawa, H., Abe, K., Hirota, M. and Ishii, T. (1981) 'Mass Spectrometric determination of spin adducts in Spin trapping technique', *Chemistry Letters*, 10(7), 1049-1052.
- Sultana, R., Perluigi, M. and Butterfield, D.A. (2006) 'Protein Oxidation and Lipid Peroxidation in Brain of Subjects with Alzheimer's disease: Insights into Mechanism of Neurodegeneration from Redox Proteomics', *Antioxidants & Redox Signaling*, 8(11-12), 2021-2037.
- Sun, J.G., Jurisicova, A. and Casper, R.F. (1997) 'Detection of deoxyribonucleic acid fragmentation in human sperm: Correlation with fertilization in vitro', *Biology of Reproduction*, 56(3), 602-607.
- Surai, P.F. and Dvorska, J.E. (2007) 'Strategies to enhance antioxidant protection and implications for the wellbeing of companion animals', <https://en.engormix.com/pets/articles/strategies-enhance-antioxidant-protection-t33671.htm> {accessed on 04/04/2018}.
- Suto, D., Ikeda, Y., Fujii, J. and Ohba, Y. (2006) 'Structural Analysis of Amino Acids, Oxidised by Reactive Oxygen Species and an Antibody against N-Formylkynurenine', *J Clin. Biochem. Nutr*, 38(2), 1-5.
- Swartz, H.M., Khan, N. and Khramtsov, V.V. (2007) 'Use of electron paramagnetic resonance spectroscopy to evaluate the redox state in vivo', *Antioxid Redox Signal*, 9(10), 1757-1771.
- Takahashi, S., Takahashi, I., Sato, H., Kubota, Y., Yoshida, S. and Muramatsu, Y. (2001) 'Age-related changes in the concentrations of major and trace elements in the brain of rats and mice', *Biol Trace Elem Res*, 80(2), 145-158.
- Tavafi, M. (2013) 'Complexity of diabetic nephropathy pathogenesis and design of investigations', *J Renal Inj Prev*, 2(1), 59-62.
- Themann, C., Teismann, P., Kuschinsky, K. and Fergert, B. (2001) 'Comparison of two independent aromatic hydroxylation assays in combination with intracerebral microdialysis to determine hydroxyl free radicals', *Journal of Neuroscience Methods*, 108(1), 57-64.



- Tian, Y.W., Sun, S.H., Xie, J.P., Zong, Y.L., Nie, C. and Guo, Y.L. (2007) 'Detection of Radical Adducts with Small Molecular Weights by Matrix-Assisted Laser Desorption/Ionisation with Fourier Transform Mass Spectrometry', *Chinese Journal of Chemistry*, 25(8), 1139-1144.
- Toyokuni, S. (1996) 'Iron-induced carcinogenesis: the role of redox regulation', *Free Radic Biol Med*, 20(4), 553-566.
- Tring, W. (2018) 'Vac Aero International Inc', < <https://vacaero.com/information-resources/vacuum-pump-technology-education-and-training/153727-five-main-reasons-for-using-vacuum.html> > [accessed: 4/7/18]
- Trinity, J.D., Broxterman, R.M. and Richardson, R.S. (2016) 'Regulation of Exercise Blood Flow: Role of Free Radicals', *Free Radic Biol Med*, 98, 90-102.
- Truss, C.O. (1984) 'Metabolic Abnormalities in Patients with Chronic Candidiasis: The Acetaldehyde Hypothesis', *J Orthomolecular Psychiatry*, 13(2), 66-93.
- Tsuboi, K.K., Thompson, D.J., Rush, E.M. and Schwartz, H.C. (1981) 'Acetaldehyde-Dependent Changes in Hemoglobin and Oxygen Affinity of Human Erythrocytes', *Hemoglobin*, 5(3), 241-50.
- Turnbull, S., Tabner, B.J., El-Agnaf, O.M.A., Twyman, L.J. and Allsop, D. (2001) 'New evidence that the Alzheimer  $\beta$ -amyloid peptide does not spontaneously form free radicals: An ESR study using a series of spin-traps', *Free Radical Biology and Medicine*, 30(10), 1154-1162.
- Turner, R.N. (1996) 'Free radicals and disease: the toxemia hypothesis', *Complementary Therapies in Medicine*. 4(1), 43-47.
- Uttara, B., Singh, A.V., Zamboni, P. and Mahajan, R.T. (2009) 'Oxidative Stress and Neurodegenerative Diseases: A Review of Upstream and Downstream Antioxidant Therapeutic Options', *Current Neuropharmacology*, 7(1), 65-74.

- Vandenberk, S. and Peeters, J. (2003) “The reaction of acetaldehyde and propionaldehyde with hydroxyl radicals: experimental determination of the primary H<sub>2</sub>O yield at room temperature”, *Journal of Photochemistry and Photobiology A: Chemistry*, 157(2-3), 269-274.
- Van Ruth, S.M., Roozen, J.P. and Jansen, F.J. (2000) ‘Aroma profiles of vegetable oils varying in fatty acid composition vs. concentrations of primary and secondary lipid oxidation products’, *Nahrung*, 44(5), 318-322.
- Velavan, S., Nagulendran, K., Mahesh, R. and Begum, V.H. (2007) ‘*In vitro* antioxidant activity of *Asparagus racemosus* root’, *Pharmacognosy Magazine*, 3(9), 26-33.
- Valentova, K. and Ulrichova, J. (2003) ‘*Smilax officinalis* and *Lepidium meyenii* prospective Andean crops for the prevention of chronic diseases’, *Biomedical papers*, 147(2), 119-130.
- Van 't Erve, T.J., Kadiiska, M.B., London, S.J. and Mason, R.P. (2017) ‘Classifying oxidative stress by F<sub>2</sub>-isoprostane levels across human diseases: A meta-analysis’, *Redox Biol*, 12, 582-599.
- Vas, G. and Vekey, K. (2004) ‘Solid-phase microextraction: A powerful sample preparation tool prior to mass spectrometric analysis’, *J Mass Spectrom*, 39, 233-254.
- Vidal, M.J.L., Plaza-Bolanos, P., Romero-Gonzales, R. and Frenich, A.G. (2009) ‘Determination of pesticide transformation products: a review of extraction and detection methods’, *Journal of Chromatography A*, 1216 (40), 6767-6788.
- Vinna, J., Gomez-Cabera, M.C., Lloret, A., Marquez, R., Minana, J.B., Pallardo, F.V. and Sastre, J. (2008) “Free Radicals in Exhaustive Physical Exercise: Mechanism of Production, and protection by Antioxidants”, *IUBMB Life*, 50(4-5), 271-277.
- Vinson, J.A. (2006) ‘Review of oxidative stress in cataracts. *Pathophysiology*’, 13(151-162).
- Vita, M., Abdel-Rehim, M. and Nilsson, C. (2005) ‘Stability, pKa and plasma protein binding of roscovitine’, *Journal of Chromatography B*, 821(1), 75-80.

- Vogt, P.K. and Bos, T.J. (1990) 'jun: oncogene and transcription factor', *Adv Cancer Res*, 55, 1-35.
- Volka, M., Leibfritz, D., Moncol, J., Cronin, M. T., Mazur, M. and Telser, J. (2007) 'Free radicals and antioxidants in normal physiological functions and human disease', *Int J Biochem Cell Biol*, 39(1), 44-84.
- Vonlaufen, A., Wilson, J.S., Pirola, R.C. and Apte, M.V. (2007) 'Role of alcohol metabolism in chronic pancreatitis', *Alcohol Research & Health*, 30(1), 38-54.
- Voulgaridou, G., Anestopoulos, I., Franco, R., Panayiotidis, M.I. and Pappa, A. (2011) 'DNA damage induced by endogenous aldehydes: current state of knowledge', *Mutation Research/Fundamental and Molecular Mechanisms of Mutagenesis*, 711(1-2), 13-27.
- Vu, D.C., Ho, T., Vo, P.H., Carlo, G., McElroy, J.A., Davis, A.N. and Lin, C.H. (2018) 'Determination of volatile organic compounds in child care centers by thermal desorption gas chromatography-mass spectrometry', *Analytical Methods*, 10(7), 730-742.
- Walker, J.R., Fairfull-Smith, K.E., Anzai, K., Lau, S., White, P.J., Scammells, P.J. and Bottle, S.E. (2011) 'Edaravone containing isoindoline nitroxides for the potential treatment of cardiovascular ischaemia', *Med. Chem. Commun*, 436-441.
- Wang, D., Wang, J., Liu, Y., Zhao, Z., Liu, Q. (2016) 'Roles of Chinese herbal medicines in ischemic heart diseases (IHD) by regulating oxidative stress', *International Journal of Cardiology*, 220, 314-319.
- Wang, F., Lei, L. and Wu, L. (2005) 'NO spin trapping and EPR studies on the photochemistry of aliphatic aldehydes', *Magn Reson Chem*, 43(2), 156-165.
- Webb, C.B. (2013). 'Antioxidant drugs' In *Canine and Feline Gastroenterology* (pp 477-480). Elsevier: St. Louis, Missouri.

- Wei, T., Chen, C., Hou, J., Xin, W. and Mori, A. (2000) 'Nitric oxide induces oxidative stress and apoptosis in neuronal cells', *Biochimica et Biophysica Acta (BBA)-Molecular Cell Research*, 1498(1), 72-79.
- Woolfenden, E. (2012). Chapter 10 - *Thermal Desorption for Gas Chromatography A2* - Poole, Colin F. In *Gas Chromatography* (pp. 235-289). Amsterdam: Elsevier.
- Woolfenden, E. (2010) 'Sorbent-based sampling methods for volatile and semi-volatile organic compounds in air. Part 2. Sorbent selection and other aspects of optimizing air monitoring methods', *Journal of Chromatography A*, 1217(16), 2685-2694.
- Xu, Y., Gu, Y. and Qian, S.Y. (2012) 'An advanced Electron Spin Resonance (ESR) spin-trapping and LC/(ESR)/MS technique for the study of lipid peroxidation', *Int J Mol Sci*, 13(11), 14648-14666.
- Yildirim, Z., Ucgun, N.I., Tildirim, F. (2011) 'The role of oxidative stress and antioxidants in the pathogenesis of age-related macular degeneration', *Clinics*, 66(5):743-746.
- Young, I.S. (2001) 'Measurement of total antioxidant capacity', *Journal of Clinical Pathology*, 54(5), 339.
- Yu, B P. (1994) 'Cellular defences against damage from reactive oxygen species', *Physiological reviews*, 76, 139-162.
- Yue Qian, S., Kadiiska, M.B., Guo, Q. and Mason, R.P. (2005) 'A novel protocol to identify and quantify all spin trapped free radicals from in vitro/in vivo interaction of HO.- and DMSO: LC/ESR, LC/MS, and dual spin trapping combinations', *Free Radic Biol Med*, 38(1), 125-35.
- Zakhari, S. (2006) 'Overview: How is alcohol metabolized by the body?', *Alcohol Research & Health*, 29(4), 245-254.
- Zelzer, S., Mangge, H., Oberreither, R., Bernecker, C., Gruber, H. J., Prüller, F. and Fauler, G. (2015) 'Oxidative stress: Determination of 4-hydroxy-2-nonenal by gas

- chromatography/mass spectrometry in human and rat plasma', *Free Radical Research*, 49(10), 1233-1238.
- Zeng, Z., Zhang, H., Chen, J. Y., Zhang, T. and Matsunaga, R. (2008) 'Flavor volatiles of rice during cooking analyzed by modified headspace SPME/GC-MS', *Cereal Chemistry*, 85 (2), 140–145.
- Zhang, X., Li, S.Y., Brown, R. A. and Ren, J. (2004) 'Ethanol and acetaldehyde in alcoholic cardiomyopathy: from bad to ugly en route to oxidative stress', *Alcohol*, 32(3), 175-186.
- Zhang, X., Liao, Y., Qian, R., Wang, H. and Guo, Y. (2005) 'Investigation of Radical Cation in Electrophilic Fluorination by ESI-MS', *Organic Letters*, 7(18), 3877-3880.
- Zhang, X., Wang, H. and Guo, Y. (2006) 'Interception of the radicals produced in electrophilic fluorination with radical traps (Tempo, Dmpo) studied by electrospray ionisation mass spectrometry', *Rapid Communications in Mass Spectrometry*, 20(12), 1877-1882.
- Zhang, Y.K., and Maples, K.R. (2002) 'Synthesis and EPR Evaluation of the Nitron PBN-[*tert*-<sup>13</sup>C] for Spin Trapping Competition', *Zeitschrift fur naturforschung B*, 57(1), 127-131.
- Zhao, Z., Ni, M., Li, X. and Buekens, A. (2016) 'Thermal desorption for remediating PCB-contaminated soil', *International Journal of Environment and Pollution*, 60(1-4), 171-189.
- Zhang, Z. and Pawliszyn, J. (1993) 'Headspace solid-phase microextraction', *Analytical Chemistry*, 65(14), 1843-1852.
- Ziegler, D.V., Wiley, C.D. and Velarde, M.C. (2015) 'Mitochondrial effectors of cellular senescence: beyond the free radical theory of ageing', *Ageing Cell*, 14(1), 1-7.
- Zielonka, J., Gębicki, J., and Gryniewicz, G. (2003) 'Radical scavenging properties of genistein', *Free Radical Biology and Medicine*, 35(8), 958-965.

- Zimatkin, S.M., Pronko, S.P., Vasiliou, V., Gonzalez, F.J. and Deitrich, R.A. (2006) 'Enzymatic mechanisms of ethanoloxidation in the brain', *Alcohol.Clin.Exp.Res*, 30, 1500–1505.
- Zinellu, E., Zinellu, A., Fois, A.G., Carru, C. and Pirina, P. (2016) 'Circulating biomarkers of oxidative stress in chronic obstructive pulmonary disease: a systematic review', *Respiratory Research*, 17(1), 150-160.
- Zoia, L. and Argyropoulos, D.S. (2010) 'Detection of ketyl radicals using  $^{31}\text{P}$  NMR spin trapping', *Journal of Physical Organic Chemistry*, 23(6), 505-512.
- Zoia, L., Perazzini, R., Crestini, C. and Argyropoulos, D.S. (2011) 'Understanding the radical mechanism of lipoxygenases using  $^{31}\text{P}$  NMR spin trapping', *Bioorganic & Medicinal Chemistry*, 19(9), 3022-3028.
- Zukiel, R., Nowak, S., Barciszewska, A. and Barciszewska, M.Z. (2004) 'A simple epigenetic method for the diagnosis and classification of brain tumors', *Molecular Cancer Research*, 2(3), 196-202.

# Appendix

## Fenton reaction with $d_3$ -acetaldehyde $\{CD_3C(H)O\}$ and $d_6$ -PBN

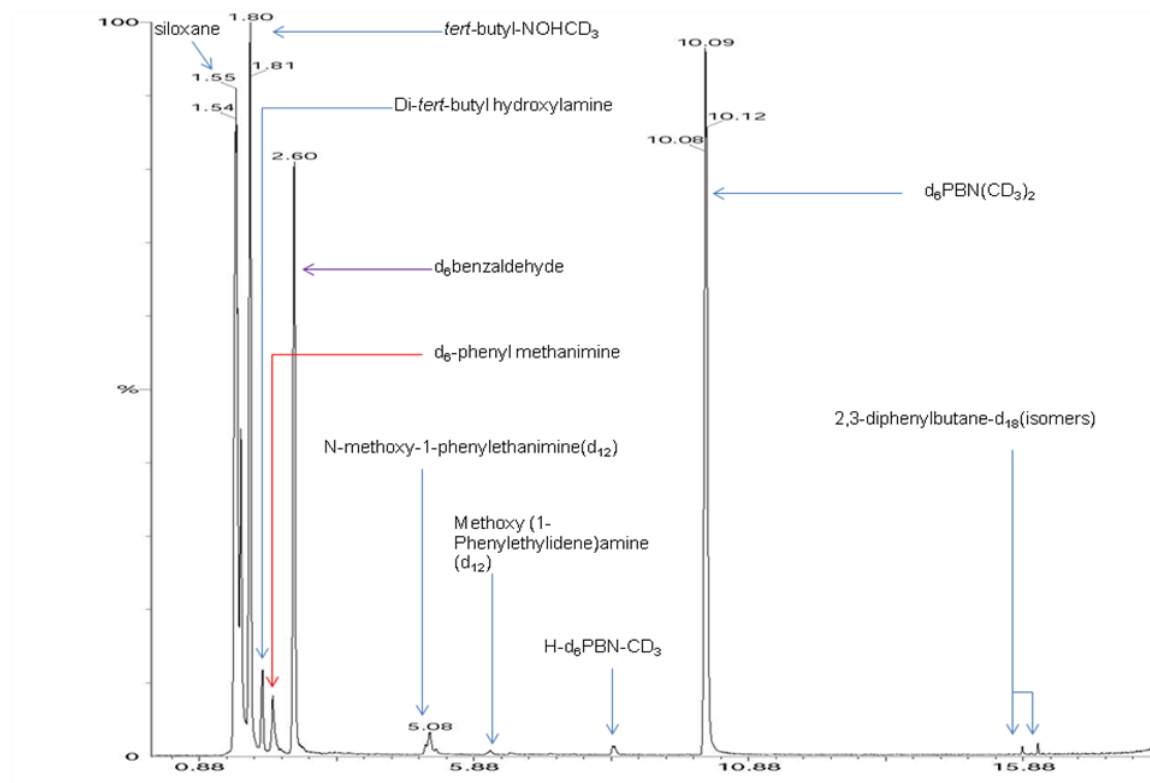


Figure A1: The total ion chromatogram (TIC) obtained from the headspace Thermal desorption TD-GC-MS analysis of the Fenton reaction containing  $d_3$ -acetaldehyde  $\{CD_3C(H)O\}$  and  $d_6$ -PBN.

Figure 1 shows the detection of tert-butylhydroaminoxyl- $CD_3$  ( $R_t$  1.67 minutes), deuterated paraldehyde- $d_9$  ( $R_t$  1.81), di-*tert*-butyl( $d_9$ ) hydroxylamine ( $R_t$  2.02 minutes),  $d_6$ -phenyl methanimine ( $R_t$  2.23 minutes),  $d_6$ -benzaldehyde ( $R_t$  2.61 minutes), N-methoxy-1-phenylethanimine( $d_{12}$ ) ( $R_t$  5.08 minutes), methoxy-(1-phenylethylidene)amine ( $d_{12}$ ) ( $R_t$  6.32 minutes), hydrogen & deuterium-methyl adduct of PBN (H-PBN- $CD_3$ ;  $R_t$  8.40 minutes), a di-deuterium-methyl adduct of the  $d_6$ -PBN ( $d_6PBN-(CD_3)_2$ ;  $R_t$  10.27 minutes) and 2,3-diphenylbutane ( $d_{18}$ ) isomers ( $R_t$  15.91 and 16.25 minutes). For a detailed analysis of EI-mass spectra see sections 3.3 – 3.12 of chapter 3.



### Self-aldol condensation of acetaldehyde into paraldehyde

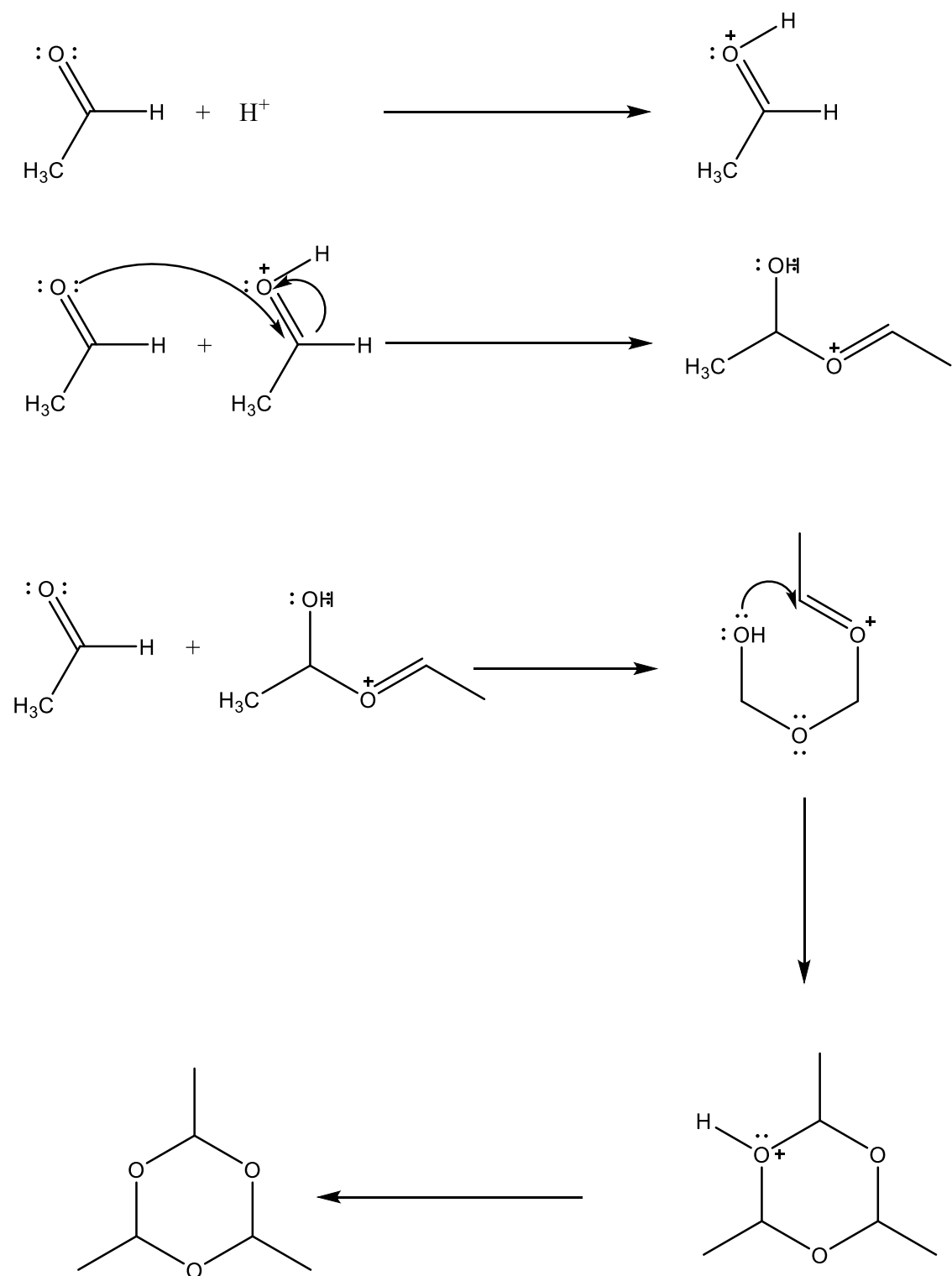


Figure A2: Aldol condensation of acetaldehyde into paraldehyde (Hill, Miessner & Ohlmann, 1989; Georgieff, 1966)

## Standard mass spectrum of 2-methylcyclopentenone

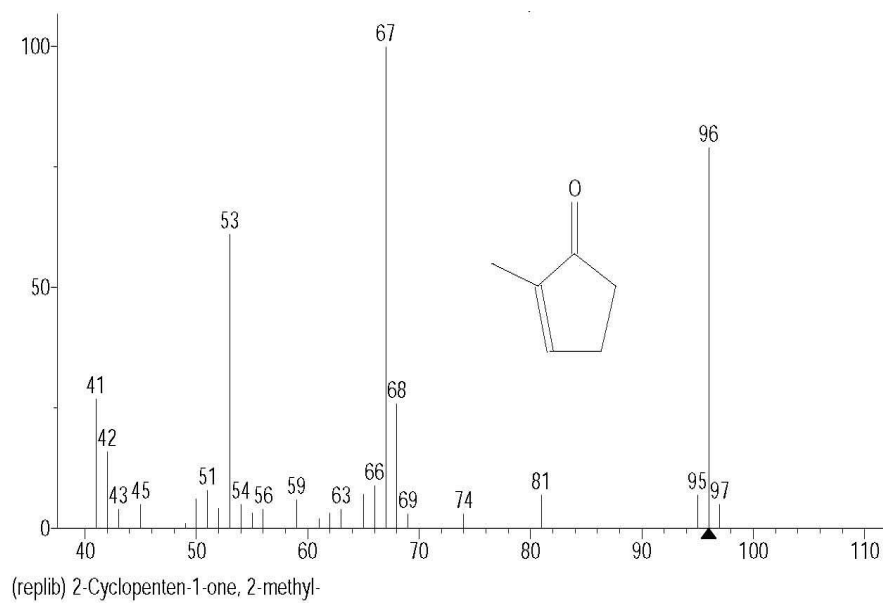


Figure A3: Standard mass spectrum of 2-methylcyclopentenone

## Comparison chromatograms for the Fenton reaction containing 4-methoxy-TEMPO and acetaldehyde using TD-GC-MS

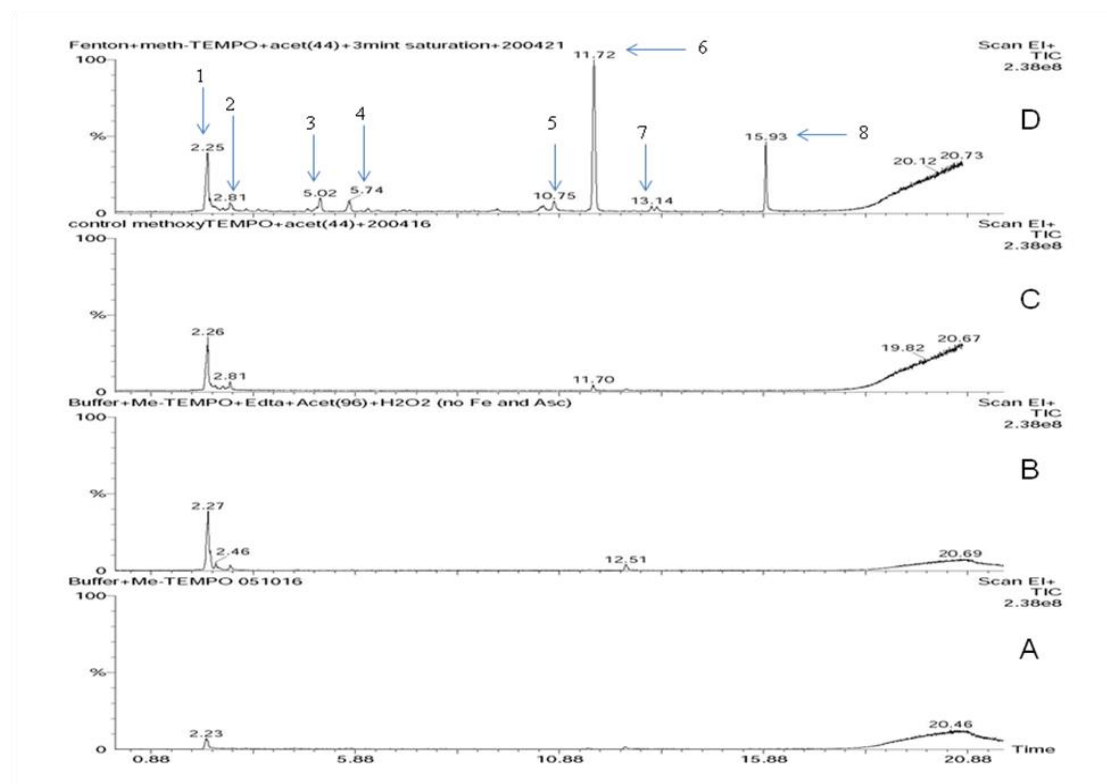


Figure A4: Comparison of chromatograms: Chromatograms generated for control experiments containing 4-methoxy-TEMPO (spin trap) and acetaldehyde (secondary source of radicals), whereby the headspace was extracted for a sample containing (A) phosphate buffer and spin trap. (B) All Fenton reagents (section 2.2.1) except iron and ascorbic acid. (C) All Fenton reagents (section 2.2.1) except iron. (D) The Fenton reaction (From bottom to top respectively).

There were eight peaks in the chromatogram when the Fenton reaction was carried out containing acetaldehyde and 4-methoxy-TEMPO. It can be seen clearly in above comparative chromatogram that the peaks at 2.25 & 2.81 minutes are present in control reactions as well which is evident that either they are impurities or the products of non-radical mechanism which are occurring alongside the Fenton reaction.

Peaks indicated with numbers 3-8 are the products of the Fenton reaction as they are present in a chromatogram obtained by the headspace analysis of the Fenton reaction containing spin trap and acetaldehyde (figure A4: D). For a detailed analysis of EI-mass spectra see sections 5.8.